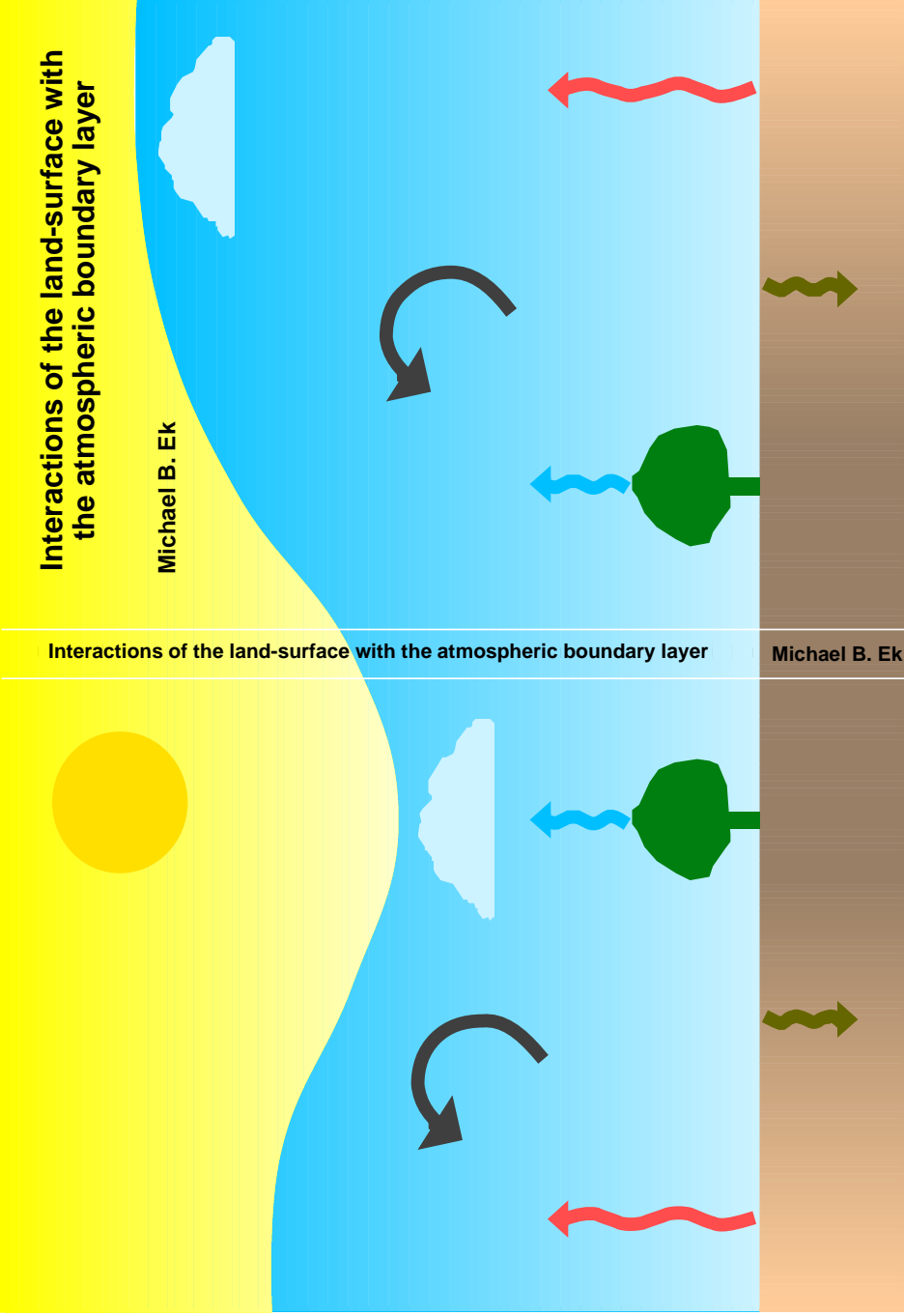


Interactions of the land-surface with the atmospheric boundary layer

Michael Bryan Ek

19 May 2005
18.30 EDT



thesis cover

**Interactions of the land-surface with
the atmospheric boundary layer**

**Interacties van het landoppervlak
met de atmosferische grenslaag**

Michael Bryan Ek

Promotor:

Prof.dr. A.A.M. Holtslag

Hoogleraar Meteorologie en Luchtkwaliteit, Wageningen Universiteit

Samenstelling promotiecommissie:

Dr. Joan Cuxart - Universitat de les Illes Balears, Palma de Mallorca, Spain

Dr. Huug van den Dool - Climate Prediction Center, NCEP, Camps Springs, USA

Prof.dr.ir. Bart van den Hurk - Universiteit Utrecht en KNMI, De Bilt

Prof.dr. Pavel Kabat - Wageningen Universiteit en Alterra

Prof.dr. Peter Troch - Wageningen Universiteit

Interactions of the land-surface with the atmospheric boundary layer

Michael Bryan Ek

Proefschrift
ter verkrijging van de graad van doctor
op gezag van de rector magnificus
van Wageningen Universiteit,
Prof.dr.ir. L. Speelman,
in het openbaar te verdedigen
op dinsdag 10 mei 2005
des namiddags te vier uur in de Aula.

CIP-gegevens Koninklijke Bibliotheek, Den Haag

Ek, M. B.

Interactions of the land-surface with the atmospheric boundary layer / M. B. Ek

Thesis Wageningen University - With ref. - With summary in Dutch.

ISBN 90-8504-172-4

Subject headings: Land-atmosphere interaction / Atmospheric boundary layer /

Land-surface modeling / Boundary-layer modeling / Soil moisture / Boundary-layer clouds.

Cover page

The development of clouds in the atmospheric boundary layer involves a number of land and atmospheric processes and interactions that may compete, in one case yielding clouds over moist soils, and in another case yielding clouds over dry soils.

Abstract

We study daytime land-atmosphere interaction using a one-dimensional (column) coupled land-surface – atmospheric boundary-layer (ABL) model and data sets gathered at Cabauw (1978, central Netherlands) and during the Hydrological and Atmospheric Pilot Experiment – Modélisation du Bilan Hydrique (HAPEX-MOBILHY, 1986, southwest France). The sensitivity of this interaction to the parameterization of soil hydraulic processes shows that the effects on surface fluxes and boundary layer development are largest for dry to moderate values of soil moisture, particularly for bare soil conditions. Boundary-layer clouds are controlled by the evolution of relative humidity (RH) at the boundary-layer top, which involves the interaction of soil moisture, surface heating, initial ABL conditions, and the moisture content and temperature stratification above the ABL with a number of competing feedback mechanisms. A fractional cloud cover formulation is developed based on a Gaussian distribution of total-water RH at the ABL top, where the distribution includes both turbulent variations (as a function of ABL-top dry air entrainment) and mesoscale variations (as a function of horizontal domain size); the modeled cloud cover is found to be more sensitive to the specified mean vertical motion than to the adjustable coefficients in the cloud cover formulation. Various improvements are made to the land-surface model and tested against data in off-line model runs without parameter tuning; using this improved land-surface model, coupled ABL – land-surface model runs yield realistic daytime surface fluxes and atmospheric profiles. Finally, it is shown in coupled land-atmosphere modeling, analytically, and with data that the effect of soil moisture is to increase ABL-top RH tendency and thus cloud cover only if the stability above the ABL is not too weak (and there is sufficient initial ABL RH, and air above the ABL not too dry), while for weak stability above the ABL, drier soils yield a greater ABL-top RH tendency and thus cloud cover (again, with sufficient initial ABL RH, and air above the ABL not too dry).

Foreword

This thesis was initiated while I was a visiting scientist at the Royal Netherlands Meteorological Institute (KNMI) in De Bilt during 1995-1996, and continued at Oregon State University/College of Oceanic and Atmospheric Sciences (OSU/COAS) in Corvallis, Oregon, USA, drawing on my past work as well as new research. It was completed while a University Corporation for Atmospheric Research visiting scientist at the National Centers for Environmental Prediction/Environmental Prediction Center (NCEP/EMC) in Suitland, Maryland, USA, with frequent visits to KNMI, then later to Wageningen University/Meteorology and Air Quality.

My interest in meteorology and the weather began at a young age, afterall, in Oregon you always watch the weather hoping for a break in the rain. The sun does generally show itself sometime during July and/or August. At age 13 I did a report on "The study of clouds" (Oregon, remember), and at 14 on the way home from an oceanography field trip to the Pacific coast I saw a funnel cloud that later formed into a tornado (a rare event in Oregon). From the school bus I made the bold prediction that it would start hailing; to the amazement of my fellow students, moments later it did. This was my first (and probably still best) weather forecast. I'd like to thank my parents (sadly now both deceased) for their support in my interest in science, especially my mother, Patricia, who encouraged me to keep studying math "...because you're good at it, Michael, and perhaps you will be able to use it in some way..." despite my questioning what it was good for, other than becoming a math teacher! My family and friends have listened (sometimes with interest!) about how the "land-surface" and "atmospheric boundary layer" affect them; my nephew thinks it's "cool" that I get to study clouds. They have patiently endured my explanations that I had "more to do", and that I was "almost done" with my thesis (e.g. Su and Alan, Peggy and Pad, John and Clare, Wayne and Dee Dee, my sister Karen and her

family, and Paula – thanks a lot). The cover page illustration was made following suggestions by my artistic daughter, Laura Ek, with help from her brilliant younger brother and sister, Bryan and Susanna.

I want to thank my many colleagues, all of whom I consider friends: At OSU, Larry Mahrt (my M.S. advisor), Hua-Lu Pan (on my M.S. committee, now at NCEP/EMC), Wayne Gibson and Nimal Gamage (computing, science, and internet help), Richard Cuenca ("Here Mike, read this book to learn something about plants"), Larry Boersma ("Here Mike, read this book to learn something about soils"), and Gad Levy (my marine boundary layer associate, previously at OSU and the University of Washington, and now with NorthWest Research Associates in Seattle). I must mention that I owe a lot to Larry Mahrt ("Mike, read a book to learn something ...*anything!*") since he so kindly asked me to work with him after my operational meteorology sojourn in Alaska and Seattle; he introduced me to many other great researchers and projects. (By the way, thanks to John Eise, a fellow fire weather and snow avalanche/mountain weather forecaster and field worker in Alaska; John is now a National Weather Service Science and Operations Officer in Wisconsin.) At NCEP I wish to thank Ken Mitchell for his previous cooperation while I was still at OSU, and now his continuing support of my collaboration with colleagues in The Netherlands and elsewhere after I came to work with him at NCEP. Suru Saha, also at NCEP, via her incredible charm, provided ongoing "encouragement" (read: pushing) for me to finish my thesis, as did Dag Lohmann and Curtis Marshall. I wish to thank a former contract monitor, Sam Chang (now at a research lab in Adelphi, Maryland) who I worked with on several papers.

At KNMI and Wageningen, I must thank Bert Holtslag (my Ph.D. advisor) for his valuable inspiration and guidance, along with his continued encouragement ...and patience, Fred Bosveld (from scientific to thesis-administrative support), Anton Beljaars and Bart van den Hurk for many valuable land-surface and boundary layer discussions (my former KNMI office mates, in the old building and then in the "Units"; Anton is now at ECMWF; when I returned to OSU from KNMI, Bart bought my bicycle – it was stolen within a month), Erik van Meijgaard (who put up with me so often when I visited his former officemate at KNMI, Bert), Aad van Ulden (during his visit to Oregon, and my later visits to KNMI) and Pier Siebesma for their ideas on boundary layer mixing and clouds, Henk de Bruin (the first Dutch scientist I met when he visited OSU) as well as Bas van de Wiel, Gert-Jan Steeneveld, Jordi Vila, and Dirk

Burose-Schuettmeyer (among others) for more discussions on the land-surface and boundary layers, Kees van den Dries (great help with computers and the internet), and Reinder Ronda (his thesis in Latex was my starting template). Also, Bert and Fred and their families provided and continue to provide wonderful friendship with me and my family, especially when we lived in The Netherlands; Anton helped me deal with the phone company ("...but they need a telephone *before* they return to America...") and residency issues ("...don't bother – you'll return home before they find out you're even here..."). Also, many of these people and others need to be acknowledged for their role (either direct or indirect) in helping to develop and improve the model I have been able to work with over the years.

As far as working environment, I found that I got a lot done at coffee shops (not Dutch "coffeeshop"), i.e. at "The Beanry" and elsewhere in Corvallis, Oregon (where there are many espresso bars) when I started the work on my thesis, and at "Jitterz" (Candace and her baristas) in North Beach, Maryland when I completed my writing, plus elsewhere in between. I have also had many lively discussions with my colleagues about land-surface and boundary-layer issues (among other topics) over beer. (Ideas from such discussions were often greatly amended later over coffee.) Thanks also go to the several Macintosh computers that have served me well during the research and writing of this thesis (with an occasional PC or Linux box thrown in for good measure).

Finally, here's something amusing. Returning from a trip, I was thinking about how I might use my previous work with Larry Mahrt on the daytime evolution of boundary-layer relative humidity (Chapter 3) in the research for Chapter 6. With *lots* of scribbling (next page) I came up with a derivation showing the various land and atmospheric influences in a rather simple equation and corresponding phase diagram (Equation 6.1/Figure 6.10). A woman sitting next to me on the plane asked, "What are you doing?!" I said, "Showing the influence of soil moisture on boundary-layer cloud initiation." She responded with a long and puzzled, "Oh...?"

Michael Ek
Chesapeake Beach, Maryland, USA
13 April 2005

Contents

1	Introduction	1
1.1	Land-atmosphere interaction	1
1.2	Motivation and outline of thesis	5
2	Variation in soil parameters: Implications for modeling surface fluxes and atmospheric boundary-layer development	9
2.1	Introduction	10
2.2	Soil hydraulics and thermodynamics	10
2.3	Modeling and the heterogeneity of soil properties	14
2.4	Modeling results	14
2.4.1	Bare soil	15
2.4.2	Full vegetation	18
2.5	Summary	23
3	Daytime evolution of relative humidity at the boundary-layer top	25
3.1	Introduction	26
3.2	Boundary-layer relative humidity	28
3.2.1	Boundary-layer warming and growth	31
3.2.2	Dry air entrainment	32
3.2.3	Influence of soil moisture and surface evaporation	33
3.2.4	Large scale vertical motion	35
3.2.5	Small boundary-layer growth	36
3.3	HAPEX-MOBILHY data analysis	37
3.3.1	Aircraft data	37
3.3.2	Simple models	41
3.4	Boundary-layer model simulations	43

3.4.1	Evolution stages	47
3.4.2	Influence of soil moisture	49
3.5	Conclusions	53
4	A formulation for boundary-layer cloud cover	55
4.1	Introduction	56
4.2	Relative humidity models of cloud cover	57
4.3	Relative humidity variance	68
4.3.1	Turbulent scale variation of relative humidity	68
4.3.2	Vertical velocity variance	72
4.3.3	Mesoscale variation of relative humidity	72
4.4	Cloud transmission of solar radiation	73
4.5	Model testing	74
4.6	Conclusions	80
5	Evaluation of a land-surface scheme at Cabauw	83
5.1	Introduction	84
5.2	Cabauw site and data set	85
5.3	Land-surface scheme	86
5.3.1	Transpiration and canopy conductance	87
5.3.2	Root density and soil hydraulics	90
5.3.3	Soil thermodynamics	92
5.3.4	Model geometry and initial conditions	94
5.4	Land-surface modeling sensitivity tests	95
5.4.1	Canopy conductance	95
5.4.2	Root distribution	98
5.4.3	Soil heat flux	101
5.4.4	Surface fluxes and sensitivity to initial soil moisture	105
5.5	Summary	107
6	Influence of soil moisture on boundary-layer cloud development	111
6.1	Introduction	112
6.2	Cabauw site and data set	114
6.3	Coupled Atmospheric boundary layer-Plant-Soil (CAPS) model	116
6.4	Model evaluations	119
6.4.1	Land-surface modeling results (atmospheric forcing)	119
6.4.2	Atmospheric boundary-layer modeling results (surface forcing)	121

6.4.3	Coupled modeling results (surface-atmosphere interaction) . . .	126
6.5	Impact of soil moisture on ABL cloud development	129
6.5.1	Coupled model results	129
6.5.2	Analytical results	130
6.5.3	Discussion	135
6.6	Summary	139
7	Summary and perspective	141
7.1	Summary	141
7.2	Perspective	145
A	Coupled Atmospheric boundary layer–Plant–Soil model	149
A.1	Surface radiation scheme	151
A.1.1	Incoming solar radiation	151
A.1.2	Albedo	153
A.1.3	Downward atmospheric radiation	153
A.2	Surface fluxes and surface exchange coefficients	153
A.2.1	Surface fluxes	153
A.2.2	Surface exchange coefficients	154
A.3	Land-surface scheme	157
A.3.1	Prognostic land-surface equations	157
A.3.2	Potential evaporation calculation	158
A.3.3	Surface evapotranspiration	163
A.3.4	Soil hydraulics	166
A.3.5	Soil thermodynamics	167
A.3.6	Surface temperature	168
A.4	Atmospheric boundary-layer scheme	169
A.4.1	Prognostic boundary-layer equations	169
A.4.2	Boundary layer turbulence	170
A.4.3	ABL height	174
A.4.4	ABL cloud cover formulation	177
B	Relative humidity tendency at the ABL top	179
	Bibliography	183
	Samenvatting	203

Curriculum vitae	205
List of peer-reviewed publications by the author	207
First-author publications	207
Co-author publications	208

Chapter 1

Introduction

1.1 Land-atmosphere interaction

Life on earth depends directly on solar energy and the availability of water. Evaporation of water from the land-surface and water bodies eventually generates clouds and may result in precipitation that infiltrates into the ground and percolates downward, increasing soil moisture that is critical for agricultural and native plant growth. Figure 1.1 shows the relevant processes in the hydrological cycle, of which evaporation, precipitation, and infiltration and percolation are a part, with runoff and groundwater flow into rivers, lakes, and oceans completing that cycle. Surface evaporation consists of plant transpiration, direct evaporation of water from the soil surface, and evaporation of canopy-intercepted water from precipitation or dew (together often called evapotranspiration), in addition to open-water evaporation.

Over land, just how much water evaporates depends on the surface and soil conditions (e.g. type and coverage of vegetation, soil moisture, and other factors), as well as the incoming solar ("shortwave") and atmospheric ("longwave") radiation (energy) absorbed at the surface. In addition, the air temperature, humidity, and wind near the surface play a role in evaporation. Figure 1.2 shows the relevant energy processes in the land-atmosphere system, where the solar energy absorbed at the surface is reduced from the top-of-atmosphere value due to reflection and absorption by clouds, back-scatter by air, and reflection by the surface. The atmospheric energy reaching the surface is due to the emission of longwave radiation from clouds (liquid water) and "greenhouse" gases in the atmosphere (carbon dioxide, water vapor, and other

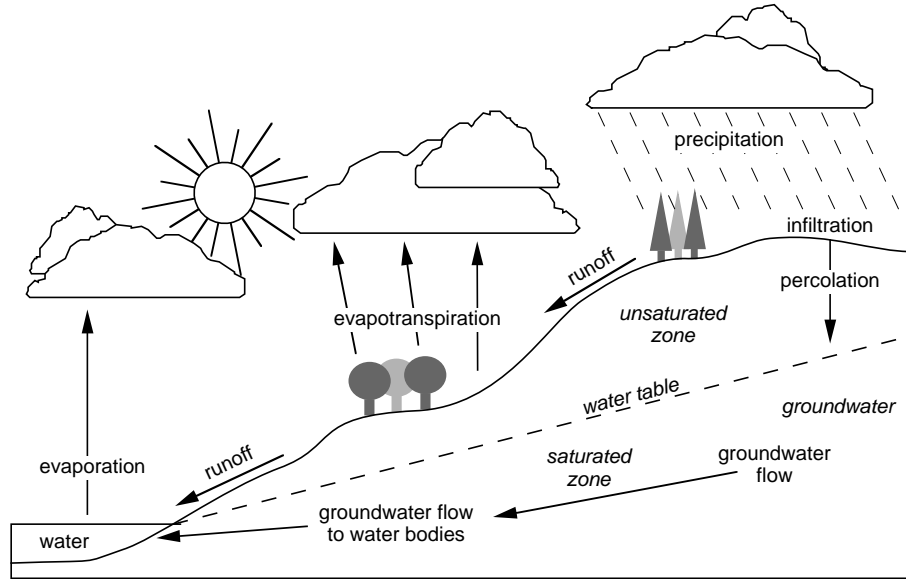


Figure 1.1: Components and processes in the hydrological cycle.

trace gases), and increases with increasing temperature, and increased concentrations of liquid water and greenhouse gases. We note that for the land-atmosphere system, there is net outgoing longwave radiation (radiated to space) in order to balance the incoming solar energy.

For the surface energy budget to balance over land, energy not used in evaporation (latent heat flux) then penetrates into the ground (soil heat flux), is re-emitted as outgoing terrestrial (longwave) radiation, and heats the atmosphere (sensible heat flux). The soil heat flux depends on the soil moisture and temperature, soil texture, and vegetation overlying the ground surface, and may be into (typically during day) or out of (typically at night) the ground, but approximately balances over long time scales (i.e. an annual cycle). Terrestrial radiation depends on the surface skin temperature, so with a greater temperature the terrestrial radiation increases. Finally, the sensible heat flux is determined by the surface roughness, low-level wind, and temperature gradient between the surface and low-level atmosphere. The sensible (latent) heat flux may be downward, in which case heat (moisture, e.g. as dew) is transported to the surface; this is more typical of nocturnal conditions.

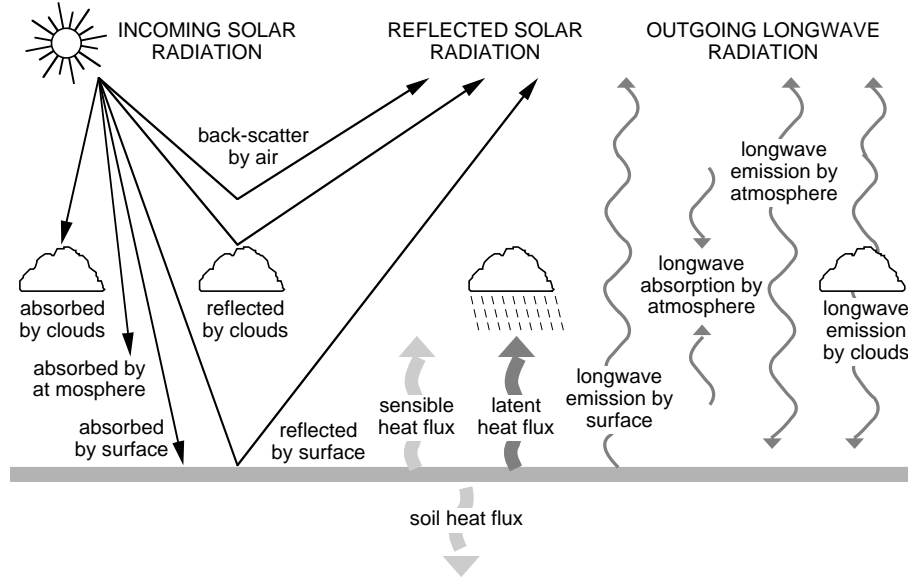


Figure 1.2: The land-atmosphere energy budget for typical daytime conditions.

The latent and sensible heat fluxes are turbulent processes at the surface and are affected by the evolution of the temperature, humidity, and wind fields in the overlying atmospheric boundary layer (ABL). The ABL is defined as the lowest part of the atmosphere that is directly influenced by the motions and processes at and near the earth's surface. Under the right conditions, ABL clouds form as a coupled response to surface fluxes, the ambient state of the ABL, and interactions of the ABL with the free atmosphere above. Friction of the wind at the surface and convective heating from the surface increase the depth of turbulent mixing in the ABL and interaction with the surface; typically over land the evolution of temperature, humidity, and wind fields generally follows a diurnal time scale.

In order to better understand and model the cycles of water and energy necessary for weather and climate, we must study interactions between the land and atmosphere. As noted by Richardson (1922), "The atmosphere and the upper layers of the soil or sea form together a united system. This is evident since the first few meters of ground has a thermal capacity comparable with 1/10 that of the entire atmospheric column standing upon it, and since buried thermometers show that its changes for temperature are considerable. Similar considerations apply to the sea and to the ca-

capacity of the soil for water.”

In weather and climate models, we require a realistic hydrometeorological representation of land-atmosphere interactions for different atmospheric regimes on many spatial and temporal scales, from larger scales (e.g. as in Figures 1.1 and 1.2), to the smaller scales of diurnal interaction between the land-surface and ABL (see Figure 6.1 in Chapter 6, for example). The subject of this thesis is directed mostly towards land-atmosphere interactions on the diurnal time scale. According to Betts (2004), “Usually we rely on simple models to gain understanding, but hydrometeorology is too complex for that, and too important for us to be satisfied with rough approximations. ...we have to do much better – we must understand how well the models represent physical processes and feedbacks.”

Many studies have been undertaken over the past several decades in examining land-atmosphere interaction. We briefly review here (and then more completely in subsequent chapters) some of these studies that address such interaction on a variety of scales. Charney et al (1977) showed the interactive role of albedo and evaporation on convective clouds and precipitation in semi-arid regions using a global general circulation model. Garrett (1982) demonstrated the importance of including soil and vegetation in cloud formation in the convective atmospheric boundary layer in a regional model. He noted that evapotranspiration retards boundary-layer growth, and if retarded enough, convective rainfall decreases, suggesting that cloudiness is reduced compared to regions with stronger surface heating. Anthes (1984) examined the effect of mesoscale variations in vegetation on surface heating and the resulting changes to local circulations and convective precipitation. Pan and Mahrt (1987) examined the interaction of soil moisture and boundary-layer development (for initially wet soils), describing three stages: potential (high) evaporation, a rapid decrease of evaporation, and near-equilibrium (low) evaporation, with corresponding boundary-layer evolution, and variations for different soil textures and atmospheric forcings.

Avissar and Pielke (1989) accounted for the subgrid variability of surface features using a micrometeorological model of the soil-plant-atmosphere system incorporated in a mesoscale model to show the importance of surface spatial heterogeneity in generating local circulations. Blyth et al (1994) used a mesoscale model including boundary layer and land-surface components (i.e. Noilhan and Planton 1989) to demonstrate that the impact of re-evaporation of forest canopy-intercepted water in-

creases rainfall compared with a bare-soil domain. Holtslag and Ek (1996) examined the sensitivity of the land-atmosphere coupling to the specification of the surface roughness for heat. Brubaker and Entekhabi (1996) used an analytical model coupling energy and water balances to explore land-atmosphere interaction and found that local positive feedbacks act to preserve and reinforce droughts.

Betts et al (1996) reviewed land-atmosphere interaction on time scales from diurnal to seasonal (and longer) based on observational and global modeling perspectives. In an observational study, Freedman et al (2001) analyzed boundary layer cumulus clouds and the changes in their impact on land-atmosphere interaction due to changes in Bowen ratio, lifting condensation level, and boundary layer depth from early spring through summer. Findell and Eltahir (2003a) developed measures using the low-level humidity and the elevated temperature lapse rate to characterize the role of soil moisture and atmospheric profiles in convective initiation, distinguishing three types of early-morning conditions, i.e. those favoring convection over dry soils, those favoring convection over wet soils, and those that will allow or prevent convection, independent of the surface conditions. They applied this method to observations over the continental United States (Findell and Eltahir 2003b) to investigate how different atmospheric regimes influence local land-atmosphere feedbacks.

1.2 Motivation and outline of thesis

The underlying research question that provides the motivation for this thesis is, "What is the nature of land-atmosphere interaction, or more specifically, the diurnal interaction of the land-surface and the atmospheric boundary layer?" Also, as a tool to advance our understanding, "How can we model these land-atmosphere interactions with simple, robust and still realistic methods?" To address these questions we must carefully examine land-surface and atmospheric boundary layer processes on the diurnal time scale, and the corresponding model formulations used to represent them, trying to increase our understanding in order to close those observational and modeling gaps.

The chapters in this thesis are individually published in the reviewed literature as stand-alone papers. As such, some overlap occurs between this introduction, the chapters, and the summary. Land-atmosphere processes and interactions are studied using the one-dimensional (column) Coupled - Atmospheric boundary layer - Plant -

Soil (CAPS) model (also known as the Oregon State University (OSU) land-surface – atmospheric boundary-layer model), and is described in parts in the chapters, and in greater detail in Appendix A. For model formulation development and verification, we use observational data sets gathered at Cabauw (spring 1978, central Netherlands) and during the Hydrological and Atmospheric Pilot Experiment – Modélisation du Bilan Hydrique (HAPEX-MOBILHY, spring-summer 1986, southwest France). The goals of the thesis are then dealt with in five additional chapters, a summary, and two appendices.

Chapter 2 examines land surface-ABL interaction with a perspective on the influence of soil hydraulic and thermal properties. Using the CAPS model, we study the effect of the variation in soil properties on modeled surface fluxes and ABL evolution using data taken during HAPEX-MOBILHY.

Chapter 3 studies land surface-ABL interaction with a focus on the evolution of ABL-top relative humidity and the potential for ABL cloud initiation. This evolution depends on the initial and external conditions, and a number of land-surface and ABL interactions that sometimes compete. We again use the HAPEX-MOBILHY data set for analysis, and verification of a number of coupled land-surface – ABL model runs.

Chapter 4 has as its focus the development of a boundary-layer cloud cover formulation using HAPEX-MOBILHY data, with a relative humidity approach that is extended to account for horizontal variations in humidity. Since ABL clouds attenuate incoming solar radiation, their representation is important in determining surface fluxes and interaction with and development of the ABL. Subsequent model tests are then made using the cloud cover formulation.

Chapter 5 evaluates the land-surface scheme (from the CAPS model) using a data set from Cabauw, Netherlands. Uncoupled (land-only) model runs are used to assess the performance of the plant and soil formulations, along with a number of alternate parameterizations. The resulting "best" version of the land-surface scheme is then determined and used for coupling with the ABL (i.e. in Chapter 6).

Chapter 6 addresses the role of soil moisture in ABL evolution and ABL cloud initiation, from analytical, observational, and modeling perspectives. We utilize the land-surface scheme from Chapter 5, and use or extend the results from Chapters 2,

3, and 4 to make further land surface-ABL model runs using the Cabauw data set.

Chapter 7 provides an overview of results presented in this thesis, and discusses possible future research.

Appendix A reviews the details of the various formulations employed in the CAPS model: the simple surface radiation, land-surface, and ABL schemes. Appendix B gives the details for the derivation of the boundary-layer top relative humidity tendency equation from Chapter 6.

Chapter 2

Variation in soil parameters: Implications for modeling surface fluxes and atmospheric boundary-layer development

This chapter is published as Ek, M. and R. H. Cuenca, 1994: Variation in soil parameters: Implications for modeling surface fluxes and atmospheric boundary-layer development. *Boundary-Layer Meteorology*, **70**, 369-383.

©Copyright 1994 by Kluwer Academic Publishers

Abstract

Soil texture can be heterogeneous, however for land surface-atmospheric modeling purposes it is often considered homogeneous at a particular point and described by empirical equations which have been formulated to describe "average" hydraulic and thermodynamic processes in the soil. Large deviations in the variables and coefficients used in these empirical equations have been previously documented. One of the coefficients is varied by plus-and-minus one standard deviation about its mean, and tested in a coupled atmospheric-plant-soil model. Results of model simulations show that the effects on surface fluxes and boundary layer development are largest for dry to moderate values of soil moisture, particularly for bare soil conditions.

2.1 Introduction

To properly describe the interaction between the land surface and atmospheric boundary layer, one must adequately describe heat and moisture movement at the surface and within the soil since the soil layer represents both a source and sink of heat and moisture to and from the atmosphere. In an effort to simulate these complicated interactions, coupled atmospheric-plant-soil models use formulations which describe the soil physics of the processes included in the model. Many researchers have used the soil moisture potential formulation described in Clapp and Hornberger (1978) (henceforth CH78) and Cosby et al (1984) in soil moisture and heat diffusion equations. However, these empirical formulations are valid for an "average" or homogeneous soil and parameters in these formulations have been shown to have large standard deviations for typical heterogeneous soils. Using a one-dimensional coupled atmospheric boundary-layer-plant-soil model, we examine the effect on simulation results of the variation about the mean of soil moisture potential from data presented in CH78. These results give an insight to one aspect of the affect of natural variability of land surfaces and the potential effect on surface fluxes and atmospheric boundary-layer development.

2.2 Soil hydraulics and thermodynamics

The time-tendency of water transport in the soil (following Hillel 1980) is given as

$$\frac{\partial \Theta}{\partial t} = \frac{\partial K_{\Theta}}{\partial z} + \frac{\partial}{\partial z} \left(D_{\Theta} \frac{\partial \Theta}{\partial z} \right), \quad (2.1)$$

where Θ (dimensionless) is volumetric soil moisture content, K_Θ (m s^{-1}) is hydraulic conductivity, and D_Θ ($\text{m}^2 \text{s}^{-1}$) is soil water diffusivity. The one-dimensional heat conduction equation is

$$C_T \frac{\partial T}{\partial t} = \frac{\partial}{\partial z} \left(K_T \frac{\partial T}{\partial z} \right), \quad (2.2)$$

where C_T ($\text{J m}^{-3} \text{K}^{-1}$) is the volumetric heat capacity, T ($^\circ\text{C}$) is soil temperature, and K_T ($\text{W m}^{-1} \text{K}^{-1}$) is thermal conductivity. The surface fluxes of heat and moisture represent upper boundary conditions for (2.1)-(2.2).

Hydraulic conductivity and soil water diffusivity are given as

$$K_\Theta = K_{\Theta_s} \left(\frac{\Theta}{\Theta_s} \right)^{2b+3}, \quad (2.3)$$

$$D_\Theta = \left(\frac{bK_{\Theta_s}\psi_s}{\Theta_s} \right) \left(\frac{\Theta}{\Theta_s} \right)^{b+2}, \quad (2.4)$$

where K_{Θ_s} is the saturation hydraulic conductivity, Θ_s is the saturation volumetric soil moisture content, b is an empirically-derived coefficient, and ψ_s (m) is the saturation soil moisture potential (negative), all a function of soil texture as determined by CH78 who cited the method presented earlier in Campbell (1974). Following Al Nakshabandi and Kohnke (1965), the thermal conductivity is expressed as

$$K_T = \left\{ \begin{array}{ll} 420 \exp([- \log_{10}(100|\psi|)] + 2.7), & \log_{10}(100|\psi|) \leq 5.1 \\ 0.1722, & \log_{10}(100|\psi|) > 5.1 \end{array} \right\}, \quad (2.5)$$

and is a function of the soil moisture potential (ψ), where

$$\psi = \psi_s \left(\frac{\Theta}{\Theta_s} \right)^{-b}. \quad (2.6)$$

CH78 used 1446 samples to determine the mean values and standard deviations of ψ_s , Θ_s and b as a function of soil texture. Over 300 soil samples of the original set were neglected because they were considered by CH78 to be anomalous. CH78 qualified their results, citing the heterogeneous nature of soils, and indicated that "blind use of these average values may give erroneous results".

Comparison of values of K_Θ , D_Θ , K_T , and ψ from (2.3)-(2.6) shows them to be strongly dependent on the soil moisture content (Figure 2.1). Of the three values

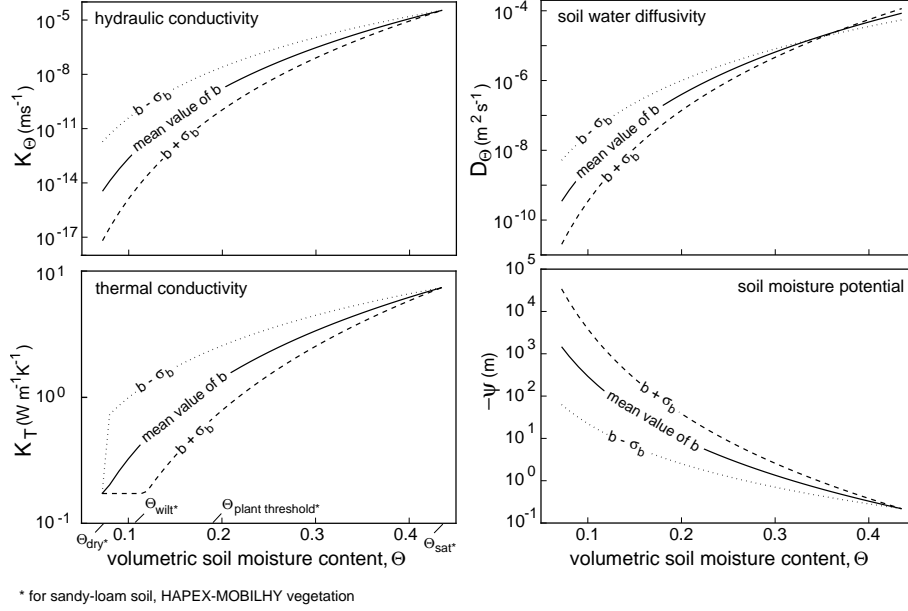


Figure 2.1: Variation of hydraulic conductivity (K_Θ), soil water diffusivity (D_Θ), thermal conductivity (K_T), and soil moisture potential (ψ) versus volumetric soil moisture content (Θ) for sandy-loam soil using the mean value of b (solid line), and the mean value of b plus or minus one standard deviation ($b \pm \sigma_b$; dashed/dotted lines) following CH78.

(ψ_s , Θ_s and b) from CH78, the variability in the exponent b has the largest effect on resulting values of K_Θ , D_Θ , K_T , and ψ over a range of soil moisture conditions (e.g for sandy-loam, Figure 2.1, Table 2.1). For very low values of soil moisture, the ratio of Θ to Θ_s in (2.3), (2.4), and (2.6) approaches zero regardless of the value of the exponent b . For very high values of soil moisture, this ratio approaches unity, so that there is an asymptotic bound in the extremes of soil moisture. Therefore, the largest differences between the modeled values of surface fluxes, temperatures and other variables should occur for moderate values of soil moisture. We shall examine the effect of variations in the exponent b on simulations using a coupled atmospheric boundary-layer-plant-soil model.

Table 2.1: Soil parameters for sandy-loam soil (from Clapp and Hornberger 1978) with values of hydraulic conductivity (K_Θ), soil water diffusivity (D_Θ), thermal conductivity (K_T), and soil moisture potential (ψ) using the mean value of b , and the mean value of b plus and minus one standard deviation ($b \pm \sigma_b$) under moist and dry volumetric soil moisture conditions.

sandy-loam soil parameters				
b	σ_b	$-\psi_{sat}$ [m]	Θ_{sat}	$K_{\Theta_{sat}}$ [ms ⁻¹]
4.90	1.75	0.218	0.435	3.45×10^{-05}

soil moisture content, Θ		hydraulic conductivity, K_Θ [ms ⁻¹]		
		$b - \sigma_b$	b	$b + \sigma_b$
moist	0.255	2.41×10^{-08}	3.72×10^{-08}	5.74×10^{-09}
dry	0.114	1.35×10^{-10}	1.25×10^{-12}	1.15×10^{-14}

soil moisture content, Θ		soil water diffusivity, D_Θ [m ² s ⁻¹]		
		$b - \sigma_b$	b	$b + \sigma_b$
moist	0.255	5.44×10^{-06}	2.14×10^{-06}	8.39×10^{-07}
dry	0.114	8.61×10^{-08}	8.26×10^{-09}	7.93×10^{-10}

soil moisture content, Θ		thermal conductivity, K_T [W m ⁻¹ K ⁻¹]		
		$b - \sigma_b$	b	$b + \sigma_b$
moist	0.255	5832.3	3886.4	2589.8
dry	0.114	1938.8	700.7	253.2

soil moisture content, Θ		soil moisture potential, $-\psi$ [m]		
		$b - \sigma_b$	b	$b + \sigma_b$
moist	0.255	1.2	3.0	7.6
dry	0.114	14.8	154.2	1606.9

2.3 Modeling and the heterogeneity of soil properties

The use of the CH78 soil properties appears to have widespread acceptance in the atmospheric modeling community where land-surface interactions are considered. The CH78 soil properties have been used in the Simple Biosphere (SiB) model (Sellers et al 1986), the Biosphere-Atmosphere Transport Scheme (BATS, Dickinson et al 1993), the land-surface parameterization scheme of Noilhan and Planton (1989), and models described in Siebert et al (1992), Kondo et al (1990), Schädler (1990), Mahrt and Pan (1984), and others.

In modeling and observational studies, Zepp and Belz (1992) and Vandenberg and Louters (1988) acknowledged that spatial heterogeneity can affect soil properties. Bougeault et al (1991) and McCumber and Pielke (1981) discuss the importance of soil moisture in modeling, and that there was a natural variability of hydraulic properties in soils. Wetzal and Chang (1987) noted the variability of the soil properties, focusing instead on the heterogeneity of soil moisture and its effect on area-averaged evaporation. In sensitivity tests with the BATS model, Wilson et al (1987) showed that changes in soil texture had the largest effect on model results in the NCAR Community Climate Model. Mascart et al (1991) chose to calibrate the soil functions directly to experimental data in HAPEX-MOBILHY, citing the wide variation in soil physical parameters. A similar method was employed by Ács et al (1991). Entekhabi and Eagleson (1989) used probability density functions of soil moisture to account for the spatial heterogeneity of soil hydraulic conditions for use in a GCM. Using probability density functions in a "statistical-dynamical approach", Avissar (1992) addressed heterogeneity of soil moisture and other surface properties. Abramopoulos et al (1988) used composited soil characteristics to account for spatial heterogeneity of soil moisture, but offline testing of the ground hydrology model from the GISS GCM showed minimal sensitivity to soil hydraulic properties. Avissar and Pielke (1989) assumed a mosaic of homogeneous patches in a mesoscale model to account for the effect of spatial heterogeneity.

2.4 Modeling results

For the model sensitivity tests in this study, we use the Oregon State University (OSU) one-dimensional coupled atmospheric-plant-soil model that was developed to

simulate the interactions of the atmospheric boundary layer, vegetation and soil. The atmospheric boundary layer model (Troen and Mahrt 1986) is coupled with an active two-layer soil model (Mahrt and Pan 1984), and a basic plant canopy submodel (Pan and Mahrt 1987) modified to include the interactive effect of vegetation following Noilhan and Planton (1989) and Jacquemin and Noilhan (1990). The OSU model has been formulated for inclusion in large-scale models where the computational efficiency is important, yet the equations used are comprehensive enough to approximate the physical processes thought to be most important. The model has been used as a stand-alone for a number of sensitivity experiments under different geophysical conditions (e.g. Holtslag et al 1990, Ek and Mahrt 1991a, Holtslag and Boville 1993, Ek and Mahrt 1994, Huang and Lyons 1994, Holtslag and Ek 1994, and others).

The following sensitivity tests are made to assess the effect of uncertainties in the soil equations (2.3)-(2.6) on the daytime evolution of surface conditions and subsequent boundary-layer development for bare soil and full vegetation conditions. Multiple model simulations are made using a wide range of soil moisture conditions, initially uniform with depth for a given initial soil moisture. Three different values of the exponent b are used in (2.3), (2.4), and (2.6): the mean value (identified as the *mean b* case), the mean plus one standard deviation of b (identified as the *+ b* case), and the mean minus one standard deviation of b (identified as the *- b* case).

2.4.1 Bare soil

We begin with simulations for bare soil since it is anticipated that the effects will be the greatest. We use data from HAPEX-MOBILHY (André et al 1988) to initialize the model. For bare soil we use a roughness length of 10^{-2} m for momentum and 10^{-3} m for heat (Garratt 1992). We exclude the effect of an albedo change over bare soil with changing soil moisture and fix the albedo at 0.15, a representative value for bare soil in HAPEX-MOBILHY (Bessemoulin et al 1987). Following Pan and Mahrt (1987), we use an air-dry volumetric soil moisture content of 0.07 for the sandy-loam soil in HAPEX-MOBILHY; the air-dry value (Θ_d) is the volumetric soil moisture content where direct evaporation from the surface vanishes. Geostrophic wind is assumed constant from the north at about 3 m s^{-1} with a prescribed subsidence of about 1.5 cm s^{-1} at 2 km linearly increasing to zero at the surface (Jacquemin and Noilhan 1990). We initiate the model using 0600 LST radiosonde data over the pine forest in SW France for 16 June 1986 (Brutsaert and Parlange 1992) and examine the

subsurface, surface and lower atmospheric conditions, and boundary-layer depth at 1200 LST after six hours of model integration.

Conditions at first change steadily, then more rapidly as the volumetric soil moisture content in the upper (Θ_1) and lower (Θ_2) soil layers increases above the air-dry value from one model simulation to the next (Figure 2.2). Latent heat flux (LE) increases with associated decreases in surface temperature (T_s) and sensible heat flux (H). This leads to a decrease in both the upper soil layer temperature (T_{s1} , 0-5 cm) and air temperature (T_a , at 20 m) which gives a modest increase in net radiation (R_n), and an increase in specific humidity of the air (q_a , at 20 m) resulting in a decrease in the potential evaporation (E_p). The lower soil layer temperature (T_{s2} , 5-100 cm) is largely unaffected due to its distance from the surface. The low-level wind speed (U) first increases as the boundary layer depth (h) becomes shallower and excludes lower momentum air above 2 km; from the initial wind profile there is a peak in wind speed around 2 km. Wind speed then decreases as the boundary layer continues to become shallower and excludes higher momentum air from above. A threshold volumetric soil moisture content of about 0.20 defines the upper end of a transition zone (the region between the vertical dotted lines for the *mean b* case, Figure 2.2) where the increasing latent heat flux equals the decreasing potential evaporation. Above this soil moisture content conditions change slowly. In the transition zone the soil heat flux (G) increases slightly with increasing soil moisture (increased conductivity), despite a decrease in the surface-soil temperature gradient. At the upper end of the transition zone there is a sharp drop in the soil heat flux as the surface-soil temperature gradient reaches a minimum. Above this point the soil heat flux slowly increases again as the soil moisture and thermal conductivity increase with a nearly constant temperature gradient between the surface and upper soil layer.

For the simulations using the *mean b* value (dashed lines, Figure 2.2), soil hydraulic and thermal conductivity, and soil water diffusivity are smaller compared to the *mean b* (solid lines) and *-b* simulations (dotted lines). For the *+b* case, this results in decreased upward movement of soil water so the latent heat flux is smaller, leaving a higher soil moisture content in the upper soil layer of the model. Consequently, the sensible heat flux and the surface and air temperatures are greater, as is the potential evaporation. The temperature in the upper soil layer is greater for the *+b* case due to a greater surface temperature despite the reduced downward heat transport, the exception being at soil moisture values near the air-dry value where the lower thermal

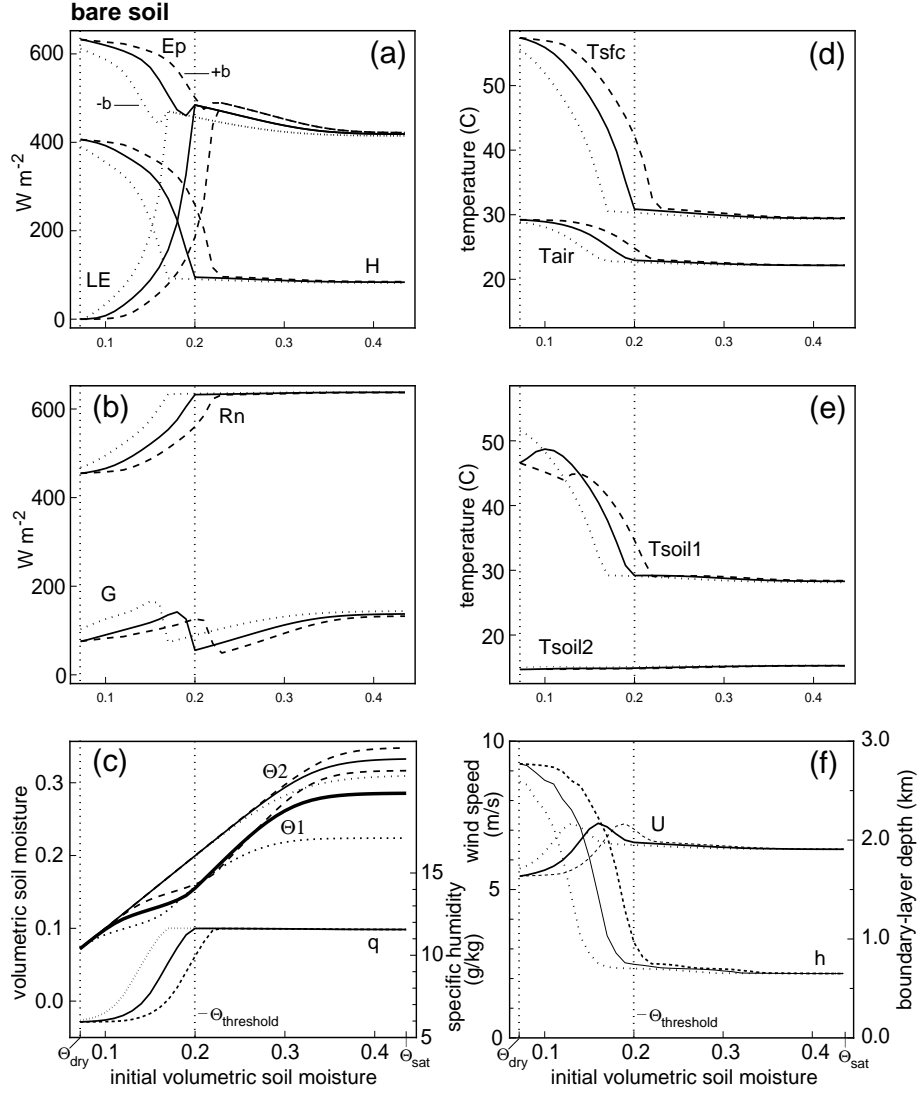


Figure 2.2: Simulations for bare soil with model output at 1200 LST for multiple six-hour integrations where the initial soil moisture content is varied from dry to moist conditions for the *mean b* (solid), *+b* (dashed) and *-b* (dotted) cases; (a) potential evaporation (E_p), sensible (H) and latent (LE) heat fluxes, (b) net radiation (R_n) and soil heat flux (G), (c) atmospheric specific humidity (q_a), and volumetric soil moisture content in the upper (Θ_1 ; thick lines) and lower (Θ_2 ; thin lines) soil layers, (d) surface (T_s) and air (T_a) temperatures, (e) upper (T_{s1}) and lower (T_{s2}) soil temperatures, and (f) wind speed (U) and boundary-layer depth (h).

conductivity is important. The temperature in the lower soil layer is only slightly less for the $+b$ case (compared to the *mean* b and $-b$ cases) due to the diminished downward transport of heat. The soil moisture content in the lower soil layer is nearly the same for all three b simulations in the transition zone because of the inertia of the lower soil layer and due to its distance from the surface. For the $+b$ simulations, the transition zone extends from the air-dry value to $\Theta = 0.22$, while for the $-b$ case it extends only to $\Theta = 0.18$.

As the soil moisture reaches saturation, the components of the surface energy balance and the potential evaporation, the air, soil and surface temperatures, the specific humidity, and the wind speed and boundary-layer depth all approach the same values. However, above the transition zone and approaching soil moisture saturation, the soil moisture content in the both soil layers becomes markedly different for the three different b simulations due to the increasing importance of soil water diffusivity (drainage). For the $+b$ case the soil moisture content is generally the greatest since drainage is less than for the *mean* b and $-b$ cases. Maximum differences in the volumetric soil moisture content between the $+b$ and $-b$ simulations are on the order 0.10 for the upper soil layer soil moisture, and 0.025 for the lower soil layer.

Except for soil moisture contents mentioned above, the differences between the $+b$ and $-b$ simulations are the largest for dry to moderate soil moisture contents, especially near the bare soil threshold moisture value. Maximum differences for the potential evaporation, and sensible and latent heat fluxes are several hundred W m^{-2} , with net radiation and soil heat flux differences on the order of 50 to 100 W m^{-2} . Maximum differences between $+b$ and $-b$ simulations are on the order of 10 C for surface temperature, several degrees for the air and upper soil layer temperatures, and only small differences for the lower soil layer temperature. Maximum differences are on the order of several g kg^{-1} for specific humidity; maximum wind speed differences are on the order of 1 m s^{-1} or less. Differences in the boundary-layer depth between the $+b$ and $-b$ simulations show dramatic contrast with 1 km or more in much of the transition zone.

2.4.2 Full vegetation

We repeat the series of model sensitivity tests but now use full vegetation coverage as in HAPEX-MOBILHY. The full vegetation simulations require the use of a canopy

resistance formulation which follows Noilhan and Planton (1989) and Jacquemin and Noilhan (1990) for the pine forest in HAPEX-MOBILHY where resistance responds to incoming solar radiation, temperature, atmospheric vapor pressure deficit and soil moisture content. This interaction can complicate interpretation of the model results. The lowest soil moisture value in this set of simulations is the wilting point of vegetation ($\Theta = 0.114$), which is higher than the air-dry value for sandy-loam soil; the saturation value remains the same. Additionally, a plant threshold value of $\Theta = 0.195$ describes the soil moisture content where plant transpiration is no longer reduced due to limiting soil moisture and then depends on atmospheric demand, as well as the remaining factors affecting canopy resistance. The root zone extends through both soil layers with transpiration from a soil layer weighted linearly by the depth of each soil layer. Following the HAPEX-MOBILHY observational study of Mahrt and Ek (1993), we use a roughness length of 2.35 m for momentum and 4.5×10^{-4} m for heat. We use the observed albedo of 0.10 for the pine forest determined from aircraft observations (Hildebrand 1988).

Conditions change rapidly as the volumetric soil moisture content in the upper (Θ_1) and lower (Θ_2) soil layers increases above the wilting point from one model simulation to the next (Figure 2.3)¹. As in the bare soil simulations, the same general trends exist and similar explanations describe the behavior of the different variables with increasing initial soil moisture content. However, the removal of moisture from the soil via transpiration has a moderating influence with less extreme changes in the different variables shown. In the transition zone for these full vegetation simulation (the region between the vertical dotted lines for the *mean b* case, Figure 2.3), latent heat flux increases steadily and is determined by both the soil water content and atmospheric demand. At the plant threshold soil moisture value, potential evaporation (atmospheric demand) levels off and slowly decreases with a similar trend in the actual evaporation since soil moisture is no longer limiting. Because canopy resistance is still nonzero, actual evaporation remains less than the potential.

Although thermal conductivity remains important in describing soil heat transport, the effect of hydraulic conductivity becomes less important for the full vegetation

¹Although verification is not the goal of this study, we show heat and moisture flux data from HAPEX-MOBILHY (Mahrt 1991, Gash et al 1989, Hildebrand 1988) with the model results (Figure 2.4). Aircraft flux measurements disagree because of different flight leg and filter lengths used in flux calculations. Note the scatter in the flux measurements between the aircraft and forest tower values which makes comparison and model verification difficult.

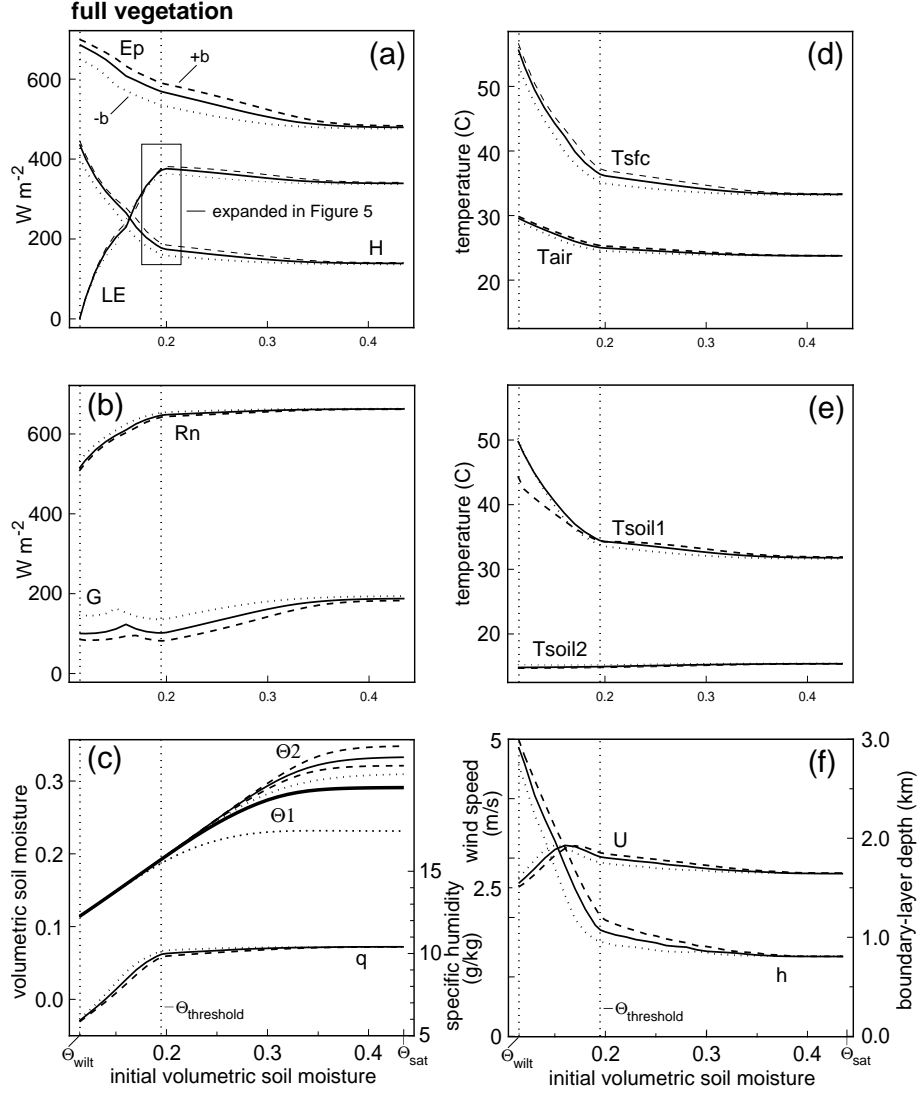


Figure 2.3: Simulations for full vegetation with model output at 1200 LST for multiple six-hour integrations where the initial soil moisture content is varied from dry to moist conditions for the *mean b* (solid), *+b* (dashed) and *-b* (dotted) cases; (a) potential evaporation (E_p), sensible (H) and latent (LE) heat fluxes, (b) net radiation (R_n) and soil heat flux (G), (c) atmospheric specific humidity (q_a), and volumetric soil moisture content in the upper (Θ_1 ; thick lines) and lower (Θ_2 ; thin lines) soil layers, (d) surface (T_s) and air (T_a) temperatures, (e) upper (T_{s1}) and lower (T_{s2}) soil temperatures, and (f) wind speed (U) and boundary-layer depth (h).

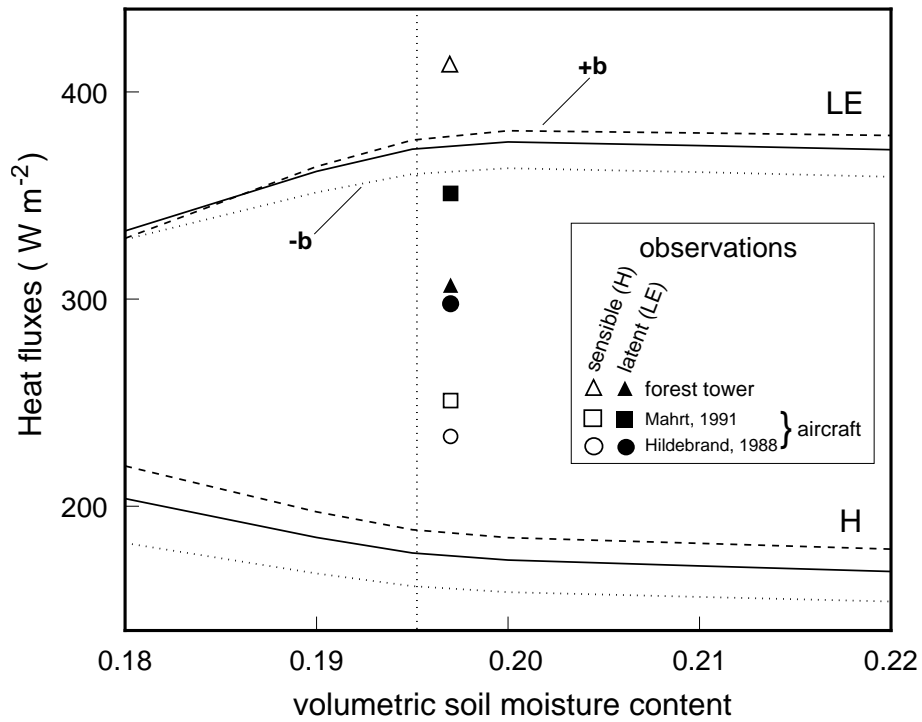


Figure 2.4: Modeled sensible and latent heat fluxes (as in Figure 2.3) and observed sensible (open symbols) and latent (solid symbols) heat fluxes from HAPEX-MOBILHY for 16 June 1986 where the layer-averaged soil moisture content was 0.197; observed fluxes from forest tower data via Gash et al (1989, triangles), and aircraft data via Mahrt (1991, squares) and Hildebrand (1988, circles).

simulations (compared to the bare soil simulations) since plants provide a direct conduit for soil moisture to the surface, removing moisture directly from each of the soil layers. Soil moisture is depleted evenly with depth for both shallow and deep soil moisture reservoirs, so there are virtually no differences between the three b cases in the transition zone, while for the bare soil simulations differences are greater. Soil water diffusivity (drainage) is important at higher soil moisture contents and there are large differences between the three b cases as initial soil moisture increases to saturation.

As with the bare soil simulations, the differences between the $+b$ and $-b$ simulations are again largest for dry to moderate soil moisture contents, especially near the plant threshold soil moisture value. Maximum differences are about 100 W m^{-2} for potential evaporation, about 50 W m^{-2} for sensible heat flux, and about 25 W m^{-2} for the latent heat fluxes. Soil heat flux differences on the order of 50 W m^{-2} are similar to the bare soil simulations, with even smaller differences in net radiation. Maximum differences between $+b$ and $-b$ simulations are on the order of a few degrees C for the surface temperature, and about 1 C for the air and upper soil layer temperatures (except several degrees for the upper soil layer under very dry conditions). As with the bare soil simulations, there are only small differences for the lower soil layer temperature between the $+b$ and $-b$ cases. Maximum differences are on the order of 0.5 g kg^{-1} for specific humidity; maximum wind speed differences are on the order of 0.5 m s^{-1} or less. Differences in the boundary-layer depth between the $+b$ and $-b$ cases are not as great as in the bare soil simulations, but still show a large contrast with about 500 m near the upper end of the transition zone. In summary, for the full vegetation simulations the differences between the $+b$, *mean b* and $-b$ cases are generally less compared to the bare soil simulations, although usually of the same sign.

One exception in sign is the temperature in the upper soil layer. Since surface temperatures compare fairly closely between the three b simulations (a few degrees difference, compared to 5 to 10 C for the bare soil simulations), with reduced thermal conductivity for the $+b$ case, heat movement downward into the soil is less resulting in a lower temperature in the upper soil layer compared to the *mean b* and $-b$ cases. This results in the large differences in soil heat flux which causes the large potential evaporation differences.

Another exception in sign is the latent heat flux under dry soil conditions. For

the $+b$ simulation the latent heat flux is slightly greater than the *mean* b and $-b$ simulations, presumably because of the greater potential evaporation. As the initial soil moisture approaches the plant threshold value, the latent heat flux increases for all three b simulations, but now the $+b$ case has slightly lesser values compared to the *mean* b and $-b$ cases. This may be due to increasing difference between the values of specific humidity for the three b simulations, where the $+b$ case has the lowest specific humidity. (In the canopy resistance formulation, lower specific humidity, or greater atmospheric vapor pressure deficit, causes a higher resistance, and lesser evaporation.)

2.5 Summary

As per the warning of Clapp and Hornberger (1978), caution must be exercised when mean soil properties are used if standard deviations of these properties are large. This study has found that variations in a soil parameter, the exponent b in (2.3), (2.4), and (2.6), can have an impact on the modeled surface energy balance and resulting atmospheric boundary-layer development. The largest effect on surface fluxes and atmospheric conditions was for dry to moderate soil moisture conditions, especially for bare soil. As with all sensitivity tests, the above results do not indicate general rules, but only provide examples for a specific set of initial conditions and parameter values. That is, variations in the surface fluxes, temperatures and other variables that are identified for the bare soil and full vegetation simulations in this study will depend on both soil texture, vegetation type, and initial atmospheric conditions.

The results of this study indicate the importance of accounting for variations in soil hydraulics and thermodynamics in a one-dimensional model. As with subgrid variations in atmospheric and surface variables, the effect of these variations should be investigated further. The influence on the surface energy balance and subsequent boundary-layer development has important implications in land-surface parameterizations which can directly influence the performance of large-scale models.

Acknowledgements. The suggestions by Dr. Sam Chang of the Phillips Laboratory (Hanscom AFB, Mass.) and the detailed comments by an anonymous reviewer are greatly appreciated. This research was supported by the U.S. Geological Survey, Department of the Interior, under USGS award number 14-08-0001-G1890, and the NOAA Climate and Global Change Program under award number NA36GP0369.

Chapter 3

Daytime evolution of relative humidity at the boundary-layer top

This chapter is published as Ek, M. and L. Mahrt 1994: Daytime evolution of relative humidity at the boundary-layer top. *Monthly Weather Review*, **122**, 2709-2721.

©Copyright 1994 by American Meteorological Society

Abstract

Data from the HAPEX-MOBILHY field program and results from a one-dimensional model of the soil and atmospheric boundary layer are analyzed to study the day-time evolution of the relative humidity at the boundary-layer top. This evolution is thought to control the development of boundary-layer clouds. This study examines the dependence of boundary-layer relative humidity on soil moisture, large-scale vertical motion, and the moisture content and temperature stratification above the boundary layer. The response of the boundary-layer relative humidity to external forcing involves competing mechanisms and the net effect on relative humidity is difficult to predict without complete analysis of the relative humidity tendency equation.

As one example, drier soil leads to smaller boundary layer specific humidity but also leads to cooler temperatures at the boundary-layer top due to greater boundary layer growth. When the latter effect dominates, the relative humidity at the boundary layer top is greater over drier soil. In contrast, drier soil leads to lower relative humidity at the boundary-layer top when the air above the boundary layer is strongly stratified or quite dry. These and other nonlinear interactions are posed in terms of a detailed analysis of the budget equation for boundary-layer top relative humidity.

3.1 Introduction

The daytime evolution of the boundary layer moisture field and potential for boundary layer cloud development depends, in part, on soil moisture, large scale vertical motion, and the "dryness" of the air above the growing boundary layer. These dependencies can sometimes contribute to unexpected changes of the boundary-layer relative humidity through nonlinear interactions shown in Figure 3.1.

Consider the following two examples. Strong low-level subsidence inversions normally suppress the development of boundary layer clouds. However with low sun angle and moist soil conditions, boundary layer relative humidity may increase with a strong low-level inversion and lead to the development of boundary layer stratus. As a second example, dry soil conditions are normally expected to reduce the probability of boundary-layer cloud development. However, with less surface evaporation or transpiration, greater surface heating leads to deeper boundary-layer growth which can sometimes lead to boundary-layer cloud development in spite of weaker surface

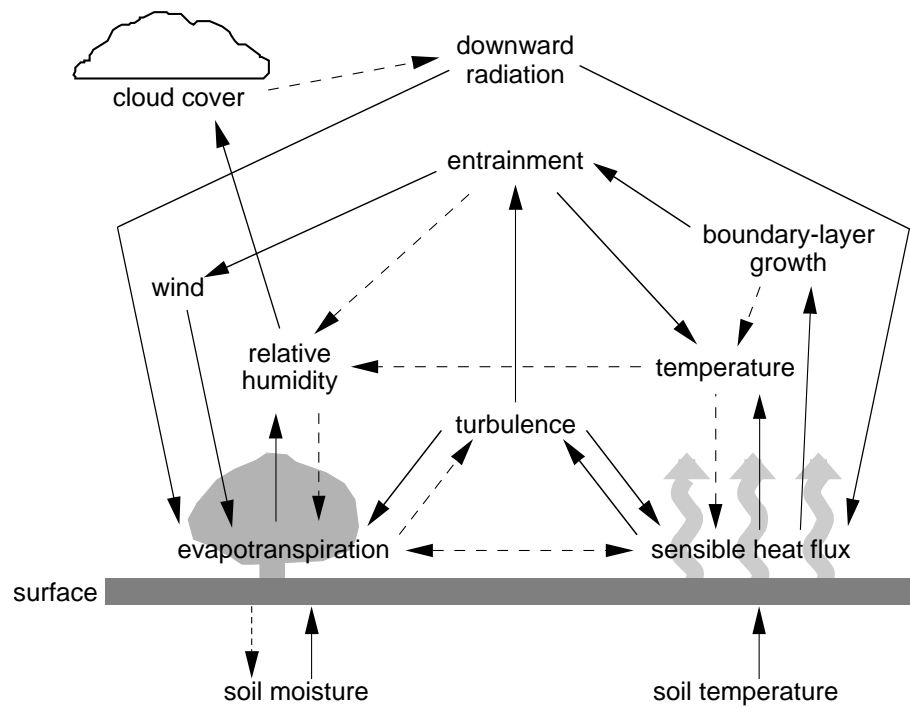


Figure 3.1: Suspected important interactions between the surface and boundary layer for conditions of daytime surface heating. Solid arrows indicate the direction of feed-backs which are normally positive (leading to an increase of the recipient variable). Dashed arrows indicate negative feedbacks. Two consecutive negative feedbacks make a positive one. Note the many positive and negative feedback loops which may lead to increased or decreased relative humidity and cloud cover.

evaporation (see Otterman et al 1990, Rabin et al 1990, Lanicci et al 1987, Colby 1984). The prediction of one outcome versus the other in these examples depends on external conditions and complex boundary-layer interactions.

To study the above boundary-layer interactions, the daytime evolution of the boundary layer relative humidity field using data from HAPEX-MOBILHY (Hydrological and Atmospheric Pilot Experiment - Modélisation du Bilan Hydrique, André et al 1988) will be examined. The data is interpreted using a simple one dimensional model which couples the atmospheric boundary layer, vegetation and soil. The ensuing study will focus on the evolution of relative humidity near the top of the growing daytime boundary layer.

3.2 Boundary-layer relative humidity

To understand the physics of the examples described in the Introduction the tendency equation for relative humidity (RH) is analyzed

$$\begin{aligned}\frac{\partial}{\partial t}RH &= \frac{\partial}{\partial t} \left(\frac{q}{q_s} \right) \\ &= \frac{1}{q_s} \frac{\partial q}{\partial t} - \frac{RH}{q_s} \frac{\partial q_s}{\partial t} \\ &= \frac{1}{q_s} \frac{\partial q}{\partial t} - \frac{RH}{q_s} \frac{dq_s}{dT} \frac{\partial T}{\partial t},\end{aligned}\tag{3.1}$$

where q is the specific humidity, q_s is saturation specific humidity, dq_s/dT is the slope of the saturation specific humidity-temperature curve, and T is temperature. With well-mixed conditions, the relative humidity reaches a maximum near the boundary-layer top which will be the reference level for the following developments. The relative humidity tendency combines the separate influences of changes in moisture and changes in temperature, the first and second terms on the right-hand-side of (3.1), respectively, where these tendencies are influenced by different boundary-layer and land-surface processes. This development is continued to explicitly account for these different processes.

Assuming a well-mixed boundary layer, the temperature tendency is expressed as

$$\frac{\partial T}{\partial t} = \frac{\partial}{\partial t} \left[\theta \left(\frac{p}{p_s} \right)^{R/c_p} \right],\tag{3.2}$$

which can be eventually written as

$$\frac{\partial T}{\partial t} = \left(\frac{p}{p_s}\right)^{R/c_p} \frac{\partial \theta}{\partial t} + \frac{T}{p} \frac{R}{c_p} \frac{\partial p}{\partial t}, \quad (3.3)$$

where θ is potential temperature, p is pressure, p_s is surface pressure, R is the gas constant, c_p is specific heat of air, and the equation of state and the definition of potential temperature have been used. Using the hydrostatic approximation and neglecting the local change of pressure at a fixed height, the pressure tendency can be written as

$$\frac{\partial p}{\partial t} = \frac{\partial p}{\partial z} \frac{\partial h}{\partial t} = -\rho g \frac{\partial h}{\partial t} = -\frac{pg}{RT} \frac{\partial h}{\partial t}, \quad (3.4)$$

where h is the boundary-layer depth, z is height, ρ is air density, and g is gravity. Substituting (3.4) into (3.3) gives

$$\frac{\partial T}{\partial t} = \left(\frac{p}{p_s}\right)^{R/c_p} \frac{\partial \theta}{\partial t} \frac{g}{c_p} \frac{\partial h}{\partial t}. \quad (3.5)$$

Substituting (3.5) into (3.1) then gives

$$\frac{\partial}{\partial t} RH = \frac{1}{q_s} \frac{\partial q}{\partial t} - \frac{RH}{q_s} \frac{dq_s}{dT} \left[\left(\frac{p}{p_s}\right)^{R/c_p} \frac{\partial \theta}{\partial t} - \frac{g}{c_p} \frac{\partial h}{\partial t} \right], \quad (3.6)$$

To avoid modeling the vertical structure of specific humidity, well-mixed conditions in specific humidity as well as potential temperature are assumed. The equations for the boundary-layer moisture and thermodynamic budgets from Tennekes (1973) are

$$\begin{aligned} \frac{\partial q}{\partial t} &= -\frac{(\overline{w'q'_s} - \overline{w'q'_h})}{h}, \\ \frac{\partial \theta}{\partial t} &= -\frac{(\overline{w'\theta'_s} - \overline{w'\theta'_h})}{h}, \end{aligned} \quad (3.7)$$

where $\overline{w'q'}$ and $\overline{w'\theta'}$ are the moisture and heat fluxes, respectively, and the subscripts s and h refer to the surface and the level just below the boundary-layer top, respectively. Substituting (3.7) into (3.6) gives

$$\frac{\partial}{\partial t} RH = \frac{1}{hq_s} (\overline{w'q'_s} - \overline{w'q'_h}) - \frac{RH}{q_s} \frac{dq_s}{dT} \left[\left(\frac{p}{p_s}\right)^{R/c_p} \frac{(\overline{w'\theta'_s} - \overline{w'\theta'_h})}{h} - \frac{g}{c_p} \frac{\partial h}{\partial t} \right]. \quad (3.8)$$

To simplify the "bookkeeping", variable coefficients are defined as

$$\begin{aligned}
C_\theta &= -\frac{\overline{w'\theta'_h}}{\overline{w'\theta'_s}}, \\
C_q &= \frac{\overline{w'q'_h}}{\overline{w'q'_s}}.
\end{aligned} \tag{3.9}$$

Under many conditions, $C_\theta \approx C$, where $C = (\overline{w'\theta'_v})_h / (\overline{w'\theta'_v})_s$ and is often found in the literature. In daytime boundary layers, the value of C_θ is typically thought to range between 0.2-0.5 (Betts et al 1990, Tennekes and Driedonks 1981, Carson 1973) but can be much larger in cases of significant shear generation of turbulence and weak surface heating (Nicholls and LeMone 1980). The value of C_q is more variable, exceeding unity in the drying boundary layer (Mahrt 1991, Betts et al 1990, Steyn 1990) and often becoming 0.5 or less in the moistening boundary layer (Grant 1986, Nicholls and Reading 1979, and others).

Substituting (3.9) into (3.8), the relative humidity tendency equation becomes

$$\frac{\partial}{\partial t} RH = c_0 \overline{w'q'_s} - c_0 C_q \overline{w'q'_s} + c_1 \overline{w'\theta'_s} (1 + C_\theta) + c_2 h \frac{\partial h}{\partial t}, \tag{3.10}$$

where

$$\begin{aligned}
c_0 &= \frac{1}{hq_s}, \\
c_1 &= c_0 RH \frac{dq_s}{dT} \left(\frac{p}{p_s} \right)^{R/c_p}, \\
c_2 &= c_0 RH \frac{dq_s}{dT} \frac{g}{c_p}.
\end{aligned} \tag{3.11}$$

The four terms on the right hand side of (3.10) are (left-to-right):

1. Increasing relative humidity due to surface evapotranspiration,
2. Decreasing relative humidity due to entrainment of dry air from above the boundary layer ($C_q > 0$); or less commonly, increasing relative humidity due to entrainment of moister air from above the boundary layer ($C_q < 0$),
3. Decreasing relative humidity due to surface sensible heat flux and entrainment of warmer air at the boundary layer top (boundary-layer warming), and

4. Increasing relative humidity due to increasing boundary layer depth where for a given potential temperature, the temperature at the boundary layer top decreases with boundary layer growth.

The importance of these different effects in different atmospheric situations is now estimated.

3.2.1 Boundary-layer warming and growth

In this section, the influence of moisture changes on the evolution of relative humidity is neglected, in which case the relative humidity at the boundary-layer top changes due to adiabatic cooling from boundary-layer growth and due to the turbulent heat flux. The importance of boundary-layer heating with respect to the boundary-layer growth can be expressed as the ratio of term 3 to term 4 in (3.10):

$$\left(\frac{p}{p_s}\right)^{R/c_p} \frac{\overline{w'\theta'_s}(1+C_q)}{\left(\frac{g}{c_p}h\frac{\partial h}{\partial t}\right)^{-1}}. \quad (3.12)$$

The boundary-layer warming can be neglected if it is small compared to $g/c_p(\partial h/\partial t) \approx 1^\circ\text{C}/100\text{m}$ ($\partial h/\partial t$). This condition is met during the late morning rapid growth period, but otherwise the heating term cannot be categorically neglected.

For the simplified case where the mean vertical motion and horizontal advection are small, the turbulence is generated primarily by buoyancy effects and where the time rate of change of the inversion strength is small compared to the boundary-layer heating rate, the boundary-layer depth tendency may be approximated as (Tennekes 1973, Betts 1973)

$$\frac{\partial h}{\partial t} = \frac{\overline{w'\theta'_s}(1+C_q)}{h\gamma_\theta}, \quad (3.13)$$

where γ_θ is the vertical gradient of potential temperature above the boundary layer. Then the time rate of change of relative humidity at the boundary-layer top is

$$\frac{\partial}{\partial t}RH = -\frac{RH}{hq_s}\frac{dq_s}{dT}(1+C_q)\left[\left(\frac{p}{p_s}\right)^{R/c_p} - \frac{1}{\gamma_\theta}\frac{g}{c_p}\right]\overline{w'\theta'_s}. \quad (3.14)$$

The ratio of the effects of boundary-layer growth to the boundary-layer warming from (3.12) assumes the approximate form

$$\frac{1}{\gamma_\theta} \frac{g}{c_p} \left[\left(\frac{p}{p_s} \right)^{R/c_p} \right]^{-1}. \quad (3.15)$$

If the stratification of potential temperature is small compared to g/c_p ($\approx 1^\circ\text{C}/100\text{m}$), the influence of the surface heat flux on the boundary-layer growth effect will exceed the direct effect of boundary-layer warming. This condition is easily met in those late morning periods where the boundary layer has consumed the nocturnal surface inversion and grows rapidly through the residual layer remaining from the mixed layer of the previous day. This condition is approximated in many atmospheric situations, including that of the standard atmosphere. However, in general the boundary-layer warming term must be included.

If the air aloft is quite dry, (3.15) will overestimate the increase of relative humidity because of neglect of entrainment drying of the boundary layer, the subject of section 3.2.2.

3.2.2 Dry air entrainment

For cases where boundary-layer warming can be neglected compared to the boundary-layer growth, only the additional influence of changes of moisture need be considered. The relative humidity at the boundary-layer top increases with time unless the boundary layer dries at a rate which exceeds the boundary-layer growth term. This can occur only with rapid entrainment of dry air. To study the case of boundary-layer drying, the dry-air entrainment is approximated as

$$-\overline{w'q'}_h = \Delta q \frac{\partial h}{\partial t}, \quad (3.16)$$

where Δq is the change of specific humidity across the boundary-layer top which is normally negative and the mean vertical motion is zero (analogous to Tennekes 1973, his equation 1; see also Ball 1960, Kraus and Turner 1967, Lilly 1968). Then the ratio of the magnitude of the effects of surface evaporation and boundary-layer growth to the effect of entrainment drying is

$$\frac{1}{C_q} - RH \frac{dq_s}{dT} \frac{g}{c_p} \frac{h}{\Delta q}. \quad (3.17)$$

Note that (3.17) is independent of the boundary-layer growth rate since the dry-air entrainment (term 2 in (3.10)) and boundary-layer growth (term 4 in (3.10)) are

both linearly proportional to the growth rate.

Since C_q is likely to be large when Δq is large and vice versa, (3.17) must be evaluated on a case-by-case basis. The analyses in sections 3.3 and 3.4 suggest that the relative humidity at the boundary-layer top will normally increase during the day in which case (3.17) exceeds unity. This is not surprising since boundary-layer clouds are more likely to develop as the boundary layer deepens. However the above analysis provides a framework for estimating how fast the relative humidity increases with time prior to cloud development and whether cloud formation will be possible. Additionally, the daytime evolution of the real atmospheric boundary layer is significantly influenced by soil moisture and the large scale vertical motion, the subject of sections 3.2.3 and 3.2.4.

3.2.3 Influence of soil moisture and surface evaporation

Greater soil moisture leads to boundary-layer moistening which acts to increase the relative humidity, but also leads to weaker surface heating and weaker boundary-layer growth which may in turn lead to smaller values of relative humidity at the boundary-layer top. As a result of these opposing influences, the net effect of soil moisture changes on relative humidity at the boundary-layer top and the potential for boundary-layer cloud development cannot be simply predicted.

To study the influence of soil moisture, note that the boundary-layer growth due to surface heating is inversely related to the surface moisture flux through the surface energy balance

$$\rho c_p \overline{w'\theta'}_s = R_n - G - \rho L_v \overline{w'q'}_s, \quad (3.18)$$

where R_n is the net radiation, L_v is the latent heat of evaporation and G is the soil heat flux.

Substituting (3.18) into the relative humidity tendency equation 3.10 and using the simplified expression for the convectively generated mixing depth (3.13) yields

$$\frac{\partial}{\partial t} RH = \frac{1}{hq_s} \left[\overline{w'q'}_s (1 - C_q) + \left(\frac{A^*}{\gamma_\theta} - B^* \right) \left(\frac{R_n - G}{\rho L_v} - \overline{w'q'}_s \right) \right], \quad (3.19)$$

where

$$\begin{aligned}
A^* &= RH \frac{dq_s}{dT} \frac{L_v}{c_p} (1 + C_q) \frac{g}{c_p}, \\
B^* &= RH \frac{dq_s}{dT} \frac{L_v}{c_p} (1 + C_q) \left(\frac{p}{p_s} \right)^{R/c_p}.
\end{aligned} \tag{3.20}$$

Collecting the direct influence of the surface evaporation on the boundary-layer moisture with the indirect effect of the surface moisture flux on reduction of boundary-layer growth, (3.19) becomes

$$\frac{\partial}{\partial t} RH = \frac{1}{hq_s} \left[\overline{w'q'}_s \left(1 - \frac{A^*}{\gamma_\theta} + B^* \right) - \overline{w'q'}_h + \left(\frac{A^*}{\gamma_\theta} - B^* \right) \left(\frac{R_n - G}{\rho L_v} \right) \right]. \tag{3.21}$$

The entrainment term, $\overline{w'q'}_h$, normally acts to decrease relative humidity.

Surface evaporation acts to increase relative humidity at the boundary-layer top if

$$\frac{\gamma_\theta(1 + B^*)}{A^*} > 1. \tag{3.22}$$

This situation occurs with strong stratification in which case the primary role of surface evaporation is to moisten the boundary layer. Then greater soil moisture and evaporation increase the relative humidity at the boundary-layer top and thus increase the probability of boundary-layer cloud development, as in Hammer (1970) and Barnston and Schikedanz (1984). This interaction is sometimes used to construct a feedback mechanism in extended drought or desertification arguments, i.e. that drier soil leads to lower relative humidity at the boundary-layer top (Oglesby and Erickson 1989, Namias 1988, Trenberth et al 1988, and others).

On the other hand, if the stratification above the boundary layer is weak, (3.22) < 1 , then the relative humidity tendency is strongly influenced by the boundary-layer growth term. As a result, the main influence of surface evaporation on relative humidity is to reduce the boundary-layer growth term and thus reduce relative humidity at the boundary-layer top. Therefore with weak stratification, drier soil increases the probability of boundary-layer cloud development, as in Otterman et al (1990), Rabin et al (1990), and others.

The above arguments are based on a number of simplifications leading to (3.22). Drought scenarios are further complicated by the interdependence of $\overline{w'q'_h}$, γ_θ , A^* and B^* , and the necessity to include cloud feedback mechanisms; both are beyond the scope of this discussion. Even in the above oversimplified example, the role of soil moisture is complex indicating that construction of desertification scenarios can be misleading.

3.2.4 Large scale vertical motion

To estimate the influence of the mean vertical motion w_h on the relative humidity tendency, 3.10 is differentiated with respect to the mean vertical motion and again neglect the direct influence of surface heating on the relative humidity to obtain

$$\frac{\partial}{\partial w_h} \frac{\partial}{\partial t} RH = - \left[\frac{\overline{w'q'_s}(1 - C_q)}{q_s h^2} \right] \frac{\partial h}{\partial w_h} + \frac{g}{c_p} \frac{RH}{q_s} \frac{dq_s}{dT}, \quad (3.23)$$

where it is noted that $(\partial/\partial w_h)(\partial h/\partial t) = 1$. Even though the entrainment rate is normally time-dependent, the complex physics of this equation can be qualitatively examined in terms of scale values for the case of a time-independent entrainment rate w_e and mean vertical motion

$$h = (w_e + w_h)t. \quad (3.24)$$

Then $\partial h/\partial w_h = t$ and (3.23) becomes

$$\frac{\partial}{\partial w_h} \frac{\partial}{\partial t} RH = - \left[\frac{\overline{w'q'_s}(1 - C_q)}{q_s h^2} \right] t + \frac{g}{c_p} \frac{RH}{q_s} \frac{dq_s}{dT}. \quad (3.25)$$

This equation represents the change of relative humidity tendency with respect to changes of mean vertical motion. For the case of mean subsidence ($w_h < 0$), negative values of terms on the right hand side of (3.25) indicate greater positive tendency of relative humidity and therefore greater relative humidity. The change of relative humidity ΔRH over time period T^* due to enhanced subsidence Δw_h (< 0) would be

$$\Delta RH = -\Delta w_h T^* \left[\frac{T^* (\overline{w'q'})_s (1 - C_q)}{q_s h^2} + \frac{g}{c_p} \frac{RH}{q_s} \frac{dq_s}{dT} \right]. \quad (3.26)$$

The first term represents the increase of relative humidity due to "trapping" of evaporated surface moisture in a thinner boundary layer. The second term represents the slower rate of relative humidity decrease at the boundary-layer top due to slower

boundary-layer growth. The relative importance of the first term is accumulative and thus increases with time. Therefore, the initial influence of subsidence is to cause decreasing values of the relative humidity at the boundary-layer top as a result of slower boundary-layer growth compared to the case without subsidence.

However, after the time scale

$$\tau = \frac{g}{c_p} RH \frac{dq_s}{dT} h^2 [\overline{w'q'_s}(1 - C_q)]^{-1}, \quad (3.27)$$

the net influence of the subsidence is to increase the relative humidity through "trapping" of boundary-layer moisture. Then subsidence and reduced boundary-layer growth may increase the probability of boundary-layer cloud development (Mahrt and Pierce 1980). With larger surface moisture flux and weaker entrainment of dry air (C_q small), the stage at which the subsidence acts to increase the relative humidity begins sooner. In winter with a thin boundary-layer depth, the time scale from (3.27) will be small and the main influence of subsidence will be to increase the relative humidity through trapping of moisture.

On the other hand, if this time is comparable to, or large compared to the period of mixed layer development, then the main influence of subsidence is the decrease of boundary-layer depth leading to smaller relative humidity at the boundary-layer top compared to the case of no subsidence.

3.2.5 Small boundary-layer growth

When boundary-layer growth is small, typically in the early morning or later afternoon over land or in the quasi-steady marine boundary layer, the boundary-layer growth term in the relative humidity tendency equation can be ignored. Then the relative humidity tendency is determined by surface evaporation, boundary-layer warming and dry air entrainment.

To estimate the relative importance of increased relative humidity at the boundary-layer top due to surface evaporation compared to decreased relative humidity due to boundary-layer warming and dry entrainment, involves the ratio

$$\overline{w'q'_s} \left[RH \frac{dq_s}{dT} \left(\frac{p}{p_s} \right)^{R/c_p} \overline{w'\theta'_s}(1 + C_\theta) + \overline{w'q'_s} C_q \right]^{-1}, \quad (3.28)$$

which can be rewritten as

$$L_v \overline{w'q'}_s \left[RH \frac{dq_s}{dT} \frac{L_v}{c_p} \left(\frac{p}{p_s} \right)^{R/c_p} c_p \overline{w'\theta'}_s (1 + C_\theta) + L_v \overline{w'q'}_s C_q \right]^{-1}, \quad (3.29)$$

and reduces to

$$\frac{1}{\beta B^* + C_q}, \quad (3.30)$$

where β is the (surface) Bowen ratio and B^* is defined in section 3.2.3. When the ratio (3.30) is greater than unity the relative humidity will increase with time. For example, over land in the early morning or afternoon when boundary-layer growth and entrainment are weak, a low Bowen ratio leads to increasing relative humidity at the boundary-layer top.

The above analysis provides a framework for studying the evolution of the boundary-layer top relative humidity. The examples cited above have not exhausted the important possibilities. Other important examples include the slowly varying marine boundary layer. In this study, the terms in 3.10 are now evaluated by examining observations taken during HAPEX-MOBILHY.

3.3 HAPEX-MOBILHY data analysis

3.3.1 Aircraft data

To evaluate the terms in the relative humidity tendency equation 3.10 aircraft observations made at multiple levels in the boundary layer on a fair-weather day during HAPEX-MOBILHY (André et al 1988) are examined. During this field program considerable attention was devoted to aircraft moisture measurements (Eloranta et al 1989). On 13 June 1986 atmospheric conditions were the most homogeneous across the experimental domain compared to other flight days, and boundary-layer cloud fractions averaged 10% or less. This aircraft flight was from 0853 to 1354 UTC (=solar time) and included the morning rapid boundary-layer growth.

Boundary-layer depth is estimated using relative humidity profiles from the five aircraft slant soundings (Figure 3.2a). Relative humidity combines the influences of decreasing moisture and increasing temperature with height to provide a sharper

delineation of the boundary-layer top (Mahrt 1976). Fractional cloud cover is determined using an upward-looking solar radiometer (Ek and Mahrt 1991a) and is the average cloud cover for the horizontal aircraft flight legs between soundings. Flux measurements from the aircraft horizontal flight legs were computed using a high pass filter with a 5-km wavelength (Mahrt 1991), with mid- and upper-level flights after the rapid growth of the boundary layer. Surface flux values are taken as an average of the low-level flights nearest to the sounding time.

During slower boundary-layer growth after 1100, flux profiles (Figure 3.2, insert) are used to determine ratios of the boundary-layer top fluxes to the surface fluxes (the values of C_θ and C_q defined in (3.9)). A linear fit to the average flux values at each of the three aircraft flight levels is extrapolated to the boundary-layer top, yielding values of $C_\theta = 0.67$ and $C_q = 0.33$. C_θ is larger than the more theoretical free convection value of 0.2 because of the observed wind shear on this day, about $5 \text{ m s}^{-1}/100 \text{ m}$ at the boundary-layer top.

The value of C_q is expected to be larger during the rapid growth of the boundary layer when entrainment is strong. Aircraft flux measurements from the middle and upper boundary-layer are unavailable during the rapid growth of the boundary layer before 1100, so the value of C_q is estimated from aircraft sounding moisture profiles using a graphical integration method. This method follows Stull (1988, his equation 11.2.2c) applied to moisture flux expressed in finite difference form so that

$$C_q = \Delta h \frac{\Delta q}{\Delta t} \frac{1}{(\overline{w'q'})_s}, \quad (3.31)$$

where Δh is the change in the boundary-layer depth between the two soundings, Δq is the average time change in the specific humidity over the layer between the two boundary-layer tops, and Δt is the time between aircraft soundings. The large-scale subsidence and advection of moisture appear to be small compared to the boundary-layer growth rate during this time since specific humidity is constant with time above the growing boundary layer. The value of C_q exceeds unity during rapid growth of the boundary layer, implying boundary-layer drying; C_q is less than unity after 1100, implying vertical convergence of moisture flux and daytime boundary-layer moistening. Temperature advection does seem to be important during this period so that soundings could not be used to estimate C_θ . Therefore, C_θ is assigned the same value as estimated from aircraft fluxes later in the day. C_θ is constrained by the turbulence

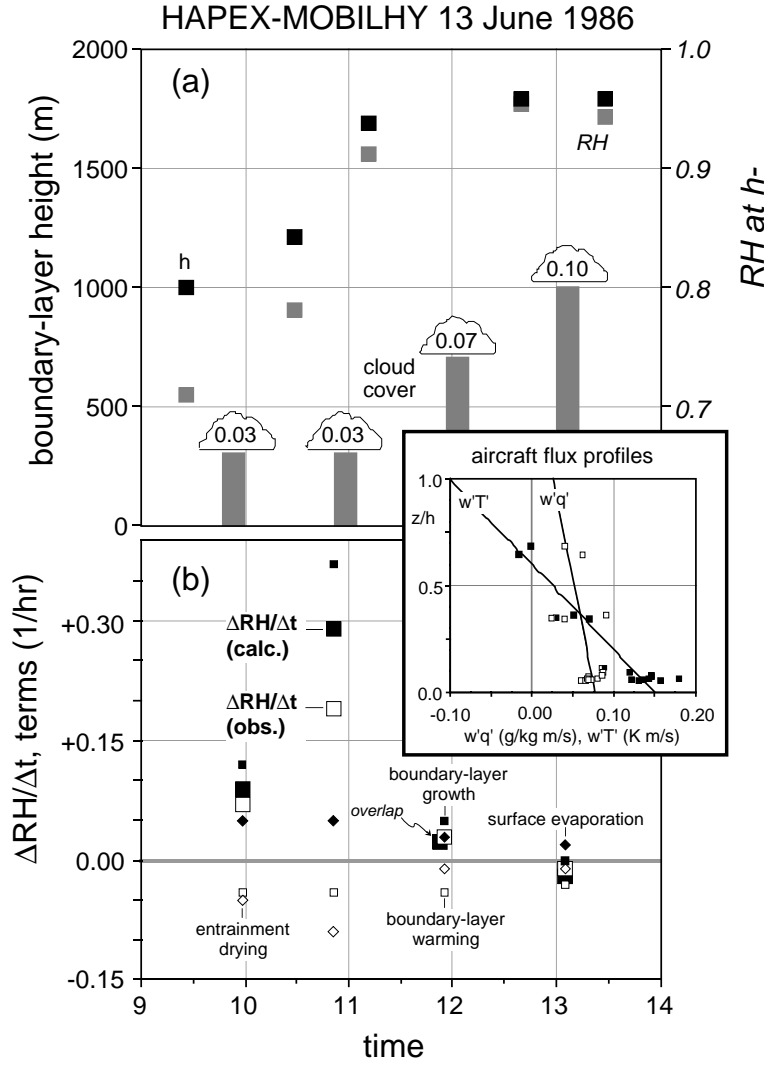


Figure 3.2: (a) Observed boundary-layer depth, relative humidity at boundary-layer top, and fractional cloud cover; (insert) heat and moisture aircraft flux profiles; and (b) observed relative humidity tendency at the boundary-layer top; and tendency terms and computed relative humidity tendency evaluated from 3.10 from aircraft data for 13 June 1986 in HAPEX-MOBILHY.

energy budget and is expected to be less variable than C_q .

Centered time-differencing is used to estimate tendency terms from 3.10 for four different times (Table 3.1; Figure 3.2b)¹. Atmospheric conditions on 13 June show rapid growth of the boundary-layer until 1100 (Figure 3.2a). The boundary-layer growth term dominates the relative humidity tendency during this period (Figure 3.2b, Table 3.1), with the observed relative humidity increasing from about 0.70 to more than 0.95. The small fractional cloud cover was observed to increase during the rapid boundary-layer growth, similar to Johnson’s (1977) findings that cumulus convection over Florida first developed during the late morning rapid growth period. Additionally, even though the observed average relative humidity was less than 1.0, clouds formed because of spatial variations of relative humidity (Betts 1983, Wilde et al 1985, Ek and Mahrt 1991a).

Relative to the other terms, the boundary-layer growth term dominates only during the period of rapid boundary-layer growth before 1100, with the rest of the relative humidity tendency terms in (3.10) becoming important in the early afternoon after boundary-layer growth diminishes. Note that the relative humidity tendency is over-predicted during the rapid growth of the boundary layer (Table 3.1), perhaps because of errors in the estimates of the effects of entrainment during the period of rapid boundary-layer growth. In the early afternoon the relative humidity becomes approximately time-independent with a value of about 0.95.

Evaluation of (3.30) for the case of negligible boundary-layer growth is valid in the early afternoon near the end of the flight (section 3.2.5). During this period the value of (3.30) is less than unity predicting that the relative humidity will decrease

¹Increasing or decreasing the values of C or C_q by a factor of two changes the relative humidity tendency by about 0.05 hr^{-1} or less. Typical errors in the surface flux measurements on the order of 20% yield differences in the relative humidity tendency equation on the order of 0.01 hr^{-1} . Errors in the flux measurements are particularly large in the upper part of the boundary layer where the scale of the transporting eddies is large. The errors are estimated as $\sigma_{flux} n^{-1/2}$, where σ_{flux} is the standard deviation of the flux and n is the number of independent flux measurements, yielding estimates of $0.005 \text{ (m s}^{-1}\text{C)}$ for the heat flux (30% of the mean flux value) and $0.019 \text{ (m s}^{-1}\text{)(g kg}^{-1}\text{)}$ for the moisture flux (almost 40% of the mean flux value) for this day. Estimating boundary-layer depth subjectively from relative humidity profiles, errors on the order of 100 m hr^{-1} in the boundary-layer depth tendency might be expected, which gives a difference in the relative humidity tendency of about 0.05 hr^{-1} . These potential errors in estimating tendency terms are less important when the boundary-layer growth term dominates the relative humidity tendency.

Table 3.1: Values of C_θ and C_q , tendency terms and relative humidity tendency from (3.10), and observed relative humidity tendency for 13 June 1986 in HAPEX-MOBILHY, with tendencies extrapolated to hourly values for easier interpretation.

time (UTC)	C_θ	C_q	surface evap.	dry-air entrain.	ABL warming	ABL growth	RH tendency	
							(calc)	(obs)
9.97	0.67	0.82	0.06	-0.05	-0.04	0.12	+0.09	+0.07
10.85	0.67	2.05	0.05	-0.09	-0.04	0.37	+0.29	+0.19
11.93	0.67	0.33	0.03	-0.01	-0.04	0.05	+0.03	+0.03
13.07	0.67	0.33	0.02	-0.01	-0.03	0.00	-0.02	-0.01

(as observed) because of the dominance of dry air entrainment and boundary-layer warming over surface evaporation.

3.3.2 Simple models

Although the radiosonde data set does not provide flux values, it does allow partial evaluation of the relative humidity tendency from 3.10. The aircraft case study of 13 June in HAPEX-MOBILHY shows that the relative humidity tendency in the morning is dominated by the boundary-layer growth term, a term that can be estimated from radiosonde data. For the 13 June aircraft data, the observed relative humidity tendency is modestly correlated with the boundary-layer growth term (oversized squares, Figure 3.3a).

To supplement the above aircraft analysis, boundary-layer radiosonde data for 10 fair weather days during HAPEX-MOBILHY 1986 are examined (Brutsaert and Parlange 1992). Radiosondes were launched from the forest clearing at the central site of Lubbon at approximately two-hour intervals (0600-1800). The boundary-layer top is determined by visual inspection of sounding profiles of relative humidity. Although the instantaneous radiosonde observations are less reliable estimates of the mean structure of the boundary-layer compared to aircraft slant soundings, the radiosonde data set provides a larger sample size. We restrict our analysis to the cases where boundary-layer growth exceeds 100 m/hr. At smaller growth rates the uncertainties in the radiosonde data set make estimates of the boundary-layer growth less reliable.

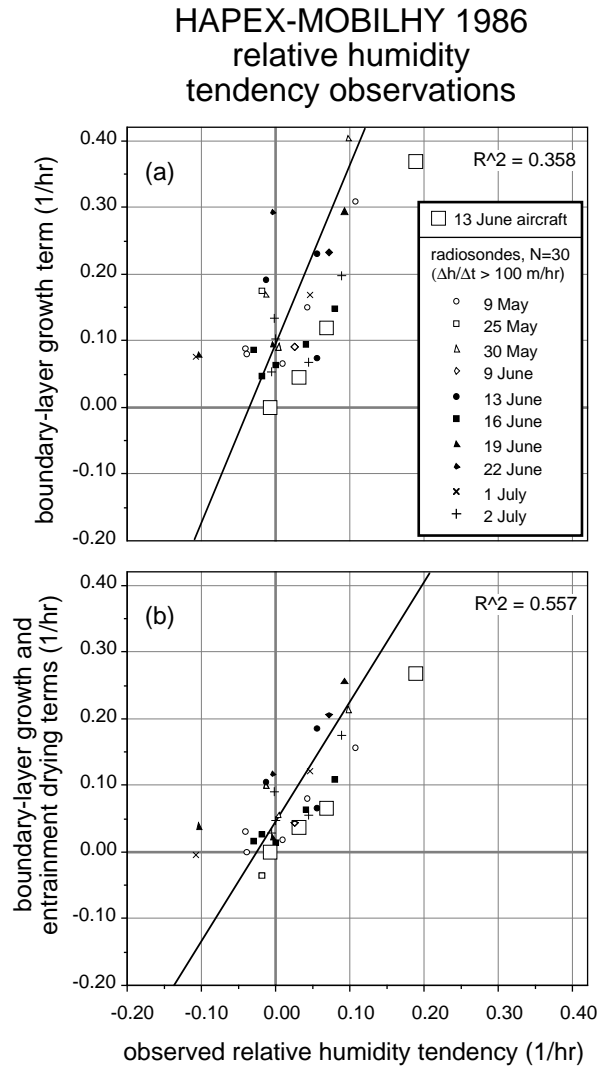


Figure 3.3: Observed relative humidity tendency and terms in the relative humidity tendency equation evaluated from radiosonde data for 10 days in HAPEX-MOBILHY 1986 (13 June aircraft data in oversized symbols), (a) observed relative humidity tendency versus the boundary-layer growth term alone, (b) observed relative humidity tendency versus the sum of the boundary-layer growth and entrainment drying terms.

From the radiosonde data set, the boundary-layer growth term in 3.10 is computed and modest correlation with the observed relative humidity tendency at the boundary-layer top is found (Figure 3.3a). The regression equation using the boundary-layer growth term alone is

$$\frac{\Delta RH}{\Delta t} = a_0 + a_1 BLG, \quad (3.32)$$

where $a_0 = 0.112$ and $a_1 = 0.862$, and BLG is the boundary-layer growth term from 3.10 in finite difference form. To generalize (3.32), (3.16) is used to construct a rough estimate of the boundary-layer top entrainment flux and the entrainment drying term. The observed relative humidity tendency is linearly regressed with the boundary-layer growth and entrainment drying terms to obtain

$$\frac{\Delta RH}{\Delta t} = b_0 + b_1 (BLG + DAE), \quad (3.33)$$

where $b_0 = 0.047$ and $b_1 = 0.867$, and DAE is the dry air entrainment term using (3.16) in finite difference form. The correlation between the observed relative humidity tendency and that predicted from (3.33) increases when this entrainment drying term is included (Figure 3.3b). The generality of (3.32) - (3.33) is not known and additional data sets are required before (3.33) can be considered a useful prediction of boundary-layer cloud formation.

3.4 Boundary-layer model simulations

All the terms in 3.10 are now evaluated from sensitivity tests utilizing the Oregon State University one-dimensional coupled atmospheric-plant-soil model which was developed to simulate the interactions of the atmospheric boundary layer, vegetation and soil. The atmospheric boundary layer model (Troen and Mahrt 1986, Holtslag et al 1990, Holtslag and Boville 1993) is coupled with an active two-layer soil model and a simple vegetated surface (Pan and Mahrt 1987) using the Penman-Monteith formulation. For the sensitivity tests, data from the pine forest region in southwest France taken during HAPEX-MOBILHY is used (André et al 1988, Noilhan and Planton 1989), with a momentum roughness length of 1.0 m, and a smaller value of 10^{-2} m for the roughness length for heat following Mahrt and Ek (1993). Geostrophic winds and vertical motion values are taken from the mesoscale analysis described in Jacquemin and Noilhan (1990). Mean vertical motion is specified to increase linearly

Table 3.2: Summary of initial conditions for model sensitivity tests.

13 June 1986, HAPEX-MOBILHY	
Prototype	geostrophic wind, northeast at 10 m/s subsidence, 2 cm/s at 5 km average volumetric soil moisture content, $\Theta = 0.15$
Dry soil	$\Theta = 0.07$, model vegetation wilting point
Moist soil	$\Theta = 0.435$, model soil moisture saturation
Dry aloft	RH ≈ 0.80 near surface, decreasing to 0.20 at 3 km
Moist aloft	RH ≈ 0.80 near surface, increasing to 0.95 at 3 km

22 June 1986, HAPEX-MOBILHY	
Prototype	geostrophic wind, southwest at 12 m/s subsidence, 3.5 cm/s at 5 km average volumetric soil moisture content, $\Theta = 0.12$
Dry soil	$\Theta = 0.07$, model vegetation wilting point
Moist soil	$\Theta = 0.435$, model soil moisture saturation

with height from zero at the surface and is fitted to an "observed" layer averaged value centered at 2 km, and a 12-hour averaged value centered at 1200 UTC (=solar time). Geostrophic wind is assumed constant with time.

We first make a prototype simulation for the 13 June case, initiating the model using the 0600 radiosonde data (Figure 3.4). While the data does not allow formal verification, the model results for 13 June compare favorably with the observed conditions (Figure 3.5a). Modeled relative humidity near the boundary-layer top is about 0.10 larger than that observed by the aircraft and radiosonde data earlier in the observing period, but agrees more closely with data later in the day. For the prototype model simulation, apparently advection was not important and the subsidence value was reasonably well estimated (Ek and Mahrt 1991a). A summary of initial conditions for model sensitivity tests is shown in Table 3.2.

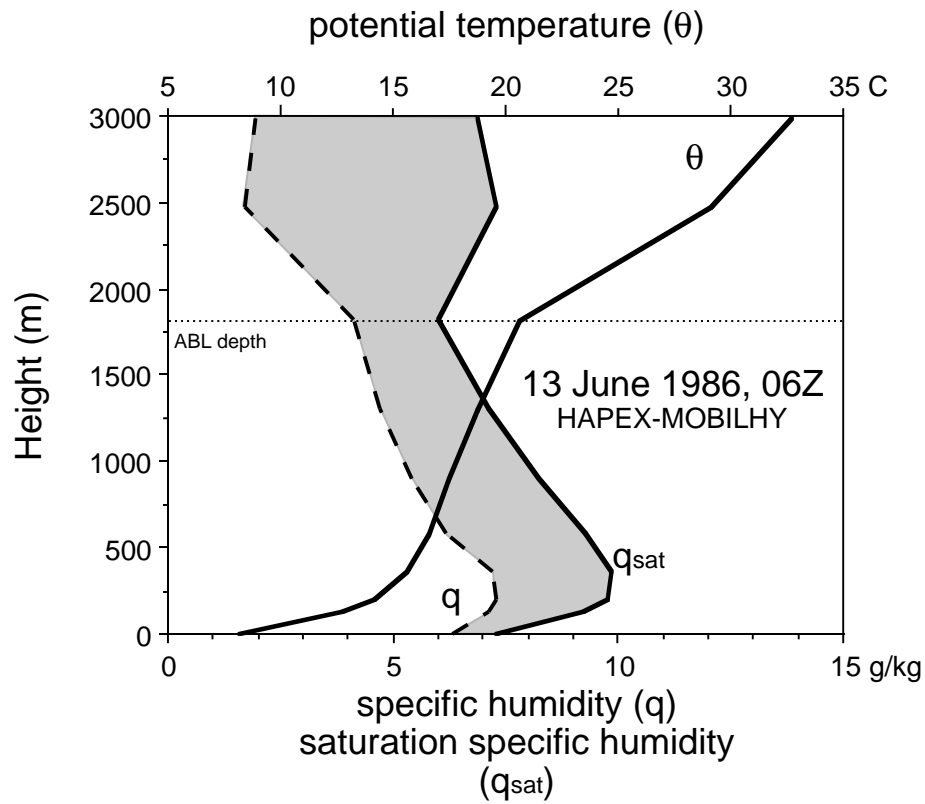


Figure 3.4: Radiosonde data profiles at 0600 for 13 June 1986 in HAPEX-MOBILHY showing saturation specific humidity (q_{sat}), specific humidity (q), and potential temperature (θ) used in model initiation, and the approximate observed maximum afternoon boundary-layer depth (dotted line).

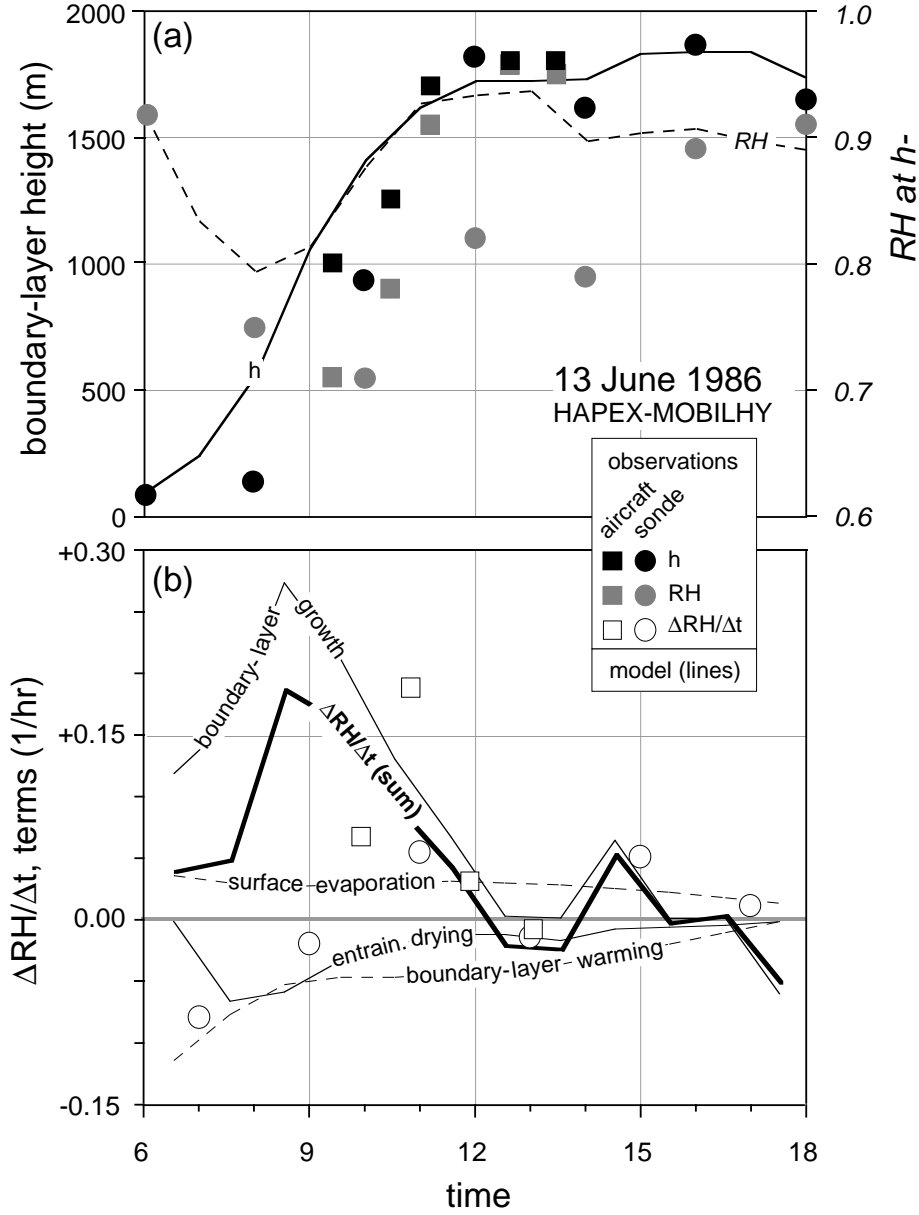


Figure 3.5: Daytime evolution of (a) the boundary-layer depth and relative humidity at the boundary-layer top, and (b) the four relative humidity tendency terms and total relative humidity tendency from 3.10 for the prototype model simulation (solid lines), and aircraft and radiosonde observations (symbols defined in insert) for 13 June 1986 in HAPEX-MOBILHY.

3.4.1 Evolution stages

Four stages of moisture development occur on 13 June, which also occurred to various degrees on other days during HAPEX-MOBILHY. We briefly discuss these stages for the prototype simulation in terms of the relative humidity tendency terms (Figure 3.5b) and the evolution of relative humidity near the boundary-layer top (Figure 3.6). On 13 June, the observed boundary layer was relatively moist and grew to about 1800 m by midday.

Stage 1: Early Morning Moistening (0600-0700) - Surface fluxes are weak with weak turbulent moisture flux convergence and moistening of the shallow boundary layer. Due to surface heating, however, at the top of the boundary layer temperature increases sufficiently for relative humidity to decrease.

Stage 2. Mid/Late-Morning Rapid Growth (0700-1100) - Boundary layer growth becomes rapid with stronger vertical moisture flux divergence induced by dry air entrainment. This flux divergence decreases the boundary-layer specific humidity; however, the relative humidity near the boundary-layer top increases due to the large boundary-layer growth term in 3.10.

Stage 3. Early Afternoon (1100-1500) - After the rapid growth stage, boundary-layer specific humidity increases slightly due to vertical convergence of the turbulent moisture flux. This flux convergence is associated with reduced boundary-layer growth and reduced dry air entrainment and increasing surface evapotranspiration. However, the relative humidity at the boundary-layer top decreases slowly with time due to the slight excess of the boundary-layer warming term over surface evaporation term.

Stage 4. Mid/Late Afternoon Diminishing Surface Fluxes (1500-1800) - Surface fluxes decrease and the change in relative humidity at the boundary-layer top is small.

Aspects of the first two stages are documented in previous studies. Coulman (1978) shows moisture flux convergence and boundary-layer moistening in the early morning when boundary-layer growth is weak, followed by stronger boundary-layer growth with moisture flux divergence and boundary-layer drying (see Mahrt 1991). Segal et al (1991) show similar results where the low-level moisture increases in early morning in the shallow boundary layer, then decreases rapidly as the morning surface

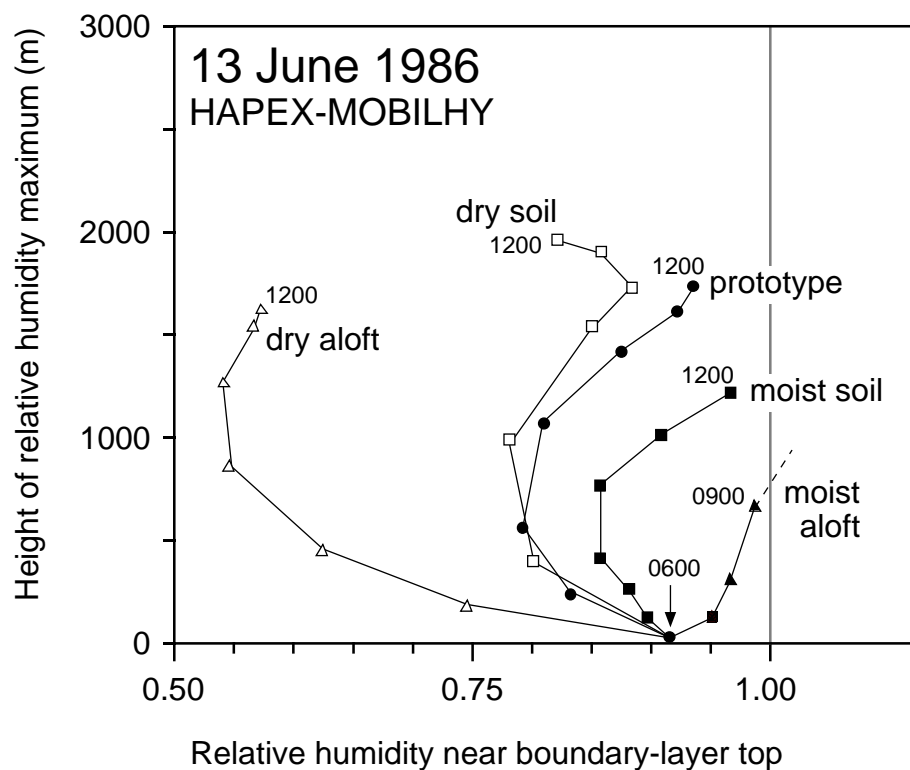


Figure 3.6: Daytime evolution of relative humidity near the boundary-layer top for the different model sensitivity tests described in section 3.4 for 13 June 1986 in HAPEX-MOBILHY.

inversion is eroded by a growing boundary layer. This same rapid moisture decrease also occurred at the forest tower near the central site (Figure 3.7) and at some of the surface observing network (12 surface stations) for 13 June 1986 in HAPEX-MOBILHY. However, after the initial moisture decrease, there is a steady increase throughout the rest of the day at the forest tower site corresponding to a moistening boundary layer ($C_q < 1$). Compare this to 22 June 1986 in HAPEX-MOBILHY (discussed further below) where low-level moisture increases in the early morning shallow boundary layer, and then decreases due to the growing boundary layer. This decrease continues throughout the day of 22 June which is identified as a boundary-layer drying day with $C_q > 1$.

The model simulations are terminated at noon since the relative humidity at the boundary-layer top exceeds 1.0 in the afternoon for several of the simulations in which case a cloud model would be required. As expected, drier (moister) air above the boundary layer leads to more (less) dry air entrainment and lower (greater) relative humidity at the boundary-layer top (Figure 3.6).

3.4.2 Influence of soil moisture

The influence of soil moisture on relative humidity varies dramatically according to initial atmospheric conditions and the prescribed mean subsidence. The effect of soil moisture on relative humidity tendency described by (3.22) involves the opposing influences of boundary-layer moistening and reduced boundary-layer growth due to surface evaporation. For 13 June, (3.22) is greater than unity during most of the day because of significant temperature stratification above the boundary layer. This suggests that the main influence of surface evaporation for this day is to increase the relative humidity at the boundary-layer top. When the soil is specified to be dry (Figure 3.6, Table 3.2), greater surface heating leads to more rapid boundary-layer growth. The increase of relative humidity due to greater boundary-layer growth is opposed by the effects of stronger surface heating, dry air entrainment and decreased surface evaporation. As a result, the decrease of soil moisture exerts little net effect on the relative humidity at the boundary-layer top before noon (Figure 3.6). However, by noon when boundary-layer growth diminishes, relative humidity at the boundary-layer top decreases with time due to stronger surface heating compared to the prototype case. For the case of very moist soil, boundary-layer growth diminishes by noon due to less surface heating. Then the greater surface evaporation leads to

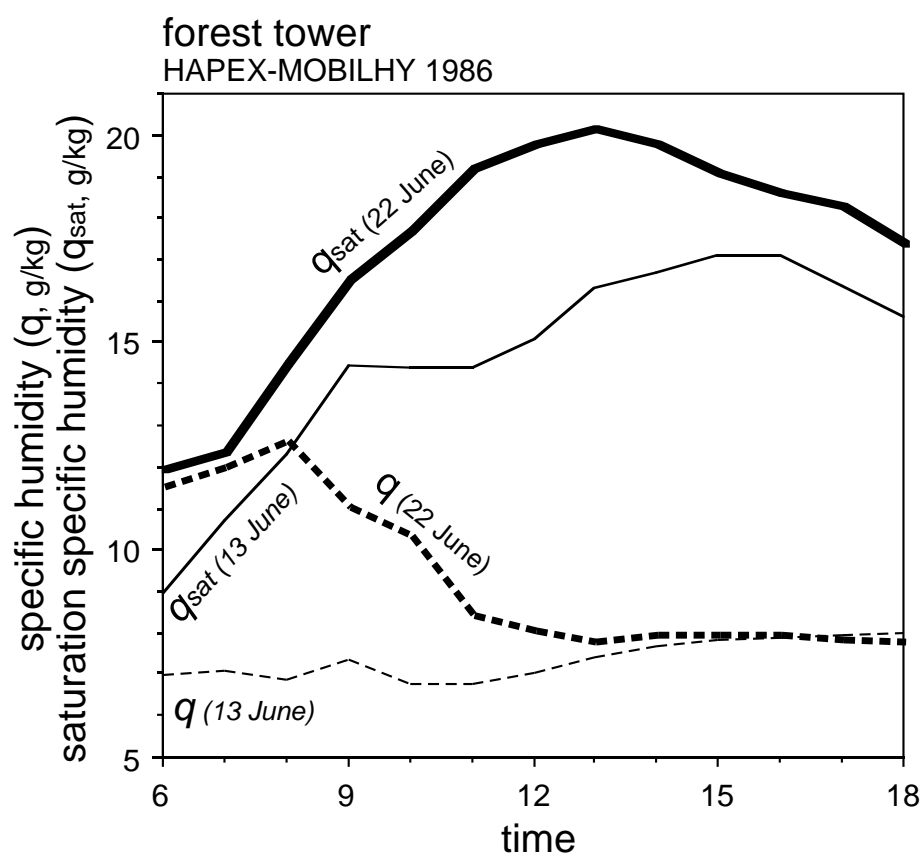


Figure 3.7: Time series of specific humidity and saturation specific humidity at the forest tower site in HAPEX-MOBILHY for 13 and 22 June 1986.

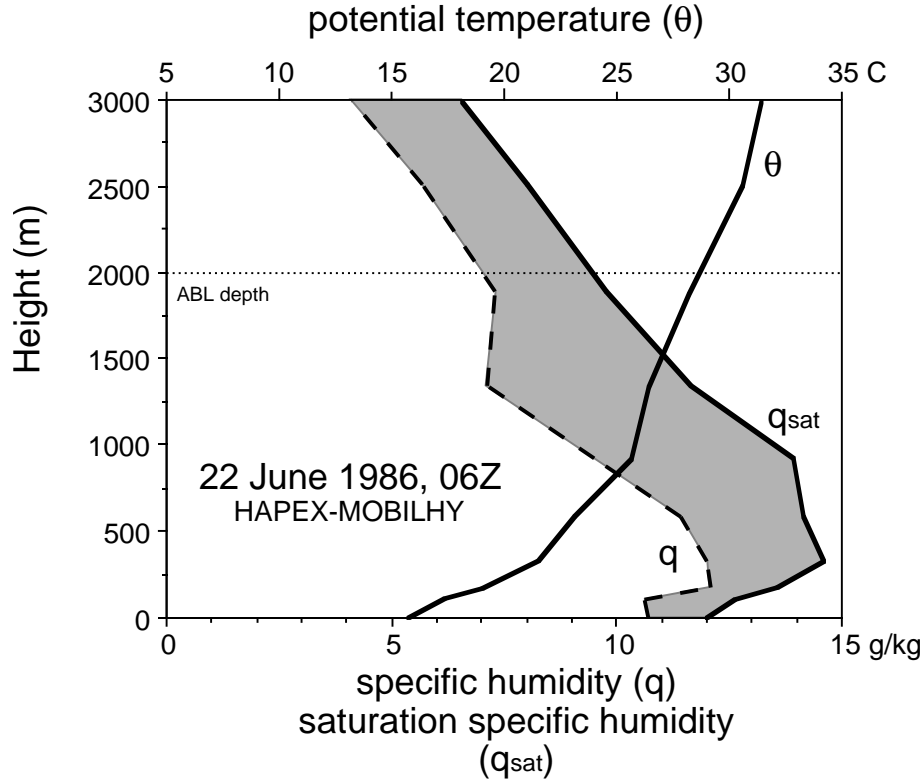


Figure 3.8: As in Figure 3.4 except for 22 June 1986 in HAPEX-MOBILHY.

greater relative humidity compared to the prototype case.

To further examine the effect of temperature stratification and moisture aloft on the relative humidity tendency, sensitivity tests are made for 22 June 1986 in HAPEX-MOBILHY, again initiating the model using 0600 radiosonde data (Figure 3.8, Table 3.2). On 22 June, the observed boundary layer was relatively dry but with greater moisture aloft. Temperature stratification was weaker which allowed for deeper boundary-layer growth compared to 13 June. The greater spatial inhomogeneity on 22 June precludes analysis of the relative humidity tendency in the same manner as the more spatially homogeneous case on 13 June.

Repeating the same soil moisture sensitivity tests above for 22 June indicates that the soil moisture exerts the opposite influence on the relative humidity at the

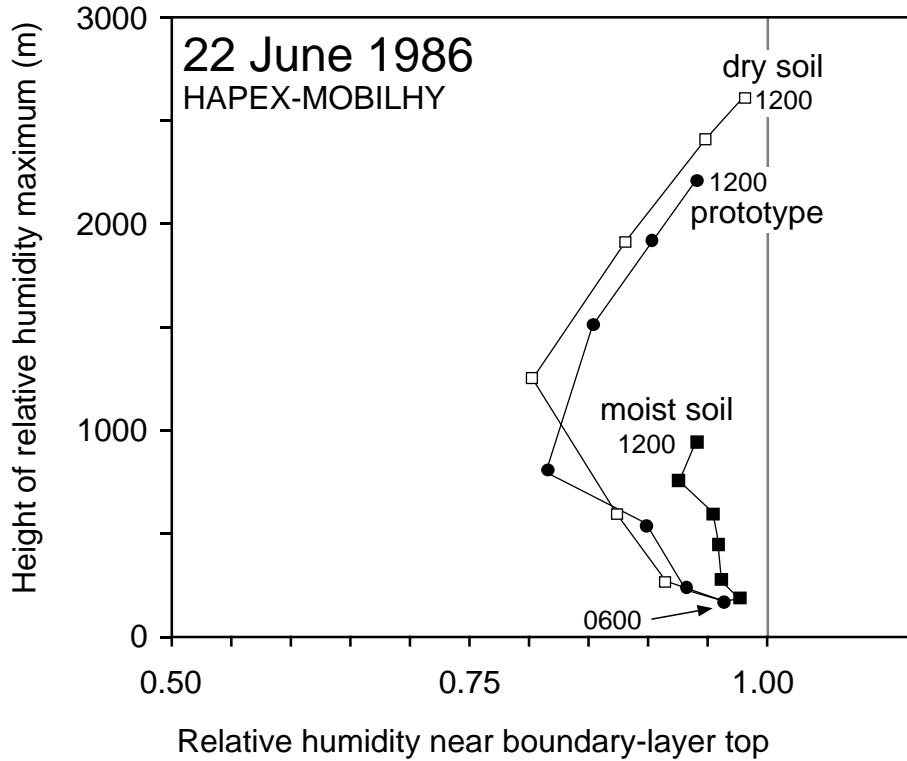


Figure 3.9: As in Figure 3.6 except for 22 June 1986 in HAPEX-MOBILHY.

boundary-layer top compared to 13 June. With dry soil and weaker temperature stratification, the boundary layer grows rapidly. The influence of dry air entrainment is only modest because the air aloft is relatively moist (Figure 3.9). As a result, the relative humidity at the boundary-layer top is greater for drier soil compared to the prototype case! For moist soil conditions, the influence of greater surface evaporation on relative humidity is largely offset by slower boundary-layer growth, so the relative humidity at the boundary-layer top is smaller for moist soil compared to the drier soil case.

From a more general point of view, drier soil may or may not decrease relative humidity and cloud development at the boundary-layer top, depending on temperature stratification and moisture aloft. Therefore the role of soil moisture cannot be simply predicted as assumed in some climate feedback arguments.

All three model simulations for the 22 June case overpredict the observed relative humidity by 0.05 to 0.10, possibly due to the exclusion of modest dry air advection at upper levels after the model initialization at 0600. Note that this overprediction cannot be ameliorated by adjusting soil moisture.

As possible implications of the above sensitivity tests, consider typical high plains conditions or regions of synoptic scale subsidence where the air above the boundary layer is quite dry (Palmén and Newton 1969). Then drier soil and resulting large boundary-layer growth is more likely to decrease the relative humidity at the top of the boundary layer. In contrast, consider typical conditions further east with moist southerly flow aloft. Then drier soil conditions and greater boundary-layer growth can lead to larger relative humidity at the boundary-layer top.

Plants provide a conduit for deep soil moisture to the atmosphere. The effect of moistening due to transpiration is offset by weaker surface heating and resulting weaker boundary-layer growth. Then the relative humidity for a fully vegetated surface (simulation not shown) is similar to values for the bare soil case for a range of initial conditions. As with all sensitivity tests, the above results do not indicate general rules, but only provide examples for a specific set of initial conditions and parameter values.

3.5 Conclusions

Aircraft observations from a case-study fair weather day in HAPEX-MOBILHY have been analyzed to evaluate terms in the tendency equation for relative humidity at the boundary-layer top 3.10. These findings were extended to include ten days of radiosonde data, and simulations with a one-dimensional numerical model for two contrasting days in HAPEX-MOBILHY. The analyses indicate that the adiabatic decrease of the boundary-layer top temperature during the morning rapid boundary-layer growth exerts the strongest influence on the relative humidity tendency. That is, as the boundary-layer top grows to lower pressure, the temperature and saturation vapor pressure decrease for a given potential temperature. Of course the potential temperature and specific humidity of the boundary layer are both changing, so that the net change of relative humidity at the boundary layer top is the difference between several effects as represented by 3.10. Based on analysis of HAPEX-MOBILHY data,

a simple version of the relative humidity tendency equation (3.33) is constructed. However (3.33) requires comparison with additional data sets before it can be assessed as a predictive tool.

If the air aloft is characterized by weak stratification and is not too dry, the relative humidity at the boundary-layer top and probability of cloud initiation might increase more rapidly over dry surfaces than over wet surfaces. In this case, the more rapid growth over dry surfaces is the main influence on relative humidity at the boundary-layer top. This case appears to explain increased convection and cloud development over surfaces of large sensible heat flux compared to surfaces with enhanced moisture flux (Otterman et al 1990, Rabin et al 1990, and others). However, if the air above the boundary layer is characterized by significant stratification, the boundary-layer relative humidity is generally greater over moist surfaces where boundary-layer growth is weaker (Hammer 1970, Barnston and Schikedanz 1984). This case includes the drought feedback mechanism of dry spring soil conditions where reduced soil moisture reduces the probability of precipitation thus intensifying drought conditions (Oglesby and Erickson 1989, Namias 1988, Trenberth et al 1988, and others); this scenario is more likely to occur with dry air aloft in which case the more rapid growth of the boundary layer over dry surfaces leads to entrainment drying of the boundary layer. Previously proposed drought scenarios are generally valid only for a specific parameter regime. Modeling drought conditions as well as forecasting boundary-layer cloud development requires adequate representation of several different boundary-layer interactions controlling the relative humidity field.

Acknowledgements. The detailed comments by reviewers Alan Betts and Doug Lilly are greatly appreciated. This material is based upon work supported by the Phillips Laboratory under contract F19628-91-K-0002, and the NOAA Climate and Global Change Program under award number NA36GP0369. The National Center for Atmospheric Research is acknowledged for the use of the King Air research aircraft in HAPEX-MOBILHY.

Chapter 4

A formulation for boundary-layer cloud cover

This chapter is published as Ek, M. and L. Mahrt, 1991: A formulation for boundary-layer cloud cover. *Annales Geophysicae*, **9**, 716-724.

©Copyright 1991 by Springer-Verlag

Abstract

Subgrid variability of moisture complicates the formulation of boundary-layer cloud cover in large-scale numerical models. When spatial fluctuations of relative humidity are large, boundary-layer clouds first form at a lower spatially averaged relative humidity. Using data from HAPEX-MOBILHY, we construct a fractional cloud cover formulation which uses relative humidity based on spatially averaged variables and accounts for the influences of turbulent and subgrid mesoscale variations of relative humidity. The turbulent variability of relative humidity near the boundary-layer top is formulated in terms of dry air entrainment. The mesoscale subgrid variability is specified as a function of horizontal grid size based on HAPEX-MOBILHY analyses. The cloud cover formulation is applied in a one-dimensional atmospheric boundary-layer model. However, the modeled cloud cover is found to be more sensitive to the specified mean vertical motion than to the adjustable coefficients in the cloud cover formulation.

4.1 Introduction

Formulation of cloud cover and the associated attenuation of downward solar radiation is an important aspect of practical models of the atmospheric boundary layer. Development of boundary-layer clouds reduces surface heating and evapotranspiration. Relatively little attention has been devoted to construction of simple formulations of boundary-layer cloud cover.

Most existing simple formulations can be roughly classified into two classes: those formulations using some form of relative humidity (Mitchell and Hahn 1990, Saito and Baba 1988, Slingo 1987, 1980, Chu 1986, Dickinson 1985, Albrecht 1981, Chu and Parrish 1977) and those formulations based on a frequency distribution of the lifted condensation level (Betts 1983, Wilde et al 1985). The latter class of models seems to possess more physics which can be potentially related to turbulence statistics, whereas the former class is easier to implement in a numerical model. In this investigation, we develop a model of cloud cover which utilizes aspects of both classes of formulations by analyzing data from HAPEX-MOBILHY conducted in the southwest of France in 1986 (André et al 1988).

The present study will indicate that turbulent scale variations of relative humidity

and subgrid mesoscale inhomogeneity are both important factors in the formulation for grid-averaged cloud cover in large-scale numerical models. A simple formulation of transmission of solar radiation through boundary-layer clouds will also be adopted. We will incorporate this cloud cover formulation into a one-dimensional atmospheric boundary-layer model and simulate cloud cover development for 12 days during HAPEX-MOBILHY.

4.2 Relative humidity models of cloud cover

The proposed model will follow those formulations that use relative humidity since this quantity is available from numerical models and does not require a link between surface processes and cloud development. We will also follow Wilde et al (1985) and Betts (1983) and assume a frequency distribution of variables (relative humidity for our study) in order to account for variability on turbulent scales. We also include mesoscale subgrid variability to allow for application to large-scale models.

The simplest formulation of cloud cover which is based on the fractional relative humidity (RH) near the top of the boundary layer can be summarized in a framework based on a "scaled relative humidity"

$$RH_* = \frac{RH - RH_{crit}}{RH_t - RH_{crit}}. \quad (4.1)$$

This function vanishes as RH decreases to the critical relative humidity RH_{crit} , and approaches unity when RH approaches the threshold value RH_t (Mitchell and Hahn 1990), normally chosen to be 1.0. A general model of boundary-layer fractional cloud cover A_c is then formulated as

$$A_c = \begin{cases} 0, & RH_* \leq 0 \\ RH_*^p, & RH_* > 0 \end{cases}. \quad (4.2)$$

With formulation (4.1)-(4.2), boundary-layer clouds are first predicted when the grid-averaged relative humidity exceeds RH_{crit} . Cloud cover reaches 1.0 when the grid-averaged relative humidity reaches RH_t . The Slingo model (1980, 1987) uses the average relative humidity in the 950-850 mb layer with $p = 2$ and $RH_t = 1.0$, while $RH_{crit} = 0.80$ near the surface and decreases with height. The Dickinson model (1977) corresponds to $RH_t = 1.0$, $RH_{crit} = 0.85$ and $p = 2$, while the Chu model (1986) corresponds to $RH_t = 1.0$, $RH_{crit} \approx 0.57$ and $p \approx 1.32$. The different values

of RH_{crit} used by these models presumably take into account the vertical depth and horizontal scale of the grid volume over which averaging is implied. For a given average relative humidity, a larger subgrid volume is more likely to contain at least some clouds, and thus corresponds to a lower value of RH_{crit} .

Mitchell and Hahn (1990) allow 1.0 cloud cover with a grid averaged relative humidity of less than 1.0 (corresponding to a value of $RH_t < 1.0$) to allow for a thin layer of clouds within a thicker vertical grid layer. Models by Saito and Baba (1988), Albrecht (1981) and Chu and Parrish (1977) all use relative humidity, but cannot be reduced to the format of (4.1)-(4.2).

In our observational analyses, average relative humidity refers to the relative humidity computed from spatially averaged moisture and temperature from aircraft data at a single level. To study the relationship between cloud cover and relative humidity at the boundary-layer top, we estimate the fractional cloud cover using records of downward solar radiation data from aircraft flight legs collected by the NCAR King Air during HAPEX-MOBILHY. This data set consists of 12 days with varying cloud amounts in the boundary layer and minimal cloud cover above the boundary layer. Frequency distributions of the downward solar radiation are computed from one-second observations (approximately 80-m segments) along the aircraft flight leg. Under a partial cloud cover the resulting frequency distributions of solar radiation (Figure 4.1) are bimodal due to cloudy areas and clear areas. As a result, a threshold value of solar radiation can be defined for each flight leg to determine the local existence of overhead boundary-layer clouds without sensitivity to the exact numerical choice of the threshold value.

To illustrate the dependence of cloud cover on scale, we compute average cloud cover from aircraft data over horizontal scales from one to 50 km (Figure 4.2). With no averaging, the cloud cover is either clear or totally overcast. As the horizontal scale increases, the cloud cover distribution becomes less bimodal as averaging combines both clear and cloudy regions. As the scale increases to the record length, the cloud cover approaches the record mean value. The effect of horizontal scale and spatial averaging on cloud cover is discussed further in Hughes and Henderson-Sellers (1983).

Observations from the 18 available upper-level flight legs from ten days in HAPEX-MOBILHY (Figure 4.2 and Table 4.1) indicate that the observed boundary-layer cloud

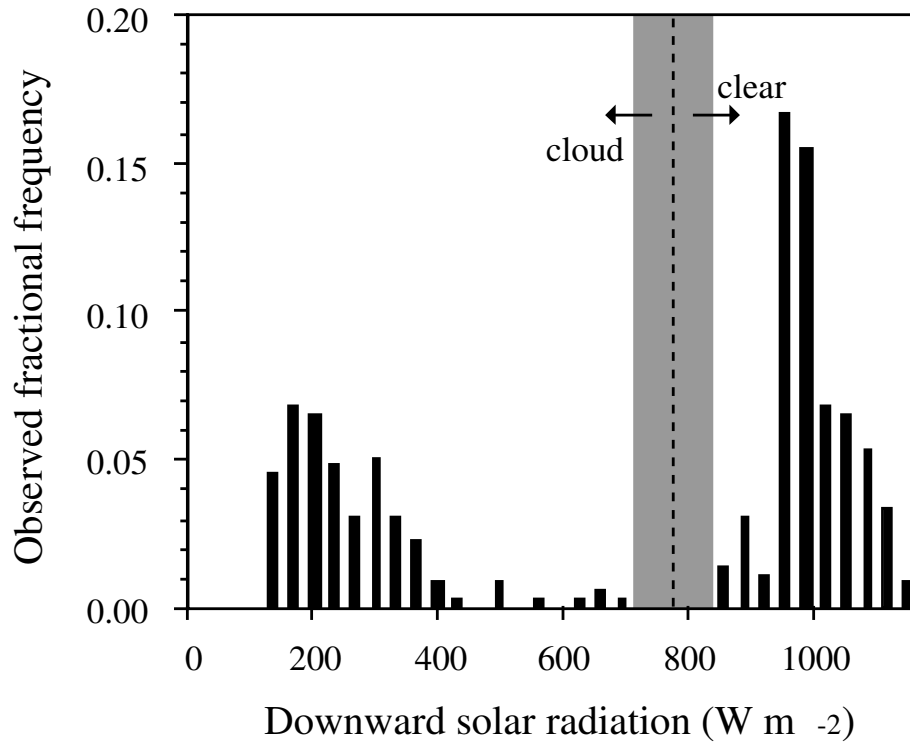


Figure 4.1: Frequency distribution of downward solar radiation from a flight leg just below cloud base in HAPEX-MOBILHY on 21 May 1986 with a fractional cloud cover of 0.38.

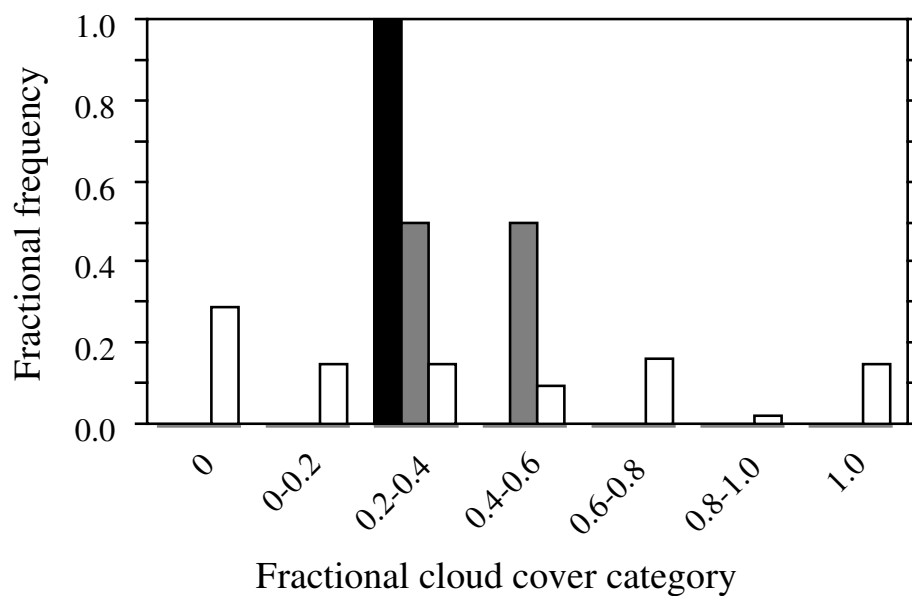


Figure 4.2: Frequency of occurrence for different cloud cover categories from the flight leg in Figure 4.1 for different horizontal scales of averaging: 1-km (white), 10-km (hatched) and 50-km (black).

cover is indeed related to the relative humidity at the boundary layer top, at least for the data of this study. To estimate this relative humidity we have assumed well-mixed unsaturated conditions between the aircraft level and the boundary-layer top, in which case the relative humidity increases with height at an approximate rate of 0.05/100 m. The computation of this height-adjusted relative humidity undoubtedly leads to some of the scatter and is not valid for a thick overcast layer.

We have used only aircraft legs in the upper 45% of the boundary layer. When clouds developed, the aircraft legs were flown immediately below the cloud base. Data from the 8 July flight were discarded because of undetermined instrumentation problems corresponding to relative humidity values greater than 1.0 in clear air. Three other individual flight legs were discarded because the horizontally-averaged relative humidity computed from the aircraft leg disagreed with the relative humidity from the nearest aircraft sounding by 0.10 or more. Finally, one flight leg was discarded where the cloud layer was 450 m thick corresponding to moist adiabatic stratification in which case the relative humidity height adjustment procedure is not valid.

From our data we see that the average relative humidity over the approximately 50-km flight legs must reach about 0.90 before significant cloud cover forms (Figure 4.3). This high value is partly related to the absence of vertical averaging. For averaged relative humidity less than 1.0, the partial cloud cover appears to be greater with significant spatial variability of relative humidity at the aircraft level (Figure 4.3). However, the scatter between days is large partly due to the neglect of the height-dependence of relative humidity variance. The flight levels are below the upper 10% of the boundary layer where moisture variance is expected to reach a sharp peak (Lenschow et al 1980).

In order to allow for spatial variability of relative humidity, a relationship between cloud cover and relative humidity can be posed in terms of an assumed frequency distribution of relative humidity (Figure 4.4). Here relative humidity is generalized using total water relative humidity (vapor plus liquid); that is, values greater than 1.0 occur in clouds. For an average relative humidity less than 1.0 (Figure 4.4a), greater cloud cover is more likely with larger variation of relative humidity. For an average relative humidity greater than 1.0 (Figure 4.4b), larger variation of relative humidity leads to smaller cloud cover. As an example, increased variation of relative humidity in stratocumulus corresponds to more dry pockets and decreased cloud cover. The

Table 4.1: Observed boundary-layer cloud cover, aircraft-level relative humidity (RH) and standard deviation of relative humidity on the mesoscale (aircraft-level σ_{RHmeso}) and on the turbulent scale (aircraft-level σ_{RHturb}), height-adjusted relative humidity (height-adjusted RH), non-dimensional aircraft flight level (z/h), and contributions to the turbulent scale variance of relative humidity from the three terms in (4.12): temperature variance term (T -term $\times 10^{-5}$), moisture variance term (q -term $\times 10^{-5}$) and temperature-moisture correlation term (r_{Tq} -term $\times 10^{-5}$). This data set is for the 18 upper-level flight legs, each approximately 50 km long, from ten days in HAPEX-MOBILHY.

date (1986)	cloud cover	aircraft level			height-adj. RH	z/h	(4.12) terms		
		RH	σ_{RHmeso}	σ_{RHturb}			T	q	r_{Tq}
9 May	0.41	0.82	0.048	0.030	0.98	0.63	3	76	6
9 May	0.27	0.79	0.026	0.022	0.98	0.59	2	45	-1
24 May	0.43	0.84	0.044	0.037	1.01	0.62	3	122	12
24 May	0.79	0.94	0.045	0.025	1.14	0.62	3	55	3
6 June	0.64	0.85	0.048	0.031	1.04	0.60	3	88	7
6 June	0.70	0.81	0.057	0.043	0.98	0.67	2	171	6
6 June	0.52	0.83	0.069	0.045	1.01	0.71	4	178	19
9 June	0	0.60	0.032	0.022	0.57	0.58	1	41	5
9 June	0	0.59	0.020	0.021	0.65	0.56	1	38	4
16 June	0	0.69	0.023	0.013	0.78	0.61	1	15	1
16 June	0	0.67	0.021	0.019	0.76	0.57	2	27	7
19 June	0	0.69	0.047	0.035	0.76	0.71	4	85	30
19 June	0	0.69	0.043	0.027	0.77	0.69	3	54	15
22 June	0.02	0.73	0.054	0.029	0.89	0.59	2	71	6
1 July	0.60	0.96	0.031	0.021	1.27	0.59	3	32	8
2 July	0	0.76	0.030	0.023	0.79	0.82	2	35	10
2 July	0	0.73	0.026	0.030	0.76	0.84	3	60	23
11 July	0	0.65	0.039	0.022	0.72	0.63	1	39	5

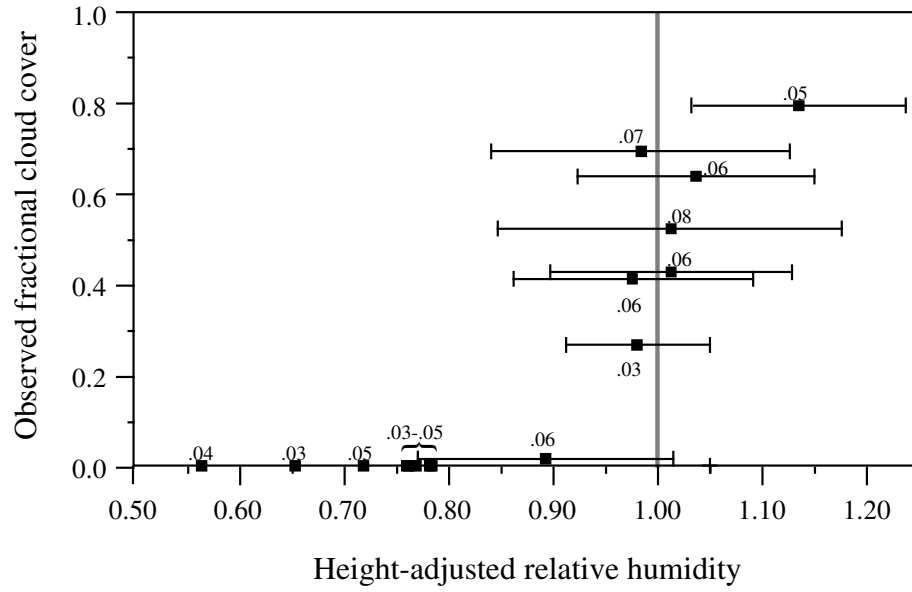


Figure 4.3: 50-km horizontal averages of cloud cover versus height-adjusted relative humidity (RH) for $z/h > 0.55$ with bars showing $\pm 2\sigma_{RH}$ for those values of RH greater than about 0.90; the standard deviation of relative humidity (σ_{RH}) is calculated from raw temperature and moisture data at the aircraft flight level.

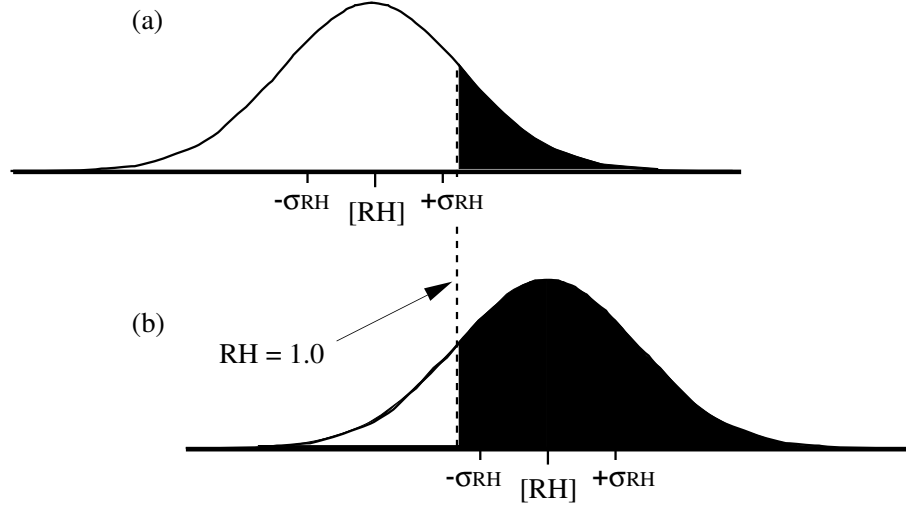


Figure 4.4: Sketch of theoretical cloud cover (dark region) for a Gaussian distribution of relative humidity with the average total water relative humidity (a) less than 1.0 and (b) greater than 1.0.

two example frequency distributions of relative humidity shown in Figure 4.5 indicate that the spatial variability of relative humidity is greater on the day with rapid growth of the boundary layer into overlying dry air (22 June 1986) and less on the day where entrainment of dry air is weak (1 July 1986).

For simplicity we will construct a formulation of fractional cloud cover which assumes a Gaussian distribution of relative humidity and predicts the mean and variance of relative humidity from variables available from a simple atmospheric boundary-layer model. The observed distributions of relative humidity in HAPEX-MOBILHY indicate skewness toward larger values (Figure 4.5) although the tendency is not sufficiently well-defined to construct a more sophisticated distribution function. Mathematically, the fractional boundary-layer cloud cover can be represented by

$$A_c = f\{\overline{RH}, \sigma_{RH}\}, \quad (4.3)$$

where \overline{RH} is the spatially averaged relative humidity and σ_{RH} is the standard deviation of relative humidity which determines the Gaussian distribution, here approximated by a ninth-order polynomial fit. The fractional cloud cover is the area under

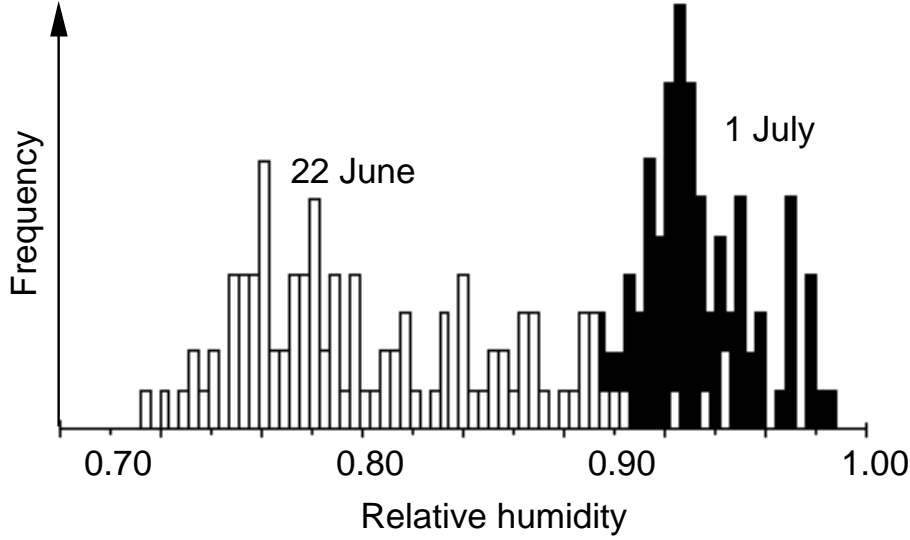


Figure 4.5: Relative humidity distribution for two days in HAPEX-MOBILHY. 22 June 1986 is characterized by large entrainment of dry air into the boundary layer while 1 July is characterized by weaker entrainment.

the Gaussian curve greater than $RH = 1.0$ (Figure 4.4).

The variation of relative humidity near the boundary-layer top involves both turbulent scale variations and those mesoscale variations not resolved by the horizontal grid of large-scale models. For simplicity, we assume that the mesoscale and turbulent fluctuations of relative humidity are uncorrelated. We can then write

$$\sigma_{RH} = (\sigma_{RH_{turb}}^2 + \sigma_{RH_{meso}}^2)^{\frac{1}{2}}, \quad (4.4)$$

where $\sigma_{RH_{turb}}^2$ is the turbulent scale variance of relative humidity and $\sigma_{RH_{meso}}^2$ is the mesoscale variance of relative humidity. In this study, turbulent fluctuations of relative humidity are computed from the aircraft data using a high-pass filter with a 5-km cutoff wavelength.

The cloud cover formulation from (4.3)-(4.4) using the observed height-adjusted relative humidity and aircraft level standard deviation of relative humidity seems to approximate the cloud cover determined from the aircraft radiation observations (Fig-

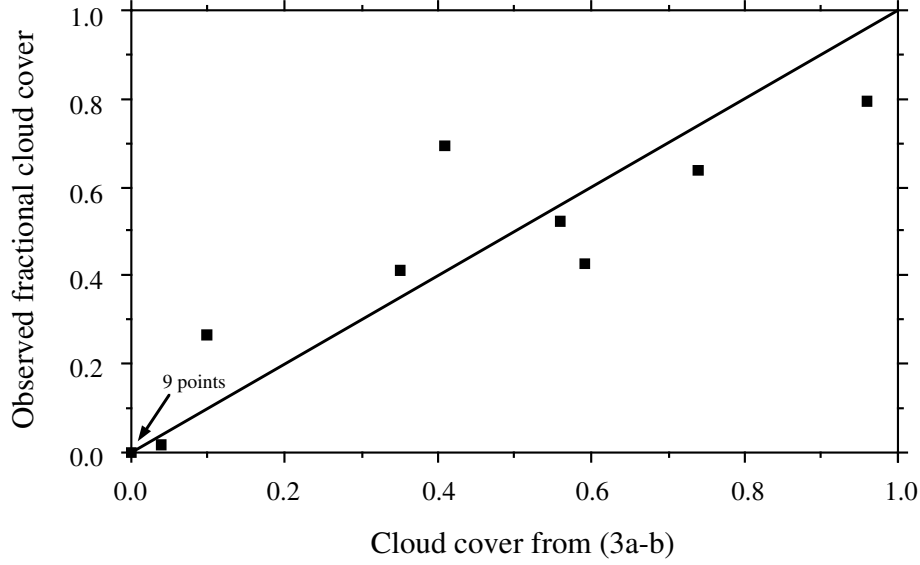


Figure 4.6: Cloud cover calculated from (4.3)-(4.4) using observed values of height-adjusted relative humidity and σ_{RH} versus observed cloud cover determined from aircraft radiation data for 18 upper-level flight legs from ten days in HAPEX-MOBILHY.

ure 4.6). Using a calibrated constant σ_{RH} reduces the accuracy of (4.3)-(4.4) but not significantly compared to the uncertainty in the data. As an example, choosing a constant value of $\sigma_{RH} = 0.05$ describes much of the variation of the observed cloud cover (Figure 4.7). Alternatively, calibrating formulation from (4.1)-(4.2) by choosing $RH_{crit} = 0.90$ and $RH_t = 1.05$ leads to a comparable approximation. The coefficient RH_t exceeds 1.0 when applied to a single level because the cloud cover may be less than 1.0 even when the total water relative humidity exceeds 1.0 (Figure 4.7).

In the present study we allow σ_{RH} to depend on the physical situation which will allow for more flexibility when considering diverse atmospheric conditions. Starting with the variance equation for relative humidity variance, $\sigma_{RH_{turb}}$ is described in sections 4.3.1 and 4.3.2; the subgrid mesoscale variance of relative humidity ($\sigma_{RH_{meso}}$) is described in sections 4.3.3 and modeled as an increasing function of horizontal grid size.

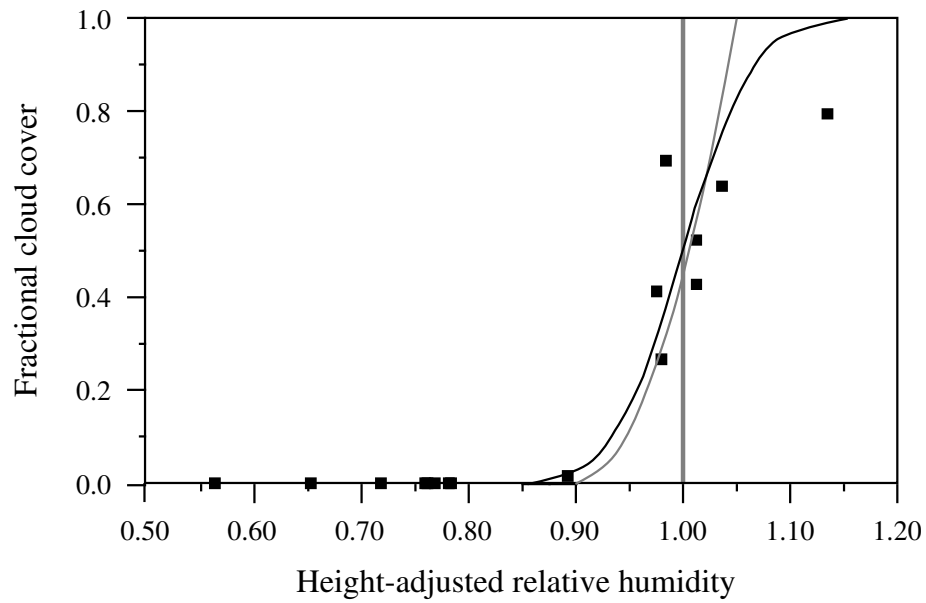


Figure 4.7: Modeled cloud cover as a function of relative humidity for formulation (4.1)-(4.2) (dashed line) and formulation (4.3)-(4.4) with $\sigma_{RH} = 0.05$ (solid line) calibrated in section 4.2, and observed height-adjusted relative humidity versus observed cloud cover (solid squares).

4.3 Relative humidity variance

In the upper part of the boundary layer, temperature and moisture tend to be negatively correlated on turbulent scales due to entrainment of warmer drier air between cooler moist updrafts. This negative temperature-moisture correlation corresponds to larger spatial variation of relative humidity.

Mesoscale variations of the surface energy budget often also lead to variations of relative humidity (Mahrt 1991). In regions of moist surface conditions, greater evapotranspiration leads to less energy available to heat the atmosphere; conversely, dry surfaces correspond to greater sensible heat flux at the surface and warmer air temperatures. With variations between warm dry air and cool moist air, both temperature and moisture variations act in concert to produce variations of relative humidity. Mesoscale moisture variations may be systematically larger than temperature variations for a variety of conditions (Mahrt 1991). Since these variations may be on a subgrid scale, they must be considered in the formulation of cloud cover based on relative humidity. This effect decreases the value of relative humidity required for the initial onset of boundary-layer clouds in formulations of the form (4.1)-(4.2) or (4.3)-(4.4).

We arbitrarily define turbulent scales as those less than 5 km and mesoscale variations as those greater than 5 km. For this reason, we compute the moisture flux and variances using a Tangent-Butterworth filter with a 5-km cutoff wavelength. With this partition, dry downdrafts between individual cloud elements are turbulent scale variations. The upper limit to the mesoscale circulations included in this calculation will be roughly 100 km corresponding to the length of the record.

We now study the variation of relative humidity in the boundary layer in terms of equations for relative humidity variance.

4.3.1 Turbulent scale variation of relative humidity

To compute the turbulent variation of relative humidity near the boundary-layer top, we express the relative humidity (RH) in terms of the specific humidity (q), and partition variables into record means (\bar{x}) and perturbations (x') to obtain

$$RH = \overline{RH} + RH' = \frac{\overline{q} + q'_s}{\overline{q}_s + q'_s}. \quad (4.5)$$

Assuming that the perturbation saturation specific humidity q'_s is small compared to the mean value (\overline{q}), we approximate (4.5) as

$$\overline{RH} + RH' = \frac{1}{\overline{q}}(\overline{q}_s + q'_s)\left(1 - \frac{q'_s}{\overline{q}_s}\right). \quad (4.6)$$

Carrying out the multiplication on the right hand side, rearranging, and subtracting \overline{RH} from both sides, we obtain

$$RH' = \frac{1}{\overline{q}_s} \left(-\overline{RH}q'_s + q'_s - \frac{q'_s q'_s}{\overline{q}_s} \right). \quad (4.7)$$

Squaring (4.7) and averaging, the turbulent scale relative humidity variance (σ_{RHturb}^2) becomes

$$\sigma_{RHturb}^2 = \frac{1}{\overline{q}_s^2} \left[\overline{RH}^2 \sigma_{q_s}^2 + \sigma_q^2 + \frac{\overline{q_s'^2 q'^2}}{\overline{q}_s^2} + 2\overline{RH} \left(-\overline{q'_s q'} + \frac{\overline{q_s'^2 q'}}{\overline{q}_s} - \frac{\overline{q'_s q'^2}}{\overline{q}_s} \right) \right], \quad (4.8)$$

where $\sigma_{q_s}^2$ and σ_q^2 are the variances of saturation specific humidity and specific humidity, respectively, where again overlines indicate averaging. Assuming $q' \ll \overline{q}$ and again using $q'_s \ll \overline{q}_s$, we neglect third- and fourth-order perturbation terms, so (4.8) becomes approximately

$$\sigma_{RHturb}^2 = \frac{\overline{RH}^2 \sigma_{q_s}^2}{\overline{q}_s^2} + \frac{\sigma_q^2}{\overline{q}_s^2} - \frac{2\overline{RH} \overline{q'_s q'}}{\overline{q}_s^2}. \quad (4.9)$$

The linearized Clausius-Clapeyron equation can be written as

$$q'_s = \left(\frac{dq_s}{dT} \right) T'. \quad (4.10)$$

Assigning the perturbation values to be the record standard deviations, the Clausius-Clapeyron equation becomes

$$\sigma_{q_s}^2 = \left(\frac{dq_s}{dT} \right)^2 \sigma_T^2. \quad (4.11)$$

Using this, (4.9) may be rewritten as

$$\sigma_{RHturb}^2 = \left[\overline{RH} \left(\frac{dq_s}{dT} \right) \frac{\sigma_T}{\overline{q}_s} \right]^2 + \left(\frac{\sigma_q}{\overline{q}_s} \right)^2 - 2\overline{RH} \left(\frac{dq_s}{dT} \right) \frac{r_{Tq} \sigma_T \sigma_q}{\overline{q}_s^2}. \quad (4.12)$$

The first term on the right-hand side of (4.12) is the RH variance due to the temperature variance, the second term is due to the moisture variance, and the third term is due to the correlation between temperature and moisture (r_{Tq} is the temperature-specific humidity correlation). In the upper part of the boundary layer below cloud base, the moisture variance term computed from aircraft data in HAPEX-MOBILHY is much larger than the other two terms (Table 4.1).

Since the contribution from the other two terms in (4.12) is small, we choose to express σ_{RHturb}^2 as a function of the moisture variance term. Then (4.12) reduces to

$$\sigma_{RHturb}^2 = f \left\{ \left(\frac{\sigma_T}{\overline{q_s}} \right)^2 \right\}, \quad (4.13)$$

where f is an undetermined function to be estimated empirically from HAPEX-MOBILHY data. Unfortunately, simple models of the boundary layer do not predict moisture variance and similarity relationships for moisture fluctuations are unreliable near the boundary-layer top.

We can transform (4.13) by relating σ_q to the moisture flux

$$\sigma_q = \frac{\overline{w'q'}}{r_{wq}\sigma_w}. \quad (4.14)$$

Then (4.13) becomes

$$\sigma_{RHturb}^2 = f \left\{ \left(\frac{\overline{w'q'}}{r_{wq}\sigma_w\overline{q_s}} \right)^2 \right\}. \quad (4.15)$$

Boundary-layer models can predict $\overline{w'q'}$ and $\overline{q_s}$. (4.15) is preferable to (4.13) because similarity expressions for σ_w are thought to be more reliable than those formulations for moisture fluctuations. Furthermore the vertical motion-specific humidity correlation (r_{wq}) in the upper boundary layer appears to be less variable than the moisture variance required for (4.13). Therefore we proceed to explore the applicability of (4.15) by assuming the function f to depend linearly on its argument and ignoring the variation of r_{wq} . Then (4.15) becomes

$$\sigma_{RHturb}^2 = C_1 + C_2 \left[\left(\frac{\overline{w'q'}}{r_{wq}\sigma_w\overline{q_s}} \right)^2 \right]. \quad (4.16)$$

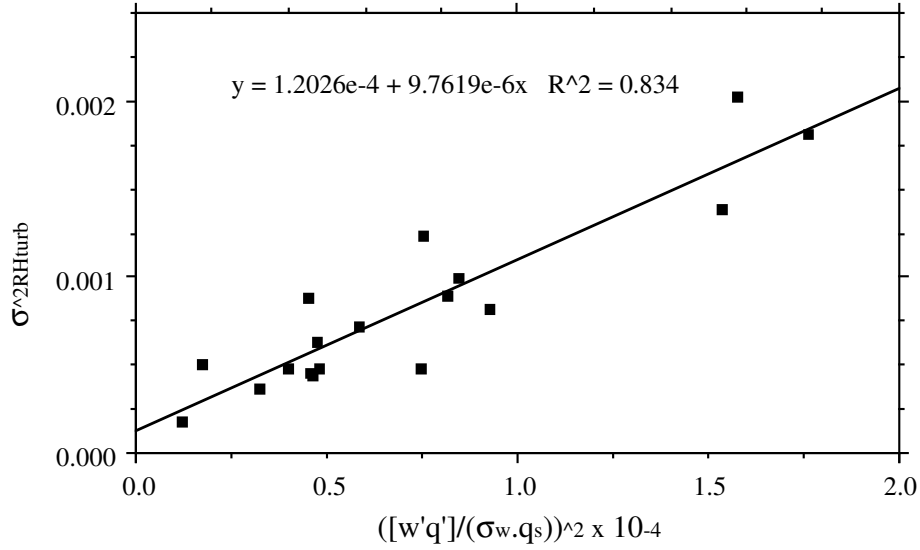


Figure 4.8: Relationship between the turbulent variance of relative humidity and the moisture entrainment flux (2nd term on right hand side in (4.16)). The y-intercept provides an estimate of C_1 while the slope is C_2 in (4.16).

Using the 18 upper-level flight legs from HAPEX-MOBILHY, linear regression yields $C_1 = 0.00014$, and $C_2 = 9.75$ (Figure 4.8). A comparison of the linear regression model based on (4.16) (Figure 4.8) with the observed values of the moisture variance term (Table 4.1) indicates that the parameterization of moisture variance by (4.16) apparently does not seriously increase the scatter. The coefficient C_1 in (4.16) is expected to absorb the smaller contributions from the temperature variance and temperature-moisture correlation terms (first and third terms on the right hand side) in (4.12). The coefficient C_2 absorbs the contribution from r_{wq}^2 in (4.15).

The large percentage of the variance explained by the linear model (4.16) is of unknown generality. For example, in the case of downward transport of moisture, as may occur in the stable nocturnal boundary layer, the second term in (4.16) must be omitted. Then the turbulent variability of relative humidity is small and large values of average relative humidity are probably needed to produce cloud cover.

4.3.2 Vertical velocity variance

For unstable conditions, we use the similarity formulation for vertical velocity variance from Lenschow et al (1980)

$$\sigma_w^2 = 1.8 \left(\frac{z}{h} \right)^{\frac{2}{3}} \left(1 - 0.8 \frac{z}{h} \right)^2 w_*^2, \quad (4.17)$$

where z is height, h is boundary-layer depth, and w_* is the convective velocity scale. For the stable case, we use Stull's (1988) relationship based on the data of Caughey et al (1979)

$$\sigma_w^2 = 2.5 \left[1 - \left(\frac{z}{h} \right)^{0.6} \right] u_*^2, \quad (4.18)$$

where u_* is the friction velocity.

For weakly unstable conditions, we evaluate both (4.17) and (4.18) and take the maximum of these two expressions. This allows σ_w to be determined by either mechanical or convective generation of turbulence depending on which one is larger.

We will include turbulent scale contributions (4.16)-(4.18) to the relative humidity variation through application of (4.4) in the model simulations reported in section 4.5.

4.3.3 Mesoscale variation of relative humidity

Mesoscale variations of relative humidity are related to surface inhomogeneity and transient mesoscale disturbances. With larger horizontal grid size, more of the mesoscale motions become "subgrid" so that we would expect the mesoscale standard deviation $\sigma_{RH_{meso}}$ to increase with grid size. Then for relative humidity less than one, the chance of some cloud cover increases with the horizontal size of the grid area.

To examine the effect of grid size on relative humidity variations, we compute 5-km averages of relative humidity for the 18 upper-level flight legs in HAPEX-MOBILHY. We then determine the ensemble average of the standard deviations of the 5-km averaged relative humidity ($\sigma_{RH_{meso}}$) over 10, 25, 50 and 100 km segments. An expression for the dependence of $\sigma_{RH_{meso}}$ on horizontal scale (grid size) is constructed as a least square fit to a logarithmic function (Figure 4.9) and is of the form

$$\sigma_{RH_{meso}}^2 = a_0 + a_1 \Delta x + a_2 \ln(\Delta x), \quad (4.19)$$

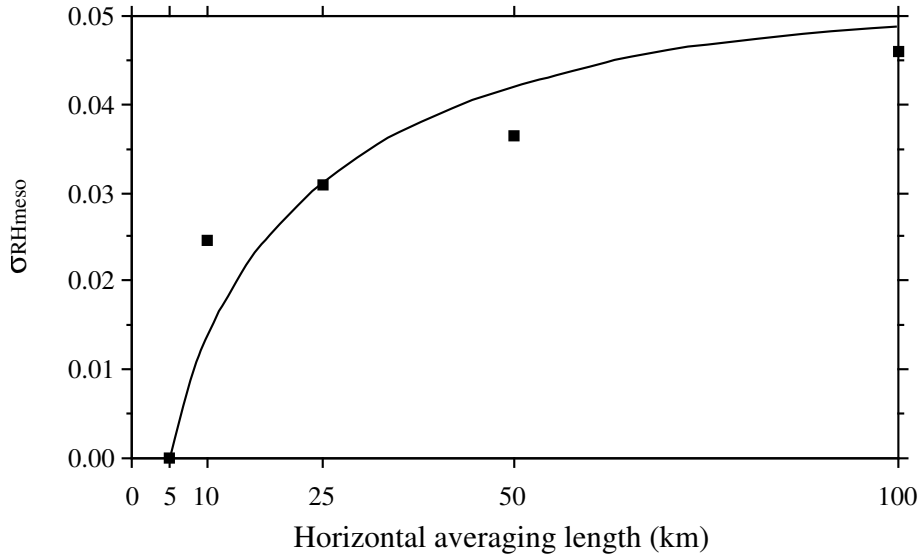


Figure 4.9: Logarithmic least squares fit of the mesoscale standard deviation of relative humidity to the horizontal averaging length.

where $a_0 = -0.03$, $a_1 = -0.00015 \text{ km}^{-1}$, $a_2 = 0.02$ and Δx is the horizontal scale in kilometers; (4.19) is valid for $\Delta x \geq 5 \text{ km}$. A better fit to the data can be constructed with a higher-order relationship, however, this may not be justified by the data. In particular the mesoscale variability of relative humidity changes substantially between different days (Table 4.1). We will include the mesoscale contribution (4.19) to the relative humidity variation through application of (4.4) in the model simulations reported in section 4.5.

4.4 Cloud transmission of solar radiation

Transmission of solar radiation through the fractional cloud cover determines the amount of radiation that reaches the surface. The formulation of this transmission may be as important as the prediction of fractional cloud cover itself. Expressions for transmission of solar radiation through clouds (Fairall et al 1990, Kasten and Czeplak 1980, Stephens 1978), are based on functions of solar elevation, cloud thickness, liquid water content, and cloud geometry. In the current simple version of our atmospheric boundary-layer model, solar elevation is available while the other factors are not.

Therefore, we choose a transmission function with an implicitly fixed optical depth following Liou (1976) where the fraction transmitted $t_{S\downarrow}$ is approximated as

$$t_{S\downarrow} = 0.06 + 0.17 \sin \phi, \quad (4.20)$$

where ϕ is solar elevation angle (0° overhead, 90° at the horizon). The total incoming solar radiation $S\downarrow$ reaching the surface (before reflection) is then calculated as

$$S\downarrow = S_{cs\downarrow}(1 - A_c + t_{S\downarrow}A_c), \quad (4.21)$$

where $S_{cs\downarrow}$ is the incoming clear sky solar radiation (incident at the top of the boundary layer).

4.5 Model testing

We incorporate the fractional cloud cover formulation ((4.3)-(4.4), (4.16)-(4.19)) into a simple atmospheric boundary-layer model which was developed to simulate the interactions of the atmospheric boundary layer, soil, and vegetation. The atmospheric boundary-layer model (Troen and Mahrt 1986, Holtslag et al 1990) is coupled with an active two-layer soil model (Mahrt and Pan 1984) and a primitive plant canopy model (Pan and Mahrt 1987).

The following comparisons of the atmospheric boundary-layer model with HAPEX-MOBILHY data attempt to study the sensitivity of the cloud cover formulation to the less-than-perfect information from the rest of the boundary-layer model. In addition to the various model assumptions, errors in the one-dimensional model result from the external specification of the mean vertical motion and the variable geostrophic wind, and from the omission of horizontal advection of temperature and moisture.

We implement the cloud cover formulation at the level of maximum relative humidity which is normally the first level below the boundary-layer top. We choose those 12 days from the HAPEX-MOBILHY data set for model testing when minimal cloud activity occurred above the boundary layer and a radiosonde data set is available. Of the ten days used in determining coefficients for the cloud cover formulation, seven are used in model testing, while three are not selected because they lack radiosonde data. Radiosondes launched from the central site in HAPEX-MOBILHY at Lubbock at 0600

LST provide initial atmospheric conditions for model simulations. Mean vertical motion is specified to increase linearly with height from zero at the surface and is fitted to an "observed" layer averaged value centered at 2 km, and a 12-hour averaged value centered at 1200 LST taken from the mesoscale analysis described in Jacquemin and Noilhan (1990). Geostrophic winds are estimated from a layer average of the actual winds at approximately 1500 m from the 0600 LST soundings and are assumed to be height-independent. Equating the initial wind and the geostrophic wind prevents unrealistic inertial oscillations. Other details concerning the model input data are included in Holtslag and Ek (1996), Pinty et al (1989) and Bougeault et al (1989). In addition, we assume a horizontal scale for our model simulations of roughly 100 km and therefore use a value of $\sigma_{RHmeso} = 0.05$. Model simulations begin at 0600 LST and are integrated for 12 hours.

Sequential aircraft legs provide an ensemble average of the spatial averages of fractional cloud cover for the approximate period of aircraft flights from 1300-1500 LST. Surface observations of downward solar radiation in the forest clearing at Lubbon provide an independent assessment of the range of fractional cloud cover for the two-hour period centered at 1400 LST (Table 4.2).

Model simulations of fractional cloud cover averaged over the period 1300-1500 LST tend to be higher than the observed fractional cloud cover values (Table 4.2). The overprediction may be due to systematic errors in the modeled surface evapotranspiration which affects surface heating and subsequent boundary-layer growth. The modeled fractional cloud cover is particularly sensitive to uncertainties in the mean vertical motion and sometimes sensitive to the omission of horizontal advection as discussed below. In contrast, the modeled prediction of the cloud cover is not as sensitive to the values of the coefficients in the cloud cover formulation! The model is least sensitive to the coefficient C_1 . Changing the value of the coefficient C_2 in the relationship for σ_{RHturb} (in (4.16)) by $\pm 50\%$ alters the modeled fractional cloud cover by a maximum of 0.12. The estimated uncertainty of C_2 for the σ_{RHturb} formulation (in (4.16)) is only about $\pm 10\%$ based on envelopes of the data in Figure 4.8.

The observed value of σ_{RHmeso} varies significantly from day to day (Table 4.1). We have carried out preliminary case studies which show that mesoscale variations of the boundary-layer depth lead to spatial variations of cloud cover. The mesoscale variation of relative humidity measured by the aircraft are at constant level and do

Table 4.2: Midday cloud cover from aircraft and surface observations, and from the cloud formulation in the atmospheric boundary-layer model simulations for 12 days in HAPEX-MOBILHY.

date (1986)	ABL cloud cover obs.		cloud model simulations
	aircraft	surface	
9 May	0.37	0-0.70	1.00
19 May	0.07	0-0.05	0.12
21 May	0.40	0-0.70	0.98
24 May	0.33	0-0.75	1.00
25 May	0	0	0
30 May	0.50	0-0.85	0.45
6 June	0.73	0-0.85	1.00
13 June	0.03	0	0.62
16 June	0	0	0
19 June	<0.01	0-0.20	0.33
22 June	<0.01	0-0.35	1.00
1 July	0.48	0-0.30	0.56

not account for the need to obtain the relative humidity near the variable top of the boundary layer. Within the framework of the present model, this problem can be statistically reduced by specifying a larger value of the mesoscale variation of relative humidity. Increasing $\sigma_{RH_{meso}}$ widens the Gaussian distribution of relative humidity (Figure 4.4) which leads to more model prediction of partly cloudy conditions. However, the modeled relative humidity on several days is sufficiently greater or smaller than 1.0 so as not to be affected by even doubling $\sigma_{RH_{meso}}$. Therefore, adjustment of $\sigma_{RH_{meso}}$ is not adopted.

Model simulations are now conducted to examine the sensitivity of the fractional cloud cover formulation to changes of the mean vertical motion specified in the one-dimensional model. We incrementally change the vertical motion from -6.0 cm s^{-1} to $+2.0 \text{ cm s}^{-1}$ at 2 km to form a series of simulations. This is carried out for the 12 HAPEX-MOBILHY days (Figure 4.10). The change of cloud cover from clear to overcast is normally concentrated over a relatively narrow range of vertical motion values which defines a cloud transition. The values of the vertical motion defining the cloud transition range vary from day to day depending on boundary-layer characteristics. For example, an increase of vertical motion from 1.0 to 1.5 cm s^{-1} on 25 May leads to an increase of cloud cover from clear to overcast. The range of mean vertical motion values separating clear and cloudy conditions is proportional to the modeled standard deviation of relative humidity (3b, 13-16). However, typically a change of less than 1.0 cm s^{-1} can significantly alter the modeled relative humidity at the boundary-layer top, changing the cloud cover between clear and overcast. This change of vertical motion may be less than the accuracy to which it can be computed from observations. These tests underscore the sensitivity of boundary-layer growth and cloud cover to the vertical motion specified in the atmospheric boundary-layer model.

The specified values of vertical motion completely suppress modeled cloud development or initiate complete model cloud development (Table 4.2) on seven of the twelve days studied. Only in cases where the specified mean vertical motion corresponds to values in the cloud transition, is partial cloud cover predicted. Because of this sensitivity to vertical motion and the substantial uncertainties of the specified vertical motion, the testing of the cloud model appears inconclusive. The inability to assess the mean vertical motion in field programs may be a generic difficulty for testing models with field data in cloud transition cases.

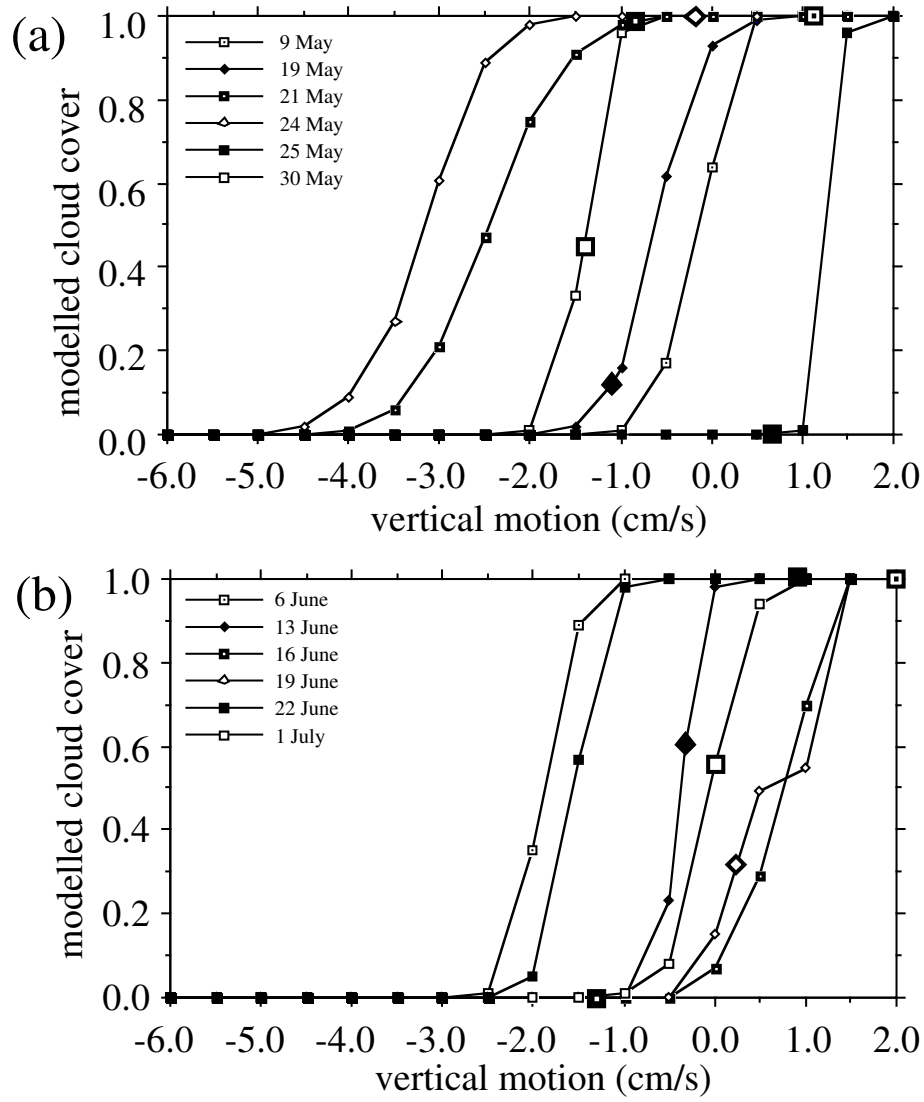


Figure 4.10: Fractional boundary-layer cloud cover and vertical motion at 2 km for model simulations during HAPEX-MOBILHY in (a) May and (b) June and July. Cloud cover values are averaged from 1300-1500 LST. Oversized symbols indicate the vertical motion value used in the model simulations of cloud cover shown in Table 4.2.

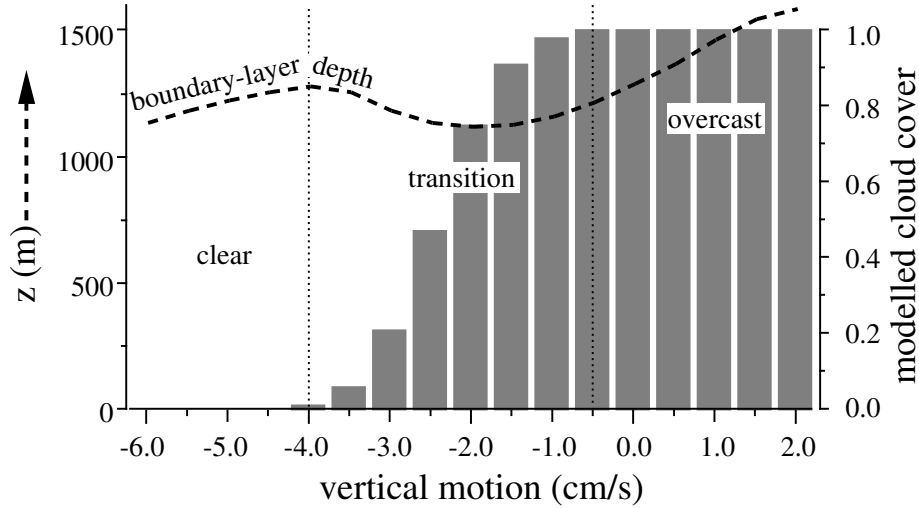


Figure 4.11: Relationship of the afternoon cloud cover and boundary-layer depth to the mean vertical motion for the 21 May 1986 set of model simulations using HAPEX-MOBILHY data.

Nevertheless, the model tests do indicate interesting interactions between cloud cover and vertical motion. For example, reduced subsidence normally leads to greater boundary-layer growth. However, cloud cover resulting from mean rising motion can eventually lead to smaller boundary-layer depths compared to the cloud-free cases with subsidence. With rising motion and cloud development, boundary-layer growth due to surface heating is reduced (Figure 4.11). Since the boundary layer in this case grows primarily due to the rising motion and not to entrainment, drying of the boundary layer by entrainment is reduced and the cloud cover is maintained resulting in smaller boundary-layer growth. Inverting this argument, the boundary layer may be deeper with weak subsidence than with weak rising motion because prevention of cloud cover leads to greater surface heating. Of course, with strong subsidence, the boundary layer becomes shallower compared to either the case of weaker subsidence or rising motion (Figure 4.11).

The neglect of horizontal advection in the model can also lead to large model errors for the boundary-layer depth and fractional cloud cover. For example on 22 June, omission of low-level horizontal advection of cool dry air in the model appar-

ently contributes to an overestimation of the boundary-layer depth by 700 m and false prediction of overcast when in fact observed clouds did not develop. On 21 May, omission of low-level horizontal advection of warm dry air may account for the underprediction of the boundary-layer depth by 600 m and prediction of nearly complete overcast compared to the observed cloud cover of 0.40. Inclusion of observed advection data described in Jacquemin and Noilhan (1990) fails to improve the model forecast on the first day, but dramatically improves the forecast on the second day. On the remaining 10 days, including the observed advection did not systematically improve model performance.

4.6 Conclusions

Spatially averaged boundary-layer cloud cover (A_c) is expected to depend on both the spatially averaged relative humidity (RH) and the spatial variability of RH (i.e. σ_{RH}). With greater σ_{RH} , clouds first form at a lower average relative humidity. In this study, the averaged RH is computed from spatially averaged aircraft measurements in the upper part of the boundary layer in HAPEX-MOBILHY. For this data, turbulent and mesoscale variations of RH contribute about equally to the total subgrid variation of RH and A_c for a hypothetical horizontal grid size of about 50-100 km. In the upper part of the boundary layer, σ_{RH} is large partly because of the significant moisture fluctuations and their negative correlation with temperature fluctuations.

From this data analysis, an expression for A_c is formulated in terms of turbulent variations of RH based on dry air entrainment and boundary-layer similarity theory. The subgrid mesoscale variation of RH is determined to be a function of horizontal grid size based on HAPEX-MOBILHY data. The data suggest that σ_{RH} varies significantly from day to day. Testing the A_c formulation in a one-dimensional atmospheric boundary-layer model indicates more sensitivity of the modeled cloud cover to the specified vertical motion field than to the adjustable coefficients of the cloud cover formulation. Horizontal advection of heat and moisture appear to be important on some of the days.

Section 4.2 examines simplified versions of the cloud cover formulation that neglect the variation of σ_{RH} which might be more appropriate when computing constraints are important. These studies should be extended to additional data sets to test the

performance of the proposed cloud cover formulation ((4.3)-(4.4), (4.16)-(4.19)) under more diverse geographic and atmospheric conditions. Future observations which emphasize cloud base statistics would reduce uncertainties apparent in the above studies.

Acknowledgements. The useful comments of A. A. M. Holtslag, Sam Chang, Ken Yang, and James Coakley are greatly appreciated, as well as the computational work of Wayne Gibson and technical assistance provided by Susanna M. Bremer and Jacob H. Jensen. This material is based upon work supported by the Phillips Laboratory under contract F19628-88-K-001, and the National Science Foundation under grant ATM-8820090. The National Center for Atmospheric Research is acknowledged for computer resources and the use of the King Air research aircraft in HAPEX-MOBILHY.

Chapter 5

Evaluation of a land-surface scheme at Cabauw

This chapter is published as Ek, M., and A. A. M. Holtslag, 2005: Evaluation of a land-surface scheme at Cabauw. *Theoretical and Applied Climatology*, **80**, 213-227, doi:10.1007/s00704-004-0101-4.

©Copyright 2005 by Springer-Verlag

Abstract

We study the response of the land-surface to prescribed atmospheric forcing for 31 May 1978 at Cabauw, Netherlands, using the land-surface scheme from the Coupled Atmospheric boundary layer - Plant - Soil (CAPS) model. Results from model runs show realistic daytime surface fluxes are produced using a canopy conductance formulation derived from Cabauw data (for 1987, a different year), and *un-tuned* parameterizations of root density (near-uniform with depth) and soil heat flux (reduced thermal conductivity through vegetation). Sensitivity of model-calculated surface heat fluxes to initial values of soil moisture is also examined. Results of this study provide the land-surface "base state" for a coupled land-atmosphere modeling study.

5.1 Introduction

Land-surface schemes are an important part of the parameterization in any atmospheric model, and as such, their evaluation has received much attention (e.g. see the PILPS overviews by Henderson-Sellers et al 1993, 1995). Often these schemes are evaluated for a long period of time, however, mostly only limited long-term data sets are available to test the details of the schemes. In this paper we focus on an evaluation of a state-of-the-art land-surface scheme for a daytime case at Cabauw, Netherlands, but explore the details with an extensive data set. Using *a priori* formulations and parameters for the important land-surface processes, we test sensitivities of modeled surface fluxes. The diurnal variation of the land surface is an important issue because of its influence on atmospheric boundary-layer (ABL) development (e.g., see Ek and Holtslag 2004).

Developments in numerical weather prediction (NWP) and atmospheric climate models have focused increased attention on land-surface processes (e.g. Viterbo and Beljaars 1995 and references therein). Many of these developments have been pursued in an effort to bring the parameterization of land-surface processes within NWP models in line with developments in the plant and soil physics communities, thereby recognizing progress in these associated disciplines. For example, Ek and Cuenca (1994) and Cuenca et al (1996) examined the response of the ABL to variations in soil hydraulic properties; Peters-Lidard et al (1997, 1998) examined the effect of vegetation and soil thermal properties on soil heat flux; and Beljaars and Bosveld (1997) examined the influence of evaporative control on surface moisture flux by the vegeta-

tion at Cabauw.

The case study by Holtslag et al (1995) examined ABL model runs driven by observed surface fluxes, and reproduced the observed boundary-layer structure for a case study at Cabauw reasonably well. But in coupled land-surface – ABL model runs they found that they could not reproduce observed fluxes and boundary-layer structure using a simpler land surface scheme. Here we use the same case study day as Holtslag et al (1995), but use the more sophisticated land-surface scheme from the Coupled Atmospheric boundary layer-Plant-Soil (CAPS) model originally developed at Oregon State University. This land-surface scheme has been used in a stand-alone mode for a number of sensitivity experiments under different geophysical conditions (e.g. Kim and Ek 1995, Chen et al 1996) and as part of the Project for Intercomparison of Land-surface Parameterization Schemes (PILPS, e.g. Chang and Ek 1996a, T. H. Chen et al 1997, Liang et al 1998, Lohmann et al 1998, Qu et al 1998, Wood et al 1998, Chang et al 1999); the study by Chang et al (1999) includes a comprehensive description of the current physics in the CAPS model land-surface scheme.

The purpose of this study is to examine "stand-alone" (or "offline") model runs of the CAPS model land-surface scheme forced by observed atmospheric and downward radiation measurements at Cabauw to assess the ability of our scheme to properly partition the incoming radiation into surface heat fluxes and outgoing radiation. Specifically, we will explore assumptions made and examine alternatives for (1) canopy conductance (which affects the partition between latent and sensible heat flux), (2) root density characterization, and (3) soil heat flux parameterization. These tests allow us to isolate the processes responsible for surface fluxes without ABL interaction in an attempt to determine the "best" version of the land-surface scheme for coupling with the ABL (e.g., as in Ek and Holtslag 2004). We first describe the data set at Cabauw (section 5.2), then give an overview of the components in the CAPS model land-surface scheme relevant to this study (section 5.3), followed by model sensitivity runs (section 5.4), and then a summary (section 5.5).

5.2 Cabauw site and data set

In this study we use observations made on 31 May 1978 at the Cabauw site in central Netherlands that provide a comprehensive data set for model initialization and verification. The region surrounding the Cabauw site is rather flat for a distance of at least

20 km, with many fields and scattered canals, villages, orchards and lines of trees. One of the main branches of the Rhine, the River Lek, flows about one kilometer south of the Cabauw site, approximately 45 km east of the North Sea.

The Cabauw site itself is located in an open field nearly completely covered by short grass which extends for several hundred meters in all directions, and a series of shallow, narrow ditches that provide drainage for the site. Under the sod layer (3 cm) the soil consists of heavy clay down to about 0.6 m, with a nearly saturated peat layer below. Soil moisture measurements using neutron probe were taken covering the study day at three sample sites in the micromet tower plot adjacent to the Cabauw tower; measurements were made at 10 cm intervals down to 50 cm, and at 1 m (Wessels 1983). While 31 May 1978 was during the beginning of a "dry-down" period, soil moisture values were still sufficiently high so that transpiration was not overly limited. There had not been any precipitation for a week, and this was to last three more weeks into later June before the next substantial precipitation event.

The 213 m tower at the Cabauw site includes sensible and latent heat fluxes determined from profile and Bowen ratio methods. Incoming solar and longwave radiation, low-level surface and soil temperatures, and low-level specific humidity measurements were made at the micrometeorological site adjacent to the Cabauw tower (within 200 m). The downward longwave radiation is suspect, however, being anomalously low. An estimate of downward longwave radiation is made as a residual by taking the difference between the observed net radiation, and the sum of the net solar radiation and outgoing terrestrial (longwave) radiation (computed from the infrared radiometer assuming an emissivity of one). Soil heat fluxes were measured by transducers buried at depths of 5 and 10 cm; surface soil heat flux was inferred from extrapolation of these measurements (Beljaars and Bosveld 1997). See Monna et al (1987) and Wessels (1984) for further information on Cabauw observations.

5.3 Land-surface scheme

The CAPS model land-surface scheme consists of multiple soil layers (Mahrt and Pan 1984), and a simple plant canopy (Pan and Mahrt 1987) modified to include the effect of vegetation using a "big leaf" approach for canopy conductance (inverse of canopy resistance) following Noilhan and Planton (1989, hereafter NP89) and Jacquemin and Noilhan (1990). This more empirically-based approach for canopy conductance fol-

lows the original work by Jarvis (1976) and Stewart (1988) where canopy conductance is modeled as a function of atmospheric forcing and soil moisture availability. Alternate more recent "physiologically-based" formulations for canopy conductance as a function of CO₂ assimilation will not be utilized in this study, e.g. Jacobs (1994), Sellers et al (1996), Sen et al (2000), Ronda et al (2001).

5.3.1 Transpiration and canopy conductance

Evaporation in our scheme is calculated as

$$E = \beta_{E_p} f_{\Theta} E_p, \quad (5.1)$$

where β_{E_p} is the potential evaporation fraction, f_{Θ} is the fractional availability of root-zone soil moisture (described further below), and E_p is the potential evaporation (a function of atmospheric forcing). The potential evaporation fraction, β_{E_p} , is the ratio of actual evaporation to the potential evaporation and accounts for the reduction in actual evaporation from potential evaporation due to the stomatal control by plants, here related to *atmospheric* conditions; β_{E_p} can be related to canopy conductance (g_c) by equating the bulk aerodynamic forms of E and $\beta_{E_p} E_p$ which yields

$$\begin{aligned} \beta_{E_p} &= E/E_p \\ &= \frac{(\rho \delta q)/(1 + g_a/g_c)}{\rho g_a \delta q} \\ &= \frac{g_c}{g_c + g_a}, \end{aligned} \quad (5.2)$$

where ρ is air density, δq is the land-atmospheric specific humidity deficit, and g_a is aerodynamic conductance (inverse of aerodynamic resistance), the product of the wind speed and the surface exchange coefficient, which in turn is a function of surface roughness and atmospheric stability via Monin-Obukhov similarity theory. Surface exchange coefficients (and thus surface fluxes) are calculated by iterating an implicit formula of the Monin-Obukhov similarity functions described in Beljaars and Holtslag (1991)¹.

¹This replaces the previous method in our scheme which used an explicit dependence on the near-surface bulk Richardson number to determine surface exchange coefficients following Louis (1979) and Louis et al (1982). This step was taken because of a limitation in the application of the Louis formulation for cases where the ratio of the momentum to heat roughness is large, as demonstrated in Holtslag and Ek (1996), and explored further in van den Hurk and Holtslag (1997). See Beljaars and Holtslag (1991) for further discussion on this issue as applied to the Cabauw site.

The "big-leaf" development for canopy conductance by NP89 follows the original approach of Jarvis (1976) and Stewart (1988) where canopy conductance (g_c) is modeled as a function of the species-dependent maximum stomatal conductance (g_{cmax}) and several reduction factors as

$$g_c = g_{cmax} f_{S\downarrow} f_T f_q, \quad (5.3)$$

where $f_{S\downarrow}$, f_T , and f_q are functions of atmospheric forcing (incoming solar radiation, air temperature, and atmospheric vapor pressure deficit, respectively), all functions of plant species, with values between 0 and 1. (In our scheme we exclude the usual dependence of g_c on root-zone soil moisture availability, f_Θ , and instead include it directly as a linear reduction factor in the calculation of E via (5.1).) As an alternate to NP89 (yet still following the Jarvis-Stewart approach), we also include the Cabauw-specific canopy conductance formulations for *atmospheric* forcing (as in (5.3)) derived by Beljaars and Bosveld (1997, hereafter BB97) based on an evaluation of the annual 1987 Cabauw data set used in PILPS phase 2a (hereafter PILPS2a, T. H. Chen et al 1997). (Note that the BB97 parameterization for canopy conductance is based on an annual data set from 1987, a year different from our case study.) The NP89 and BB97 canopy conductance functions for atmospheric forcing are

factor	NP89 formulation	BB97 formulation
$f_{S\downarrow} =$	$(a + \frac{g_{cmax}}{g_{cmin}})(a + 1)^{-1}$	$(\frac{S\downarrow(b_{1S\downarrow} - b_{2S\downarrow})}{b_{1S\downarrow}S\downarrow + b_{2S\downarrow}(b_{1S\downarrow} - 2S\downarrow)})$
$f_T =$	$1.0 - a_T(T_{ref} - T_a)^2$	1.0
$f_q =$	$1 - a_q(\delta e)$	$(1 + b_q(\delta q_a - \delta q_r))^{-1}$

(5.4)

where $a = (1.1/LAI)(S\downarrow/a_{S\downarrow})$, LAI is leaf area index, $S\downarrow$ is incoming solar radiation, T_a , δe_a and δq_a are the air temperature, and atmospheric vapor pressure and specific humidity deficits, respectively, at the first model level (i.e. 20 m in the study here), and the other coefficients and constants are defined in Table 5.1.

The expression for root-zone soil moisture availability (f_Θ) included in (5.1) is

$$f_{\Theta_i} = \left\{ \begin{array}{ll} 1 & \Theta_i \geq \Theta_{fcp} \\ \frac{\Theta_i - \Theta_w}{\Theta_{fcp} - \Theta_w} & \Theta_w < \Theta_i < \Theta_{fcp} \\ 0 & \Theta_i \leq \Theta_w \end{array} \right\}, \quad (5.5)$$

Table 5.1: CAPS model land-surface scheme parameters for Cabauw. Note that λ_{T0} is the initial value corresponding to the Cabauw soil type and initial soil moisture content in the upper soil layer.

description	parameter	value	units
vegetation fraction	σ_f	0.97	-
momentum roughness	z_{0m}	0.15	m
thermal roughness	z_{0h}	2.35×10^{-5}	m
soil moisture (nondimensional volumetric)			
porosity	Θ_{sat}	0.600	-
field capacity	Θ_{fc}	0.491	-
wilting point	Θ_{wilt}	0.314	-
vegetation: NP89 formulation with Cabauw (PILPS2a) parameter set			
maximum canopy conductance	g_{cmax}	0.0426	m s^{-1}
minimum canopy conductance	g_{cmin}	5×10^{-5}	m s^{-1}
leaf area index	LAI	1.7	-
solar coefficient	$a_{S\downarrow}$	100	W m^{-2}
thermal coefficient	a_T	0.0016	K^{-2}
reference temperature	T_{ref}	298.0	K
humidity coefficient	a_q	0.024	mb^{-1}
vegetation: BB97 formulation with Cabauw parameter set			
maximum canopy conductance	g_{cmax}	0.0386	m s^{-1}
solar coefficient 1	$b_{1S\downarrow}$	1000	W m^{-2}
solar coefficient 2	$b_{2S\downarrow}$	230	W m^{-2}
humidity coefficient	b_q	0.02	kg g^{-1}
humidity deficit threshold	δq_r	3.0	g kg^{-1}
soil heat flux			
bare soil thermal conductivity	λ_{T0}	0.601	$\text{W m}^{-1} \text{K}^{-1}$
thermal conductivity coefficient	Λ_T	7.0	$\text{W m}^{-2} \text{K}^{-1}$

where Θ , Θ_{fcp} , and Θ_w are the volumetric soil moisture contents corresponding to the actual, field capacity, and wilting point values, respectively, and the subscript i refers to a given soil layer in the root zone. The total effect (i.e. on transpiration) of root-zone soil moisture availability is then determined by summing f_{Θ_i} over all (root-zone) soil layers as

$$f_{\Theta} = \sum_{i=1}^n N_i f_{\Theta_i}, \quad (5.6)$$

where n is the total number of soil layers in the root zone (three in the study here, with one subroot layer, so four total soil layers), and N_i is the fractional root density for a particular soil layer ($\sum N_i = 1$).

5.3.2 Root density and soil hydraulics

Studies have shown the relevance of root density distribution for improved transpiration modeling (i.e. Ács 1994, Viterbo and Beljaars 1995, Desborough 1997, Colello et al 1998). A uniform root density is assumed where soil layers in the root zone are equally-weighted by their fraction of the total root zone depth. A non-uniform root density may be specified which varies with depth; this is commonly done in many land-surface schemes so that the relative contribution of a particular soil layer to the total transpiration is non-uniform. A non-uniform fractional root density may lead to non-uniform (for a given soil layer) depletion of soil moisture in the root zone, which may be realistic in that plants often have a higher root density near the surface.

For the PILPS2a numerical experiments at Cabauw (T. H. Chen et al 1997), it was suggested that plants could be represented by 70 percent root density in the upper 10 percent of the root zone, and 30 percent in the lower 90 percent of the root zone. As an additional comparison, the land-surface scheme in the ECMWF model had assumed one-third of the root density in each of the three root zone soil layers which corresponds to a decreasing root density with depth since the soil layer thickness increases with depth (Viterbo and Beljaars 1995); this has been updated to account for differences between vegetation types (van den Hurk et al 2000).

In contrast, a general concept commonly used among plant and soil scientists (Richard Cuenca 1999, personal communication) suggests that the fractional root density is assumed to be 40 percent in the upper quarter of the root zone, with the fractional root density decreasing by 10 percent with each subsequent quarter

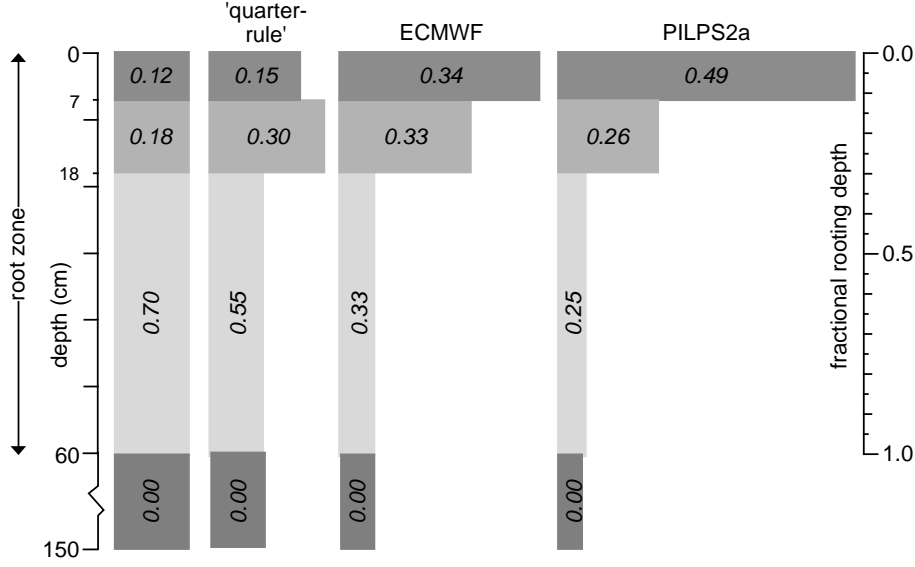


Figure 5.1: Schematic representation of various choices for root density distributions for soil layers in the CAPS model land-surface scheme.

of the soil root zone depth. This "quarter-rule", distribution is much closer to the uniform-with-depth root distribution than in the ECMWF model, or that suggested for PILPS2a at Cabauw. A variation on the quarter-rule root distribution is to exclude the "sod" layer which contains no roots (i.e. the upper 3 cm of the root zone at Cabauw, BB97). For the quarter-rule root distribution used in this study, we take the average root density of the two root density distributions which average both the inclusion and exclusion of the sod layer, which leads to a slightly higher root density in the second soil layer. Figure 5.1 shows a schematic representation of the various root distributions with depth.

It should be pointed out that our function for root-zone soil moisture availability (5.5), depends on *relative* soil moisture availability in the root zone and is retained over the corresponding BB97 function derived for Cabauw (formulation not shown) which depends on the *actual* volumetric soil moisture content. The rationale for this is as follows: since no soil moisture measurements were available at Cabauw for 1987, the f_{Θ} function derived by BB97 was based on ECMWF model-generated soil moisture output. The ECMWF model uses soil-texture-specific hydraulic properties (e.g.

saturated soil moisture content) following Clapp and Hornberger (1978) (or Cosby et al 1984), an approach commonly used in the meteorological land-surface modeling community. However, for the Cabauw site, *in situ* measurements of soil moisture at Cabauw are not consistent with the "standard" values cited in Clapp and Hornberger for a heavy clay soil found at the Cabauw site, e.g. for 31 May 1978 the soil moisture content in lower soil layers at Cabauw *exceeds* the saturated volumetric soil moisture content according to the "standard" clay values cited in Clapp and Hornberger, i.e. $\Theta_{sat} = 0.468$ (Figure 5.2). As such, we must either make some sort of relative adjustment to the Clapp and Hornberger approach to make it applicable to Cabauw, or find a suitable alternative. Since the Cabauw soils have been evaluated in terms of a van Genuchten (1980) formulation for soil hydraulic processes, we adopt this method using locally-derived parameters specific to the clay soils at Cabauw (Jager et al 1976)².

As noted earlier, the Cabauw soil has a heavy clay content in the root zone (upper 60 cm), with an increasing peat content below this level in the subroot zone. In its current form, our land-surface scheme does not accommodate different soil textures with depth, so we must choose soil properties that most appropriately represent the soil at Cabauw for the purposes of this study. On shorter (e.g. diurnal) time scales the root zone will have more direct interaction with the atmosphere through plant transpiration, as compared to the subroot zone which operates on longer (e.g. seasonal) time scales. As such in this study we adopt the properties of a clay soil. We choose the specific soil parameters for the 18-60 cm soil layer at Cabauw, as opposed to the 0-18 cm layer (which differ slightly), since the 18-60 cm layer (although with a lower root density than the 0-18 cm layer) is still expected to dominate root zone processes because of a greater thickness and overall root content.

5.3.3 Soil thermodynamics

Soil heat flux (G) is often formulated (i.e. from McCumber and Pielke 1981, following Al Nakshabandi and Khonke 1965) as

$$G = \lambda_{T0} \Delta T / \Delta z, \quad (5.7)$$

²An advantage in using van Genuchten (over Clapp and Hornberger) is that van Genuchten is more widely accepted in the soil physics community, with many soil data sets evaluated in terms of van Genuchten, including Cabauw. See BB97 for details on Cabauw soils and the van Genuchten formulation applied to Cabauw soils.

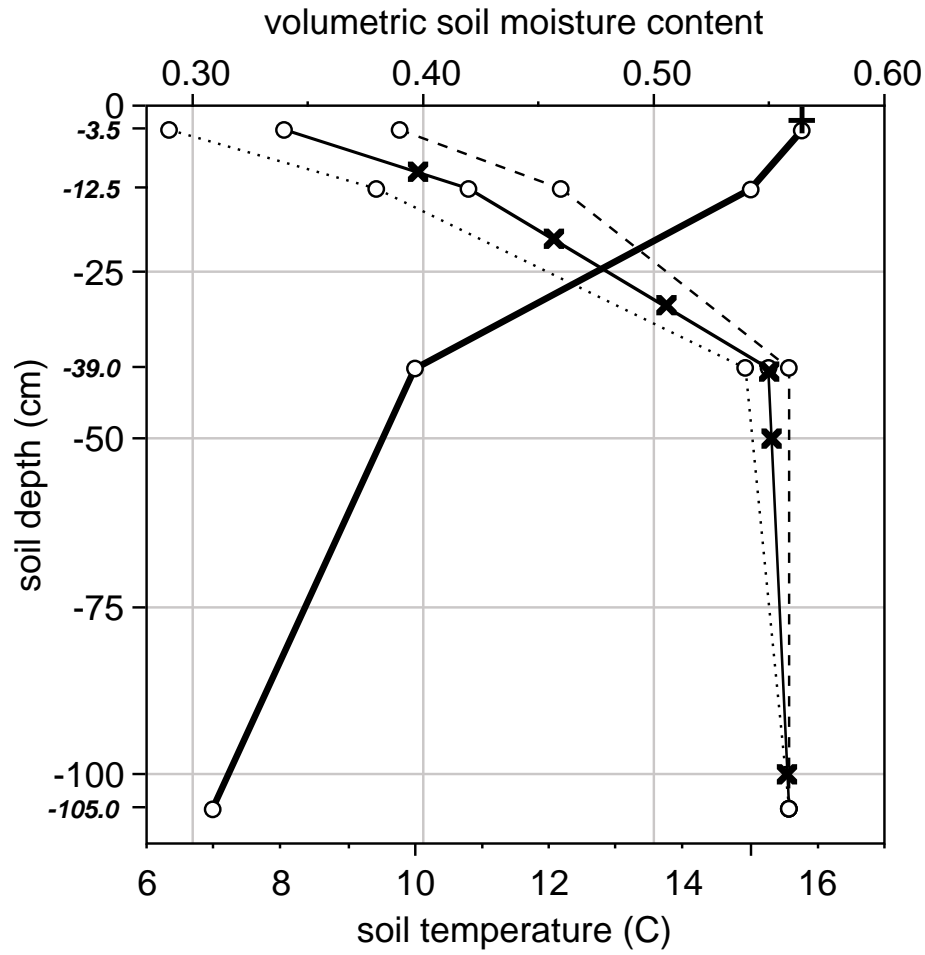


Figure 5.2: Initial soil moisture profiles for 31 May 1978 at Cabauw, Netherlands: observed (\times), initial model soil moisture reference profile interpolated to model soil level mid-points (\circ & solid line), and drier and wetter initial soil moisture profiles used in sensitivity tests (\circ & dotted line, and \circ & dashed line, respectively); and observed soil temperature at -2 cm (+) and initial model soil temperature reference profile (\circ & heavy solid line).

where λ_{T0} is the "bare-soil" thermal conductivity (a function of soil texture and soil moisture content), and $\Delta T/\Delta z$ is the temperature gradient between the surface and center of the upper soil layer. However, in the presence of a vegetation layer, soil heat flux is reduced because of lowered heat conductivity through vegetation (Peters-Lidard et al 1997, and others). This has been demonstrated by Viterbo and Beljaars (1995) in the ECMWF model land-surface scheme where they suggest a simpler formulation to deal with this effect where G is computed as the product of an empirical coefficient (appropriate to Cabauw) and the temperature difference between the surface and the (center of the) upper soil layer (3.5 cm), i.e.

$$G = \Lambda_T \Delta T, \quad (5.8)$$

where Λ_T is a fixed constant "thermal conductivity" (Table 5.1). This formulation draws upon earlier work by van Ulden and Holtslag (1985), and implicitly accounts for the reduction of soil heat flux in the presence of vegetation. Van den Hurk et al (1995), van den Hurk and Beljaars (1996), and van den Hurk et al (2000) describe refinements to this approach where the value of Λ_T varies depending on land-surface classification, e.g. bare ground, sparse vegetation, etc.

5.3.4 Model geometry and initial conditions

We set the depth of the first soil layer in our model the same as in the ECMWF model (7 cm) in order to use the same coefficient (Λ_T) to calculate soil heat flux at Cabauw since this coefficient was calibrated for a 7-cm depth (section 5.3.3). Following BB97, our subsequent soil layers match the bottom of the "higher root density" zone (18 cm depth), a zone of "lower root density" down to the bottom of the root zone (60 cm), with a subroot zone below (1.5 m total depth), and an implicit soil column bottom (for temperature) at 3.0 m (see Figure 5.1).

We initialize our land-surface scheme using soil moisture observations interpolated to the mid-point of the model soil levels (Wessels 1983, Figure 5.2). (Sensitivity of the initial soil moisture conditions will also be explored.) Soil temperature is initialized at the first model soil layer (-3.5 cm) using -2 cm observations; this difference is not expected to be significant at this time of day. Soil temperature observations are not available below 2 cm, so to initialize soil temperatures at subsequent model soil levels we make approximations from the average of the previous week, month, and three-months 2-m air temperatures, respectively, for the lowest three model levels, with the

annual 2-m air temperature used as the implicit bottom temperature.

5.4 Land-surface modeling sensitivity tests

5.4.1 Canopy conductance

Before making any model runs, we first examine the observed daytime evolution of surface conductance which can be determined by inverting the Penman-Monteith equation (Monteith 1965) using the observed surface fluxes, temperature and specific humidity measurements, given the surface roughness for momentum (z_{0m}) and heat (z_{0h}) for the Cabauw site (i.e. from Beljaars and Holtslag 1990, Beljaars and Holtslag 1991, De Rooy and Holtslag 1999). This yields a surface conductance directly inferred from observations ("observed" in Figure 5.3) along with an inferred aerodynamic conductance (g_a , not shown). The surface conductance values here are negligibly affected by bare soil fluxes since the vegetation fraction at Cabauw is very nearly equal to one, hence the surface conductance is essentially a bulk *canopy* conductance (g_c). (Unlike canopy conductance, modeled values of g_a cannot be explicitly determined *a priori* in the same manner. Subsequent model runs yield g_a values somewhat underpredicted, though not significantly. As such, use of the prescribed wind speed and the apparently appropriate surface layer stability formulation are suitable for our model runs.)

We test the modeled canopy conductance formulations described in section 5.3 using observations taken throughout the day (31 May 1978) at Cabauw necessary for these formulations. We use a combined approach with BB97 for maximum canopy conductance (g_{cmax}) and the effect of atmospheric conditions on canopy conductance ($f_{S\downarrow}$, f_T , f_q in (5.3)), our expression for the effect of root-zone soil moisture availability on evaporation ((5.1) and (5.5)) using observed soil moisture (Figure 5.2), and the quarter-rule root distribution (all described previously in section 5.3). With this approach (hereafter the "reference" canopy formulation), we see that the canopy conductance is somewhat underpredicted in the morning hours, and slightly overpredicted in the afternoon, though still quite adequately represented (Figure 5.3). It is important to re-emphasize that the reference canopy conductance here is calibrated to Cabauw for a 1987 data set, but not specifically to our 31 May 1978 case study day.

The formation of overnight dew and subsequent evaporation from the grass canopy during the first few hours after sunrise is a possible explanation for the lower-than-

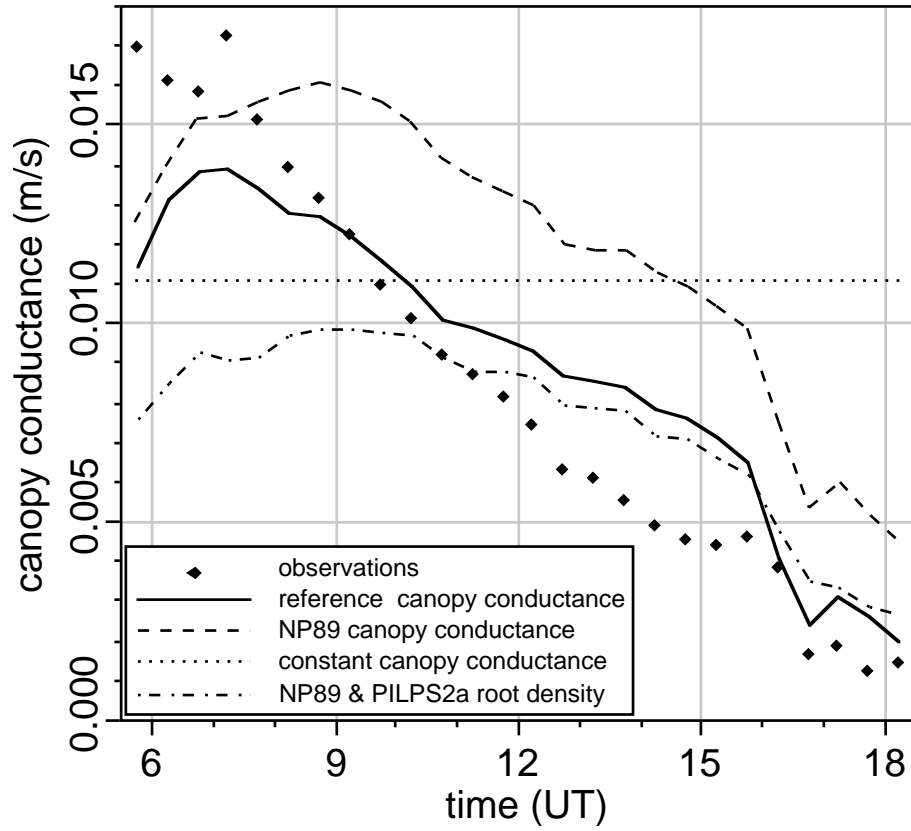


Figure 5.3: Canopy conductance inferred from observations for 31 May 1978 at Cabauw (solid diamonds), versus different canopy conductance formulations: reference approach (solid line), NP89 with quarter-rule root density (dashed line), NP89 with PILPS2a root density (dot-dashed line), and constant canopy conductance (dotted line). See text for further details.

observed values of modeled canopy conductance during 06-09 UT (Figure 5.3). That is, there may be an underestimation of the observed canopy conductance due to evaporation of canopy water after 06 UT, where evaporation of canopy water has a larger moisture conductance value than the conductance for plant transpiration. Lacking an explicit measurement or indicator of canopy wetness, we utilize nighttime observations of the latent heat flux to estimate the canopy water content, which for a period from 00-04 UT was downward (suggesting dewfall). However, calculations indicate that subsequent evaporation starting after 04 UT would have been sufficient to evaporate the accumulated canopy water before 06 UT, the initial time for model runs. As such, our underestimation of canopy conductance during the 06-09 UT period may be attributable to some other reason, perhaps less certainty in the observed surface fluxes at this time.

We also use the NP89 formulation (section 5.3.1) for the effect of atmospheric conditions on canopy conductance with the corresponding PILPS2a parameter set for Cabauw which was based on a "standard" grassland category ((5.3); Table 5.1), but using our expression for the effect of root-zone soil moisture availability on canopy conductance, and the quarter-rule root distribution. (In this way, it represents a "fair" test between the BB97 and NP89 canopy conductance formulations for the atmospheric part of the canopy conductance formulations.) In this case the NP89/PILPS2a-Cabauw formulation greatly overpredicts the canopy conductance throughout most of the day. For comparison, the PILPS2a root distribution is substituted for the quarter-rule root distribution, and yields a canopy conductance that is underpredicted in the morning hours, with conductance values similar to the reference canopy conductance approach during the afternoon hours.

Using our reference approach for canopy conductance described above (and in section 5.3.1), the quarter-rule root distribution (section 5.3.2), and the ECMWF soil heat flux formulation (section 5.3.3), we drive our land-surface scheme using the observed atmospheric forcing and downward radiation measurements (Figure 5.4) at the Cabauw site at each timestep (hereafter our "reference" model run). This allows us to evaluate the model performance in terms of its ability to properly partition available incoming energy into upward longwave radiation, and sensible, latent, and soil heat fluxes without ABL interaction. In our reference model run, a slight underprediction in canopy conductance in the morning (Figure 5.3) leads to an underprediction of the latent heat flux with the opposite case during the afternoon, while sensible heat flux is

generally well-predicted, though slightly high during mid-day (Figure 5.5). Replacing the reference approach for canopy conductance with that by NP89 for Cabauw via PILPS2a, the latent (*sensible*) heat flux is slightly under (*similarly*) predicted in the morning, though greatly over (*under*) predicted in the afternoon. (The effect of using the PILPS2a root distribution will be explored in section 5.4.2.)

Using a constant value for canopy conductance (Figure 5.3) represents the average value for this particular day fairly well, though it underpredicts the observed canopy conductance in the morning and overpredicts canopy conductance in the afternoon, with a corresponding slight under (*similar*) prediction of the latent (*sensible*) heat flux in the morning, and a stronger over (*under*) prediction in the afternoon (Figure 5.5). This is consistent with the findings of Holtslag et al (1995) for this same case study day, though in their coupled land-atmosphere model runs the biases were more exaggerated due to apparently unfavorable feedbacks between the ABL and their simpler representation of the land surface.

The results here suggest that our reference approach for canopy conductance at Cabauw, along with the quarter-rule root distribution and the ECMWF soil heat flux formulation, is the better choice as our reference model run, which we will then compare with subsequent model runs in this study. Three additional sets of sensitivity tests are made where we explore the effect on the surface fluxes of using alternate representations of root distribution, of soil heat flux, and finally sensitivity to initial soil moisture conditions.

5.4.2 Root distribution

We again drive our land-surface scheme using the observed atmospheric forcing at the Cabauw site, and explore the effect of using different root density distributions. A uniform-with-depth root density distribution yields results that are similar to the reference model run (which uses the quarter-rule root distribution), while using the PILPS2a root distribution yields latent (*sensible*) heat fluxes which are greatly under (*over*) predicted throughout the day (Figure 5.6). For the case using the PILPS2a root distribution, soil moisture in the upper soil layers with much higher root density is more quickly depleted (Figure 5.7), leading to the underprediction of the latent heat flux and a subsequent overprediction of the sensible heat flux. The re-charge of soil moisture in the upper soil layers is most notable during 06-09 UT, but continues

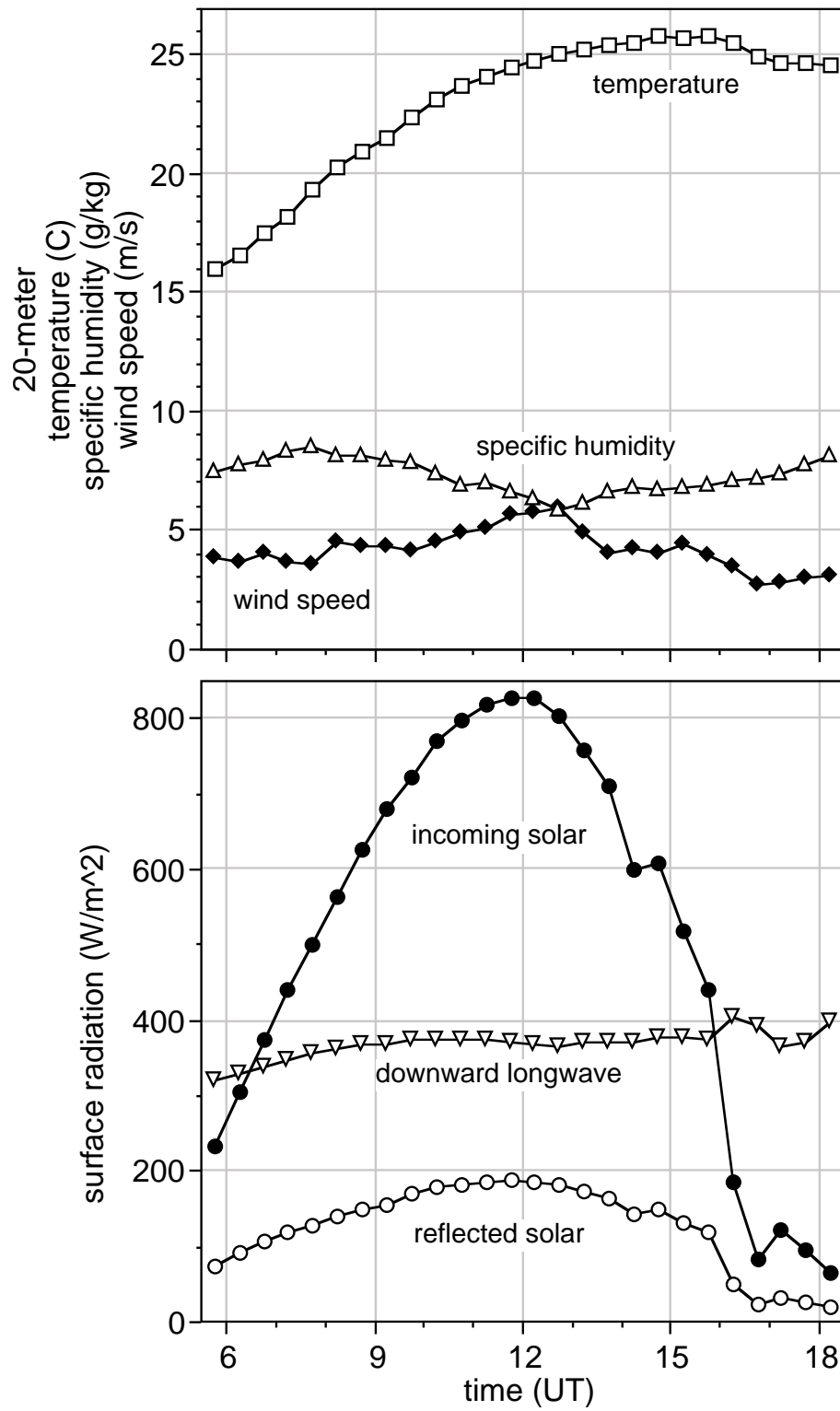


Figure 5.4: Atmospheric forcing data for 31 May 1978 at Cabauw, Netherlands: (a) 20-meter temperature, specific humidity, and wind speed, and (b) incoming and reflected solar and downward longwave radiation.

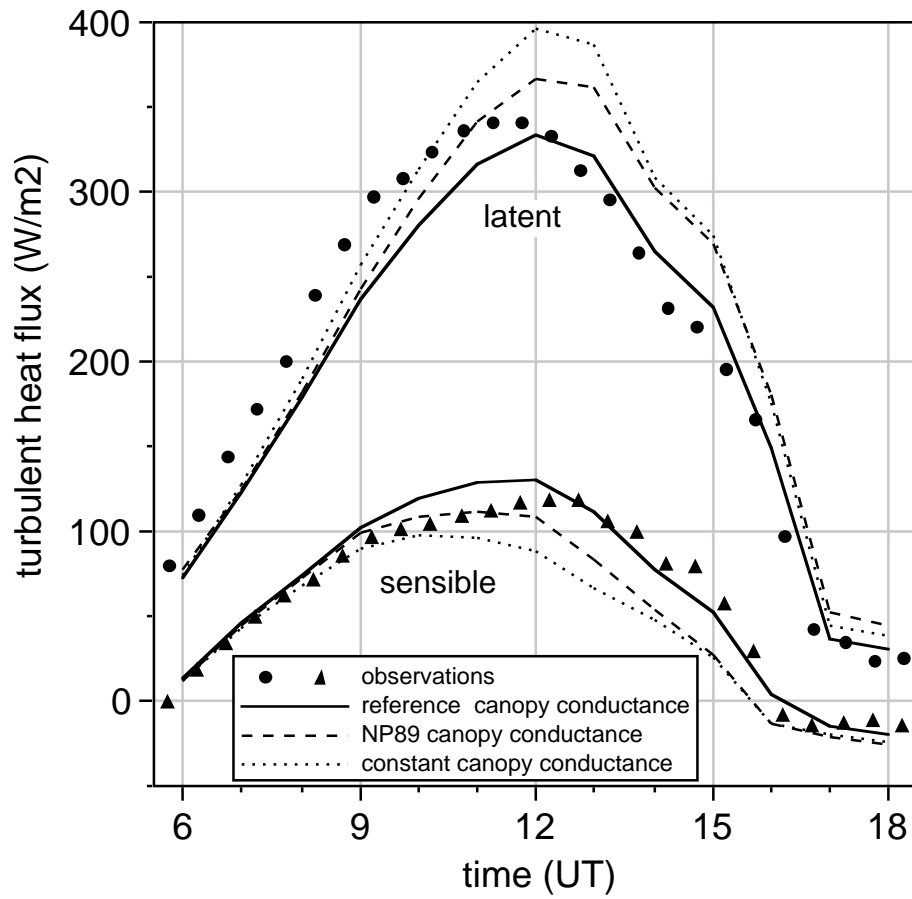


Figure 5.5: Observed latent (•) and sensible (solid triangles) heat fluxes, versus modeled heat fluxes for different canopy conductance tests: reference approach (solid line), NP89 with quarter-rule root density (dashed line), and constant canopy conductance (dotted line) for 31 May 1978 at Cabauw, Netherlands.

throughout the day for the quarter-rule or uniform-with-depth root distributions because of an excess in upward diffusion of soil moisture over soil moisture loss through drainage, and transpiration and direct soil evaporation. Lacking sub-diurnal time-scale observations of soil moisture makes it difficult to assess the nature of diurnal soil moisture evolution, though there is evidence that such soil moisture re-charge processes do occur (Richard Cuenca 2001, personal communication).

With both the quarter-rule, or with a uniform-with-depth root distribution, soil moisture from *deeper* soil layers is more available for transpiration, and is thus depleted more than with the non-uniform PILPS2a root distribution (Figure 5.7). The PILPS2a root distribution, with excessively high root density near the surface, may lead to improper rapid drying of the higher-root-density soil layers in the root zone (Zeng et al 1998). This can yield less accurate predictions of latent heat flux, and subsequently the surface energy budget. In the study here, our assumption of a near-uniform root distribution (a so-called "bulk method") is more consistent with the current level of understanding and thus preferred over root-weighted (non-uniform) methods (Desborough 1997). This may mitigate the problem of treating the root zone as static when in fact it may be rather dynamic in terms of the ability of vegetation to extract water from where it is available in the root zone, despite the root density distribution. In the case of a more non-uniform root distribution, it seems that in coupled land-surface – ABL model runs the evolution of the daytime ABL would be adversely affected, i.e. greater ABL growth due to greater sensible heat flux, though a potentially drier ABL due to smaller latent heat flux.

5.4.3 Soil heat flux

Modeled surface fluxes using the ECMWF soil heat flux formulation (representing the reference model run; section 5.3.3) are found to more closely approximate observed values, though slightly out of temporal phase (Figure 5.8). However, for the case of the soil heat flux formulation for bare soil, the soil heat flux is excessively overpredicted, and as a result of so much more energy going into soil heat flux, both the latent and sensible heat fluxes are significantly underpredicted during most of the day. Net radiation is also modeled well (not shown) indicating that the upward longwave radiation is properly represented. (Recall that the other radiation fluxes are prescribed).

For the case where the soil heat flux formulation for bare soil is used, the thermal

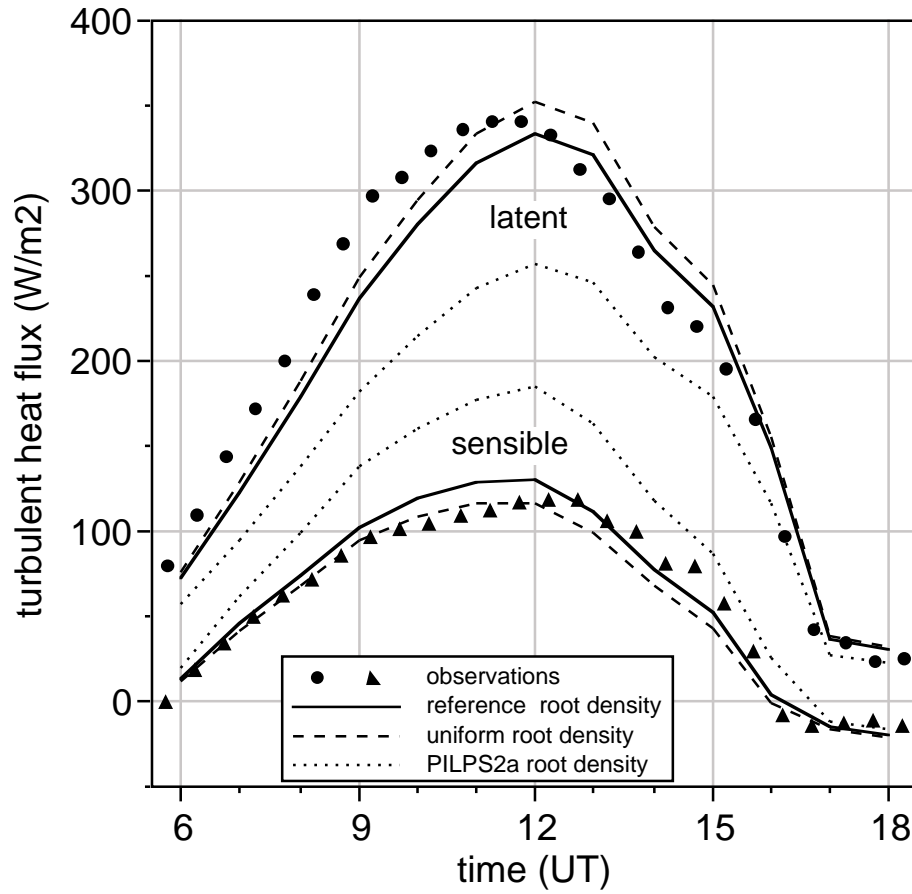


Figure 5.6: Observed latent (•) and sensible (solid triangles) heat fluxes, versus modeled heat fluxes for different root density tests: quarter-rule (solid line), uniform (dashed line), and PILPS2a (dotted line) for 31 May 1978 at Cabauw, Netherlands.

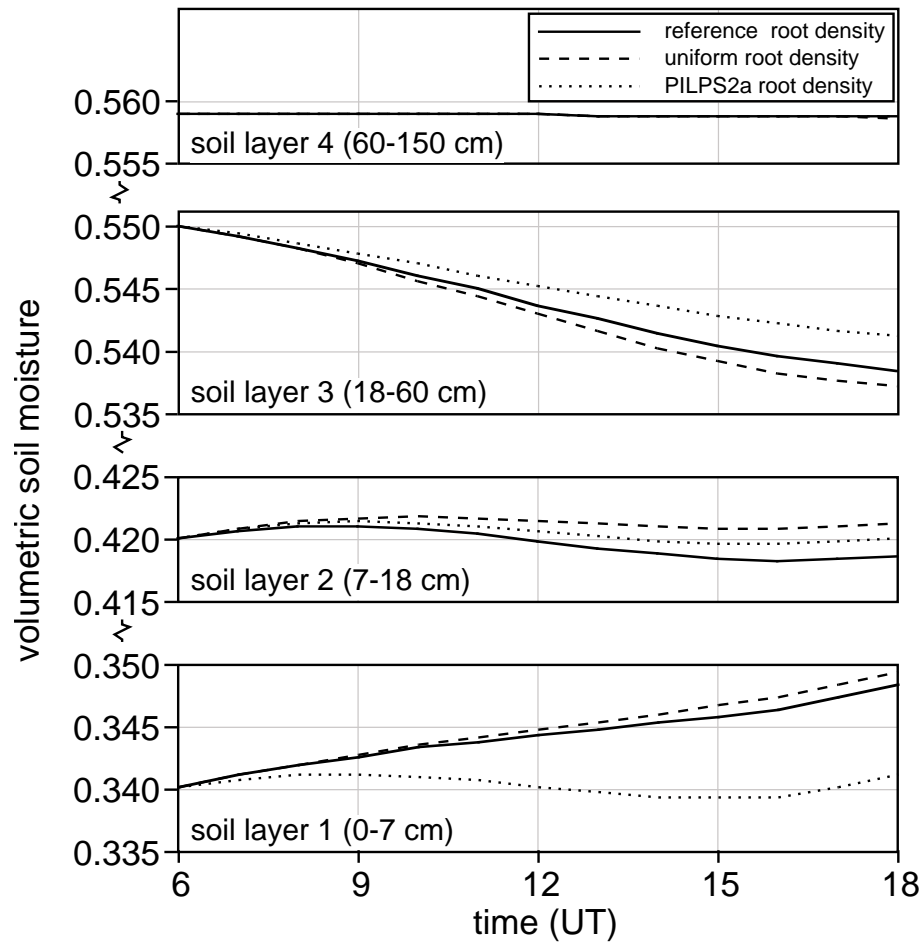


Figure 5.7: Modeled values of soil moisture for model soil layers for root density tests: quarter-rule (solid line), uniform (dashed line), and PILPS2a (dotted line) for 31 May 1978 at Cabauw, Netherlands.

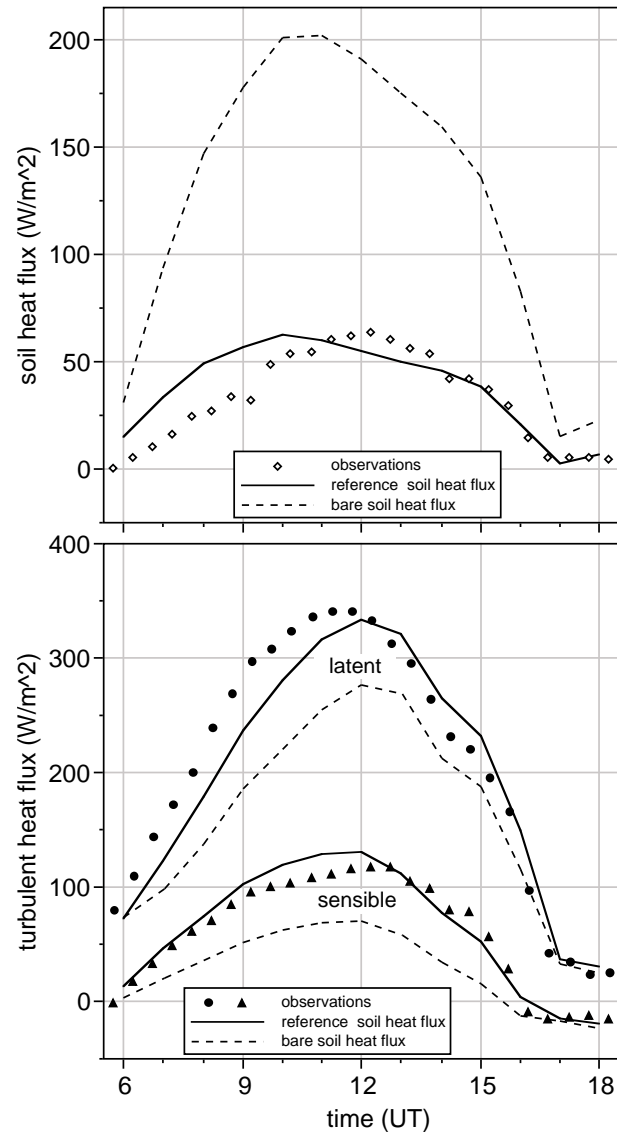


Figure 5.8: Observed (a) soil heat flux (open diamonds), and (b) latent (●) and sensible (solid triangles) heat fluxes, versus modeled heat fluxes for soil heat flux tests: ECMWF formulation (solid line) and bare soil formulation (dashed line) for 31 May 1978 at Cabauw, Netherlands.

conductivity in the upper soil layer is quite high because of a moderate soil moisture content yielding a higher soil heat flux than observed, while in reality the overlying vegetation layer would reduce the thermal conductivity which is implicitly included in the ECMWF formulation used in our reference model run. Because of the excessive soil heat flux using the base soil formulation, the resulting surface (radiative) and model soil (at -3.5 cm) temperatures are then much lower than observed, compared to the reference model run (Figure 5.9) using the ECMWF formulation. An overprediction of the soil heat flux would result in modeled values of the sensible and latent heat flux being less than observed; in coupled land-surface – ABL model runs the evolution of the daytime ABL would then be adversely affected, i.e. less ABL growth due to smaller sensible heat flux, and a potentially drier ABL due to smaller latent heat flux.

5.4.4 Surface fluxes and sensitivity to initial soil moisture

An important uncertainty in the initial conditions in these model runs is in the specification of moisture in the soil column. A change in the volumetric soil moisture by a few percent can have a notable effect on the surface fluxes, observed as well as modeled. Here we make a series of sensitivity tests and examine the 12 UT surface fluxes, varying the initial soil moisture by a realistic $\pm 5\%$ (volumetric) variation in soil moisture in the upper soil layer where it is can be quite variable, with decreasing variation with depth because of the greater certainty in temporal invariance of the measurements; the soil moisture in the bottom soil layer is not varied since it was very near saturation (Figure 5.2).

In a series of model runs, as the initial soil moisture is changed from drier to moister, as expected sensible heat flux decreases (by about 50 Wm^{-2} , -32% from drier to moister soil conditions), while latent heat flux increases (80 Wm^{-2} , +28%) (Figure 5.10). There is a subtle increase in net radiation (15 Wm^{-2} , +3%), because the surface temperature and thus outgoing longwave radiation decreases (note that the other radiation fluxes are prescribed). With a decrease in surface temperature, the gradient in soil temperature near the surface is reduced, so soil heat flux decreases (20 Wm^{-2} , -28%). These differences in surface fluxes are within the uncertainty of the observed flux measurements; changes here are rather linear with changing soil moisture because these model runs are for the land-surface only, that is, without ABL *interaction*.

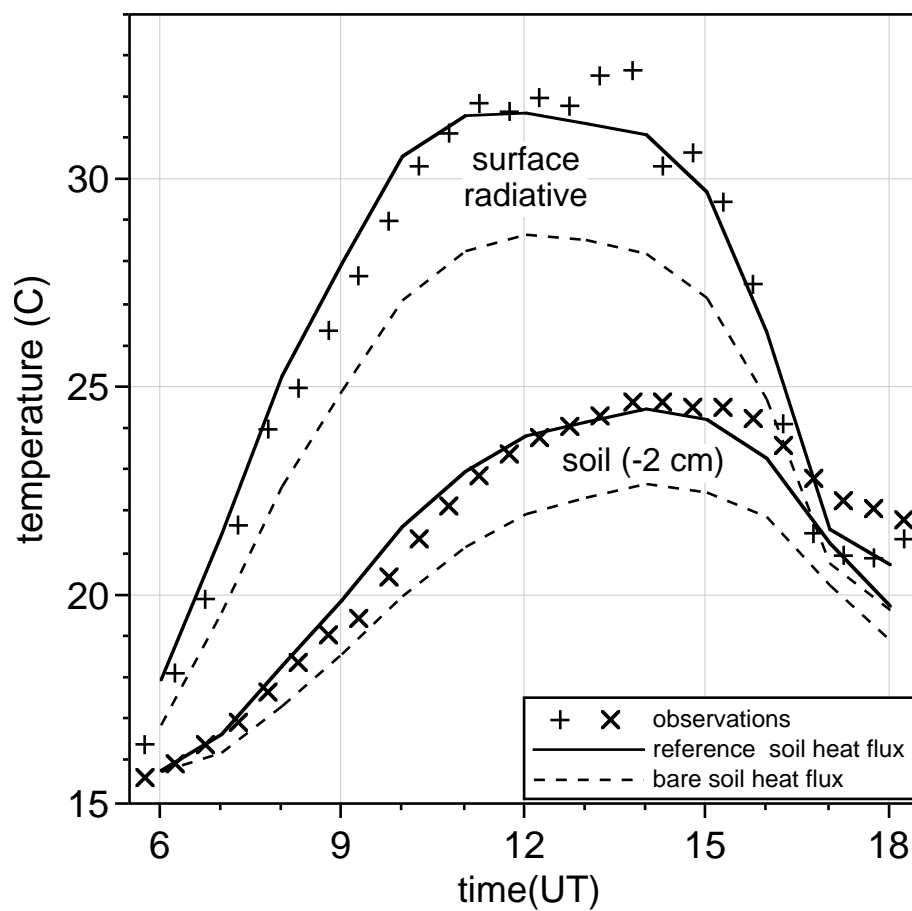


Figure 5.9: Observed surface radiative (+) and 2 cm soil (x) temperatures, versus modeled temperatures for soil heat flux tests: ECMWF formulation (solid line) and bare soil formulation (dashed line) for 31 May 1978 at Cabauw, Netherlands.

5.5 Summary

In this study our goal was to properly represent the soil-vegetation system in offline model runs for Cabauw (Netherlands) using a land-surface scheme driven by atmospheric forcing for the case study day examined (31 May 1978). Results indicate that in land-surface-only model runs, realistic daytime surface fluxes are produced using the land-surface scheme from the Coupled-Atmospheric boundary layer-Plant-Soil (CAPS) model with existing or alternate formulations, but using *un-tuned* model parameters. Model sensitivity tests included:

1. Modifications to the parameterization of canopy conductance. The locally-derived formulation specific to Cabauw (using an annual 1987 data set) was more successful in representing the canopy conductance at Cabauw than the "off-the-shelf" formulations. This suggests that classifications covering a broad land-surface category (e.g. "grassland") should be re-examined perhaps in terms of locally-derived data sets. Future work should investigate a more physically-based approach for canopy conductance based on CO₂ assimilation (e.g. Ronda et al 2001) as an alternative to the current widely-used Jarvis-Stewart empirical approach.
2. Alternatives for plant root density distribution. Nonlinear distributions that include a much higher root density near the surface, decreasing in density with depth, may not be appropriate for use in current land-surface schemes where the static treatment of roots can lead to rapid drying of the higher-root-density soil layers, and thus less accurate predictions of latent heat flux (and subsequently the surface energy budget). The "quarter-rule" used in this study is a near-uniform-with-depth root distribution, and performed quite well compared to more nonlinear distributions. A more uniform root distribution may in fact mitigate the problem of treating the root zone as static when in fact it may be rather dynamic in terms of the ability of vegetation to extract available soil water for transpiration.
3. Changes to the soil heat flux formulation. Accounting for the effect of overlying vegetation on the reduction of soil heat flux (via the ECMWF formulation) is important since this affects the amount of available energy that must be

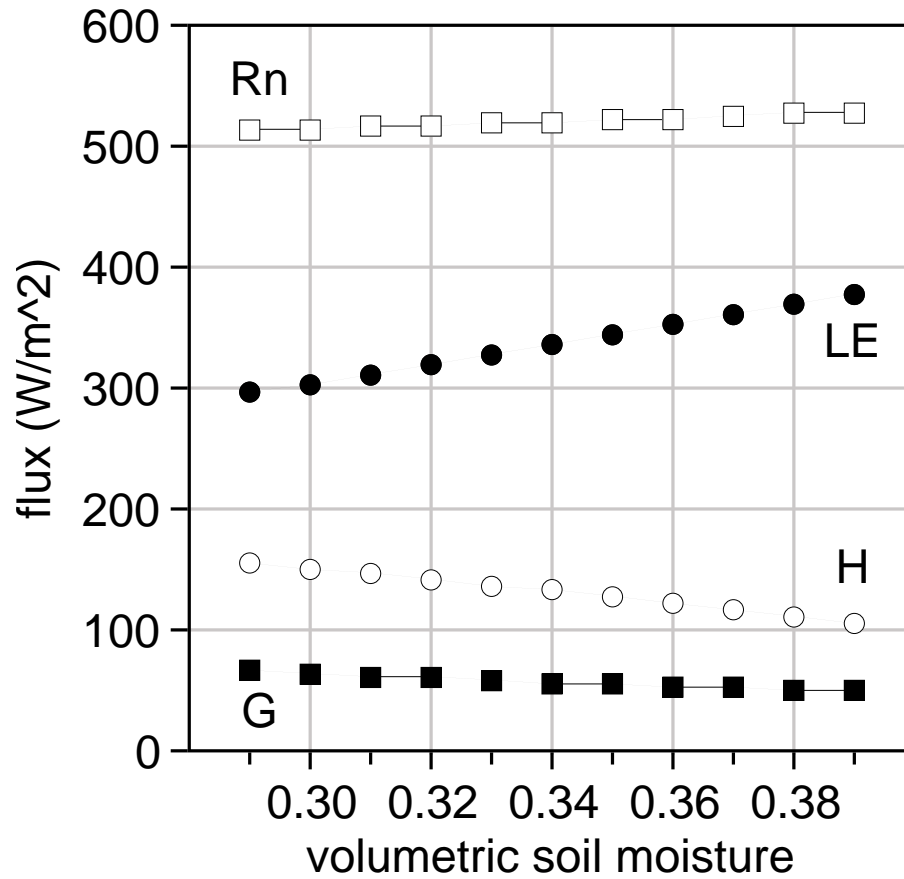


Figure 5.10: Modeled values of surface energy budget components for sensitivity tests varying initial soil moisture (Figure 2): net radiation (R_n), and sensible (H), latent (LE), and soil (G) heat fluxes for 31 May 1978 at Cabauw, Netherlands.

further partitioned into surface latent and sensible heat fluxes. As such, a simple representation of the soil heat flux as some set fraction of the net radiation is not adequate. As an alternative to the favorable ECMWF soil heat flux formulation used in the study here, vegetation can be explicitly included where the bare soil thermal conductivity is reduced by an exponential function of LAI and an empirical coefficient (described in Peters-Lidard et al 1997). A similar method uses green vegetation fraction (σ_f ; $0 \leq \sigma_f \leq 1$) instead of LAI (Ek et al 2003).

4. Sensitivity to initial soil moisture. The sensitivity of modeled surface fluxes to a variation (e.g. $\pm 5\%$ volumetric in the upper soil layer) in the initial soil moisture conditions was explored, with the resulting mid-day surface latent, sensible and soil heat fluxes varying by up to about 30% of the observed fluxes, though with the net radiation varying by less than 5%. These findings seem reasonable considering the accuracy of the surface flux and soil moisture measurements.

Regarding the use of the van Genuchten (1980) formulation for hydraulic conductivity (used in this study) as an alternative to Clapp and Hornberger (1978), IJpelaar (2000) examined regional climate model runs during the European summer of 1995, and found generally favorable results using van Genuchten. In a sensitivity study, Cuenca et al (1996) used van Genuchten versus Clapp and Hornberger in coupled land-atmosphere column model runs, and noted large differences in surface fluxes and atmospheric boundary-layer development, particularly under moderate soil moisture conditions. As such, it would be useful to repeat the study here using our "reference" model formulations and parameters to test van Genuchten versus Clapp and Hornberger, and revisit the PILPS2a (Cabauw 1987) data set, or seasonal or annual model runs for a Cabauw data set where soil moisture observations (along with surface fluxes) are available for validation, e.g. June-November 1977 and March-November 1978.

Finally, in a coupled land-atmosphere study, Ek and Holtslag (2004) used the land-surface scheme in the study here (with the "reference" model formulations and parameters) in their one-dimensional (column) land-surface – ABL model runs. In their sensitivity tests, they explored the role of soil moisture in ABL evolution and cloud development, where the outcome depends on many possible land-atmosphere interactions.

Acknowledgements. This research was supported by the NOAA Climate and Global Change Program under award number NA36GP0369, the Air Force Office of Scientific Research under contract F49620-9610058, and the Royal Netherlands Meteorological Institute (KNMI) which provided the Cabauw data set and sponsored Michael Ek as a visiting scientist on sabbatical leave from Oregon State University. We also wish to thank Fred Bosveld and Bart van den Hurk at KNMI, Anton Beljaars at ECMWF, Richard Cuenca at Oregon State University, Ken Mitchell at NCEP/EMC, and a host of other scientists at Wageningen University, KNMI, and elsewhere for their helpful comments and patience during the progress of this work.

Chapter 6

Influence of soil moisture on boundary-layer cloud development

This chapter is published as Ek, M. B., and A. A. M. Holtslag, 2004: Influence of soil moisture on boundary layer cloud development. *Journal of Hydrometeorology*, **5**, 86-99.

©Copyright 2004 by American Meteorological Society

Abstract

We study the daytime interaction of the land-surface with the atmospheric boundary layer (ABL) using a coupled one-dimensional (column) land-surface – ABL model. This is an extension of earlier work that focused on modeling the ABL for 31 May 1978 at Cabauw, Netherlands; previously it was found that coupled land-atmosphere tests using a simple land-surface scheme did not accurately represent surface fluxes and coupled ABL development. Here we utilize findings from that earlier study on ABL parameterization, and include a more sophisticated land-surface scheme. This land-surface scheme allows the land-atmosphere system to respond interactively with the ABL. Results indicate that in *coupled* land-atmosphere model runs, realistic daytime surface fluxes and atmospheric profiles are produced, even in the presence of ABL clouds (shallow cumulus). Subsequently, the role of soil moisture in the development of ABL clouds is explored in terms of a new relative humidity tendency equation at the ABL top where a number of processes and interactions are involved. Among other issues, it is shown that decreasing soil moisture may actually lead to an increase in ABL clouds in some cases.

6.1 Introduction

The interaction of the land-surface with the atmospheric boundary layer (ABL) includes many processes and important feedback mechanisms with additional interactions in the case of clouds (Figure 6.1; e.g. see Wetzal et al 1996, Pielke et al 1997, Betts 2000, Freedman et al 2001). It is the purpose of this study to explore the feedback mechanisms, in particular the role of soil moisture on ABL cloud development. The case study by Holtslag et al (1995, hereafter HMR95) examined ABL model runs driven by observed surface fluxes, and reproduced the observed boundary-layer structure for a case study at Cabauw (see also Stull and Driedonks 1987). But in their coupled land-surface – ABL model runs HMR95 found that they could not reproduce observed fluxes and boundary-layer structure using a simple land-surface scheme (using constant surface conductance). In this study we use the same case study day as HMR95, but also model land-surface – ABL interactions using an ABL scheme coupled with a more sophisticated land-surface scheme.

To this end, for the study here we use the Coupled Atmospheric boundary layer-Plant-Soil (CAPS) model that consists of coupled land-surface and ABL schemes, and

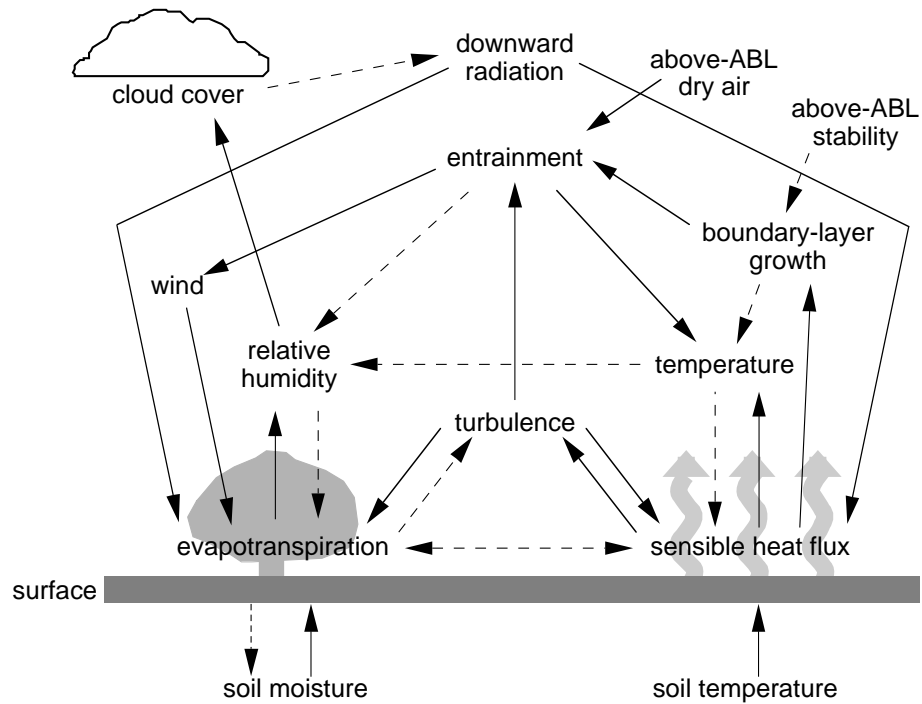


Figure 6.1: Important interactions between the surface and atmospheric boundary layer for conditions of daytime surface heating. Solid arrows indicate the direction of feedbacks that are normally positive (leading to an increase of the recipient variable). Dashed arrows indicate negative feedbacks. Two consecutive negative feedbacks make a positive one. Note the many positive and negative feedback loops that may lead to increased or decreased relative humidity and cloud cover. (Adapted from Ek and Mahrt 1994, their Figure 1.)

was developed to represent interactions of the land-surface with the ABL. Originally the CAPS model was intended for inclusion in large-scale numerical weather prediction models where computational efficiency is important, yet the equations used are comprehensive enough to approximate the physical processes thought to be most important (e.g. Holtslag et al 1990, Pan 1990, Holtslag and Boville 1993, F. Chen et al 1997, Betts et al 1997). The land-surface scheme in the CAPS model has been used in a stand-alone mode for a number of sensitivity experiments in different geophysical conditions (e.g. Kim and Ek 1995, Chen et al 1996) and for the same purpose as part of the Project for Intercomparison of Land-surface Parameterization Schemes (PILPS, e.g. T. H. Chen et al 1997, Wood et al 1998, Chang et al 1999); the study by Chang et al (1999) includes a comprehensive description of the current physics in the CAPS model land-surface scheme. In addition, a number of studies have specifically examined land-atmosphere interactions using the CAPS model in a coupled land-surface – ABL column mode (e.g. Ek and Mahrt 1994, Ek and Cuenca 1994, Huang and Lyons 1995, Cuenca et al 1996, Holtslag and Ek 1996).

In this study we first describe the data set at Cabauw (section 6.2), then give an overview of the CAPS model (section 6.3), followed by land-surface-only, ABL-only, and coupled land-surface – ABL model runs (section 6.4), then examine the influence of soil moisture on ABL cloud (shallow fair-weather cumulus) development (section 6.5), and finally a summary and conclusions (section 6.6).

6.2 Cabauw site and data set

In this study we use observations made on 31 May 1978 at or near the Cabauw site in central Netherlands that provide the necessary information for model initialization, forcing, and verification. The region surrounding the Cabauw site is rather flat for a distance of at least 20 km, with many fields and scattered canals, villages, orchards and lines of trees. One of the main branches of the Rhine, the River Lek, flows about one kilometer south of the Cabauw site, approximately 45 km east of the North Sea.

The Cabauw site itself is located in an open field nearly completely covered by short grass that extends for several hundred meters in all directions, and a series of shallow, narrow ditches that provide drainage for the site. Under the sod layer (3 cm) the soil consists of heavy clay down to about 0.6 m, with a nearly saturated peat layer below. Soil moisture measurements using neutron probe were taken covering the

study day at three sample sites in the micrometeorology tower plot adjacent to the Cabauw tower; measurements were made at 10 cm intervals down to 50 cm, and at 1 m (Wessels 1983). 31 May 1978 was the beginning of a "dry-down" period, though soil moisture values were still sufficient so that transpiration was not overly limited. There had not been any precipitation for a week, and this was to last three more weeks into later June before the next substantial precipitation event.

The 213 m tower at the Cabauw site includes atmospheric observations of winds and wind stress, temperature, and specific humidity at multiple levels, as well as sensible and latent heat fluxes determined from profile and Bowen ratio methods. Incoming solar and longwave radiation, low-level surface and soil temperatures, and low-level specific humidity measurements were made at the micrometeorological site adjacent to the Cabauw tower (within 200 m). The downward longwave radiation is suspect, however, being anomalously low. An estimate of downward longwave radiation is made as a residual by taking the difference between the observed net radiation, and the sum of the net solar radiation and outgoing terrestrial (longwave) radiation (computed from the infrared radiometer assuming an emissivity of one). Soil heat fluxes were measured by transducers buried at depths of 5 and 10 cm; surface soil heat flux was inferred from extrapolation of these measurements (Beljaars and Bosveld 1997). See Monna et al (1987) and Wessels (1984) for further information on Cabauw observations. See van Ulden and Wieringa (1996) for an extensive review of Cabauw boundary-layer research.

Four radiosondes were launched from the Cabauw site during the morning of the study day providing temperature and moisture profiles above the tower level. Additionally the data set is supplemented with information from radiosondes launched at De Bilt (about 25 km to the northeast) several times during the day providing additional measurements of wind, temperature and moisture. Because of the proximity and similarity in surface conditions, the De Bilt observations are thought to be representative for the Cabauw site, especially above the surface layer (see HMR95).

For our case study day of interest, the synoptic weather pattern over western Europe was dominated by surface high pressure with generally fair weather and light winds from the east, with a frontal system to the west of the British Isles.

6.3 Coupled Atmospheric boundary layer-Plant-Soil (CAPS) model

The Coupled Atmospheric boundary layer-Plant-Soil (CAPS) model consists of a land-surface scheme with multiple soil layers (Mahrt and Pan 1984), and a simple plant canopy (Pan and Mahrt 1987) modified to include the effect of vegetation using a "big leaf" approach for canopy conductance following Noilhan and Planton (1989), and described in Holtslag and Ek (1996). This more empirically-based approach for canopy conductance follows the original work by Jarvis (1976) and Stewart (1988) where canopy conductance is modeled as a function of atmospheric forcing and soil moisture availability. Under this approach, for this study we adopt the canopy conductance formulation more specific to Cabauw following Beljaars and Bosveld (1997) who examined the influence of vegetation evaporative control on surface moisture fluxes at Cabauw.

The soil heat flux formulation implicitly accounts for vegetation-reduced thermal conductivity (and thus soil heat flux) allowing more available energy for sensible and latent heat fluxes; this formulation follows the one used in the ECMWF TESSEL (land-surface) model (Viterbo and Baljaars 1995, van den Hurk et al 2000). This is in principle similar to the formulation described in Peters-Lidard et al (1997) that uses a more explicit dependence on vegetation density (via leaf area index). We set the depth of the first soil layer in our model the same as in the TESSEL model (7 cm; Figure 6.2) in order to use the same Cabauw-calibrated coefficient in the soil heat flux formulation. Following Beljaars and Bosveld (1997), our subsequent soil layers match the bottom of the "higher root density" zone (18 cm depth), a zone of "lower root density" down to the bottom of the root zone (60 cm), with a subroot zone below (1.5 m total depth), and an implicit soil column bottom at 3.0 m. A nonlinear root distribution with excessively high root density near the surface may lead to improper rapid drying of the higher-root-density soil layers in the root zone (Zeng et al 1998). This can yield less accurate predictions of latent heat flux, and subsequently the surface energy budget. As such, in our study here we assume a near-uniform root distribution since bulk methods (uniform root distribution) are more consistent with the current level of understanding and thus preferred over root-weighted methods (Desborough 1997). This may mitigate the problem of treating the root zone as static when in fact it may be rather dynamic in terms of the ability of vegetation to extract water from where it is available in the root zone, despite the root density distribution.

The ABL scheme uses the original combined local (K-theory) and nonlocal (boundary-layer-scale mixing) development by Troen and Mahrt (1986) with an update to non-local mixing of heat and moisture following Holtslag and Boville (1993), and quite similar to the ABL scheme used in the HMR95 study. The boundary-layer height formulation has been modified to account for boundary layers with relatively high wind speed and upper boundary-layer stratification, and includes the effect of turbulence due to surface friction under near-neutral and stable conditions (for further details see Vogelesang and Holtslag 1996).

A simple fractional boundary-layer cloud cover formulation (Ek and Mahrt 1991a) is included in the ABL scheme, which is based on a Gaussian distribution of total-water (vapor plus liquid) relative humidity near the boundary-layer top, where cloud cover is defined as the area under the Gaussian curve above saturation. The relative humidity distribution includes turbulent and mesoscale variations, where the turbulent variation is formulated in terms of dry-air entrainment at the boundary-layer top, while the mesoscale (subgrid) variation is specified as a function of horizontal grid size (assumed to be on the order of 100 km corresponding to a mesoscale relative humidity variation of 5% across the domain of central Netherlands). When spatial fluctuations of relative humidity are large, boundary-layer clouds first form at a lower spatially averaged relative humidity. This formulation was developed using HAPEX-MOBILHY data (continental fair weather cumulus), but has also shown quite favorable performance in the study of Mocko and Cotton (1995) using data from BLX (also continental fair weather cumulus) as well as from FIRE (marine stratocumulus).

With the CAPS model in a fully-interactive mode, the land-surface scheme is coupled with the ABL scheme, and ABL clouds predicted by the cloud cover formulation are allowed to alter the radiation budget at the surface (via a simple surface radiation scheme included as an option in the CAPS model) thereby affecting surface processes (e.g. fluxes). Incoming clear-sky solar and downward longwave radiation reaching the surface are calculated following the methods of Collier and Lockwood (1974) (similar to Holtslag and van Ulden 1983), and Satterlund (1979), respectively, and include solar attenuation by ABL clouds via a transmission function following Liou (1976) for "climatological" cumulus clouds, a cloud enhancement to the downward longwave radiation following Paltridge and Platt (1976), and a Cabauw-specific shortwave albedo formulation following Duynkerke (1992).

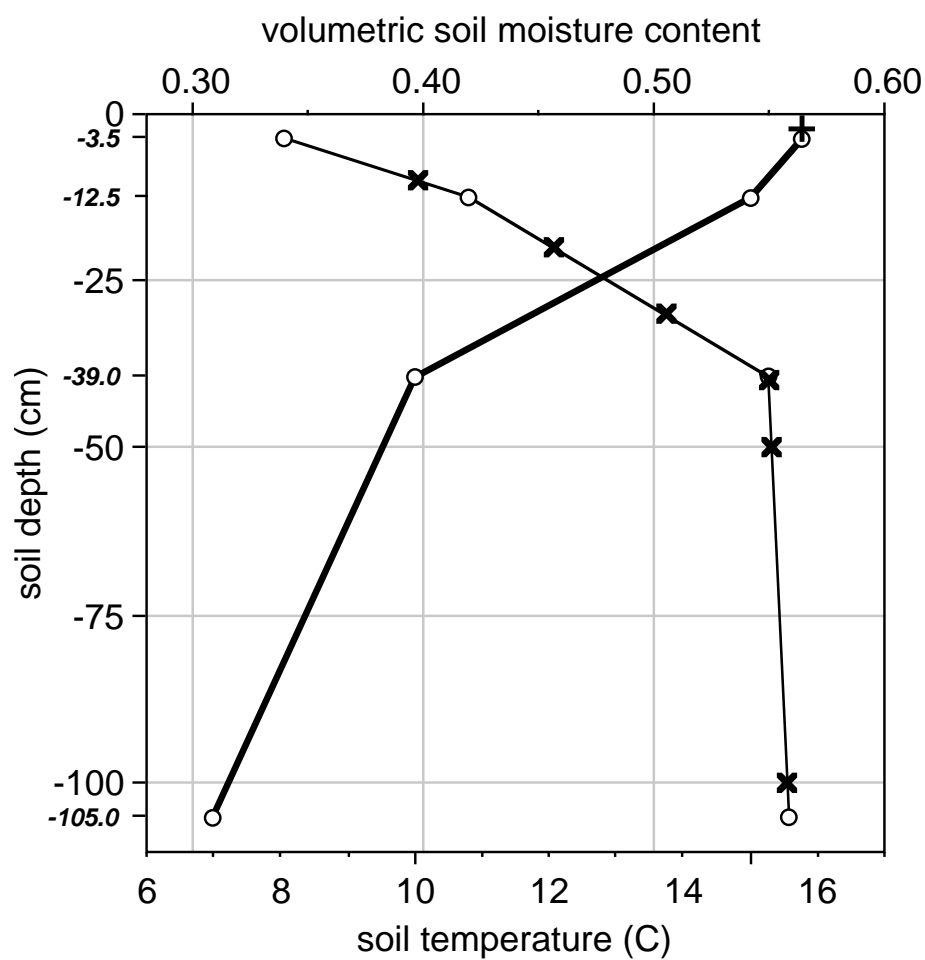


Figure 6.2: Initial soil moisture profiles for 31 May 1978 at Cabauw, Netherlands: observed (\times), initial model soil moisture reference profile interpolated to model soil level mid-points (\circ & solid line), and observed soil temperature at -2 cm ($+$) and initial model soil temperature reference profile (\circ & heavy solid line).

The lowest atmospheric model levels are at 20, 40, 80, 120, and 200 meters (matching the Cabauw tower observation heights), with 100 m vertical resolution from 200 m to a height of 2 km, then 200 m resolution above to the top of the model domain (10 km). The time step used in model runs is 180 seconds, which is felt to be appropriate for the model (vertical) resolution.

6.4 Model evaluations

We first examine model runs of the land-surface forced by atmospheric conditions, followed by model runs of the ABL forced by observed surface heat and moisture fluxes. These stand-alone or "off-line" land-surface-only and ABL-only (uncoupled) tests allow us to isolate the processes responsible for land-surface fluxes (land-surface scheme without ABL interaction) and ABL development (ABL scheme without land-surface interaction) separately before coupling the land-surface and ABL schemes. In a coupled mode, more complicated interactions and feedbacks are possible, including the formation and presence of ABL clouds.

6.4.1 Land-surface modeling results (atmospheric forcing)

We use the same case study day as HMR95, and first examine a "base state" model run to show land-surface behavior in response to observed atmospheric forcing (Figure 6.3) before making coupled land-surface – ABL model runs. We initialize our land-surface model using soil moisture observations interpolated to the mid-point of the model soil levels (Wessels 1983; Figure 6.2). Soil temperature is initialized at the first model soil layer (-3.5 cm) using -2 cm observations; this difference is not expected to be significant at this time of day. Soil temperature observations are not available below 2 cm, so to initialize soil temperatures at subsequent model soil levels we make approximations from the average of the previous week, month, and three-months 2-m air temperatures, respectively, for the lowest three model levels, with the annual 2-m air temperature used as the implicit bottom temperature.

In our land-surface model run driven by observed atmospheric conditions, the latent heat flux is slightly underpredicted (*overpredicted*) in the morning (*afternoon*), while sensible heat flux is generally well-predicted, though slightly high around mid-day (Figure 6.4a). This may be due to the slight underprediction in the canopy

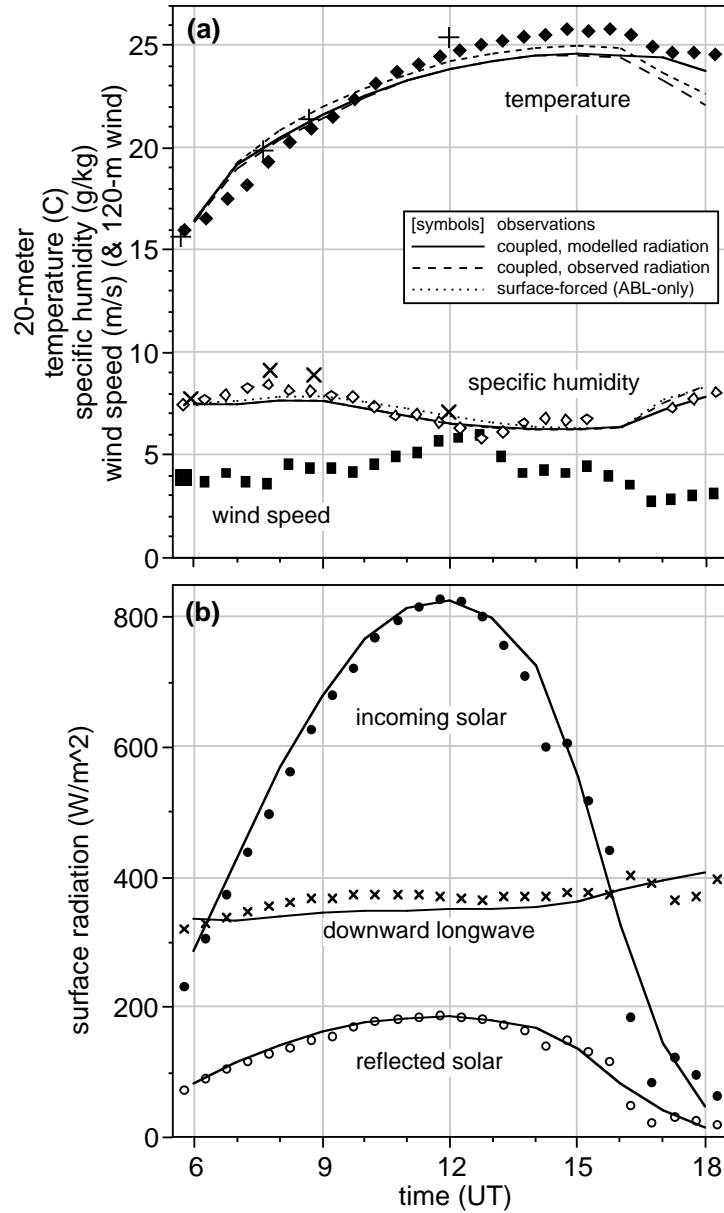


Figure 6.3: Atmospheric forcing data for 31 May 1978 at Cabauw, Netherlands: (a) 20-meter temperature, specific humidity, and wind speed (large symbols from Cabauw and De Bilt radiosonde data), and (b) incoming and reflected solar and downward longwave radiation. Also shown: (a) time series of air temperature and specific humidity for ABL-only, and coupled land-surface – ABL model runs, and (b) time series of incoming solar, reflected solar, and downward longwave radiation for coupled land-surface – ABL model runs using modeled radiation (with ABL cloud interaction).

conductance in the morning (results not shown). Net radiation and soil heat flux are generally well-predicted (Figure 6.4b), though the soil heat flux is slightly overpredicted (*underpredicted*) in the morning (*early afternoon*), with soil temperatures still comparing favorably (results not shown). These results are not completely surprising since the parameters used in the various surface formulations have been calibrated for Cabauw data, although not specifically for our case study day here (31 May 1978). (See Ek and Holtslag (2005) for a detailed study on the sensitivity of the CAPS model land-surface scheme to choices of various land-surface formulations and parameters.)

6.4.2 Atmospheric boundary-layer modeling results (surface forcing)

We also examine a "base state" model run to show ABL behavior in response to observed surface fluxes before making coupled land-surface – ABL model runs. Overall, our results are similar to those of HMR95. Following HMR95, large-scale (horizontal) advection was unknown but thought to be weak considering the synoptic situation, so this same condition is applied to the ABL model runs here. As in HMR95, we initialize the ABL scheme with temperature and specific humidity profiles (Figure 6.5a), and drive the ABL by prescribing observed fluxes on 31 May 1978 (see Figure 6.4a).

Because a column model cannot adequately represent mesoscale momentum dynamics, we prescribe the wind profile at each timestep by interpolating radiosonde wind data (above 200 m) taken at 06, 12, and 18 UT; below 200 m we use 06-18 UT interpolated 30-minute Cabauw tower wind observations that are consistent with radiosonde winds (Figure 6.5b). So we depart slightly from HMR95 where wind was modeled (though they prescribed geostrophic wind); this may also have contributed to the less accurately modeled surface fluxes in HMR95. By avoiding modeling the wind we can focus more effectively on the ABL mixing of heat and moisture, and interactions with the land-surface in the case of coupled land-surface – ABL model runs (described in section 6.4.3). This method of prescribing winds was also successfully employed by Holtslag and Ek (1996) to deal with a complicated wind situation and allowed them to focus on boundary-layer heat and moisture mixing, and interaction with the surface.

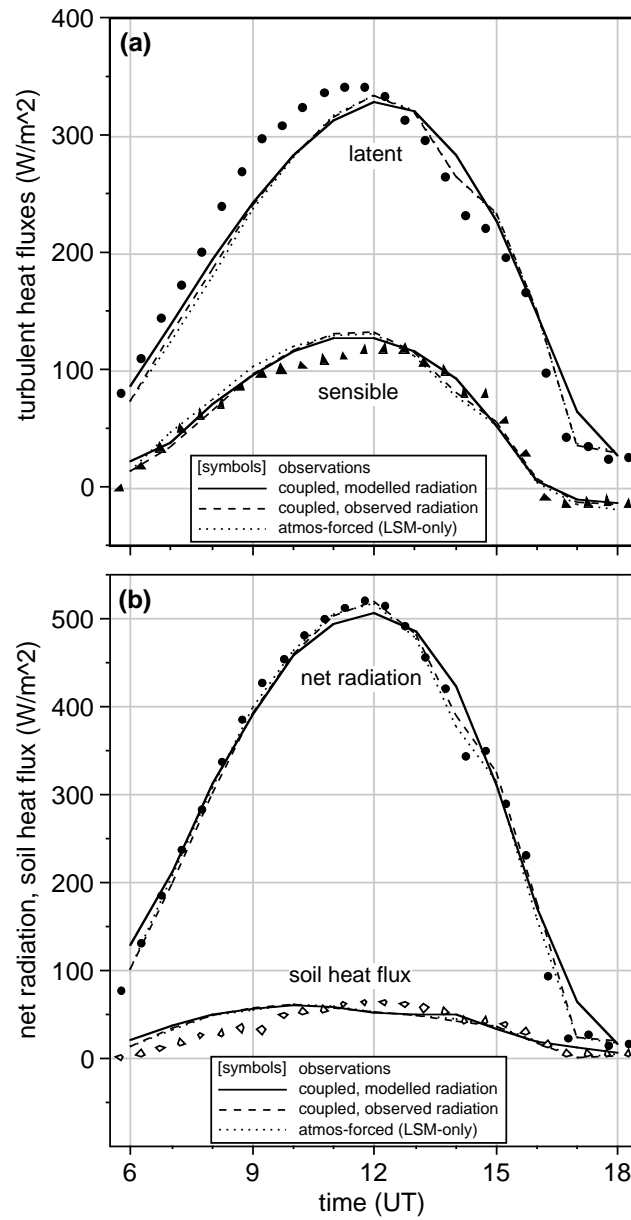


Figure 6.4: Time series of (a) latent and sensible heat flux, and (b) net radiation and soil heat flux (observations indicated by symbols), and model runs (lines) for land-surface-only, and coupled ABL-land-surface model runs using prescribed or modeled radiation (31 May 1978 at Cabauw, Netherlands).

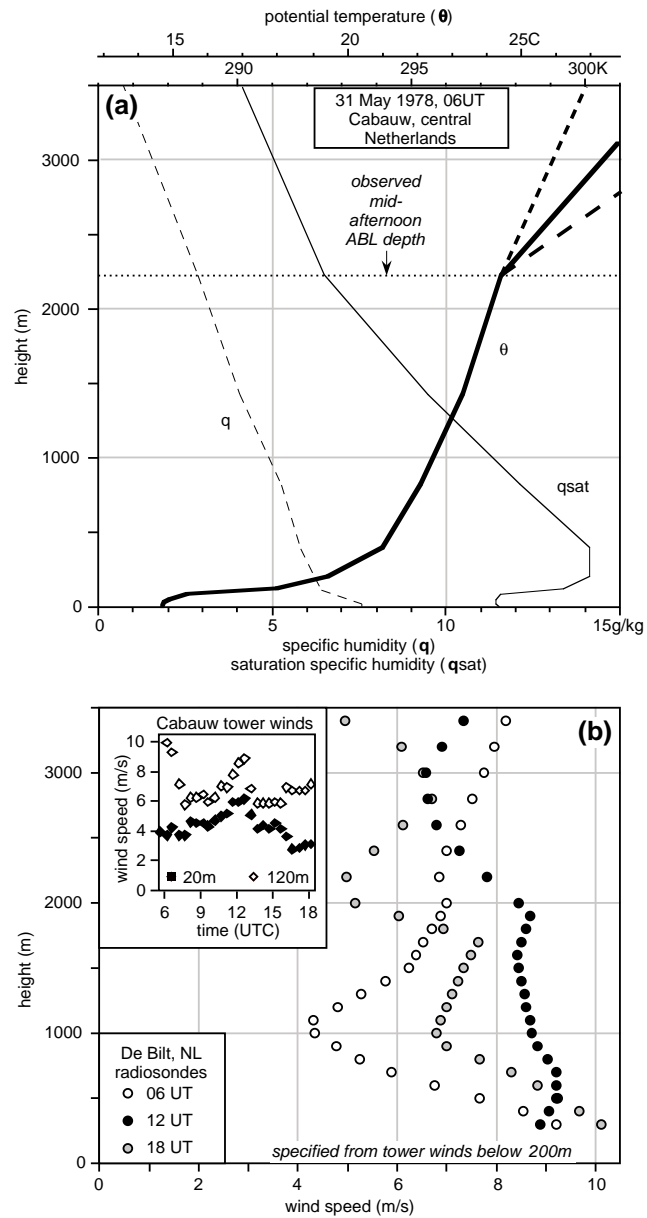


Figure 6.5: (a) Initial atmospheric profiles of potential temperature (θ), and specific humidity (q) and saturation specific humidity (q_{sat}), and (b) wind speed profiles from De Bilt radiosondes and Cabauw tower winds used for prescribing winds in model runs (31 May 1978).

Additionally, we "turn on" the ABL clouds in order to assess the performance of the ABL cloud formulation, though there is no interaction with the surface since surface fluxes are prescribed, i.e. in this phase of testing ABL clouds do not modify the surface radiation budget and subsequent ABL development. In "full" coupled land-surface – ABL testing (the subject of section 6.4.3), we include the effect of a cloud-modified surface radiation budget. (However, note that in our cloud cover formulation so far, there is no enhanced-turbulent mixing due to ABL clouds, i.e. by shallow cumulus.)

Large-scale vertical motion was not known in the HMR95 study where it was set to zero, however the prescribed vertical motion affects boundary-layer growth which influences ABL cloud development. So we first make a series of sensitivity tests of the ABL model forced by observed surface fluxes where vertical motion is varied between $\pm 1.0 \text{ cm s}^{-1}$ (at 2 km then linearly decreasing to zero at the surface). Modeled ABL clouds are first predicted in the mid-afternoon, and generally increase with increasing vertical motion (increasing boundary-layer depth), with modeled ABL cloud cover varying between near-zero and complete coverage (Figure 6.6). With increasing prescribed vertical motion, ABL clouds form and increase in their fractional coverage because with an increasingly deeper ABL, cooling at the ABL top is sufficient for the relative humidity to reach a threshold value (influenced by the ABL-top relative humidity variation) for clouds to form. For our case study day here, modeled cloud cover remains small until positive values of the prescribed vertical motion, after which cloud cover increases greatly (while boundary-layer depth increases slightly). Results suggest that a nominally small value of vertical motion ($+0.5 \text{ cm s}^{-1}$) gives a fractional ABL cloud cover that is qualitatively consistent with the synoptic weather situation described earlier, where ABL clouds (fair weather cumulus) first formed in the early-to-mid-afternoon with $3/8 - 5/8$ coverage by late afternoon across the region around Cabauw in central Netherlands. Note that using a prescribed large-scale vertical motion of zero (as in HMR95), modeled cloud coverage is quite small, though profiles and time series of temperature and specific humidity are not overly sensitive (as in HMR95) (results not shown).

In our ABL model run driven by observed surface fluxes, modeled ABL growth is slightly too vigorous in the morning hours; ABL depth is better represented in the afternoon, and during the late afternoon ABL transition to a shallow stable boundary layer (Figure 6.7). ABL growth is also slightly more vigorous in the late morning than

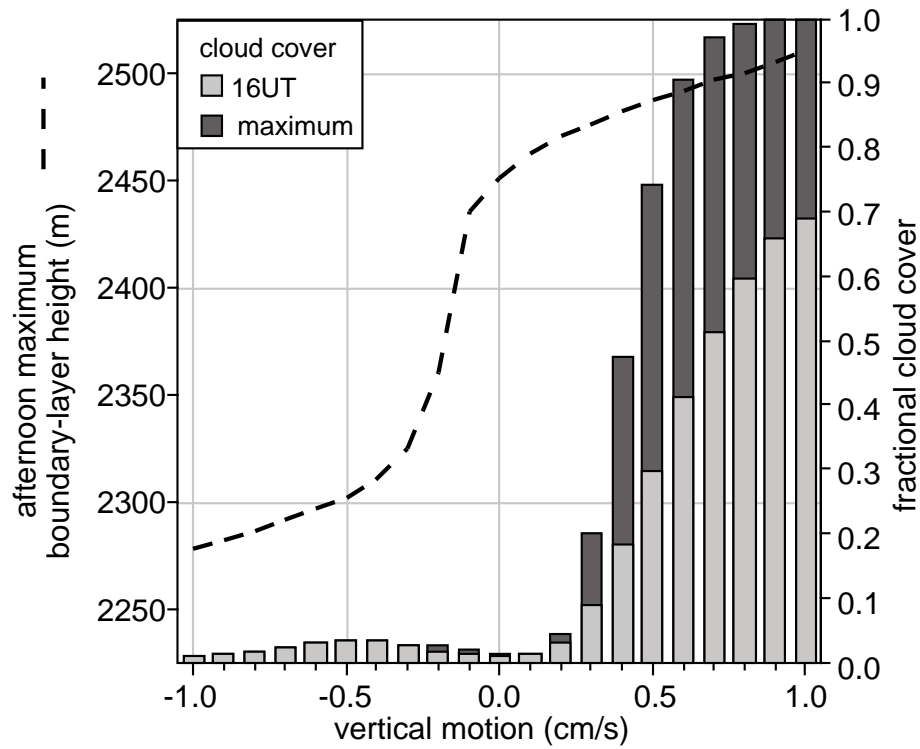


Figure 6.6: Maximum afternoon boundary-layer depth (dashed line), and 16 UT (light gray) and maximum boundary-layer (dark gray) cloud cover versus prescribed vertical motion in ABL model runs forced by observed surface fluxes (31 May 1978 at Cabauw, Netherlands).

that found in HMR95, with noontime values a few hundred meters deeper, though well-within the range of uncertainty in the observed ABL depth at De Bilt (used as an estimate for Cabauw). Mid-afternoon values of modeled ABL depth were about 400-500 m deeper than found by HMR95, though lack of observations during this period makes this comparison inconclusive. Our prescription of wind profiles throughout the model run period versus modeled winds in HMR95 may have lead to differences in diagnosed ABL height. Also recall that in our study here we have updated the ABL height formulation (described in section 6.3), though use of the original formulation for ABL height yields little difference in the development of the ABL owing to the daytime convective nature of the ABL (results not shown).

The modeled evolution of both temperature and moisture is consistent with the ABL development, and as in HMR95, the modeled 20-m (potential) temperature was found to be slightly warmer than observed in the morning hours, and about one degree cooler than observed during afternoon hours (Figure 6.3a). Specific humidity is comparable to observations though with a slightly smaller mid-morning peak that is often observed prior to late-morning rapid ABL growth (Figure 6.3a). Also note the 12 UT profiles of potential temperature and specific humidity (Figure 6.8) which show the modeled potential temperature profile cooler than observed by about 1.0 K (1.5 K) compared to Cabauw tower (*De Bilt radiosonde*) observations, and specific humidity about 0.5 g kg^{-1} greater (0.5 g kg^{-1} less) than the Cabauw tower (*De Bilt radiosonde*) observations. As in HMR95, the differences in the profiles may be attributed to modifications in the air mass not represented by the forcings, i.e. surface fluxes, and initial temperature and humidity and specified wind profiles. We refer the reader to HMR95 for further details of their sensitivity experiments on ABL response to e.g. various choices of advection, initial temperature and specific humidity profiles, and other model sensitivity tests.

6.4.3 Coupled modeling results (surface-atmosphere interaction)

In coupled runs, the model is initialized the same as in previous land-surface-only (section 6.4.1) and ABL-only (section 6.4.2) model runs, but now the land-surface is allowed to operate interactively with the ABL, but with the observed radiation at the surface prescribed for our first test. Note that if the results from coupled model runs

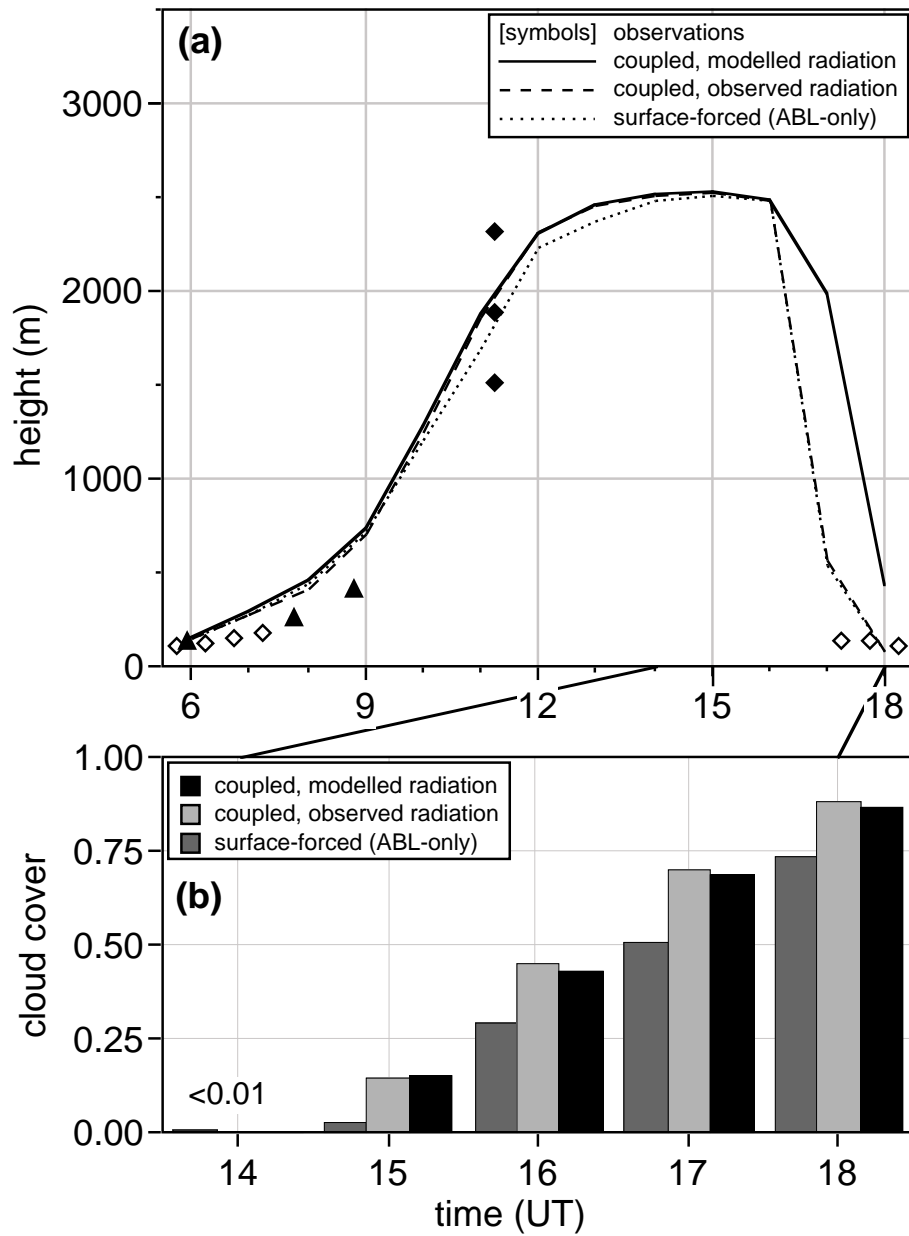


Figure 6.7: Time series of ABL height and cloud cover for ABL-only, and coupled land-surface – ABL model runs (31 May 1978 at Cabauw, Netherlands).

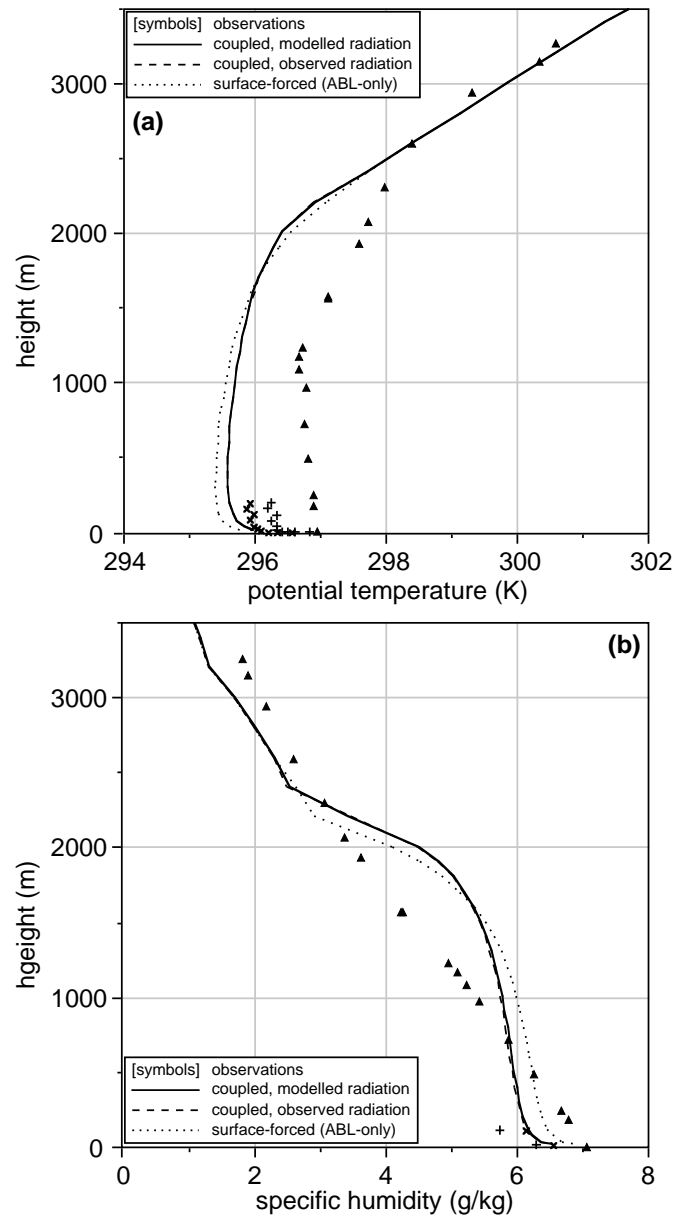


Figure 6.8: ABL profiles at 12 UT for (a) potential temperature, and (b) specific humidity for ABL-only, and coupled land-surface – ABL model runs (31 May 1978 at Cabauw, Netherlands).

improve compared to results from model runs with the land-surface scheme operating alone (atmosphere and radiation forced), or with the ABL scheme operating alone (surface forced), then compensating interactions could be responsible for any noted improvement. On the other hand, a coupled model study may reveal that the model fluxes are more representative on the ABL scale (e.g. on the order of tens of km) compared to those observed (at the Cabauw tower site). Margulis and Entekhabi (2001) explored land-atmosphere interaction using an adjoint framework, and point out the importance of using a coupled model (e.g. land-surface – ABL) in examining the sensitivity of surface parameters (versus typical uncoupled testing). In our study here, generally we hope that in coupling the land-surface and ABL schemes that the results will not diverge significantly. This appears to be the case in the coupled model runs for surface heat fluxes (Figure 6.4), and ABL development and cloud formation (Figures 6.3a, 6.7, and 6.8). (Note that in the case here, predicted ABL clouds are passive in that they do not affect the radiation reaching the surface.)

As an additional test, we utilize the simple surface radiation scheme (described in section 6.3) to predict the radiation budget at the surface. This removes an additional degree of freedom in coupled model runs so that it is more "fully interactive" (except for the specified evolution of the wind profile). The ABL cloud cover predicted by the cloud cover formulation attenuates incoming solar radiation and slightly enhances downward longwave radiation that reaches the surface, which affects land surface processes (canopy conductance, surface fluxes, etc), subsequent boundary-layer development, cloud cover, and so on. In this case, the incoming and reflected solar ($S\downarrow$ and $S\uparrow$) and downward longwave ($L\downarrow$) radiation are predicted fairly well (Figure 6.3b), which assesses the performance of our simple surface radiation scheme and the interaction with ABL clouds. The modeled surface heat fluxes (Figure 6.4) are similar to those using observed radiation, with similar results for ABL development and cloud cover (Figure 6.3a, 6.7, and 6.8).

6.5 Impact of soil moisture on ABL cloud development

6.5.1 Coupled model results

To fully explore the interaction of the land-surface with the ABL and the effect on boundary-layer cloud development, we make a series of model runs (a "reference" set)

where we change the soil moisture from quite dry to quite wet. Initial conditions and forcing are the same as in our previous coupled model runs (except here we specify a uniform soil moisture profile to better illustrate differences between model runs), and vary soil moisture from below the wilting point (Θ_{wilt}) to near saturation (Θ_{sat}). We note that for the various model runs, as we decrease the initial soil moisture from intermediate soil moisture values (close to observations, $\Theta = 0.43$) to below the wilting point, ABL cloud cover decreases to zero (Figure 6.9a), a somewhat intuitive result. However, as we increase the initial soil moisture from intermediate soil moisture values to near saturation, ABL cloud cover decreases slightly, a somewhat counter-intuitive result. Certainly there are a number of processes that account for this behavior, i.e. interactions between the land-surface, atmospheric boundary layer (including ABL clouds), free atmosphere, and initial ABL conditions (Figure 6.1).

Before attempting an explanation of this response, we also examine the role of atmospheric stability (γ_θ) above the ABL in land-surface interaction with the evolving boundary layer since γ_θ has a strong influence on boundary-layer growth. We make two additional sets of model runs as above, except now we prescribe one set with *increased* atmospheric stability above the observed afternoon boundary-layer top (compared with the reference set of model runs above), and another set with *decreased* atmospheric stability (see Figure 6.5a). We then examine the resulting afternoon ABL depth and fractional cloud cover, and the mid-day surface energy budget as it changes with changing prescribed initial soil moisture (Figure 6.9b).

The set of model runs with stronger atmospheric stability have a shallower ABL depth than the reference set and less cloud cover for drier soils, with increasing cloud cover for model runs with increased soil moisture. However, in great contrast, the set of model runs with weaker atmospheric stability above the ABL have a deeper ABL depth (as one would expect) and yet a much greater cloud cover for drier soils, with decreasing cloud cover for increasing soil moisture. This is in general agreement with the findings by Wetzal et al (1996). In section 6.5.2, we will attempt to explain this result in terms of a tendency equation for relative humidity at the ABL top.

6.5.2 Analytical results

The role of soil moisture in ABL cloud development involves a complex interaction of surface and atmospheric processes. Ek and Mahrt (1994) examined the daytime

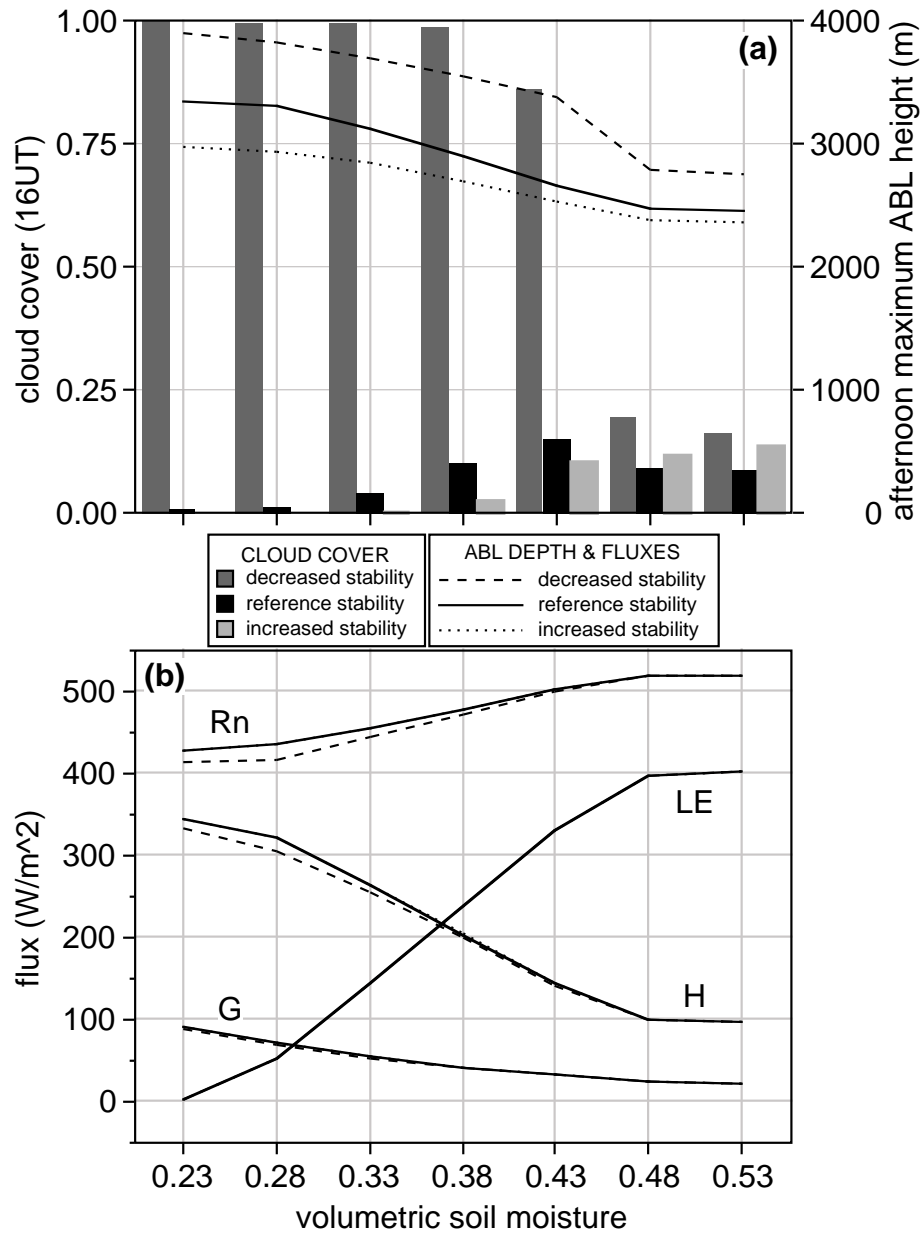


Figure 6.9: Impact of variation in volumetric soil moisture for different sets of model runs (reference, and increased and decreased above-ABL atmospheric stability) on (a) ABL depth and cloud cover, and (b) components of the surface energy budget.

evolution of ABL-top relative humidity that is expected to control ABL cloud development. They showed that the relative humidity tendency at the ABL top involves a number of competing mechanisms, with relative humidity directly *increasing* due to surface evaporation and due to ABL growth (ABL-top temperature decreases), and relative humidity directly *decreasing* due to surface sensible heat flux and due to entrainment of warm and dry air into the ABL from above. The *indirect* role of surface evaporation is to reduce surface heating, thereby competing with ABL growth that is reduced due to reduced surface heating, although this diminishes ABL-top warm- and dry-air entrainment. In a similar type of study, De Bruin (1983) examined the effect of different land-surface and ABL processes on the Priestley-Taylor parameter (used in relating surface available energy to surface evaporation).

To further understand the role of soil moisture and other factors on ABL cloud development, we extend the work of Ek and Mahrt (1994) and examine a useful new equation for relative humidity tendency at the ABL top (see Appendix B for development), given as

$$\frac{\partial RH}{\partial t} = \left(\frac{R_n - G}{\rho L_v h q_s} \right) [e_f + ne(1 - e_f)], \quad (6.1)$$

where $R_n - G$ is available energy at the surface (R_n is net radiation and G is soil heat flux), ρ is air density, L_v is latent heat, h is ABL depth, and q_s is saturation specific humidity just below the ABL top. In (6.1), e_f is the surface evaporative fraction (of surface energy available for evaporation) defined as

$$e_f = \frac{LE}{R_n - G} = \frac{LE}{H + LE}, \quad (6.2)$$

where LE ($= \rho L_v \overline{w'q'_s}$) and H ($= \rho c_p \overline{w'\theta'_s}$) are the surface latent and sensible heat fluxes, respectively.

Furthermore, $ne(1 - e_f)$ reflects the direct effects of non-evaporative processes on relative humidity tendency, where ne is given by

$$ne = L_v/c_p(1 + C_\theta) \left[\frac{\Delta q}{h\gamma_\theta} + RH \left(\frac{c_2}{\gamma_\theta} - c_1 \right) \right], \quad (6.3)$$

where c_p is specific heat, C_θ is the (negative of the) ratio of surface to ABL-top sensible heat flux, Δq is the specific humidity drop above the ABL (negative), γ_θ is the potential temperature lapse rate above the ABL, and c_1 and c_2 are functions of

surface pressure, temperature and pressure at the ABL top, and constants (see Appendix B). ne consists of three terms (each multiplied by $L_v/c_p(1 + C_\theta)$): ABL-top dry-air entrainment ($\Delta q/h\gamma_\theta$, a negative contribution to ABL-top relative humidity tendency), boundary-layer growth (RHc_2/γ_θ , a positive contribution), and boundary layer heating through surface warming and ABL-top warm-air entrainment (RHc_1 , a negative contribution).

From (6.1) we see that the relative humidity tendency is proportional to available energy and inversely proportional to ABL depth and temperature (via saturation specific humidity), while the sign of the relative humidity tendency is determined by the sign of $e_f + ne(1 - e_f)$. Examining (6.1), it is apparent that the direct role of e_f is to increase the ABL-top relative humidity, while the indirect role of surface evaporation (via reduced surface heating, and diminished ABL growth and entrainment) is found in the expression $ne(1 - e_f)$. Figure 6.10 shows how $e_f + ne(1 - e_f)$ depends on e_f versus ne , where $e_f + ne(1 - e_f)$ is the relative humidity tendency, $\partial RH/\partial t$, normalized by the available energy term, $(R_n - G)/(\rho\lambda_v h q_s)$.

When the above-ABL atmospheric stability is rather strong (larger γ_θ), or if the stability is rather weak and the above-ABL air is rather dry (larger Δq), then $ne < 1$ so that $\partial RH/\partial t$ increases as e_f increases, confirming intuition. (For the range $0 < ne < 1$, $\partial RH/\partial t > 0$ and increases with increasing e_f , while for $ne < 0$, $\partial RH/\partial t > 0$ only when e_f exceeds some threshold value which increases for increasingly negative values of ne). Here soil moisture acts to increase ABL-top relative humidity and thus increases the probability of ABL cloud development given a sufficient initial ABL relative humidity.

On the other hand, with weaker above-ABL stability (smaller γ_θ), boundary-layer growth is less restricted over drier soils than over moister soils compared to the case with stronger stability. So with above-ABL air not too dry, then $ne > 1$ so that $\partial RH/\partial t$ increases as e_f decreases, which is somewhat counter-intuitive. Here soil moisture acts to limit the increase of ABL-top relative humidity and thus decreases the probability of ABL cloud development. Note that the largest values of $\partial RH/\partial t$ are achieved for $ne > 1$ suggesting that the greatest potential for ABL cloud development is not over moist soils, but rather over dry soils with weak stability and above-ABL air not too dry.

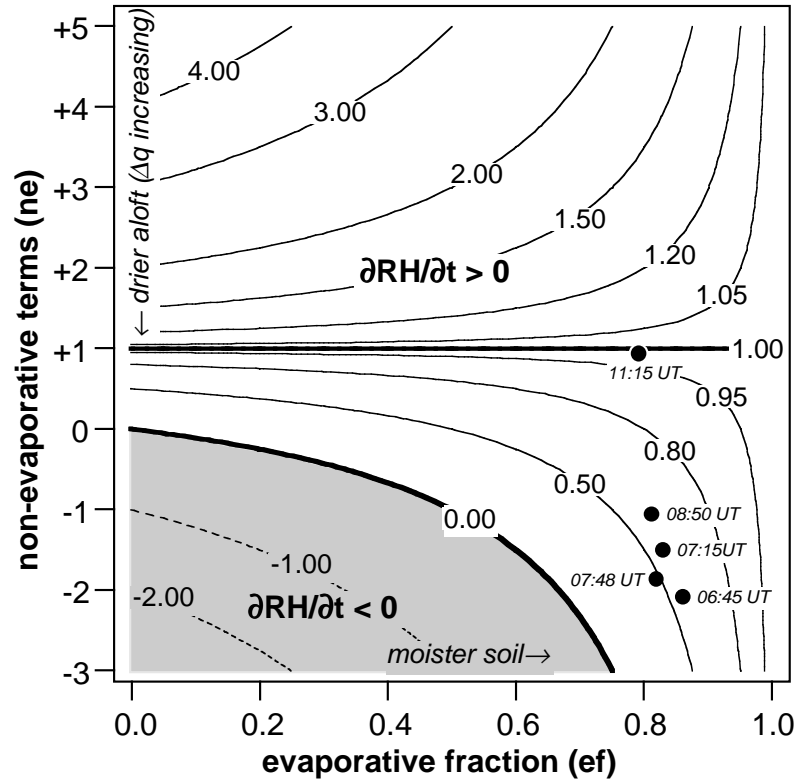


Figure 6.10: ABL-top relative humidity tendency equation, $e_f + ne(1 - e_f)$ (normalized by the available energy term), as a function of evaporative fraction (e_f) versus non-evaporative processes (ne) with Cabauw (Netherlands, 31 May 1978) values and times indicated (dots). See text for details.

From (6.1)-(6.3), note that with drier air above the ABL (increasingly negative Δq), the value of ne decreases, and that as the soil moisture increases, generally e_f increases (depending on the precise relationship between soil moisture and surface evaporation, e.g. see Wetzell and Chang 1987). But a change in stability above the ABL (γ_θ) affects both dry-air entrainment and boundary layer growth, two opposing processes in the ABL-top relative humidity tendency equation. So, only if the above-ABL specific humidity drop is greater (less negative) than some threshold $\Delta q > -RHhc_2$ (at the ABL top), will ne increase with decreasing stability, which corresponds to $ne > -L_v/c_p(1 + C_\theta)RHc_1$ (to the left of the heavy vertical dashed lines in Figure 6.11). Note that this threshold value of Δq decreases (becomes *more* negative) for increasing RH , h , and c_2 (decreasing T); this is the case at Cabauw from morning to mid-day. Finally, as $\Delta q \rightarrow 0$, $ne > 0$ for $\gamma_\theta < c_2/c_1 < \approx g/c_p \approx 1^\circ\text{C} (100 \text{ m})^{-1}$ (dry adiabatic lapse rate).

Before we proceed, we note that the outcome of (6.1)-(6.3) (as presented in Figures 6.10 and 6.11) agrees well with the output of the coupled model (confirmed by more than a thousand runs), as long as $h/-L > 5$ which is required for the assumption of mixed-layer conditions (see Holtslag and Nieuwstadt 1986).

6.5.3 Discussion

We can examine the various ABL-top relative humidity tendency terms in (6.1)-(6.3) for Cabauw data during periods of positive surface fluxes and when $h/-L > 5$ (Table 6.1; Figure 6.10). From mid-morning until mid-day, the dry-air entrainment term decreases in magnitude (becomes less negative) with time because of increasing ABL depth and a somewhat steady value of dry air above the ABL (despite decreasing atmospheric stability just above the growing ABL), while the ABL growth term increases greatly as the atmospheric stability decreases. During this same time period the ABL warming term diminishes only modestly, and the evaporative fraction increases only slightly. The effect of soil moisture is then to increase the ABL-top relative humidity ($ne < 1$), except during the mid-day rapid ABL growth when the effect of soil moisture only modestly increases ABL-top relative humidity ($ne < \approx 1$). We note that the ABL-top relative humidity increased sufficiently for ABL clouds (both modeled and observed) to form by mid to late afternoon (see discussion in section 6.4.2).

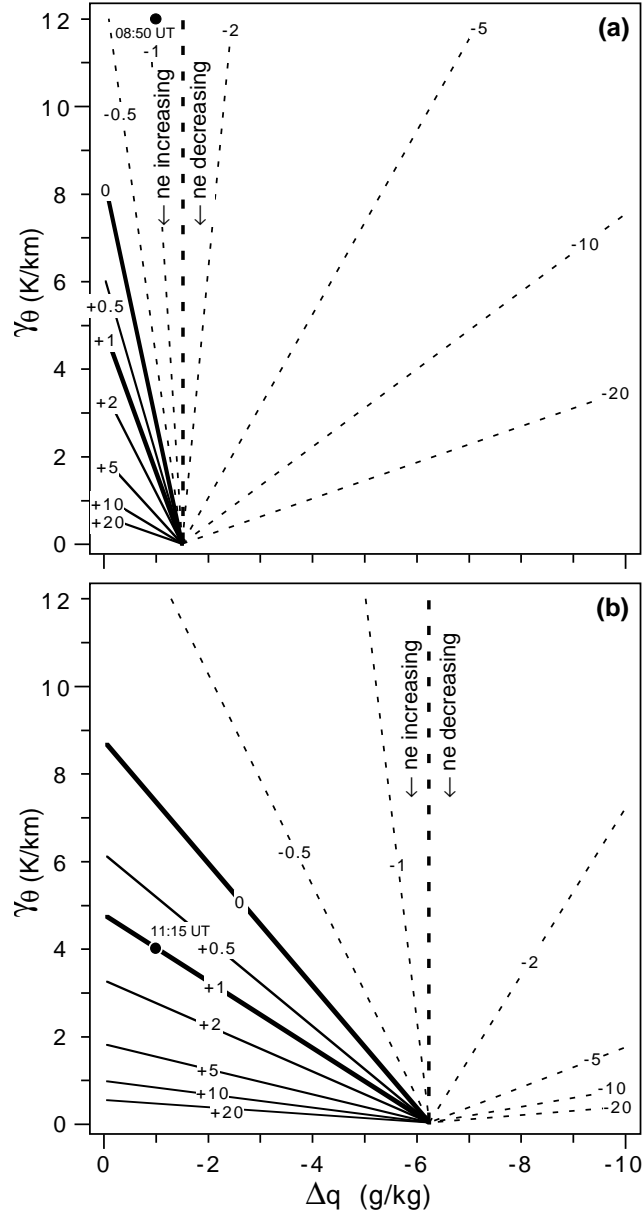


Figure 6.11: Values of ne as a function of above-ABL atmospheric stability (γ_θ) versus above-ABL specific humidity drop (Δq) for (a) morning conditions at Cabauw (Netherlands, 31 May 1978; $RH=0.80$, $h=400$ m, and $T=12.0^\circ\text{C}$ at 8:50 UT, with Cabauw value based on observations, upper left, black dot) and (b) mid-day conditions ($RH=0.90$, $h=1875$ m, and $T=5.0^\circ\text{C}$ at 11:15 UT, with Cabauw value middle left, black dot). See text for details.

Table 6.1: Quantities (top) used to evaluate the relative humidity tendency terms (bottom; non-dimensional except RH tendency) from observations via (6.1)-(6.3) for 31 May 1978 at Cabauw, Netherlands, corresponding to times at the Cabauw tower in the morning shallower boundary layer (6:45 and 7:15 UT), and radiosonde launches at Cabauw (7:48 and 8:50 UT) and at De Bilt (11:15 UT). See text for explanation.

time [UT]	$R_n - G$ [W m ⁻²]	h [m]	$(\frac{p}{p_s})^{R_d/c_p}$ [-]	T [C]	RH [-]	γ_θ [K km ⁻¹]	Δq [g kg ⁻¹]	$h/-L$ [-]
6:45	168	137	1.00	15.0	0.81	20	-1.0	6.8
7:15	211	172	0.99	15.0	0.80	18	-1.0	17.6
7:48	247	250	0.99	14.0	0.77	16	-1.0	31.0
8:50	336	400	0.99	12.0	0.80	12	-1.0	47.0
11:15	431	1875	0.94	5.0	0.90	4	-1.0	250.0
time [UT]	dry-air entrain.	ABL growth	ABL warming	ne	e_f	$ne(1 - e_f)$	$e_f +$ $ne(1 - e_f)$	dRH/dt [hr ⁻¹]
6:45	-1.09	0.67	-1.67	-2.09	0.86	-0.30	0.55	0.076
7:15	-0.96	0.73	-1.65	-1.88	0.82	-0.34	0.48	0.066
7:48	-0.75	0.76	-1.52	-1.50	0.83	-0.25	0.58	0.068
8:50	-0.62	0.95	-1.41	-1.08	0.81	-0.20	0.61	0.069
11:15	-0.40	2.51	-1.18	0.94	0.79	0.20	0.99	0.048

Table 6.2: Mid-day normalized relative humidity tendency, $e_f + ne(1 - e_f)$ ($= \partial RH / \partial t \rho L v h q_s / (R_n - G)$) for different soil moisture conditions (evaporative fractions) and atmospheric stability conditions. See text for explanation.

stability above ABL (γ_θ , [K km ⁻¹])	non-evaporative term (ne)	evaporative fraction (e_f)		
		dry (0.20)	\approx obs (0.79)	moist (0.95)
decreased (1.0)	7.28	6.021	2.315	1.314
reference (4.0)	0.94	0.949	0.987	0.997
increased (7.0)	0.03	0.224	0.797	0.953

We now focus on the rapid ABL growth period (e.g. 11:15 UT at Cabauw), during or after which ABL clouds are generally initiated, and examine the effect of changing evaporative fraction and atmospheric stability on the relative humidity tendency. Using the initial soil moisture value near that observed at Cabauw, note that as with the Cabauw observations, $ne < \approx 1$ for the reference set model run as well (Table 6.2). For a drier soil in this case, normalized relative humidity tendency decreases slightly with ABL cloud cover also decreasing. In a deeper growing boundary layer due to larger surface sensible heat flux, a larger h yields a smaller actual relative humidity tendency (see (6.1)-(6.3)), and less cloud cover (Figure 6.9a). Here stronger warm- and dry-air entrainment negates the effect of ABL-top cooling on the increase of ABL-top relative humidity. For a moister soil, normalized relative humidity tendency increases slightly, although with a shallower ABL depth the actual relative humidity tendency is less with subsequently less cloud cover. In this case the greatest relative humidity tendency (and thus cloud cover) occurs for intermediate soil moisture. This is in agreement with our assessment of the role of soil moisture on ABL cloud development based on the development in section 6.5.2.

For the two sets of model runs where the atmospheric stability above the boundary layer is changed, note that Δq is greater (less negative) than the threshold value, so that an increase (*decrease*) in atmospheric stability (γ_θ) should yield a decrease (*increase*) in ne (see section 6.5.2, Figure 6.11). So for the set of model runs with increased (stronger) atmospheric stability, ABL depth is shallower (as one would expect), and since $ne < 1$ there is a decrease in ABL-top relative humidity tendency and thus less cloud cover for drier soils (Table 6.2, Figure 6.9a), with increasing cloud cover for increasing soil moisture ($ne \approx 0$). In contrast, for the set of model runs with

decreased (weaker) atmospheric stability, ABL depth is deeper (as one would expect), and yet since $ne > 1$ there is an increase in ABL-top relative humidity tendency and thus more cloud cover for drier soils, with decreasing cloud cover for increasing soil moisture ($ne \gg 1$). Note that the largest values of $\partial RH/\partial t$ and thus ABL cloud cover are achieved for a small evaporation fraction (lower soil moisture) with weak stability ($ne \gg 1$), as was suggested in the relative humidity tendency development in section 6.5.2.

These findings are qualitatively consistent with Ek and Mahrt (1994) for HAPEX-MOBILHY data (summer 1986, southwest France) which found that on a fair-weather day with strong atmospheric stability above the ABL and a large observed evaporative fraction (via higher soil moisture) gave a similar mid-day relative humidity at the ABL top as a fair-weather case nine days later with weaker atmospheric stability and decreased soil moisture.

6.6 Summary

In this coupled model study we have examined land-atmosphere interaction using model runs with observational verification. Results indicate that in coupled land-surface – atmospheric boundary layer (ABL) model runs, realistic daytime surface fluxes and atmospheric profiles including ABL clouds are produced using the CAPS model. Both land-surface and ABL model runs yielded encouraging results operating separately, and when coupled together interactively, even in the presence of model-predicted ABL clouds. This suggests that in this coupled land-atmosphere system, processes are well-represented by the CAPS model.

The role of soil moisture on ABL cloud development was explored in terms of a new ABL-top relative humidity tendency equation, where a number of land-surface and atmospheric processes interact. It was shown with good agreement between model runs, an analytical development, and analysis of Cabauw data, that the effect of soil moisture is to increase ABL-top relative humidity tendency and thus the potential for ABL cloud formation (given sufficient initial ABL relative humidity, and above-ABL air that is not too dry) only if the stability above the boundary layer is not too weak. On the other hand, for weak stability above the boundary layer, drier soils yield a greater ABL-top relative humidity tendency and thus cloud cover. There is great interest in the study of land-atmosphere interaction and a large number of data

sets from many field programs representing diverse geophysical locations with which to study these interactions. The new relative humidity tendency equation presented here may provide a useful quantitative framework for future land-surface – ABL interaction studies in the formation of ABL clouds.

Acknowledgements. This research was supported by the NOAA Climate and Global Change Program under award number NA36GP0369, the Air Force Office of Scientific Research under contract F49620-9610058, and the Royal Netherlands Meteorological Institute (KNMI) which provided the Cabauw data set and sponsored Michael Ek as a visiting scientist. We also wish to thank Fred Bosveld and Bart van den Hurk at KNMI, Anton Beljaars at ECMWF, Larry Mahrt and Richard Cuenca at Oregon State University, Ken Mitchell at NCEP/EMC, and a host of other scientists at Wageningen University, KNMI, and elsewhere for their helpful comments, patience, and support during the progress of this work. In addition, we wish to acknowledge the useful comments from reviewer Christa Peters-Lidard at NASA/GSFC and two anonymous referees, and AMS/JHM editor Dara Entekhabi.

Chapter 7

Summary and perspective

7.1 Summary

This thesis has focused on examining land-atmosphere processes and interactions using observations and the one-dimensional (column) CAPS (or OSU) model that couples the land surface with the atmospheric boundary layer (ABL). The central aim has been to describe these processes and interactions in an effort to understand the nature of daytime land-atmosphere coupling, e.g. as illustrated in Figure 7.1.

In Chapter 2 the focus was on the influence of variations in soil properties on modeling land-surface – ABL interaction, using aircraft and surface (tower) observations from HAPEX-MOBILHY (spring-summer 1986, southwest France). Specifically, variations in the b exponent parameter from the Clapp and Hornberger (1978) formulation (commonly used in land-surface modeling) had a large impact on the magnitude of soil hydraulic and thermal properties, and subsequently on the modeled surface energy balance and resulting atmospheric boundary-layer development. Over the wide range of soil moisture conditions modeled, the largest effect was for dry to moderate soil moisture where the change in the hydraulic and thermal property curves is greatest. The effect was most notable over bare soil since for this surface condition there is no moderating influence of soil moisture removal from the soil column that is the case with transpiration for a full vegetation cover.

Clapp and Hornberger (1978) stated that caution must be exercised when mean soil properties are used if standard deviations of these properties are large, which is

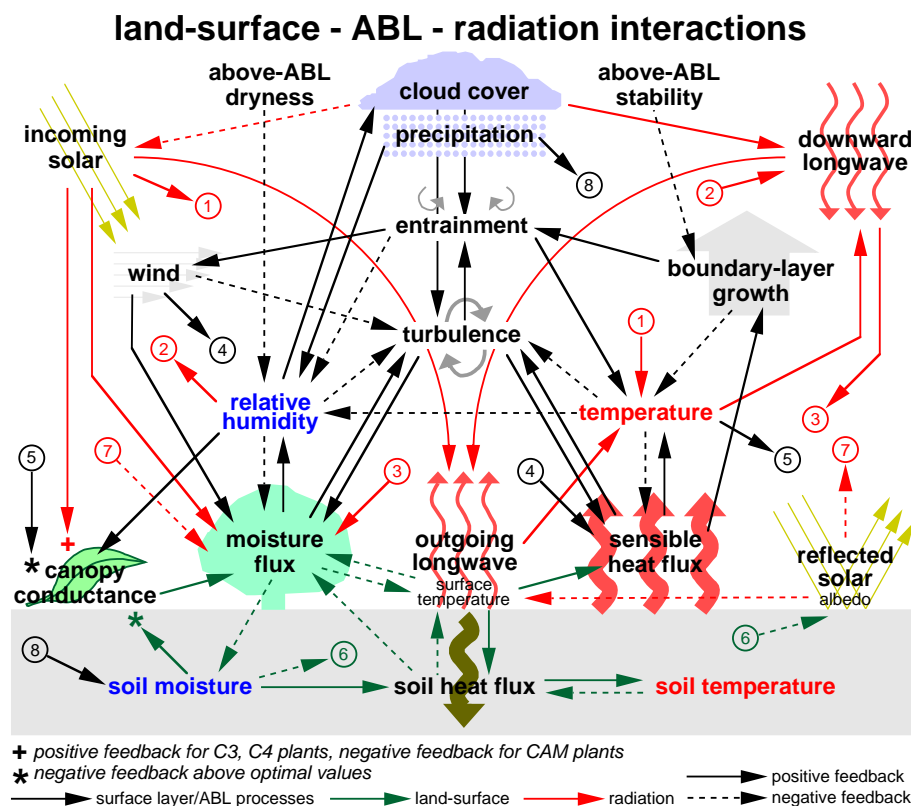


Figure 7.1: Important interactions between the land-surface and atmospheric boundary layer for conditions of daytime surface heating. Solid arrows indicate the direction of feedbacks that are normally positive (leading to an increase of the recipient variable). Dashed arrows indicate negative feedbacks. Two consecutive negative feedbacks make a positive feedback. (This is an expanded version of Figure 6.1.)

evident from this one-dimensional modeling study. Accounting for such variations in soil properties in some manner is then important to consider since this can then directly influence the performance of large-scale models.

In Chapter 3 the evolution of the relative humidity at the boundary-layer top was explored with land-surface – ABL modeling, and with surface, radiosonde, and aircraft observations from HAPEX-MOBILHY. A tendency equation for relative humidity at the ABL top was evaluated where it was found that this tendency is due to the net change of several effects, some of which are opposing: surface heat and moisture fluxes, ABL growth, and ABL-top warm- and dry-air entrainment. The analyses indicate that the adiabatic decrease of the boundary-layer top temperature during the morning rapid boundary-layer growth exerts the strongest influence on the relative humidity tendency.

If the air aloft is characterized by weak stratification and is not too dry, the ABL-top relative humidity and thus the probability of cloud initiation might increase more rapidly over dry surfaces than over wet surfaces. In this case, the more rapid growth over dry surfaces is the main influence on ABL-top relative humidity tendency. This case appears to explain increased convection and cloud development over surfaces of large sensible heat flux compared to surfaces with strong evaporation.

However, if the air above the boundary layer is characterized by significant stratification, the boundary-layer relative humidity is generally greater over moist surfaces where boundary-layer growth is weaker. This case includes the drought feedback mechanism of dry spring soil conditions where reduced soil moisture reduces the probability of precipitation thus intensifying drought conditions; this scenario is more likely to occur with dry air aloft in which case the more rapid growth of the boundary layer over dry surfaces leads to entrainment drying of the boundary layer. Previously proposed drought scenarios are generally valid only for a specific parameter regime. Modeling drought conditions as well as forecasting boundary-layer cloud development requires adequate representation of several different boundary-layer processes and interactions controlling the relative humidity field.

In Chapter 4, aircraft observations taken during HAPEX-MOBILHY were used to examine the influence of relative humidity on ABL cloud cover, where the spatially averaged cloud cover was expected to depend on both the spatially averaged and spa-

tial variability of near-ABL-top relative humidity. In the upper part of the boundary layer, the relative humidity variance is large partly because of the significant moisture fluctuations and their negative correlation with temperature fluctuations. The spatial variability of relative humidity consists of both turbulent and mesoscale variations, and with greater variation in relative humidity, clouds first form at a lower average relative humidity. For this data set, turbulent and mesoscale relative humidity variations were found to contribute about equally to the total variation of relative humidity, and that the variance of relative humidity varies significantly from day to day.

An expression for fractional cloud cover was formulated, where the turbulent relative humidity variations was based on dry-air entrainment and boundary-layer similarity theory, and the mesoscale variation of relative humidity was determined to be a function of horizontal grid size based on the HAPEX-MOBILHY experimental domain (50-100 km). Testing the cloud cover formulation in subsequent land-surface – ABL model tests indicated a greater sensitivity of the modeled cloud cover to the specified vertical motion field and to horizontal advection, than to the adjustable coefficients of the cloud cover formulation.

In Chapter 5 the goal was to properly represent the soil-vegetation system in offline model runs for Cabauw, Netherlands, in land-surface-only model tests driven by atmospheric forcing for the spring 1978 case study day examined. Results indicated that realistic daytime surface fluxes were produced with existing or alternate formulations, but using *un-tuned* model parameters. Model sensitivity tests included modifications to the parameterization of canopy conductance. The locally-derived formulation specific to Cabauw was more successful in representing the canopy conductance than the "off-the-shelf" formulations. This suggests that classifications covering a broad land-surface category (e.g. "grassland") should be re-examined perhaps in terms of locally-derived data sets.

Changes to the soil heat flux formulation were investigated, where accounting for the effect of overlying vegetation on the reduction of soil heat flux was found to be important since this affects the amount of available energy that must be further partitioned into surface latent and sensible heat fluxes. Alternatives for plant root density distribution were also examined, where nonlinear distributions that include a much higher root density near the surface, decreasing in density with depth, may not be

appropriate for use in current land-surface schemes. This may be because a static treatment of roots can lead to rapid drying of the higher-root-density soil layers, and thus lead to less accurate predictions of latent heat flux (and subsequently the surface energy budget). A more uniform root distribution may in fact mitigate the problem of treating the root zone as static when in fact the root zone may be rather dynamic in terms of the ability of vegetation to extract available soil water for transpiration.

Finally, in Chapter 6, coupled land-surface – ABL interaction was modeled using the same case study day at Cabauw and utilizing the land-surface modeling results from Chapter 5, and extending the findings from Chapters 2 and 4. Both ABL-only as well as coupled land-surface – ABL model runs yielded realistic daytime surface fluxes and atmospheric profiles, even in the presence of model-predicted ABL clouds, suggesting that in this coupled system, both land-surface and ABL processes were well-represented.

A more detailed investigation of the role of soil moisture on ABL cloud development was then explored in terms of a new ABL-top relative humidity tendency equation that depends on many possible land-surface – ABL processes, extending the results of Chapter 3. It was shown with good agreement between model runs, an analytical development, and analysis of Cabauw data, that the role of soil moisture is to increase ABL-top relative humidity tendency and thus the potential for ABL cloud formation given (1) sufficient initial ABL relative humidity, and (2) above-ABL air that is not too dry, only if (3) the stability above the boundary layer is not too weak. On the other hand, for weak stability above the boundary layer, drier soils can yield a greater ABL-top relative humidity tendency and thus more potential for cloud initiation.

7.2 Perspective

The model formulations in the studies presented in this thesis are appropriate in representing land-surface and ABL processes in mesoscale and large-scale atmospheric models, with grids that are typically 10-100 km. As such, the results presented here are then useful for mesoscale and large-scale numerical weather prediction (NWP) and in climate modeling.

From the perspective of parameterizing physical processes, future work in land-

surface modeling (e.g. for use in NWP and climate modeling) should further examine for example (1) issues of plant transpiration (canopy conductance formulations, and surface fluxes in sparse canopies), (2) the influence of long-term and deep soil conditions (e.g. soil layers and root density, soil hydraulic and thermal properties, and their spatial variability), (3) the effect on surface fluxes due to subgrid-scale motions (i.e. generated by surface inhomogeneity of surface skin temperature, soil moisture, soil temperature, etc), and (4) improvements to cold season processes (frozen soil and snowpack physics). As a specific example noted in Chapter 5, it would be useful to repeat the 1987 annual-cycle land-surface-only model runs at Cabauw undertaken during PILPS phase 2a (T. H. Chen et al 1997), in order to test the van Genuchten (1980) formulation for hydraulic conductivity that is more commonly used and robustly tested in the soil physics community, versus Clapp and Hornberger (1978) which is more popular within the meteorological community. Many of these land-surface issues are being addressed in the Noah land-surface model (used in the National Centers for Environmental Prediction (NCEP) NWP models; Ek et al 2003). The Noah model is an upgraded version of the CAPS (or OSU) land-surface model used here.

In addition, there remains the seemingly ever-present issue of the proper parameterization of surface fluxes and turbulent mixing in the stable boundary layer, with a typical model cold bias due to too little downward heat flux in the stable boundary layer. Model formulations are required to account for both spatial and temporal variability of land-surface and atmospheric conditions, but this is a difficult problem due to the uncertainty of observations taken in the often intermittently turbulent stable boundary layer. Additionally, low-level (ABL) cloud cover and downward longwave radiation are important parts of this nocturnal modeling puzzle.

The ABL cloud cover formulation presented in Chapter 4 was developed using HAPEX-MOBILHY data (continental fair weather cumulus), but has also shown quite favorable performance in the study of Mocko and Cotton (1995) using data from BLX (also continental fair weather cumulus) as well as from FIRE (marine stratocumulus); it should be extended to additional data sets to further test its performance under more diverse geographic and atmospheric conditions. Also, this formulation assumed a Gaussian distribution of relative humidity, but may be more easily represented using a simpler top-hat distribution of specific humidity (Ek 2005, unpublished manuscript). Additionally, the ABL model parameterization presented here assumes

”dry” adiabatic mixing, but can be extended to moist-conservative ABL mixing, as well as cloud-enhanced turbulence (Ek 2005, unpublished manuscript) thereby properly accounting for turbulent mixing in the cloudy boundary layer.

Finally, there is great interest in the study of land-atmosphere interaction and a large number of data sets from many field programs representing diverse geophysical locations with which to study these interactions. The new relative humidity tendency equation presented in Chapter 6 may provide a useful quantitative framework for future coupled land-surface – ABL interaction studies, such as the focus on the diurnal cycle suggested by Polcher (2004), and the ”Local Coupling” project (van den Hurk et al 2004). This work may also be extended to determine atmospheric versus soil moisture roles in the evolution of the *near-surface* relative humidity, thereby inferring soil moisture from the relative humidity tendency equation since soil moisture is a critical quantity in model initialization.

Appendix A

Coupled Atmospheric boundary layer–Plant–Soil model

The Coupled Atmospheric boundary layer - Plant - Soil (CAPS) model (also known as the Oregon State University (OSU) land-surface – atmospheric boundary-layer model; Figure A.1) operates in a one-dimensional (column) mode and represents turbulent mixing in the atmospheric boundary layer (ABL) coupled with an interactive land-surface, and simple surface radiation formulation and boundary-layer cloud cover formulation. (Over the ocean, the land-surface scheme is replaced with a specified sea surface temperature, or alternatively, an ocean mixed-layer model.) The CAPS model is suitable for inclusion in mesoscale and large-scale models, e.g. numerical weather prediction and climate models. The reader is referred to Troen and Mahrt (1986), Pan and Mahrt (1987), Ek and Mahrt (1991b), and Holtslag and Boville (1993) for details of the numerical procedures for time integration in the model.

Here we describe the physical components of the CAPS model. We begin with the calculation of radiation forcing at the surface (section A.1), followed by surface exchange coefficients (section A.2), then land-surface processes (section A.3) which determine the soil temperature and moisture content, and surface fluxes and outgoing longwave radiation (via surface temperature), and finally atmospheric boundary layer (ABL) mixing and ABL cloud cover (section A.4).

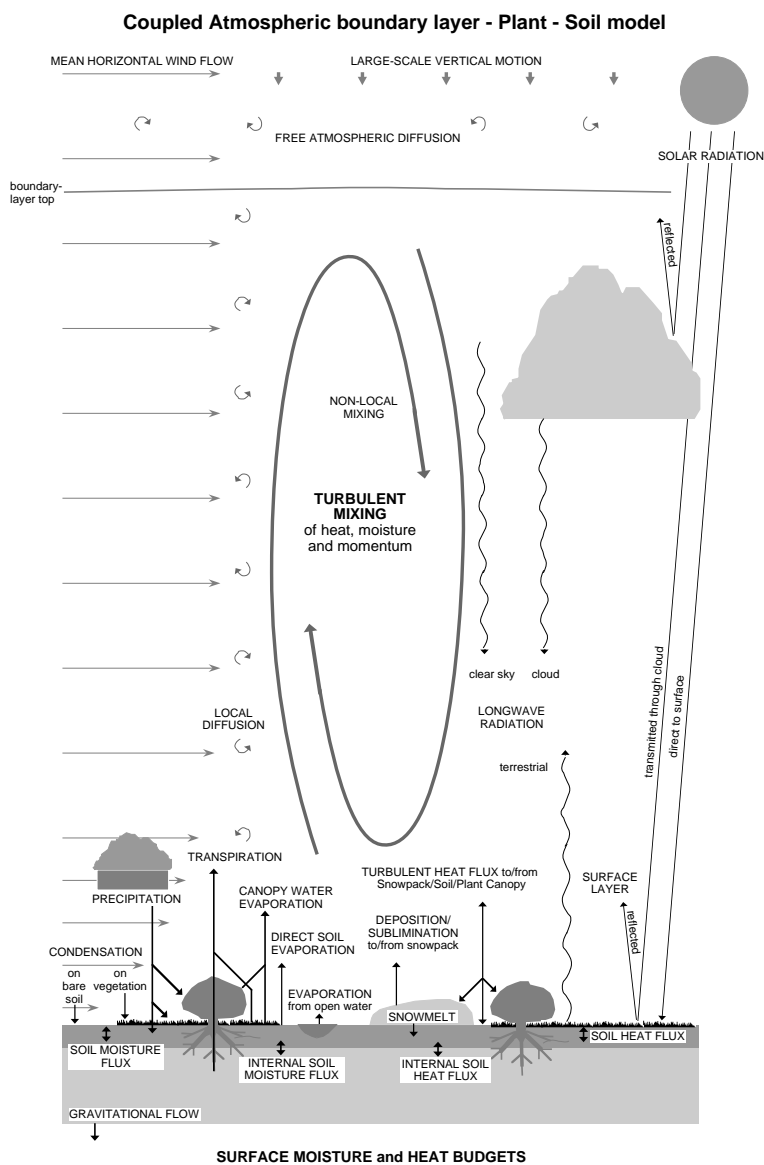


Figure A.1: The one-dimensional (column) coupled atmospheric boundary layer – plant – soil (CAPS) model that simulates the atmospheric boundary layer, vegetated surface, and underlying soil physical processes.

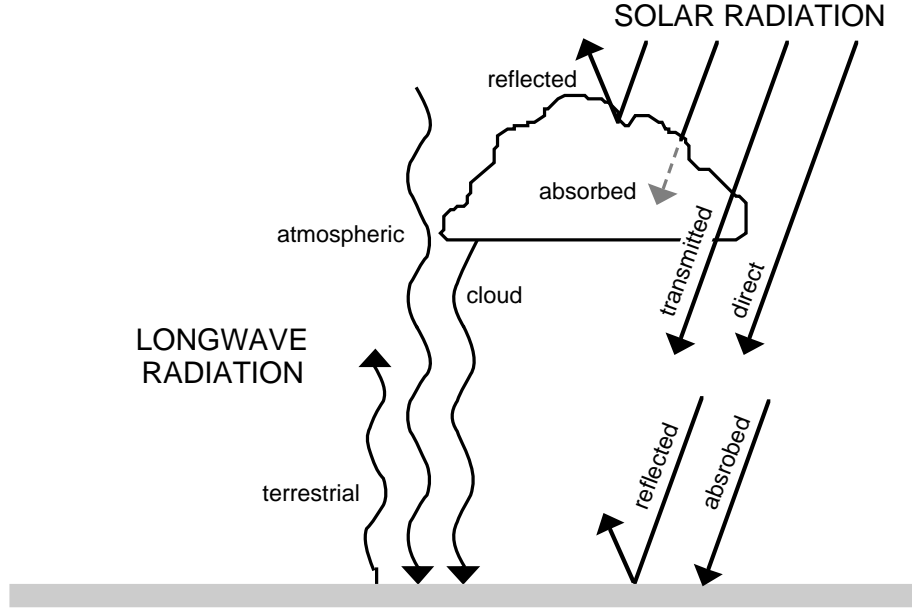


Figure A.2: Radiation in the CAPS model.

A.1 Surface radiation scheme

The simple radiation scheme determines the total downward radiation at the surface, a combination of incoming solar (shortwave) plus downward atmospheric (longwave) radiation, modified by atmospheric boundary layer clouds (Figure A.2; ABL clouds are described in section A.4.4). This incoming radiation provides energy to drive land-surface processes, surface fluxes and subsequent development of the atmospheric boundary layer. While the first order effect of radiation is to affect the available energy at the surface (including ABL cloud influence on downward radiation at the surface), the CAPS model may be coupled with a full radiation (column) scheme in order to add further detail to the ABL radiation budget, e.g. as in the nocturnal boundary layer studies described in Ha and Mahrt (2001, 2003).

A.1.1 Incoming solar radiation

Incoming solar radiation at the surface is calculated following the method of Collier and Lockwood (1974) where clear sky incoming solar radiation at the top of the atmosphere is determined, and then reduced at the surface to account for a "bulk"

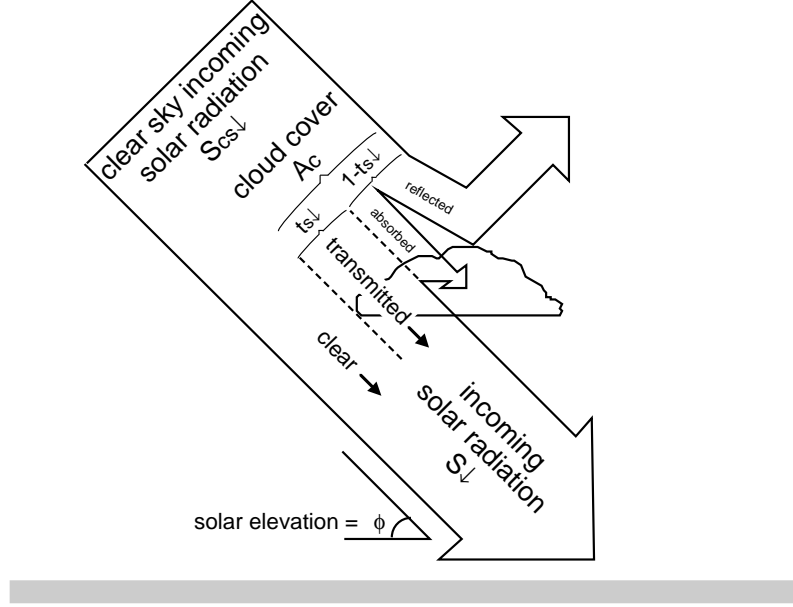


Figure A.3: Incoming solar radiation interaction with cloud cover and the terms used in the calculation of solar radiation reaching the surface.

atmospheric turbidity (see also Holtslag and van Ulden 1983), as well as the presence of ABL clouds. The equation for solar radiation as it reaches the surface is

$$S_{\downarrow} = S_{cs\downarrow}(1 - A_c + t_{S\downarrow}A_c), \quad (\text{A.1})$$

where S_{\downarrow} is solar radiation reaching the surface (that is, before any reflection), $S_{cs\downarrow}$ is the clear sky solar radiation adjusted for solar elevation and time of year, A_c is the fractional (ABL) cloud cover, and $t_{S\downarrow}$ is the fraction of solar radiation transmitted through clouds (Figure A.3). In the CAPS model transmission depends on sun angle as

$$t_{S\downarrow} = t_0 + t_1 \sin \phi, \quad (\text{A.2})$$

where ϕ is solar elevation, and $t_0 = 0.06$ and $t_1 = 0.17$ (following Liou 1976 for "climatological" cumulus clouds). More sophisticated transmission functions include cloud thickness and cloud droplet distribution (cloud optical depth), but are not adopted here for simplicity.

A.1.2 Albedo

The surface-reflected solar radiation (albedo, α) is a function of surface characteristics, but is usually taken as a constant in the CAPS model. Alternatively, albedo may be expressed as a function of solar elevation

$$\alpha = a_0 + a_1 \sin \phi, \quad (\text{A.3})$$

where a_0 and a_1 are empirical coefficients depending on surface characteristics, and ϕ is the solar elevation (e.g. following Duynkerke 1992). Additional factors affecting surface albedo include vegetation, and in the case of bare soil conditions, soil type and surface moisture, but again are not adopted here for simplicity.

A.1.3 Downward atmospheric radiation

Downward radiation atmospheric is parameterized using the method from Satterlund (1979)

$$L\downarrow = \epsilon_{ref} \sigma T_{ref}^4 + c_0 A_c, \quad (\text{A.4})$$

where $L\downarrow$ is the atmospheric radiation, ϵ is the emissivity of the atmosphere, a function of the temperature (T) and moisture at the reference level (ref) of 200 m in the model; σ is the Stefan-Boltzmann constant ($5.67 \times 10^{-8} \text{ W m}^{-2} \text{ K}^{-4}$). The second term on the left hand side accounts for the enhancement of downward atmospheric (longwave) radiation due to the presence of boundary layer cloud cover, where c_0 is a constant equal to 60 W m^{-2} (Paltridge and Platt 1976). The emissivity is expressed as

$$\epsilon_{ref} = 1.08[1 - \exp(-e_{ref}^{\frac{T_{ref}}{c_1}})], \quad (\text{A.5})$$

where e is vapor pressure (with a maximum of 0.05) and c_1 is a constant equal to $2016K$.

A.2 Surface fluxes and surface exchange coefficients

A.2.1 Surface fluxes

Given the surface values of potential temperature (θ_s) and specific humidity (q_s) obtained from the surface energy budget (described in section A.3), and the atmospheric variables updated by the boundary-layer scheme (described in section A.4),

the CAPS model determines the surface sensible (H) and latent (LE) heat fluxes, and the surface stress (τ), expressed in a bulk-aerodynamic form as

$$\begin{aligned} H &= \rho c_p C_h U_a (\theta_s - \theta_a), \\ L_v E &= \rho L_v C_q U_a (q_s - q_a), \\ \tau &= \rho C_m U_a^2, \end{aligned} \tag{A.6}$$

where H and $L_v E$ are the sensible and latent heat fluxes, respectively, and τ is the surface stress ($=\rho u_*^2$, where u_* is the surface friction velocity), ρ is air density, c_p is specific heat ($1004.5 \text{ J kg}^{-1} \text{ K}^{-1}$), and L_v is latent heat ($2.5 \times 10^6 \text{ J kg}^{-1}$), C_h , C_q , and C_m are the surface turbulent exchange coefficients for heat, moisture, and momentum, respectively (C_m is also called the drag coefficient, C_d), all functions of stability, defined below. (Here we adopt the usual convention that $C_q=C_h$.) $\theta_s - \theta_a$ and $q_s - q_a$ are the gradients in potential temperature and specific humidity, respectively, between the surface and the reference height of z_a in the atmosphere (e.g., the first atmospheric level in a model), U_a is the horizontal wind speed (at z_a) defined as

$$U_a = \sqrt{u_a^2 + v_a^2}, \tag{A.7}$$

where u_a and v_a are the horizontal wind components at z_a . As demonstrated by Beljaars (1995), to yield non-zero surface sensible and latent heat fluxes in the case of vanishing horizontal wind speed (e.g. over a model grid) under free convection conditions, an additional horizontal velocity scale proportional to the convective velocity scale (w_* , defined in section A.4) can be included in U_a to account for model subgrid scale motions.

A.2.2 Surface exchange coefficients

Surface exchange coefficients (and thus surface fluxes) are calculated by iterating an implicit formula of the Monin-Obukhov stability-dependent profile functions based on surface-layer similarity theory. This is an alternative to using the explicit approach by Louis (1979) and Louis et al (1982) based on the near-surface bulk Richardson number. There are limitations in the Louis formulations for cases where the ratio of the momentum to heat roughness is large, as demonstrated in Holtslag and Ek (1996). These limitations have been further addressed in van den Hurk and Holtslag (1997), who suggest more accurate explicit functions based on the bulk Richardson

number. We present both implicit and explicit approaches here; see Beljaars and Holtslag (1991) for a more detailed comparison.

implicit

The surface exchange coefficients for momentum and heat (and moisture) using the implicit formulations are (respectively)

$$C_m = \frac{k^2}{[\ln(z_a/z_{0m}) - \Psi_m(z_a/L) + \Psi_m(z_{0m}/L)]^2}, \quad (\text{A.8})$$

$$C_h = \frac{k^2}{[\ln(z_a/z_{0m}) - \Psi_m(z_a/L) + \Psi_m(z_{0m}/L)][\ln(z_a/z_{0h}) - \Psi_h(z_a/L) + \Psi_h(z_{0h}/L)]}, \quad (\text{A.9})$$

where k is the von Kármán constant (taken as 0.40), z_a is the atmospheric reference height (e.g., first model level height), z_{0m} and z_{0h} are the roughness lengths for momentum and heat, respectively, L is the Obukhov length, and $\Psi_{m,h}$ are the stability profile functions for momentum and heat. (As with the exchange coefficient, we assume that $\Psi_q = \Psi_h$.) The profile functions for unstable conditions (following Paulson 1970) are

$$\Psi_m = 2\ln[(1+x)/2] + \ln[(1+x^2)/2] - 2\tan^{-1}(x) + \pi/2, \quad (\text{A.10})$$

$$\Psi_h = 2\ln[(1+x^2)/2], \quad (\text{A.11})$$

where

$$x = (1 - 16z/L)^{1/4}, \quad (\text{A.12})$$

and for stable conditions (following Webb 1970) are

$$\Psi_m = \Psi_h = -5z/L. \quad (\text{A.13})$$

The Webb (1970) profile functions are fairly consistent with most data for $0 < z/L < 0.5$ (see Beljaars and Holtslag 1991). An alternate profile function for stable conditions follows Holtslag and De Bruin (1988) for up to $z/L \approx 7$

$$-\Psi_m = a\frac{z}{L} + b\left(\frac{z}{L} - \frac{c}{d}\right)\exp\left(-d\frac{z}{L}\right) + \frac{bc}{d}, \quad (\text{A.14})$$

$$\Psi_h = \Psi_m, \quad (\text{A.15})$$

where $a=0.7$, $b=0.75$, $c=5$, and $d=0.35$. This expression behaves like (A.13) for small z/L values and approaches $-\Psi_m \approx a(z/L)$ for large z/L .

explicit

Following Louis (1979) and Louis et al (1982), the surface exchange coefficients for momentum and heat (and moisture) using the explicit formulations are (respectively)

$$C_m = k^2 \frac{F_m}{[\ln(z_a/z_{0m})]^2}, \quad (\text{A.16})$$

$$C_h = \left(\frac{k^2}{R}\right) \frac{F_h}{\ln(z_a/z_{0m})\ln(z_a/z_{0h})}, \quad (\text{A.17})$$

where R , estimated as 1.0, is the ratio of the drag coefficients for momentum and heat in the neutral limit and is taken from Businger et al (1971). Here, C_m and C_h are functions of $F_{m,h}$ instead of $\Psi_{m,h}$. For unstable condition (modified by Holtslag and Beljaars 1989), $F_{m,h}$ are defined as

$$F_m = 1 - \frac{10Ri_b}{1 + 75k^2[\ln(z_a/z_{0m})]^{-2}[-Ri_b(z_a/z_{0m})]^{1/2}}, \quad (\text{A.18})$$

$$F_h = 1 - \frac{15Ri_b}{1 + 75k^2[\ln(z_a/z_{0m})]^{-1}[\ln(z_a/z_{0h})]^{-1}[-Ri_b(z_a/z_{0m})]^{1/2}}, \quad (\text{A.19})$$

and for stable conditions (modified by Holtslag and Beljaars 1989)

$$F_m = F_h = \frac{1}{1 + 10Ri_b(1 + 8Ri_b)}, \quad (\text{A.20})$$

where Ri_b is the near-surface bulk Richardson number, defined as

$$Ri_b = \frac{gz_a(\theta_{av} - \theta_{sv})}{\theta_{av}U_a^2}, \quad (\text{A.21})$$

where g is gravity, $\theta_{av} - \theta_{sv}$ is the virtual potential temperature gradient between the air θ_{av} at z_a and the surface θ_{sv} (described in section A.3).

By itself, the usual similarity theory under stable conditions leads to a significant overestimation of surface cooling. This is due to (a) failure to consider subgrid-scale spatial variability where vertical fluxes can occur in part of the grid even with large (bulk) Richardson number (Ri_b) based on grid averaged variables (Mahrt 1987), (b) poor vertical resolution where turbulence may occur in thinner layers, perhaps intermittently, even when Ri_b over the model layer is large, (c) neglect of clear air radiative cooling, (d) neglect of gravity wave momentum transport, and (e) use of a surface skin temperature from the surface energy balance (as is done, instead of temperature

at the roughness height) to compute the near-surface bulk Richardson number.

To compensate for such inadequacies, various mechanisms have been employed (and are often unreported) which include capping the allowable value of the Richardson number or specifying a minimum wind speed. An alternative to (A.20) that leads to noted improvement in model performance in the nocturnal boundary layer is the area-averaged exchange coefficient relationship of Mahrt (1987) where for stable conditions, $F_{m,h}$ are defined as

$$F_m = F_h = \exp(-\alpha_m Ri_b), \quad (\text{A.22})$$

where α_m is nominally set equal to 1.0. However, α_m is expected to depend on e.g. (a) model vertical resolution, (b) wind speed, and (c) subgrid characteristics such as standard deviation of subgrid surface skin temperature, terrain height, or some other measure of the surface inhomogeneity.

A.3 Land-surface scheme

The land-surface scheme in the CAPS model determines the surface sensible (H), latent ($L_v E$), and soil (G) heat fluxes, and the surface temperature (T_s), and has been previously described by Mahrt and Pan (1984) and Pan and Mahrt (1987), with more recent updates described in Chen et al (1996), Chang et al (1999), and Ek et al (2003). Snowpack and frozen soil physics are not described here, but can be found in detail in Chang et al (1999) and Koren et al (1999).

The prognostic variables are the volumetric soil moisture content (Θ_{soil_n} , for soil layer n) and soil temperature (T_{soil_n}), and the canopy water content (C_w). We begin with the potential evaporation calculation, followed by the canopy resistance, then the actual evapotranspiration calculation, an update to the soil moisture and canopy water, an update to surface temperature (T_s) and then soil temperatures, and finally calculation of the sensible heat flux (H) and soil heat flux (G).

A.3.1 Prognostic land-surface equations

soil moisture

Soil moisture is modeled with the prognostic equation for the volumetric water content (Θ) as

$$\frac{\partial \Theta}{\partial t} = \frac{\partial K_{\Theta}}{\partial z} + \frac{\partial}{\partial z} \left(D_{\Theta} \frac{\partial \Theta}{\partial z} \right), \quad (\text{A.23})$$

where K_{Θ} is hydraulic conductivity and D_{Θ} is the soil water diffusivity, both highly nonlinear functions of the soil water content (Θ), varying by several orders of magnitude from dry to wet soil conditions; K_{Θ} and D_{Θ} are discussed further in section A.3.4. The layer integrated form of (A.23) for the i th layer is

$$\Delta z_i \frac{\partial \Theta}{\partial t} = \left(D_{\Theta} \frac{\partial \Theta}{\partial z} + K_{\Theta} \right)_{z_{i+1}} - \left(D_{\Theta} \frac{\partial \Theta}{\partial z} + K_{\Theta} \right)_{z_i}. \quad (\text{A.24})$$

soil temperature

Soil heat transfer is treated with a prognostic equation for soil temperature (T) such that

$$C_{\Theta} \frac{\partial T}{\partial t} = \frac{\partial}{\partial z} \left(\lambda_T \frac{\partial T}{\partial z} \right), \quad (\text{A.25})$$

where C_{Θ} is the *volumetric* heat capacity of moist soil and λ_T is the soil thermal conductivity, both functions of the soil water content (Θ). C_{Θ} is linearly related to Θ , whereas λ_T is a nonlinear function of Θ and increases by several orders of magnitude from dry to wet soil conditions; C_{Θ} and λ_T are discussed further in section A.3.5. The layer-integrated form of (A.25) for the i th layer is

$$\Delta z_i C_{\Theta i} \frac{\partial T_i}{\partial t} = \left(\lambda_T \frac{\partial T}{\partial z} \right)_{z_{i+1}} - \left(\lambda_T \frac{\partial T}{\partial z} \right)_{z_i}. \quad (\text{A.26})$$

canopy water

The canopy water content (C_w) changes as

$$\frac{\partial C_w}{\partial t} = \sigma_f PD\downarrow - E_c, \quad (\text{A.27})$$

where σ_f is the plant shading factor ($0 \leq \sigma_f \leq 1$). $PD\downarrow$ is precipitation + dewfall which increases C_w , while canopy water evaporation (E_c) decreases C_w . (Precipitation is a prescribed variable in the CAPS model.)

A.3.2 Potential evaporation calculation

In order to determine the surface values of temperature and moisture (to calculate surface fluxes) it is necessary to solve the surface energy balance. As a first step we

determine the potential evaporation closely following the derivation in Mahrt and Ek (1984), except the usual Penman (1948) potential evaporation relationship is modified (as discussed below) since the surface temperature is needed to compute net radiation.

surface energy balance

We begin by evaluating the surface energy balance for the reference state of the surface but in a saturated condition

$$(1 - \alpha)S\downarrow + L\downarrow - \epsilon\sigma T_s^4 = H + L_v E_p + G, \quad (\text{A.28})$$

where α is the surface albedo and $S\downarrow$ is the incoming solar radiation at the surface (so $(1 - \alpha)S\downarrow$ is the incoming solar radiation absorbed at the surface), $L\downarrow$ is the downward atmospheric radiation, $\epsilon\sigma T_s^4$ is the upward terrestrial radiation (T_s is surface temperature), H is the sensible heat flux, $L_v E_p$ is the potential evaporation, and G is the soil heat flux. Here T_s and H are their values corresponding to the potential evaporation $L_v E_p$. ϵ is the surface emissivity (a function of surface characteristics with a value near unity, but assumed equal to 1.0 in the CAPS model land-surface package), σ is the Stefan-Boltzmann constant ($5.67 \times 10^{-8} \text{ W m}^{-2} \text{ K}^{-4}$), and L_v is latent heat (assumed constant at $2.5 \times 10^6 \text{ J kg}^{-1}$). (The left hand side of (A.28) is the net radiation, $R_n = H + L_v E_p + G$.) α , $S\downarrow$, and $L\downarrow$ are obtained from the simple surface radiation scheme in the CAPS model. In solving for potential evaporation, G is determined using variables from the previous model time step, and is updated later.

outgoing longwave radiation

The outgoing longwave radiation, σT_s^4 , is linearized as

$$\sigma T_s^4 \approx \sigma T_a^4 \left[1 + 4 \left(\frac{T_s - T_a}{T_a} \right) \right], \quad (\text{A.29})$$

where T_a is the air temperature at the first model level in the atmosphere.

sensible heat flux

Here the sensible heat flux uses a saturated surface temperature appropriate for the potential evaporation and is defined as

$$\begin{aligned}
H &= \rho c_p C_h U (\theta_s - \theta_a) \\
&= \rho c_p C_h U [(\theta_s - T_a) - (\theta_a - T_a)],
\end{aligned} \tag{A.30}$$

where ρ is air density, c_p is specific heat, C_h is the exchange coefficient for heat, θ_s is the potential temperture at the surface, and T_a , θ_a and U are the temperature, potential temperture, and wind speed at the first model level in the atmosphere, respectively. For the purpose of calculating potential evaporation, H is determined using values from the last model time step, but will be updated later. The surface potential temperature is defined as

$$\theta_s = T_s \left(\frac{p_{00}}{p_s} \right)^\kappa, \tag{A.31}$$

where p_{00} is the reference pressure (usually taken as 1000 *HPa*), p_s is the surface pressure, and $\kappa = R_d/c_p$; R_d is the gas constant. When $p_{00} = p_s$, then $\theta_s = T_s$. We will proceed with this assumption, but will also provide the general solutions for $\theta_s \neq T_s$.

soil heat flux

Soil heat flux (G) is formulated (e.g. described in McCumber and Pielke 1981) as

$$G = -\lambda_T \frac{\partial T_{s_1}}{\partial z}, \tag{A.32}$$

where λ_T is the soil thermal conductivity and $\partial T_{s_1}/\partial z$ is the soil temperature gradient in the upper soil layer. The finite difference form of (A.32) is

$$G = -\lambda_T \frac{T_s - T_{s_1}}{\Delta z}, \tag{A.33}$$

where T_s and T_{s_1} are the surface and upper soil layer temperatures, respectively, and Δz is the mid-point of the upper soil layer. As with the sensible heat flux (A.30), for the purpose of calculating potential evaporation, G is determined using values from the last model time step, but is updated later.

In the presence of a vegetation layer, soil heat flux is reduced because of reduced heat conductivity through vegetation (Figure A.4). This has been demonstrated by Viterbo and Beljaars (1995) in the ECMWF model land-surface scheme (TESSEL, van den Hurk et al 2000). They suggest a simple parameterization to deal with this

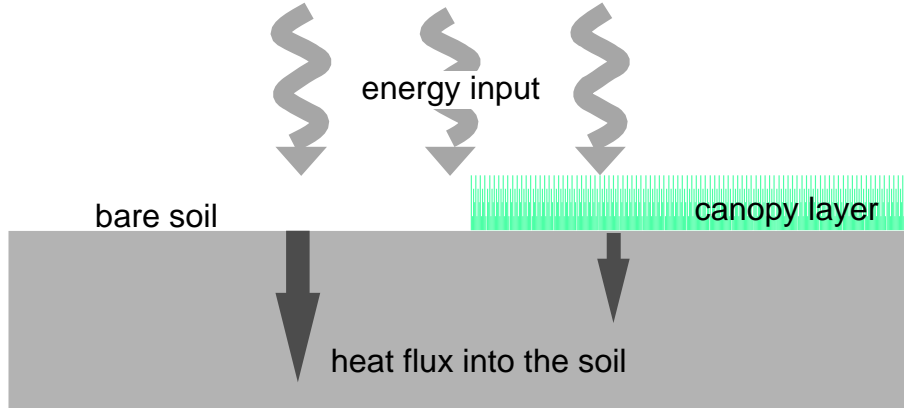


Figure A.4: Schematic showing daytime soil heat flux for bare soil versus a vegetated surface.

effect where G is computed as the product of an empirical coefficient (appropriate to the surface concerned) and the temperature difference between the surface and the center of the upper soil layer (3.5 cm in the TESSEL scheme), i.e.,

$$G = \Lambda_T \Delta T, \quad (\text{A.34})$$

where Λ_T is a fixed constant *thermal conductivity function* (e.g. $7 \text{ W m}^{-2} \text{ K}^{-1}$ for Cabauw, Netherlands). This formulation draws upon earlier work by van Ulden and Holtslag (1985), and implicitly accounts for the reduction of soil heat flux in the presence of vegetation. Van den Hurk et al (1995), van den Hurk and Beljaars (1996), and van den Hurk et al (2000) describe refinements to this approach where the value of Λ_T varies depending on land-surface classification, e.g. bare ground, sparse vegetation, etc.

λ_T and alternatives to the soil heat flux formulation in the TESSEL scheme are discussed further in section A.3.5 (see also section 2.2 in Chapter 2, and section 5.3.3 in Chapter 5).

linearized surface energy balance

We further define

$$F_n = (1 - \alpha)S\downarrow + L\downarrow - \epsilon\sigma T_a^4 - G, \quad (\text{A.35})$$

and substitute into (A.28) to obtain

$$F_n - 4\sigma T_a^4 \left(\frac{T_s - T_a}{T_a} \right) = H + L_v E_p. \quad (\text{A.36})$$

Substituting (A.30) into (A.36) we obtain

$$F_n - 4\sigma T_a^4 \left(\frac{T_s - T_a}{T_a} \right) = \rho c_p C_h U [(T_s - T_a) - (\theta_a - T_a)] + L_v E_p. \quad (\text{A.37})$$

where we have assumed that $\theta_s = T_s$.

final potential evaporation calculation

The potential evaporation is defined as

$$\begin{aligned} L_v E_p &= \rho c_p C_q U (q_{s,sat} - q_a) \\ &= \rho c_p C_h U \left[\frac{dq_s}{dT} (T_s - T_a) + (q_{a,sat} - q_a) \right], \end{aligned} \quad (\text{A.38})$$

where we make the usual assumption that the exchange coefficients for moisture and heat are equal ($C_q = C_h$). dq_s/dT is the slope of the saturation specific humidity with temperature, $q_{s,sat}$ is the surface saturation specific humidity, and $q_{a,sat}$ and q_a are the saturation and actual specific humidities at the first atmospheric model level, respectively. To explicitly eliminate T_s in our expression for potential evaporation, we solve for $T_s - T_a$ in (A.38), where

$$T_s - T_a = \left[\frac{L_v E_p}{\rho L_v C_h U} - (q_{a,sat} - q_a) \right] \left(\frac{dq_s}{dT} \right)^{-1}. \quad (\text{A.39})$$

Substituting for $T_s - T_a$ in (A.37) using (A.39), and after some rearranging, we solve for potential evaporation

$$L_v E_p = \rho c_p C_h U \left(\frac{\Delta \left[\frac{F_n}{\rho c_p C_h U} + (\theta_a - T_a) \right] + A(r+1)}{\Delta + r + 1} \right), \quad (\text{A.40})$$

where

$$\Delta = \frac{dq_s}{dT} \frac{L_v}{c_p},$$

$$\begin{aligned}
A &= \frac{L_v}{c_p}(q_{a,sat} - q_a), \\
r &= \frac{4\sigma T_a^4 R_d}{p_s c_p C_h U}.
\end{aligned}$$

For the case where $\theta_s \neq T_s$, (A.40) assumes a more general form

$$L_v E_p = \rho c_p C_h U \left(\frac{\Delta \left[\frac{F_p}{\rho c_p C_h U} + (\theta_a - T_a) \right] + A(r+1) + (A - \Delta T_a)\delta_\theta}{\Delta + r + 1 + \delta_\theta} \right), \quad (\text{A.41})$$

where $\delta_\theta = [(p_{00}/p_s)^\kappa - 1]$.

A.3.3 Surface evapotranspiration

The total surface evapotranspiration (E) has contributions from three sources: evaporation of water from the plant canopy (E_c), direct evaporation from the soil (E_d), and plant transpiration (E_t), so the total is

$$E = E_d + E_c + E_t. \quad (\text{A.42})$$

The total evaporation cannot exceed the potential evaporation (E_p) defined in (A.40), or alternatively (A.41).

canopy evaporation

The canopy evaporation of free water (E_c) is formulated as

$$E_c = \sigma_f \left(\frac{C_w}{S_w} \right)^n E_p, \quad (\text{A.43})$$

where σ_f is the plant shading factor (a fraction between 0 and 1), C_w and S_w are the actual and saturated water contents, respectively, for a canopy surface (a function of plant type), and $n = 0.5$, following Pan and Mahrt (1987) who cite earlier studies. The canopy water is filled by precipitation or dewfall, and when saturated, all additional water is assumed to fall through to the ground surface.

direct soil evaporation

To determine direct evaporation (E_d) at the air-soil interface, it is necessary to determine the rate at which the soil can provide moisture to the surface to evaporate.

We assume that evaporation may proceed at the potential rate until the surface soil moisture content decreases to an "air-dry" value, Θ_d (see Mahrt and Pan 1984, Chang et al 1999, and references therein). As a first step, we demand that the evaporation be at the potential rate in which case

$$E_p = \left[D_\Theta \left(\frac{\partial \Theta}{\partial z} \right) + K_\Theta \right] (1 - \sigma_f), \quad (\text{A.44})$$

where D_Θ is the soil water diffusivity and K_Θ is the soil hydraulic conductivity. (D_Θ and K_Θ will be discussed further below). The finite-difference form of (A.44) is

$$E_p = \left[D_\Theta \left(\frac{\Theta_s - \Theta_1}{\Delta z/2} \right) + K_\Theta \right] (1 - \sigma_f), \quad (\text{A.45})$$

where D_Θ and K_Θ are the values averaged between the surface and upper soil layer, Θ_s and Θ_1 are the volumetric soil moisture contents at the surface and upper soil model layer, respectively, and $\Delta z/2$ is the mid-point of the upper soil layer. The direct soil evaporation can proceed at a potential rate when the apparent soil moisture at the surface (obtained by solving for Θ_s in (A.45)) is greater than the air-dry value (Θ_d), that is, when the soil is sufficiently wet (demand control stage). When the soil dries out, the evaporation can only proceed at the rate by which the soil can diffuse water upward from below (flux control stage) in which case $\Theta_s = \Theta_d$ and $E_d < E_p$. Then the direct soil evaporation (in finite difference form) is

$$E_d = \left[D_\Theta \left(\frac{\Theta_d - \Theta_1}{\Delta z/2} \right) + K_\Theta \right] (1 - \sigma_f). \quad (\text{A.46})$$

plant transpiration and canopy resistance

Plant transpiration (E_t) is calculated as

$$E_t = \sigma_f k_v \left[1 - \left(\frac{C_w}{S_w} \right)^n \right] E_p, \quad (\text{A.47})$$

where k_v is the "plant coefficient" (a fraction between 0 and 1), and can be related to the commonly used expression of "canopy resistance", r_c (sometimes called "surface resistance" if the surface is not fully covered with vegetation). (See also section 5.3.1 in Chapter 5.) The canopy resistance (r_c) accounts for the reduction in transpiration due to plant stomatal control, and has been often expressed in the meteorological land-surface modeling community as a function of environmental variables, most commonly: incoming solar radiation, air temperature, specific humidity deficit of the air, and soil moisture availability. The plant coefficient (k_v) may be related to r_c by

equating the expression for transpiration used in the CAPS model land-surface scheme with the usual Penman-Monteith expression for transpiration (Monteith 1965). The following relation is then obtained for k_v

$$k_v = \frac{(r + 1 + \Delta + \delta_\theta)}{(r + 1 + \delta_\theta)(1 + r_c C_h U) + \Delta}, \quad (\text{A.48})$$

where terms have been defined above. The canopy resistance itself is given as

$$r_c = r_{cmin} (r_{cs} r_{cT} r_{cq} r_{csoil})^{-1}, \quad (\text{A.49})$$

where r_{cmin} is the minimum canopy resistance, and r_{cs} , r_{cT} , r_{cq} , and r_{csoil} are the irradiance, temperature, specific humidity deficit and soil moisture availability factors affecting the canopy resistance, where all terms here are a function of plant type and time of year; this closely follows the description of canopy resistance given in Noilhan and Planton (1989).

$$r_{cs} = \frac{a_{s1} S \downarrow a_{s2} LAI + \frac{r_{smin}}{r_{smax}}}{a_{s3} + a_{s1} S \downarrow a_{s2} LAI}, \quad (\text{A.50})$$

where LAI is the leaf area index, a_{s1} , a_{s2} , and a_{s3} are coefficients, and r_{smin} is the minimum *stomatal* resistance ($r_{smin} = r_{cmin} LAI$). $S \downarrow$ is the incoming solar radiation determined in the CAPS model surface radiation scheme.

$$r_{cT} = 1 - a_{T1} ((T_{cref} - T_a)^2), \quad (\text{A.51})$$

where a_{T1} is a coefficient, T_{cref} is a reference temperature, and T_a is the air temperature at the first model level in the atmosphere.

$$r_{cq} = 1 - a_{q1} ((q_{a,sat} - q_a)), \quad (\text{A.52})$$

where a_{q1} is a coefficient, and $q_{a,sat}$ and q_a are the saturation and actual specific humidities, respectively, at the first model level in the atmosphere.

$$r_{csoil}(\Theta_i) = \left\{ \begin{array}{ll} 0, & \Theta_i \leq \Theta_{wilt} \\ \frac{\Theta_i - \Theta_{wilt}}{\Theta_{fc} - \Theta_{wilt}}, & \Theta_{wilt} < \Theta_i \leq \Theta_{fc} \\ 1, & \Theta_{fc} < \Theta_i \end{array} \right\}, \quad (\text{A.53})$$

where $r_{csoil}(\Theta_i)$ is for a given soil layer Θ_i . Θ_{fc} is the *field capacity*, the volumetric soil moisture content above which plants are no longer water stressed, while Θ_{wilt} is the *permanent wilting point*, the volumetric soil moisture content at which transpiration ceases. The total r_{csoil} is then

$$r_{csoil} = \sum_{i=1}^n r_{csoil}(\Theta_i) g_i \frac{\Delta z_i}{\Delta z}, \quad (\text{A.54})$$

where n is the number of soil layers, g_i is the root density function for the i th soil layer, and Δz_i and Δz are the thicknesses of the i th soil layer and total soil column, respectively. (g_i is nominally set to unity for each soil layer in the land-surface scheme in the CAPS model, that is, an equal root density with depth. However, observations suggest that the root density varies with depth, perhaps higher nearer the surface or in a soil layer with a higher soil moisture content.)

A.3.4 Soil hydraulics

Clapp and Hornberger

Hydraulic conductivity (K_Θ) and soil water diffusivity (D_Θ) used in (A.23) and (A.24) are nonlinear functions of soil moisture (Θ) and change by several orders of magnitude from dry to wet soil conditions (see Ek and Cuenca 1994). They follow Clapp and Hornberger (1978) (and Cosby et al 1984) and are defined as

$$K_\Theta = K_{\Theta_s} \left(\frac{\Theta}{\Theta_s} \right)^{2b+3}, \quad (\text{A.55})$$

$$D_\Theta = \left(\frac{bK_{\Theta_s}\psi_s}{\Theta_s} \right) \left(\frac{\Theta}{\Theta_s} \right)^{b+2}, \quad (\text{A.56})$$

where K_{Θ_s} is the saturation hydraulic conductivity, Θ_s is the saturation volumetric soil moisture content, b is an empirically-derived coefficient, and ψ_s is the saturation soil moisture potential (all a function of soil type), where the actual soil moisture potential, ψ , is defined as

$$\psi = \psi_s \left(\frac{\Theta}{\Theta_s} \right)^{-b}, \quad (\text{A.57})$$

where (A.57) is also from Clapp and Hornberger (1978). (See also section 2.2 in Chapter 2.)

van Genuchten

An alternate to Clapp and Hornberger is the approach by van Genuchten (1980) where

$$K_\Theta = K_{\Theta_s} S_e^l [1 - (1 - S_e^{1/m})^m]^2, \quad (\text{A.58})$$

$$D_{\Theta} = K_{\Theta}(\partial\Theta/\partial\psi), \quad (\text{A.59})$$

where l and m are fitting parameters (functions of soil texture class and soil density), and S_e is the effective soil moisture saturation fraction defined as

$$S_e = (\Theta - \Theta_r)/(\Theta_s - \Theta_r), \quad (\text{A.60})$$

where the Θ_r is the residual volumetric soil moisture content and the other terms have been defined above. The soil moisture potential is defined as

$$\psi = \frac{1}{\alpha_s} [S_e^{-1/m} - 1]^{1/n}, \quad (\text{A.61})$$

where α_s and n are also fitting parameters, and $m = 1 - 1/n$. See Cuenca et al (1996) and Beljaars and Bosveld (1997) for further information on the van Genuchten formulation.

A.3.5 Soil thermodynamics

The thermal conductivity (λ_T) used in (A.25) is a nonlinear function of the soil moisture content (Θ), changing by a few orders of magnitude from dry to wet soil conditions, and in the absence of vegetation is the "bare soil" thermal conductivity λ_{T0} . Following Al Nakshabandi and Kohnke (1965), λ_{T0} is expressed as

$$\lambda_{T0} = \left\{ \begin{array}{ll} 420 \exp([- \log_{10}(100|\psi|)] + 2.7), & \log_{10}(100|\psi|) \leq 5.1 \\ 0.1722, & \log_{10}(100|\psi|) > 5.1 \end{array} \right\}, \quad (\text{A.62})$$

where ψ is soil moisture potential. (See also section 2.2 in Chapter 2).

An alternative to Al Nakshabandi and Khonke is the formulation by Johansen (1975) described in Peters-Lidard et al (1998), where λ_{T0} is a less non-linear function of soil moisture content, and yields more (*less*) thermal conductivity for drier (*moister*) soils. As noted in Marshall et al (2003) and Ek et al (2003), this then yields greater (*lesser*) soil heat flux, that in turn leads to a more damped (*amplified*) diurnal signal in the surface skin and near-surface (e.g. 2-m) air temperatures, and was found to improve the land-surface response in mesoscale model performance.

As discussed in section A.3.2, soil heat flux is reduced in the presence of a vegetation canopy because of reduced heat conductivity through vegetation (Figure A.4),

and is included implicitly in the soil heat flux formulation in the TESSEL land-surface scheme. An alternative is described in Peters-Lidard et al (1997) where the effect of vegetation is explicitly included, so that soil thermal conductivity is reduced by an exponential function of vegetation as

$$\lambda_T = \lambda_{T0} \exp(-\beta LAI), \quad (\text{A.63})$$

where LAI is the leaf area index, and β is an empirical coefficient equal to 0.5. Alternatively, the vegetation fraction ($0 \leq \sigma_f \leq 1$) may be used instead of LAI , where

$$\lambda_T = \lambda_{T0} \exp(-\beta' \sigma_f), \quad (\text{A.64})$$

and β' is an empirical coefficient, nominally equal to 2.0 (Ek et al 2003). (See also section 5.3.3 in Chapter 5).

The volumetric heat capacity of moist soil (C_Θ) used in A.25 includes contributions from the mineral soil itself, as well as from water and air in the soil, and is linearly related to soil moisture (Θ) as

$$C_\Theta = (1 - \Theta_{sat})c_{soil} + \Theta c_w + (\Theta_{sat} - \Theta)c_a, \quad (\text{A.65})$$

where c_{soil} is the soil heat capacity (a function of soil type, but chosen as $1.26 \times 10^6 \text{ J m}^{-3} \text{ K}^{-1}$), c_w is the heat capacity of water in the soil ($4.2 \times 10^6 \text{ J m}^{-3} \text{ K}^{-1}$), and c_a is the heat capacity of air in the soil ($1250 \text{ J m}^{-3} \text{ K}^{-1}$, which assumes an air density of $\approx 1.24 \text{ kg m}^{-3}$). (See also section 2.2 in Chapter 2.)

A.3.6 Surface temperature

To determine surface temperature (T_s) we start with the surface energy balance similar to (A.28) except now we use the actual evaporation E calculated from (A.42) instead of the potential evaporation E_p . Note that actual evaporation can be expressed as $E = \beta E_p$ where β is a factor multiplied by the potential evaporation to get the actual evaporation; β absorbs all influences that reduce the potential evaporation to the actual. The surface energy balance then becomes

$$(1 - \alpha)S\downarrow + L\downarrow - \epsilon\sigma T_s^4 = H + \beta L_v E_p + G. \quad (\text{A.66})$$

Using (A.29) and (A.30), we can rewrite this surface energy balance as

$$F - 4\sigma T_a^4 - 4\sigma T_a^4 \left(\frac{T_s - T_a}{T_a} \right) = \rho c_p C_h U [(\theta_s - T_a) - (\theta_a - T_a)] + \beta L_v E_p + G, \quad (\text{A.67})$$

where $F = (1 - \alpha)S\downarrow + L\downarrow$. Using the definition of the soil heat flux (G) from (A.33), and r from (A.41), we can solve for T_s as

$$T_s = \frac{\Delta z \rho c_p C_h U [T_a(r + 1) + (\Theta_a - T_a)] + \Delta z (F - \sigma T_a^4 - \beta L_v E_p) + \lambda_T T_{s1}}{\Delta z \rho c_p C_h U (r + 1) + \lambda_T}. \quad (\text{A.68})$$

As with the potential evaporation calculation, we can determine the surface temperature for the case where $\theta_s \neq T_s$, so (A.68) assumes a more general form

$$T_s = \frac{\Delta z \rho c_p C_h U [T_a(r + 1) + (\Theta_a - T_a)] + \Delta z (F - \sigma T_a^4 - \beta L_v E_p) + \lambda_T T_{s1}}{\Delta z \rho c_p C_h U (r + 1 + \delta_\theta) + \lambda_T}, \quad (\text{A.69})$$

where $\delta_\theta = [(p_{00}/p_s)^\kappa - 1]$.

After updating the soil moisture content, and soil and surface temperatures, an updated soil heat flux (G) can be found by re-evaluating (A.32). Similarly, the sensible heat flux (H) and components of the surface stress are updated using (A.6). The "apparent" surface specific humidity (q_s) can be determined by inverting the bulk aerodynamic relationship for latent heat flux (A.6), and is used as a boundary condition in the boundary layer scheme (section A.4).

A.4 Atmospheric boundary-layer scheme

A.4.1 Prognostic boundary-layer equations

The atmospheric boundary layer scheme in the CAPS model predicts tendencies of the potential temperature (θ), specific humidity (q), and horizontal components of the wind (\vec{V}_h) due to atmospheric turbulent mixing which combines local (gradient, or K theory) diffusion and nonlocal (boundary-layer scale) mixing (Troen and Mahrt 1986, Holtslag et al 1990, Holtslag and Boville 1993, Hong and Pan 1996). The prognostic equations for temperature, moisture, momentum, respectively, in the ABL are

$$\frac{\partial \vec{V}_h}{\partial t} = \frac{\partial}{\partial z} \left[K_m \left(\frac{\partial \vec{V}}{\partial z} - \gamma_m \right) \right] + \vec{V} \cdot \nabla \vec{V}, \quad (\text{A.70})$$

$$\frac{\partial \theta}{\partial t} = \frac{\partial}{\partial z} \left[K_h \left(\frac{\partial \theta}{\partial z} - \gamma_\theta \right) \right] + \vec{V} \cdot \nabla \theta + \frac{\partial F_{\text{rad}}}{\partial z}, \quad (\text{A.71})$$

$$\frac{\partial q}{\partial t} = \frac{\partial}{\partial z} \left[K_q \left(\frac{\partial q}{\partial z} - \gamma_q \right) \right] + \vec{V} \cdot \nabla q, \quad (\text{A.72})$$

where K_h , K_q , and K_m are the eddy diffusivities for heat, moisture, and momentum, respectively, $\gamma_{\theta,q,m}$ are nonlocal (ABL-scale) mixing terms for heat, moisture, and momentum, respectively, \vec{V} is the three-dimensional wind vector, and F_{rad} is the net radiation (sum of the incoming and outgoing solar and longwave radiation). Here we make the usual assumption of equating the diffusivity for moisture with that of heat, so $K_q = K_h$. For brevity, we only present the vertical diffusion terms (due to boundary-layer turbulent mixing), along with the advection terms ($\vec{V} \cdot \nabla \vec{V}$, θ , q) and the radiative flux divergence term ($\partial F_{\text{rad}}/\partial z$) that must be externally specified or supplied by another model.

A.4.2 Boundary layer turbulence

Eddy diffusivity

Eddy diffusivities are calculated from a prescribed profile shape as a function of boundary layer height and scale parameters derived from similarity theory (Figure A.5). In the unstable case above the surface layer ($z > z_s \equiv 0.1h$), the eddy diffusivity for momentum is defined following Troen and Mahrt (1986)

$$K_m(z) = w_s k z \left(1 - \frac{z}{h} \right)^p, \quad (\text{A.73})$$

where w_s is the boundary layer velocity scale, k is the von Kármán constant (0.4), h is boundary layer depth, and $p = 2$.

The boundary layer velocity scale is evaluated at the top of the surface layer (z_s) and defined as

$$w_s = u_* \phi_m^{-1} \left(\frac{z_s}{L} \right), \quad (\text{A.74})$$

$$= \left(u_*^3 + 15k \frac{z_s}{h} w_*^3 \right)^{1/3}, \quad (\text{A.75})$$

where u_* is the surface friction velocity, ϕ_m is the nondimensional profile function for momentum (defined below), and L is the Obukhov length, defined as

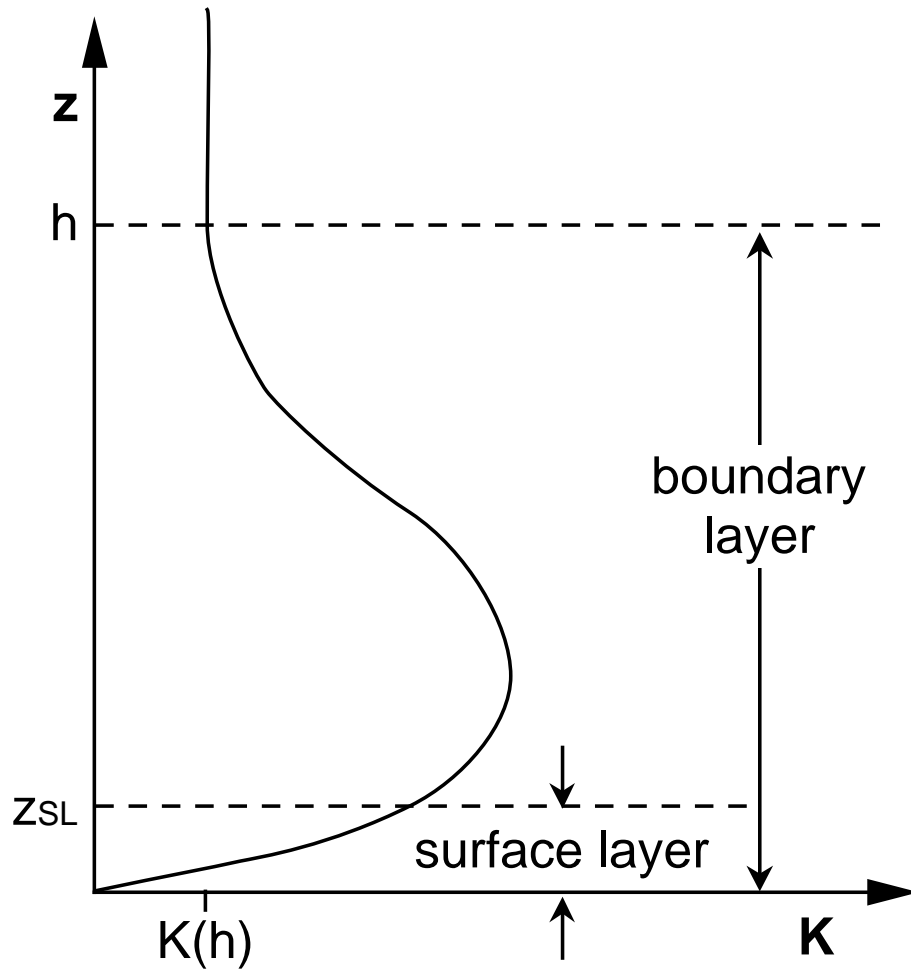


Figure A.5: Typical variation of eddy diffusivity (K) with height (z) in the boundary layer as proposed by O'Brien (1970), where z_{SL} is the depth of the surface layer, and $K(h)$ is the eddy diffusivity at the boundary-layer top (h). (Adapted from Hong and Pan 1996, their Figure 1.)

$$L = -\theta_{av} \frac{u_*^3}{gk(\overline{w'\theta'_v})_s}, \quad (\text{A.76})$$

where θ_{av} is the virtual potential temperature at an atmospheric reference level (i.e., z_a , the lowest atmospheric model level), g is gravity, w_* is the "Deardorff" convective velocity scale (defined below), and $(\overline{w'\theta'_v})_s$ is the surface virtual heat flux.

In the neutral limit (as $L \rightarrow \pm\infty$), the velocity scale $w_s \rightarrow u_*$, while in the free convection case, as wind speed vanishes, $w_s \rightarrow 0.84w_*$, where the convective velocity scale is

$$w_* = \left[\frac{gh}{\theta_{av}} (\overline{w'\theta'_v})_s \right]^{1/3}. \quad (\text{A.77})$$

The eddy diffusivity for heat (K_h) is related to the eddy diffusivity for momentum in terms of the turbulent Prandtl number (Pr)

$$K_h = K_m Pr^{-1}, \quad (\text{A.78})$$

where the turbulent Prandtl number is

$$Pr = \frac{\phi_h(z_s/L)}{\phi_m(z_s/L)} + Ck \frac{w_*}{w_s} \frac{z_s}{h}, \quad (\text{A.79})$$

where C is a coefficient set to 7.2 following Holtslag and Boville (1993). Pr is determined as the value at the top of the surface layer ($z_s = 0.1h$) using surface layer similarity theory and assumed constant above z_s . In the neutral limit, $Pr \rightarrow 1$; $Pr = 1.0$ for stable conditions. The nondimensional profile functions for temperature and momentum evaluated at z_s are defined as

$$\phi_h = \begin{cases} 6.0 & \text{very stable} \\ 1.0 + 5.0 \frac{z}{L} & \text{stable} \\ (1.0 - 15 \frac{z}{L})^{-1/2} & \text{unstable} \end{cases}, \quad (\text{A.80})$$

$$\phi_m = \begin{cases} 6.0 & \text{very stable} \\ 1.0 + 5.0 \frac{z}{L} & \text{stable} \\ (1.0 - 15 \frac{z}{L})^{-1/3} & \text{unstable} \end{cases}. \quad (\text{A.81})$$

These formulations are taken from Businger et al (1971) with modifications by Holtslag (1987). For the very stable case ($z/L > 1$) we set $z/L = 1$ (following Kondo et

al 1978) so that the profile functions remain constant.

For the stable case and in the surface layer in unstable conditions, $u_*\phi_m^{-1}(z/L)$ replaces w_s , and the eddy diffusivity for momentum is

$$K_m = u_*\phi^{-1}\left(\frac{z}{L}\right) kz \left(1 - \frac{z}{h}\right)^p, \quad (\text{A.82})$$

where $\phi_{h,m}$ now depend on z/L instead of on z_s/L . As a modification to surface layer similarity theory, the term $(1 - z/h)^p$ is included in the diffusivity for proper matching with the mixed layer ($z > z_s$).

For stable conditions, the free atmospheric diffusion parameterization following Kim and Mahrt (1992) is evaluated to account for the local generation of turbulence in the upper part of the stable boundary layer, and replaces the surface-based turbulence if greater. See Kim and Mahrt (1992) for further details.

Nonlocal mixing

The nonlocal terms ($\gamma_{\theta,q,m}$) represent mixing on the boundary-layer depth scale; γ_θ is sometimes called "countergradient" because nonlocal mixing in the upper convective boundary layer can often be upgradient (Deardorff 1966). In stable and neutral conditions, $\gamma_{\theta,q}$ are set to zero, and in unstable conditions $[(\overline{w'\theta'_v})_s > 0]$ defined following Troen and Mahrt (1986) with modifications by Holtslag and Boville (1993) as

$$\gamma_\theta = Cw_* \frac{(\overline{w'\theta'})_s}{w_s^2 h}, \quad (\text{A.83})$$

$$\gamma_q = Cw_* \frac{(\overline{w'q'})_s}{w_s^2 h}, \quad (\text{A.84})$$

where $(\overline{w'\theta'})_s$ and $(\overline{w'q'})_s$ are the surface heat and moisture flux (in kinematic units), respectively (see Figure A.6). (See also Holtslag and Moeng 1991.)

Nonlocal mixing of momentum has been explored by Frech and Mahrt (1995) and Brown and Grant (1997), but is not included because its generality had not been previously rigorously examined, so γ_m is set to zero. However, Noh et al (2003), building on this earlier work and using LES data, propose an updated γ_m expression, as well as explicit boundary-layer top entrainment, and height-dependent profiles of

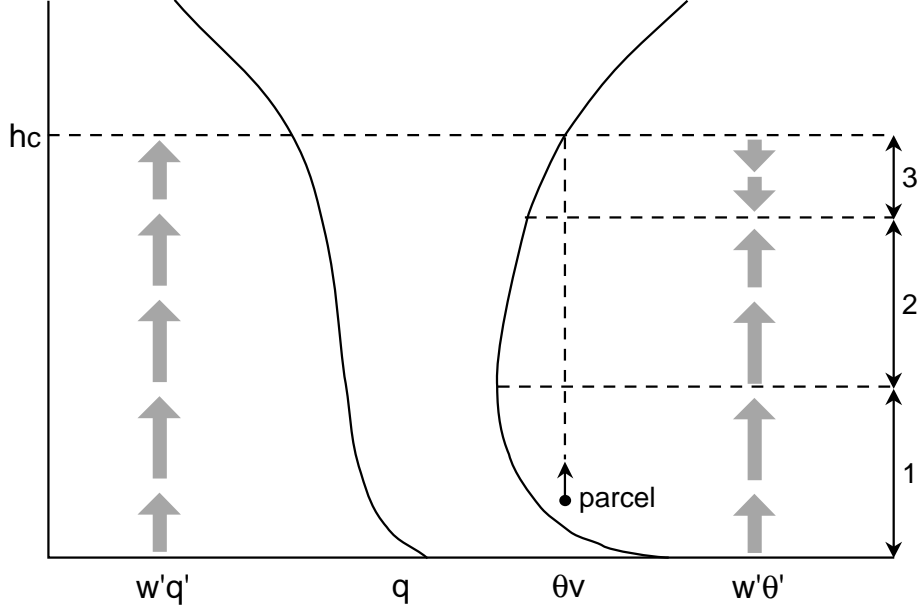


Figure A.6: Typical vertical profiles for virtual potential temperature (θ_v) and specific humidity (q) for a dry convective boundary layer. The arrows to the left illustrate the specific humidity flux ($\overline{w'q'}$), and the arrows to the right, the heat flux ($\overline{w'\theta'}$); also, a rising parcel is indicated up to its interaction height h_c . For specific humidity, its flux is typically down the local gradient, which also applies to the potential temperature in the indicated transport regions 1 and 3. But for region 2, the temperature profile is typically adiabatic and even subadiabatic higher up, while at the same time, the heat flux remains upward, arising from nonlocal transport by convective parcels, which initiate near the surface. (From Holtslag and Boville 1993, their Figure 2.)

the boundary-layer velocity scale (w_s) and turbulent Prandtl number (Pr), showing a positive impact of their changes. Currently in the model, there is no explicit entrainment, and w_s and Pr are constant with height.

A.4.3 ABL height

The boundary layer height is diagnosed as

$$h = \frac{Ri_{cr} |\vec{V}_h(h)|^2}{(g/\theta_{av})(\theta_v(h) - \theta_{av}^*)}, \quad (\text{A.85})$$

where Ri_{cr} is the critical Richardson number, θ_{av} is the reference virtual potential temperature at the first model level above the surface (z_a), g is the gravity, $\theta_v(h)$ is the virtual potential temperature at model level h , and $|\vec{V}_h(h)|$ is the magnitude of the horizontal wind at level h (Figure A.7). This approach to diagnosing the boundary layer height (following Troen and Mahrt 1986, Holtslag and Boville 1993) also requires the specification of a low-level potential temperature (θ_{av}^*), which is defined as

$$\theta_{av}^* = \begin{cases} \theta_{av} & \text{stable} \\ \theta_{av} + C \frac{(\overline{w'\theta_v})_s}{w_s} & \text{unstable} \end{cases}. \quad (\text{A.86})$$

When the boundary layer is unstable, the virtual potential temperature above the surface in (A.86) is enhanced by thermal effects in an amount that is proportional to the surface virtual heat flux. In the neutral limit, as $(\overline{w'\theta_v})_s \rightarrow 0$, $w_s \rightarrow u_*$, and $\theta_{av}^* \rightarrow \theta_{av}$.

In the original boundary-layer height formulation by Troen and Mahrt (1986), a bulk Richardson number (Ri_b) for the boundary layer is defined as

$$Ri_b = \frac{(g/\theta_{va})(\theta_{vh} - \theta_{va})h}{u_h^2 + v_h^2}, \quad (\text{A.87})$$

where g is gravity, θ_{va} and θ_{vh} are the virtual potential temperatures near the surface (e.g. at the height of the first model level, z_a) and at the boundary-layer top, respectively, h is boundary layer height, and u_h and v_h are the wind speed components at the boundary layer top. For unstable conditions, the value of θ_{va} in the expression $\theta_{vh} - \theta_{va}$ is adjusted to account for the enhanced effect of thermals in an amount that is proportional to the surface virtual heat flux (see Troen and Mahrt 1986 for details). The boundary layer depth is then diagnosed at the level where Ri_b exceeds some critical Richardson number (Ri_{cr}), set equal to 0.25 in this study because of the fine-scale vertical resolution we use in the model, though a larger value (i.e. 1.0) is appropriate for large-scale NWP models with limited resolution in the boundary-layer.

To generalize this formulation, Vogelezang and Holtslag (1996) define a similar bulk Richardson number for the boundary layer as

$$Ri_h = \frac{(g/\theta_{va})(\theta_{vh} - \theta_{va})(h - z_a)}{(u_h - u_a)^2 + (v_h - v_a)^2 + b_* u_*^2}, \quad (\text{A.88})$$

where z_a is the near-surface height (e.g. first model level), u_a and v_a are the corresponding wind speed components, b_* is an empirical coefficient (found to be on the

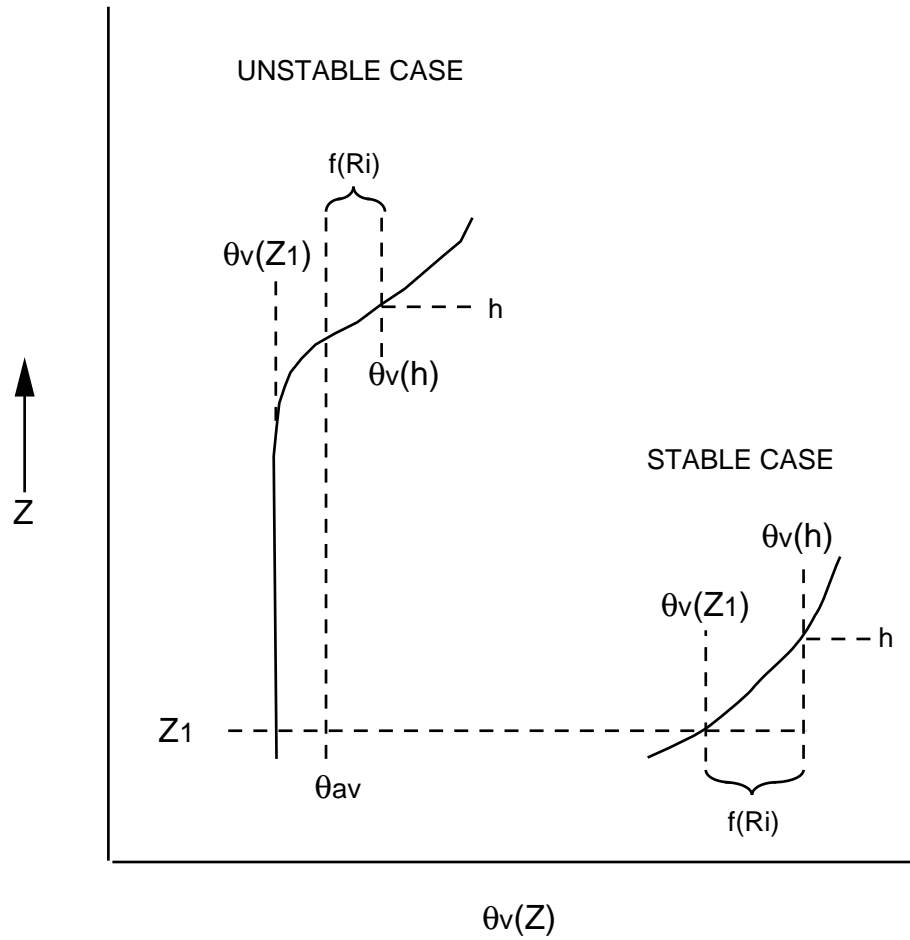


Figure A.7: Sketch of the boundary-layer depth relationship to the profile of potential temperature above the surface layer (solid profile). For the unstable case, the first vertical broken line to the right of the profile indicates the potential temperature after enhancement due to the temperature excess associated with surface heating (from A.86). For the unstable (stable) case, the second (first) vertical broken line to the right of the profile indicates the potential temperature at the boundary-layer top after deepening due to shear-generated mixing as formulated in terms of a modified bulk Richardson number (from A.85). (From Mahrt and Troen 1986, their Figure 1.)

order of 100), and u_* is the surface friction velocity. This generalization accounts for boundary layers with relatively high wind speed and upper boundary-layer stratification, and includes the effect of turbulence due to surface friction under near-neutral conditions. The corresponding boundary layer height is then

$$h = \frac{Ri_{cr}[\vec{V}_h(h) - \vec{V}_h(a)]^2}{(g/\theta_{av})(\theta_v(h) - \theta_{av}^*)}, \quad (\text{A.89})$$

where $|\vec{V}_h(a)|$ is the wind speed at the first (lowest) atmospheric level above the ground. See Vogelezang and Holtslag (1996) for further details.

A.4.4 ABL cloud cover formulation

Fractional ABL cloud cover is calculated following Ek and Mahrt (1991a; Chapter 4), and accounts for fair-weather shallow cumulus clouds. Cloud cover reduces the incoming solar radiation that modifies the surface energy balance and subsequent boundary-layer development. The model predicts cloud cover using the generalized equation

$$A_c = f(\overline{RH}, \sigma_{RH}), \quad (\text{A.90})$$

where A_c is the fractional cloud cover, \overline{RH} is the maximum relative humidity in the boundary layer (near the top), and σ_{RH} is the standard deviation of relative humidity at that level which accounts for both turbulent and subgrid mesoscale variations in relative humidity (Figure A.8). The turbulent variability of relative humidity is formulated in terms of boundary-layer top moisture flux entrainment and boundary-layer similarity theory, whereas the mesoscale subgrid variability is specified as a function of grid size (nominally based on HAPEX-MOBILHY analyses), with turbulent and mesoscale variations assumed to be uncorrelated. With unstable conditions, ABL clouds first form at lower relative humidities compared to the stable case. The fractional cloud cover is then the area under a Gaussian curve greater than $RH = 1.0$, and is approximated by a polynomial fit to a Gaussian distribution. See sections 4.2-4.3 in Chapter 4 for the specific details of relative humidity variation and the cloud cover formulation.

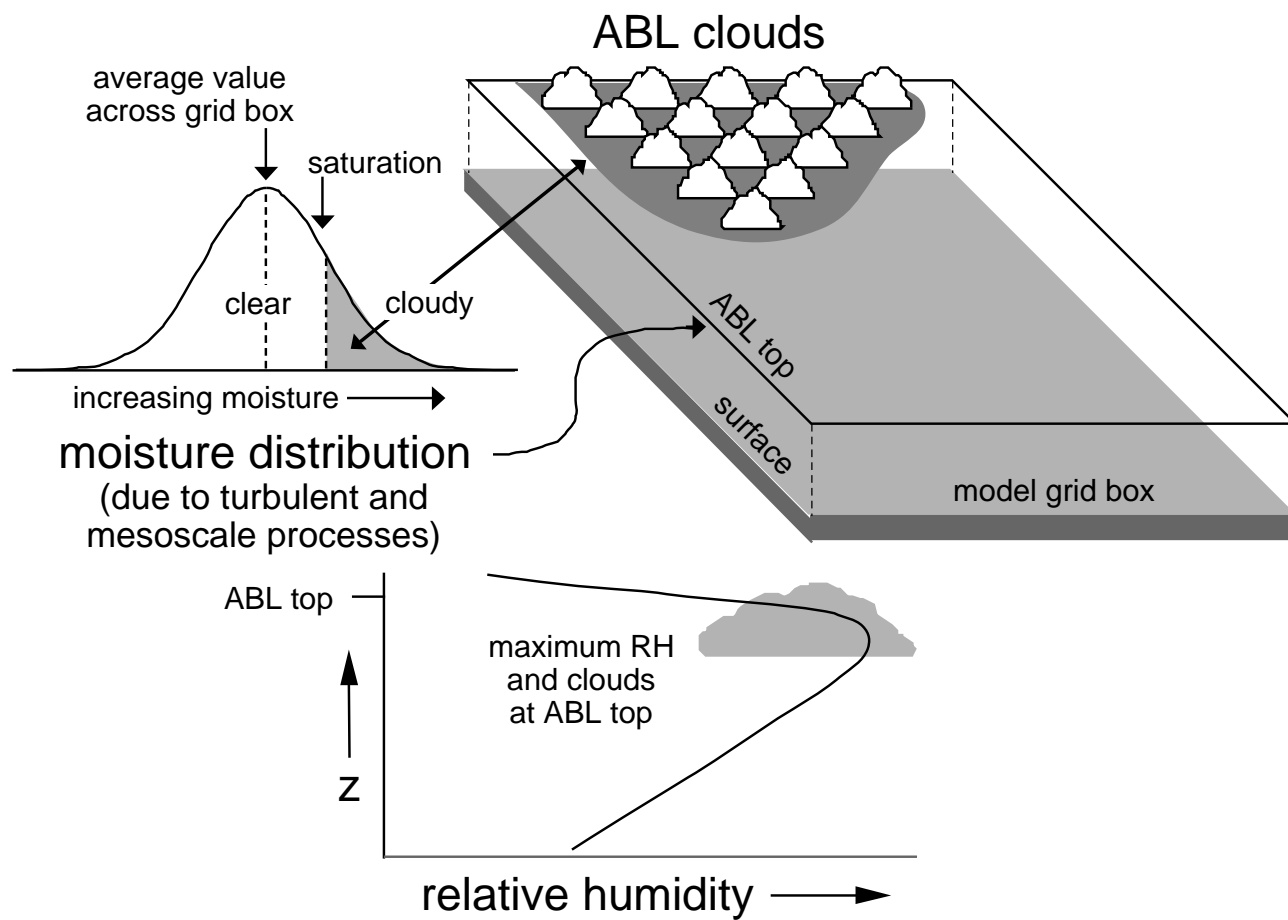


Figure A.8: Schematic showing variation of humidity and boundary-layer cloud cover.

Appendix B

Relative humidity tendency at the ABL top

Relative humidity at the atmospheric boundary layer (ABL) top is thought to control the development of ABL clouds. In order to understand the relevant processes we initially follow the development in Ek and Mahrt (1994; Chapter 3) (with a modification by Chang and Ek 1996b), and analyze the relative humidity (RH) tendency at the ABL top which may be written as

$$\begin{aligned}\frac{\partial RH}{\partial t} &= \frac{\partial}{\partial t} \left(\frac{q}{q_s} \right) = \frac{1}{q_s} \frac{\partial q}{\partial t} - \frac{RH}{q_s} \frac{\partial q_s}{\partial t} = \frac{1}{q_s} \frac{\partial q}{\partial t} - \frac{RH}{q_s} \frac{\partial}{\partial t} \left(\frac{\epsilon e_s}{p} \right) \\ &= \frac{1}{q_s} \frac{\partial q}{\partial t} + RH \left(\frac{1}{p} \frac{\partial p}{\partial t} - \frac{1}{e_s} \frac{de_s}{dT} \frac{\partial T}{\partial t} \right),\end{aligned}\tag{B.1}$$

where q is the specific humidity, q_s is saturation specific humidity ($\approx \epsilon e_s/p$), ϵ is the ratio of dry air to water vapor gas constants, e_s is saturation vapor pressure, p is air pressure, de_s/dT is the slope of the saturation vapor pressure curve, and T is temperature.

With well-mixed conditions for θ and q (typical for a dry convective boundary layer where $h/-L > 5$), the relative humidity reaches a maximum near the boundary-layer top which will be the reference level in the following development. The relative humidity tendency combines the separate influences of changes in moisture and changes in temperature, the first and second terms on the right-hand-side of (B.1), respectively, where these tendencies are influenced by different boundary-layer and land-surface

processes. This development is continued to explicitly account for these different processes. Temperature tendency in a well-mixed boundary layer can be expressed as

$$\frac{\partial T}{\partial t} = \frac{\partial}{\partial t} \left[\theta \left(\frac{p}{p_s} \right)^{R_d/c_p} \right], \quad (\text{B.2})$$

which can be eventually written as

$$\frac{\partial T}{\partial t} = \left(\frac{p}{p_s} \right)^{R_d/c_p} \frac{\partial \theta}{\partial t} + \frac{R_d T}{c_p p} \frac{\partial p}{\partial t}, \quad (\text{B.3})$$

where θ is potential temperature, p_s is surface pressure, c_p is specific heat of air, and the equation of state and the definition of potential temperature have been used. Using the hydrostatic approximation and neglecting the local change of pressure at a fixed height, the pressure tendency can be written as

$$\frac{\partial p}{\partial t} = \frac{\partial p}{\partial z} \frac{\partial h}{\partial t} = -\rho g \frac{\partial h}{\partial t} = -\frac{p g}{R_d T} \frac{\partial h}{\partial t}, \quad (\text{B.4})$$

where h is the boundary-layer depth, z is height, ρ is air density, and g is gravity. Substituting (B.4) into (B.3) gives

$$\frac{\partial T}{\partial t} = \left(\frac{p}{p_s} \right)^{R_d/c_p} \frac{\partial \theta}{\partial t} - \frac{g}{c_p} \frac{\partial h}{\partial t}. \quad (\text{B.5})$$

The Clausius-Clapeyron equation can be written as

$$\frac{1}{e_s} \frac{de_s}{dT} = \frac{L_v}{R_v T^2}, \quad (\text{B.6})$$

where L_v is latent heat. Substituting (B.5) and (B.6) into (B.1) gives

$$\frac{\partial RH}{\partial t} = \frac{1}{q_s} \frac{\partial q}{\partial t} + \frac{RH}{q_s} \left(c_2 \frac{\partial h}{\partial t} - c_1 \frac{\partial \theta}{\partial t} \right), \quad (\text{B.7})$$

where

$$c_1 = \frac{L_v}{R_v} \frac{q_s}{T^2} \left(\frac{p}{p_s} \right)^{R_d/c_p}, c_2 = \left(\frac{L_v}{R_v} \frac{q_s}{T^2} - \frac{c_p}{R_d} \frac{q_s}{T} \right) \frac{g}{c_p}. \quad (\text{B.8})$$

For our well-mixed ABL assumption we can use equations for the boundary-layer moisture and thermodynamic budgets from Tennekes (1973) (in the advection-free case)

$$\frac{\partial q}{\partial t} = \frac{(\overline{w'q'_s} - \overline{w'q'_h})}{h}, \quad \frac{\partial \theta}{\partial t} = \frac{(\overline{w'\theta'_s} - \overline{w'\theta'_h})}{h}, \quad (\text{B.9})$$

where $\overline{w'q'}$ and $\overline{w'\theta'}$ are the moisture and heat fluxes, respectively, and the subscripts s and h refer to the surface and the level just below the boundary-layer top, respectively. Substituting (B.9) into (B.7) gives

$$\frac{\partial RH}{\partial t} = \frac{(\overline{w'q'_s} - \overline{w'q'_h})}{hq_s} + \frac{RH}{q_s} \left[c_2 \frac{\partial h}{\partial t} - c_1 \frac{\overline{w'\theta'_s}(1 + C_\theta)}{h} \right], \quad (\text{B.10})$$

where $C_\theta = -\overline{w'\theta'_h}/\overline{w'\theta'_s}$, the (negative of the) ratio of surface to ABL-top sensible heat flux. (B.10) is quite similar to the relative humidity tendency equation from Ek and Mahrt (1994, their Eq. 9).

Next we assume a simple bulk well-mixed ABL (Figure B.1) so that the ABL depth tendency may be approximated as (Tennekes 1973, Betts 1973)

$$\frac{\partial h}{\partial t} = \frac{\overline{w'\theta'_s}(1 + C_\theta)}{h\gamma_\theta}, \quad (\text{B.11})$$

where γ_θ is the vertical gradient of potential temperature above the ABL. ABL-top dry-air entrainment is

$$\overline{w'q'_h} = -\Delta q \frac{\partial h}{\partial t}, \quad (\text{B.12})$$

where Δq is the change in specific humidity across the ABL top (which is normally negative, and the mean large-scale vertical motion is zero, analogous to Tennekes 1973, his Eq. 1, and others) (Figure B.1).

Substituting (B.11) and (B.12) into (B.10) eventually yields the final form of our relative humidity tendency equation

$$\frac{\partial RH}{\partial t} = \left(\frac{R_n - G}{\rho L_v h q_s} \right) [e_f + ne(1 - e_f)], \quad (\text{B.13})$$

where $R_n - G$ is available energy at the surface (R_n is net radiation and G is soil heat flux), ρ is air density, L_v is latent heat, h is ABL depth, and q_s is saturation specific humidity just below the ABL top. In (B.13), e_f is the surface evaporative fraction (of surface energy available for evaporation) defined as

$$e_f = \frac{LE}{R_n - G} = \frac{LE}{H + LE}, \quad (\text{B.14})$$

where $LE (= \rho L_v \overline{w'q'_s})$ and $H (= \rho c_p \overline{w'\theta'_s})$ are the surface latent and sensible heat fluxes, respectively, and ne is given by

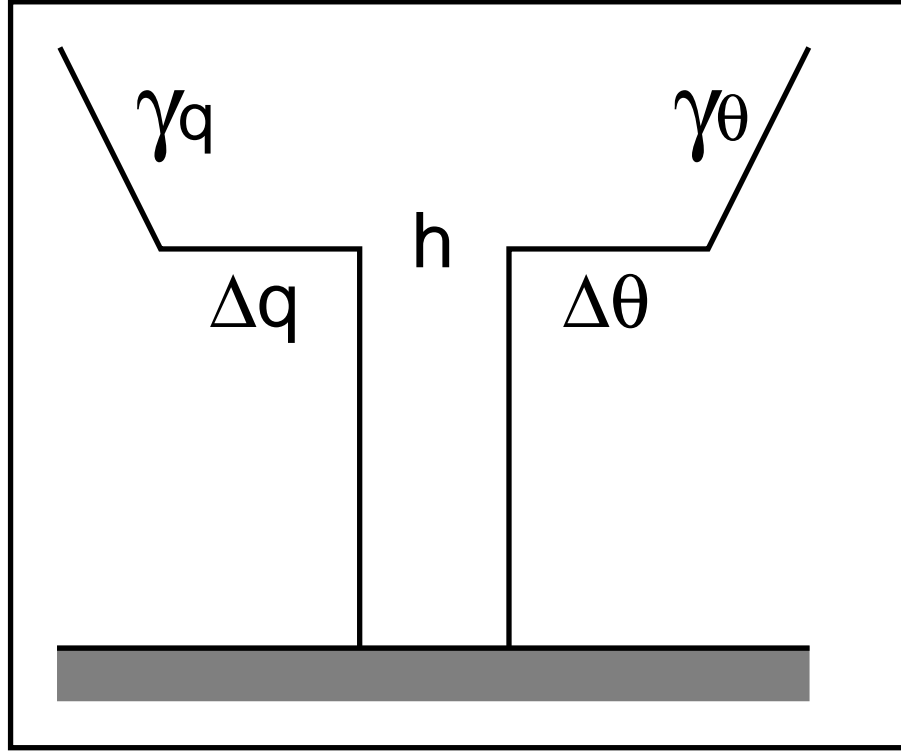


Figure B.1: Schematic of idealized well-mixed boundary layer used in analyzing the relative humidity tendency at the ABL top, where h is boundary-layer depth, Δq and γ_q are the above-ABL specific humidity drop and lapse rate, respectively, and $\Delta\theta$ and γ_θ are the above-ABL potential temperature "jump" and lapse rate (stability), respectively.

$$ne = L_v/c_p(1 + C_\theta) \left[\frac{\Delta q}{h\gamma_\theta} + RH \left(\frac{c_2}{\gamma_\theta} - c_1 \right) \right]. \quad (\text{B.15})$$

See section 6.5.2 in Chapter 6 for further discussion.

Bibliography

Abramopoulos, F., C. Rosenzweig, and B. Choudbury, 1988: Improved ground hydrology calculations for global climate models (GCMs): Soil water movement and evapotranspiration. *J. Climate*, **1**, 921-941.

Ács, R., D. T. Mihailović, and B. Rajković, 1991: A coupled soil moisture and surface temperature prediction model. *J. Appl. Meteorol.*, **30**, 812-822.

Al Nakshabandi, G., and H. Kohnke, 1965: Thermal conductivity and diffusivity of soils as related to moisture tension and other physical properties. *Agric. Meteorol.*, **2**, 271-279.

Albrecht, B. A., 1981: Parameterization of trade-cumulus cloud amounts. *J. Atmos. Sci.*, **38**, 97-105.

André, J.-C., P. Bougeault, J.-F. Mafouf, P. Mascart, J. Noilhan, and J.-P. Pinty, 1989: Impact of forests on mesoscale meteorology. *Phil. Trans. R. Soc. Lond.*, **B324**, 407-422.

André, J.-C., J.-P. Goutorbe, A. Perrier, R. H. Cuenca, L. Mahrt, and collaborators, 1988: HAPEX-MOBILHY: First results from the special observing period. *Ann. Geophysicae*, **B6**(5), 477-492.

Anthes, R. A., 1984: Enhancement of convective precipitation by mesoscale variations in vegetation covering in semi arid regions. *J. Clim. Appl. Meteorol.*, **23**, 541-554.

- Avissar, R., and R. A. Pielke, 1989: A parameterization of heterogeneous land surfaces for atmospheric models and its impact on regional meteorology. *Mon. Wea. Rev.*, **117**, 2113-2136.
- Ball, F. K., 1960: Control of inversion height by surface heating. *Quart. J. Roy. Meteorol. Soc.*, **86**, 483-494.
- Barnston, A. G., and P. T. Schikedanz, 1984: The effect of irrigation on warm season precipitation in the southern Great Plains. *J. Clim. Appl. Meteorol.*, **23**, 865-888.
- Beljaars, A. C. M., 1995: The parameterization of surface fluxes in large-scale models under free convection. *Quart. J. Roy. Meteorol. Soc.*, **121**, 255-270.
- Beljaars, A. C. M., and F. C. Bosveld, 1997: Cabauw data for the validation of land surface parameterization schemes. *J. Climate*, **10**, 1172-1193.
- Beljaars, A. C. M., and A. A. M. Holtslag, 1990: A software library for the calculation of surface fluxes over land and sea. *Environmental Software*, **5**, 60-68.
- Beljaars, A. C. M., and A. A. M. Holtslag, 1991: Flux parameterization over land surfaces for atmospheric models. *J. Appl. Meteorol.*, **30**, 327-341.
- Bessemoulin, P., Desroziers, G., Payen, M., and C. Tarrieu, 1987: Atlas des données SAMER, Programme HAPEX-MOBILHY (A quick look of the SAMER data during HAPEX-MOBILHY). Technical Report, EERM, CNRM, 42, Avenue Coriolis, 31057 Toulouse Cedex, France (in French).
- Betts, A. K., 1973: Non-precipitating cumulus convection and its parameterization. *Quart. J. Roy. Meteorol. Soc.*, **99**, 178-196.
- Betts, A. K., 1983: Thermodynamics of mixed stratocumulus layers: Saturation point budgets. *J. Atmos. Sci.*, **40**, 2655-2670.
- Betts, A. K., J. H. Ball, Beljaars, A. C. M., M. J. Miller, and P. Viterbo, 1996: The land surface-atmosphere interaction: A review based on observational and global modelling perspectives. *J. Geophys. Res.*, **101**, 7209-7225.

- Betts, A. K., 2000: Idealized model for equilibrium boundary layer over land. *J. Hydrometeorol.*, **1**, 507-523.
- Betts, A. K., 2004: Understanding hydrometeorology using global models. *Bull. Amer. Meteorol. Soc.*, **85**, 1673-1688, doi:10.1175/BAMS-85-11-1673.
- Betts, A. K., F. Chen, K. E. Mitchell, and Z. I. Janjić, 1997: Assessment of the land surface and boundary layer models in two operational versions of the NCEP Eta model using FIFE data. *Mon. Wea. Rev.*, **125**, 2896-2916.
- Betts, A. K., R. L. Desjardins, J. I. MacPherson, and R. D. Kelly, 1990: Boundary-layer heat and moisture budgets from FIFE. *Bound.-Layer Meteorol.*, **50**, 109-137.
- Blyth, E. M., A. J. Dolman, and J. Noilhan, 1994: The effect of forest on mesoscale rainfall: An example from HAPEX-MOBILHY. *J. Appl. Meteorol.*, **33**, 445-454.
- Bougeault, P., B. Bret, P. Lacarrère, and J. Noilhan, 1989: Design and implementation of a land surface processes parameterization in a mesoscale model. ECMWF Workshop Param. Fluxes over Land Surface, 24-26 Oct. 1988, Reading UK, p. 95-120.
- Bougeault, P., J. Noilhan, P. Lacarrère, and P. Mascart, 1991: An experiment with an advanced surface parameterization in a mesobeta-scale model. Part I: Implementation. *Mon. Wea. Rev.*, **119**, 2358-2373.
- Brown, A. R., and A. L. M. Grant, 1997: Non-local mixing of momentum in the convective boundary layer. *Bound.-Layer Meteorol.*, **84**, 1-22.
- Brubaker, K. L., and D. Entekhabi, 1996: Analysis of feedback mechanisms in land-atmosphere interaction. *Water Resources Res.*, **32**, 1343-1357.
- Brutsaert, W., and M. B. Parlange, 1992: The unstable surface layer above forest: Regional evaporation and heat flux. *Water Resources Res.*, **28**, 3129-3134.
- Businger, J. A., J. C. Wyngaard, Y. Izumi, and E. F. Bradley, 1971: Flux-profile relationships in the atmospheric surface layer. *J. Atmos. Sci.*, **28**, 181-189.

Campbell, G. S., 1974: A simple method for determining unsaturated conductivity from moisture retention data. *Soil Sci.*, **117**, 311-314.

Carson, D. J., 1973: The development of a dry inversion-capped convectively unstable boundary layer. *Quart. J. Roy. Meteorol. Soc.*, **99**, 450-467.

Caughey, S. J., J. C. Wyngaard, and J. C. Kaimal, 1979: Turbulence in the evolving stable layer. *J. Atmos. Sci.*, **36**, 1041-1052.

Chang, S., and M. Ek, 1996a: Sensitivity study of the CAPS model land-surface scheme using the 1987 Cabauw/PILPS data set. *Phys. Chem. Earth*, **21**, 205-210.

Chang, S., and M. Ek, 1996b: Note on "Daytime evolution of relative humidity at the boundary-layer top". *Mon. Wea. Rev.*, **124**, 1323-1326.

Chang, S., D. Hahn, C.-H. Yang, D. Norquist, and M. Ek, 1999: Validation study of the CAPS model land surface scheme using the 1987 Cabauw/PILPS dataset. *J. Appl. Meteorol.*, **38**, 405-422.

Charney, J., W. J. Quirk, S.-H. Chow, and J. Kornfield, 1977: A comparative study of the effects of albedo change on drought in semi-arid regions. *J. Atmos. Sci.*, **34**, 1366-1385.

Chen, F., Z. Janjić, and K. Mitchell, 1997: Impact of atmospheric surface-layer parameterizations in the new land-surface scheme of the NCEP mesoscale Eta model. *Bound.-Layer Meteorol.*, **85**, 391-421.

Chen, F., K. Mitchell, J. Schaake, Y. Xue, H.-L. Pan, V. Koren, Q. Y. Duan, M. Ek, and A. Betts, 1996: Modeling of land-surface evaporation by four schemes and comparison with FIFE observations. *J. Geophys. Res.*, **101**, 7251-7268.

Chen, T. H., A. Henderson-Sellers, P. Milly, A. Pitman, A. Beljaars, F. Abramopoulos, A. Boone, S. Chang, F. Chen, Y. Dai, C. Desborough, R. Dickinson, L. Duemenil, M. Ek, J. Garratt, N. Gedney, Y. Gusev, J. Kim, R. Koster, E. Kowalczyk, K. Laval, J. Lean, D. Lettenmaier, X. Liang, T.-H. Mengelkamp, J.-F. Mahfouf, K. Mitchell,

O. Nasonova, J. Noilhan, J. Polcher, A. Robock, C. Rosenzweig, J. Schaake, C. A. Schlosser, J. P. Schulz, Y. Shao, A. Shmakin, D. Verseghy, P. Wetzell, E. Wood, Y. Xue, Z.-L. Yang, and Q.-c. Zeng, 1997: Cabauw experimental results from the Project for Intercomparison of Land-surface Parameterization Schemes (PILPS), *J. Climate*, **10**, 1194-1215.

Chu, R., and D. Parrish, 1977: Humidity analyses for operational prediction models at the National Meteorological Center. NMC Office Note 140, National Meteorological Center, Washington, D. C.

Chu, C.-T., 1986: Parameterization of shallow convection in the boundary layer. Master's Thesis, Dept. Atmos. Sci., Oregon State University, Corvallis, Oregon.

Clapp, R. B., and G. M. Hornberger, 1978: Empirical equations for some soil hydraulic properties. *Water Resources Res.*, **14**, 601-604.

Colby, F. P., 1984: Convective inhibition as a prediction of convection during AVE-SESAME II. *Mon. Wea. Rev.*, **112**, 2239-2252.

Colello, G. D., C. Grivet, P. J. Sellers, and J. A. Berry, 1998: Modeling of energy, water, and CO₂ flux in a temperate grassland ecosystem with SiB2: May-October 1987. *J. Atmos. Sci.*, **55**, 1141-1169.

Collier, L. R., and J. G. Lockwood, 1974: The estimation of solar radiation under cloudless skies with atmospheric dust. *Quart. J. Roy. Meteorol. Soc.*, **100**, 678-681.

Cosby, B. J., G. M. Hornberger, R. B. Clapp, and T. R. Ginn, 1984: A statistical exploration of the relationship of soil moisture characteristics to the physical properties of soils. *Water Resources Res.*, **20**, 682-690.

Coulman, C. E., 1978: Boundary-layer evolution and nocturnal inversion dispersal - Part 1. *Bound.-Layer Meteorol.*, **14**, 471-491.

Cuxart, J., A. A. M. Holtslag, R. J. Beare, E. Bazile, A. C. M. Beljaars, A. Cheng, L. Conangla, M. Ek, F. Freedman, R. Hamdi, A. Kerstein, H. Kitagawa, G. Lenderink, D. Lewellen, J. Mailhot, T. Mauritsen, V. Perov, G. Schayes, G.-J. Steeneveld, G.

Svensson, P. Taylor, W. Weng, S. Wunsch, and K.-M. Xu, 2005: Single-column model intercomparison for a stably stratified atmospheric boundary layer. *Bound.-Layer Meteorol.* (accepted)

Cuenca, R. H., M. Ek, and L. Mahrt, 1996: Impact of soil water property parameterization on atmospheric boundary-layer simulation. *J. Geophys. Res.*, **101**, 7269-7277.

De Bruin, H. A. R., 1983: A model for the Priestley-Taylor parameter α . *J. Clim. Appl. Meteorol.*, **22**, 572-578.

De Rooy, W. C., and A. A. M. Holtslag, 1999: Estimation of surface radiation and energy flux densities from single-level weather data. *J. Appl. Meteorol.*, **38**, 526-540.

Deardorff, J. W., 1966: The countergradient heat flux in the lower atmosphere and in the laboratory. *J. Atmos. Sci.*, **23**, 503-506.

Desborough, C. E., 1997: The impact of root-weighting on the response of transpiration to moisture stress in a land surface scheme. *Mon. Wea. Rev.*, **125**, 1920-1930.

Dickinson, A., 1985: The weather prediction model. Operational numerical weather prediction system documentation paper, Meteorological Office London Road, Bracknell, U.K., No. 4, 9.13-9.15.

Dickinson, R. E., A. Henserson-Sellers, P. J. Kennedy, and M. F. Wilson, 1993: Biosphere-Atmosphere Transfer Scheme (BATS), version 1e as coupled to the NCAR community climate model. NCAR technical note, NCAR/TN-387+STR, National Center for Atmospheric Research, Boulder, Colorado, USA, 72 pp.

Duynkerke, P. G., 1992: The roughness length for heat and other vegetation parameters for a surface of short grass. *J. Atmos. Sci.*, **31**, 579-586.

Ek, M., and R. H. Cuenca, 1994: Variation in soil parameters: Implications for modeling surface fluxes and atmospheric boundary-layer development. *Bound.-Layer Meteorol.*, **70**, 369-383.

Ek, M., and A. A. M. Holtslag, 2004: Influence of soil moisture on boundary-layer

cloud development. *J. Hydrometeorol.*, **5**, 86-99.

Ek, M., and A. A. M. Holtslag, 2005: Evaluation of a land-surface scheme at Cabauw. *Theoretical Appl. Climatology*, **80**, 213-227, doi:10.1007/s00704-004-0101-4.

Ek, M., and L. Mahrt, 1991a: A model for boundary-layer cloud cover. *Annales Geophysicae*, **9**, 716-724.

Ek, M., and L. Mahrt, 1991b: OSU 1-D PBL Model User's Guide: A one-dimensional planetary boundary layer model with interactive soil layers and plant canopy, version 1.0.4, Dept. Atmospheric Sciences, Oregon State University, Corvallis, Oregon, USA. (Available from Michael Ek, NOAA Science Center, NCEP/EMC, 5200 Auth Road, Room 207, Suitland, MD 20746, USA, michael.ek@noaa.gov.)

Ek, M., and L. Mahrt, 1994: Daytime evolution of relative humidity at the boundary-layer top. *Mon. Wea. Rev.*, **122**, 2709-2721.

Ek, M., K. E. Mitchell, Y. Lin, E. Rogers, P. Grunmann, V. Koren, G. Gayno, and J. D. Tarpley, 2003: Implementation of Noah land-surface model advances in the NCEP operational mesoscale Eta model. *J. Geophys. Res.*, **108**(D22), 8851, doi:10.1029/2002JD003296.

Eloranta, E. W., R. Stull, and E. Ebert, 1989: Test of a calibration device for airborne Lyman-Alpha hygrometers. *J. Atmos. and Ocean Tech.*, **6**, 129-139.

Entekhabi, D., and P. S. Eagleson, 1989: Land-surface hydrology parameterization for atmospheric general circulation models including subgrid-scale spatial variability. *J. Climate*, **2**, 816-831.

Fairall, C. W., J. E. Hare, and J. B. Snider, 1990: An eight-month climatology of marine stratocumulus cloud fraction, albedo, and integrated liquid water. *J. Climate*, **3**, 847-864.

Findell, K. L., and A. B. Eltahir, 2003a: Atmospheric controls on soil moisture-boundary layer interactions. Part I: Framework development. *J. Hydrometeorol.*, **4**, 552-569.

- Findell, K. L., and A. B. Eltahir, 2003b: Atmospheric controls on soil moisture-boundary layer interactions. Part II: Feedbacks within the continental United States. *J. Hydrometeorol.*, **4**, 570-583.
- Frech, M., and L. Mahrt, 1995: A two-scale mixing formulation for the atmospheric boundary layer. *Bound.-Layer Meteorol.*, **73**, 91-104.
- Freedman, J. M., D. R. Fitzjarrald, K. E. Moore, and R. K. Sakai, 2001: Boundary layer clouds and vegetation-atmosphere feedback. *J. Climate*, **14**, 180-197.
- Garrett, A. J., 1982: A parameter study of interactions between convective clouds, the convective boundary layer, and a forested surface. *Mon. Wea. Rev.*, **110**, 1041-1059.
- Garratt, J. R., 1992: *The Atmospheric Boundary Layer*. Cambridge University Press, New York, 316 pp.
- Gash, J. H. C., W. J. Shuttleworth, C. R. Lloyd, J.-C. André, J.-P. Goutorbe, J. Gelpe, 1989: Micrometeorological measurements in Les Landes Forest during HAPEX-MOBILHY. *Agric. Forest Meteorol.*, **46**, 131-147.
- Grant, A. L. M., 1986: Observations of boundary layer turbulence made during the 1981 KONTUR experiment. *Quart. J. Roy. Meteorol. Soc.*, **112**, 825-841.
- Ha, K.-J., and L. Mahrt, 2001: Simple inclusion of z-less turbulence within and above the modeled nocturnal boundary layer. *Mon. Wea. Rev.*, **129**, 2136-2143.
- Ha, K.-J., and L. Mahrt, 2003: Radiative and turbulent fluxes in the nocturnal boundary layer. *Tellus*, **55A**, 317-327.
- Hammer, R. M., 1970: Cloud development and distribution around Khartoum. *Weather*, **25**, 411-414.
- Henderson-Sellers, A., A. J. Pitman, P. K. Love, P. Irannejad, and T. H. Chen, 1995: The project for intercomparison of land-surface parameterization schemes (PILPS):

Phases 2 and 3. *Bull. Amer. Meteorol. Soc.*, **76**, 1335-1349.

Henderson-Sellers, A., Z.-L. Yang, and R. E. Dickinson, 1993: The project for inter-comparison of land-surface parameterization schemes. *Bull. Amer. Meteorol. Soc.*, **74**, 489-503.

Hildebrand, P. H., 1988: Flux and sounding data from the NCAR King Air aircraft during HAPEX-MOBILHY. NCAR Technical Rept. TN-319, NCAR Boulder, CO 80307, USA.

Hillel, D., 1980: *Fundamentals of soil physics*. Academic Press, New York, 413 pp.

Holtstag, A. A. M., 1987: Surface fluxes and boundary-layer scaling: Models and applications. KNMI Sci. Rep., WR 87-02, 173 pp., Royal Netherlands Meteorological Institute (KNMI), De Bilt, Netherlands.

Holtstag, A. A. M., and A. C. M. Beljaars, 1989: Surface flux parameterization schemes; developments and experiences at KNMI. Proceed. Workshop on Parameterization of Fluxes and Land Surfaces, 24-26 Oct. 1988, 121-147, ECMWF, Reading, 1989. (Also available as KNMI Sci. Rep. 88-06, 27 pp., 1988, De Bilt, Netherlands.)

Holtstag, A. A. M., and B. Boville, 1993: Local versus nonlocal boundary-layer diffusion in a global climate model. *J. Climate*, **6**, 1825-1842.

Holtstag, A. A. M., E. I. F. de Bruijn, and H.-L. Pan, 1990: A high-resolution air mass transformation model for short-range weather forecasting. *Mon. Wea. Rev.*, **118**, 1561-1575.

Holtstag, A. A. M., and H. A. R. de Bruin, 1988: Applied modeling of the nighttime surface energy balance over land. *J. Appl. Meteorol.*, **27**, 689-704.

Holtstag, A. A. M., and M. Ek, 1996: Simulation of surface fluxes and boundary layer development over the pine forest in HAPEX-MOBILHY. *J. Appl. Meteorol.*, **35**, 202-213.

Holtstag, A. A. M., and C.-H. Moeng, 1991: Eddy diffusivity and countergradient

transport in the convective atmospheric boundary layer. *J. Atmos. Sci.*, **48**, 1689-1698.

Holtslag, A. A. M., and F. T. M. Nieuwstadt, 1986: Scaling the atmospheric boundary layer. *Bound.-Layer Meteorol.*, **36**, 201-209.

Holtslag, A. A. M., E. van Meijgaard, and W. C. de Rooy, 1995: A comparison of boundary layer diffusion schemes in unstable conditions over land. *Bound.-Layer Meteorol.*, **76**, 69-96.

Holtslag, A. A. M., and A. P. van Ulden, 1983: A simple scheme for daytime estimates of the surface fluxes from routine weather data. *J. Clim. Appl. Meteorol.*, **22**, 517-529.

Hong, S.-Y., and H.-L. Pan, 1996: Nonlocal boundary layer vertical diffusion in a medium-range forecast model. *Mon. Wea. Rev.*, **124**, 2322-2339.

Huang, X., and T. J. Lyons, 1995: On the simulation of surface heat fluxes in a land surface-atmosphere model. *J. Appl. Meteorol.*, **34**, 1099-1111.

Hughes, N. A., and A. Henderson-Sellers, 1983: The effect of spatial and temporal averaging on sampling strategies for cloud amount data. *Bull. Amer. Meteorol. Soc.*, **64**, 250-257.

IJpelaar, R. J. M., 2000: Evaluation of modified soil parameterization in the ECMWF land surface scheme. KNMI Technical Report No. 228, Royal Netherlands Meteorological Institute (KNMI), De Bilt, Netherlands.

Jacobs, C. M. J., 1994: Direct impact of atmospheric CO₂ enrichment on regional transpiration. Ph. D. thesis, Meteorology and Air Quality, Wageningen University, Wageningen, Netherlands.

Jacquemin, B., and J. Noilhan, 1990: Sensitivity study and validation of a land surface parameterization using the HAPEX-MOBILHY data set. *Bound.-Layer Meteorol.*, **52**, 93-134.

Jager, C. J., T. C. Nakken, and C. L. Palland, 1976: Bodemkundig onderzoek van twee graslandpercelen nabij Cabauw (Study of soil properties at two grassland locations near Cabauw). NV Heidemaatschppij Beheer, Arnhem, The Netherlands (in Dutch).

Jarvis P. G., 1976: The interpretation of the variations in leaf water potential and stomatal conductance found in canopies in the field. *Phil. Trans. R. Soc. Lond. B.*, **273**, 593-610.

Johansen, O., 1975: Thermal conductivity of soils (in Norwegian), Ph.D. thesis, Publ. ADA 044002, Trondheim, Norway. (English translation 637, Cold Reg. Res and Eng. Lab., Hanover, N.H., 1977.)

Johnson, R. H., 1977: Effects of cumulus convection on the structure and growth of the mixed layer over south Florida. *Mon. Wea. Rev.*, **105**, 713-724.

Kasten, F., and G. Czeplak, 1980: Solar and terrestrial radiation dependent on the amount and type of cloud. *Solar Energy*, **24**, 177-189.

Kim, J., and M. Ek, 1995: A simulation of the surface energy budget and soil water content over the Hydrologic Atmospheric Pilot Experiment - Modélisation du Bilan Hydrique forest site. *J. Geophys. Res.*, **100**, 20,845-20,854.

Kim, J., and L. Mahrt, 1992: Simple formulation of turbulent mixing in the stable free atmosphere and nocturnal boundary layer. *Tellus*, **44a**, 381-394.

Kondo, J., O. Kanechika, and N. Yasuda, 1978: Heat and momentum transfers under strong stability in the atmospheric surface layer. *J. Atmos. Sci.*, **35**, 1012-1021.

Kondo, J., N. Saigusa, and T. Sato, 1990: A parameterization of evaporation from bare soil surfaces. *J. Appl. Meteorol.*, **29**, 385-389.

Koren, V., J. Schaake, K. Mitchell, Q.-Y. Duan, F. Chen, and J. Baker, 1999: A parameterization of snowpack and frozen ground intended for NCEP weather and climate models. *J. Geophys. Res.*, **104**(D16), 19,569-19,585.

Kraus, E. B., and J. S. Turner, 1967: A one-dimensional model of the seasonal thermocline. II. The general theory and its consequences. *Tellus*, **19**, 98-105.

Lanicci, J. M., T. N. Carlson, and T. T. Warner, 1987: Sensitivity of the Great Plains environment to soil moisture distribution. *Mon. Wea. Rev.*, **115**, 2660-2673.

Lenschow, D. H., J. C. Wyngaard, and W. T. Pennell, 1980: Mean-field and second-moment budgets in a baroclinic, convective boundary layer. *J. Atmos. Sci.*, **37**, 1313-1326.

Liang, X., E. F. Wood, D. P. Lettenmaier, D. Lohmann, A. Boone, S. Chang, F. Chen, Y. Dai, C. Desborough, R. E. Dickinson, Q. Duan, M. Ek, Y. M. Gusev, F. Habets, P. Irannejad, R. Koster, K. E. Mitchell, O. N. Nasonova, J. Noilhan, J. Schaake, A. Schlosser, Y. Shao, A. B. Shmakin, D. Verseghy, K. Warrach, P. Wetzel, Y. Xue, Z.-L. Yang, and Q.-c. Zeng, 1998: The project for intercomparison of land-surface parameterization schemes (PILPS) phase 2(c) Red-Arkansas river basin experiment: 2. Spatial and temporal analysis of energy fluxes. *Global Planet. Change*, **19**, 137-159.

Lilly, D. K., 1968: Models of cloud-topped mixed layers under a strong inversion. *Quart. J. Roy. Meteorol. Soc.*, **94**, 292-309.

Liou, K.-N., 1976: On the absorption, reflection and transmission of solar radiation in cloudy atmospheres. *J. Atmos. Sci.*, **33**, 798-805.

Lohmann, D., D. P. Lettenmaier, X. Liang, E. F. Wood, A. Boone, S. Chang, F. Chen, Y. Dai, C. Desborough, R. E. Dickinson, Q. Duan, M. Ek, Y. M. Gusev, F. Habets, P. Irannejad, R. Koster, K. E. Mitchell, O. N. Nasonova, J. Noilhan, J. Schaake, A. Schlosser, Y. Shao, A. B. Shmakin, D. Verseghy, K. Warrach, P. Wetzel, Y. Xue, Z.-L. Yang, and Q.-c. Zeng, 1998: The project for intercomparison of land-surface parameterization schemes (PILPS) phase 2(c) Red-Arkansas River basin experiment: 3. Spatial and temporal analysis of water fluxes. *Global Planet. Change*, **19**, 161-179.

Louis, J.-F., 1979: A parametric model of vertical eddy fluxes in the atmosphere. *Bound.-Layer Meteorol.*, **17**, 187-202.

- Louis, J.-F., M. Tiedke, and J. F. Geleyn, 1982: A short history of the operational PBL-parameterization at ECMWF. Proceedings of the ECMWF Workshop on Planetary Boundary Layer Parameterisation, European Centre for Medium-Range Weather Forecasts, 25-27 November 1981, Reading, U.K., pp. 59-80.
- Mahrt, L., 1976: Mixed layer moisture structure. *Mon. Wea. Rev.*, **104**, 1403-1407.
- Mahrt, L., 1987: Grid-averaged surface fluxes. *Mon. Wea. Rev.*, **115**, 1550-1560.
- Mahrt, L., 1991: Boundary-layer moisture regimes. *Quart. J. Roy. Meteorol. Soc.*, **117**, 151-176.
- Mahrt, L., and M. Ek, 1984: The influence of atmospheric stability on potential evaporation. *J. Clim. Appl. Meteorol.*, **23**, 222-234.
- Mahrt, L., and M. Ek, 1993: Spatial variability of turbulent fluxes and roughness lengths in HAPEX-MOBILHY. *Bound.-Layer Meteorol.*, **65**, 381-400.
- Mahrt, L., and H.-L. Pan, 1984: A two-layer model of soil hydrology. *Bound.-Layer Meteorol.*, **29**, 1-20.
- Mahrt, L., and D. A. Pierce, 1980: Relationship of moist convection to boundary layer properties: Application to a semi arid region. *Mon. Wea. Rev.*, **108**, 92-96.
- Margulis, S. A., and D. Entekhabi, 2001: Feedback between the land surface energy balance and atmospheric boundary layer diagnosed through a model and its adjoint. *J. Hydrometeorol.*, **2**, 599-620.
- Marshall, C. H., K. C. Crawford, K. E. Mitchell, and D. J. Stensrud, 2003: The impact of the land surface physics in the operational NCEP Eta model on simulating the diurnal cycle: Evaluation and testing using Oklahoma Mesonet data. *Wea. Forecast.*, **18**, 748-768.
- Mascart, P., O. Taconet, J.-P. Pinty, and M. Ben Mehrez, 1991: Canopy resistance formulation and its effect in mesoscale models: A HAPEX perspective. *Agric. Forest*

Meteorol., **54**, 319-351.

McCumber, M. C., and R. A. Pielke, 1981: Simulation of the effects of surface fluxes of heat and moisture in a mesoscale numerical model. 1. soil layer. *J. Geophys. Res.*, **86**(C10), 9929-9938.

Mitchell, K., and D. Hahn, 1990: Objective development of diagnostic cloud forecast schemes in global and regional models. Proc. Seventh Conference on Atmospheric Radiation, Amer. Meteorol. Soc., 23-27 July, San Francisco, USA, J138-145.

Mocko, D. M., and W. R. Cotton, 1995: Evaluation of fractional cloudiness parameterizations for use in a mesoscale model. *J. Atmos. Sci.*, **52**, 2884-2901.

Monna, W. A. A., and J. G. van der Vliet, 1987: Facilities for research and weather observations on the 213-m tower at Cabauw and at remote locations. KNMI Scientific Report WP-87-5, Royal Netherlands Meteorological Institute (KNMI), De Bilt, Netherlands.

Monteith, J. L., 1965: Evaporation and environment. *Symp. Soc. Exp. Biol.*, **19**, 205-234.

Nicholls, S., and M. A. LeMone, 1980: The fair-weather boundary layer in GATE: The relationship of subcloud fluxes and structure to the distribution and enhancement of cumulus clouds. *J. Atmos. Sci.*, **37**, 2051-2067.

Nicholls, S., and C. J. Reading, 1979: Aircraft observations of the structure of the lower boundary layer over the sea. *Quart. J. Roy. Meteorol. Soc.*, **105**, 785-802.

Namias, J., 1988: The 1988 summer drought over the Great Plains - a classic example of air-sea-land interaction. *Trans. Amer. Geophys. Union*, **69**, 1067.

Noh, Y., W.-G. Cheon, S.-Y. Hong, and S. Raasch, 2003: Improvement of the K-profile model for the planetary boundary layer based on large eddy simulation data. *Bound.-Layer Meteorol.*, **107**, 401-427.

Noilhan, J., and S. Planton, 1989: A simple parameterization of land surface pro-

cesses for meteorological models. *Mon. Wea. Rev.*, **117**, 536-549.

O'Brien, J. J., 1970: A note on the vertical structure of the eddy exchange coefficient in the planetary boundary layer. *J. Atmos. Sci.*, **27**, 1213-1215.

Oglesby, R. J., and D. J. Erickson III, 1989: Soil moisture and the persistence of North American drought. *J. Climate*, **2**, 1362-1380.

Otterman, J., A. Manes, S. Rubin, P. Alpert, and D. O'C. Starr, 1990: An increase of early rains in southern Israel following land-use change? *Bound.-Layer Meteorol.*, **53**, 333-351.

Palmén, E., and C. W. Newton, 1969: *Atmospheric circulation systems: Their structure and physical interpretation*. Academic Press, New York, 603 pp.

Paltridge, G. W., and C. M. R. Platt, 1976: Radiative processes in meteorology and climatology. In *Developments in Atmospheric Science*, 5. Elsevier Scientific Publ. Co., Amsterdam, 318 pp.

Pan, H.-L., 1990: A simple parameterization scheme of evapotranspiration over land for the NMC medium-range forecast model. *Mon. Wea. Rev.*, **118**, 2500-2512.

Pan, H.-L., and L. Mahrt, 1987: Interaction between soil hydrology and boundary-layer development. *Bound.-Layer Meteorol.*, **38**, 185-202.

Paulson, C. A., 1970: The mathematical representation of wind speed and temperature profiles in the unstable atmospheric surface layer. *J. Appl. Meteorol.*, **9**, 857-861.

Penman, H. L., 1948: Natural evaporation from open water, bare soil, and grass. *Proc. Roy. Soc. London*, **A193**, 120-146.

Peters-Lidard, C. D., E. Blackburn, X. Liang, and E. F. Wood, 1998: The effect of soil thermal conductivity parameterization on surface energy fluxes and temperatures. *J. Atmos. Sci.*, **55**, 1209-1224.

Peters-Lidard, C. D., M. S. Zion, and E. F. Wood, 1997: A soil-vegetation-atmosphere

transfer scheme for modeling spatially variable water and energy balance processes. *J. Geophys. Res.*, **102**(D4), 4303-4324.

Pielke, R. A. Sr., G. Dalu, J. Eastman, P. L. Vidale, and X. Zeng, 1998: Boundary layer processes and land surface interactions on the mesoscale. In *Clear and Cloudy Boundary Layers*, A. A. M. Holtslag and P. G. Duynkerke (Eds.), Roy. Netherlands Acad. Arts and Sci., Amsterdam, 372 pp.

Pinty, J.-P., P. Mascart, E. Richard, and R. Rosset, 1989: An investigation of mesoscale flows induced by vegetation inhomogeneities using an evaporation model calibrated against HAPEX-MOBILHY data. *J. Appl. Meteorol.*, **28**, 976-992.

Polcher, J., 2004: GMPP to focus on the diurnal cycle. *GEWEX News*, **14**(1), 8.

Qu, W., A. Henderson-Sellers, A. Pitman, T. C. F. Abramopoulos, A. Boone, S. Chang, F. Chen, Y. Dai, R. Dickinson, L. Duemenil, M. Ek, N. Gedney, Y. M. Gusev, J. Kim, R. Koster, E. Kowalczyk, J. Lean, X. Liang, J.-F. Mahfouf, H.-T. Mengelkamp, K. Mitchell, O. Nasonova, J. Noilhan, A. Robock, C. Rosenzweig, J. S. C. Schlosser, J.-P. Schulz, A. Shmakina, D. Verseghy, P. Wetzels, E. F. Wood, Z.-L. Yang, and Q.-c. Zeng, 1998: Sensitivity of latent heat flux from PILPS land-surface schemes to perturbations of surface air temperature. *J. Atmos. Sci.*, **55**, 1909-1927.

Rabin, R. M., S. Stadler, P. J. Wetzels, D. J. Stensrud, and M. Gregory, 1990: Observed effects of landscape variability on convective clouds. *Bull. Amer. Meteorol. Soc.*, **71**, 272-280.

Richardson, L. F., 1922: *Weather Prediction by Numerical Processes*, Cambridge University Press, London.

Ronda, R. J., H. A. R. de Bruin, and A. A. M. Holtslag, 2001: Representation of the canopy conductance in modeling the surface energy budget for low vegetation. *J. Appl. Meteorol.*, **40**, 1431-1444.

Saito, K., and A. Baba, 1988: A statistical relation between relative humidity and the GMS observed cloud amount. *J. Meteorol. Soc. Japan*, **66**, 187-192.

- Satterlund, D. R., 1979: An improved equation for estimation longwave radiation from the atmosphere. *Water Resources Res.*, **15**, 1649-1650.
- Schädler, G., 1990: Triggering of atmospheric circulations by moisture inhomogeneities of the earth's surface. *Bound.-Layer Meteorol.*, **51**, 1-29.
- Segal, M., G. Kallos, J. Brown, and M. Mandel, 1991: Morning temporal variations of shelter level specific humidity. *J. Appl. Meteorol.*, **31**, 74-85.
- Sellers, P. J., Y. Mintz, Y. C. Sud, and A. Dalcher, 1986: A simple biosphere model (SiB) for use within general circulation models. *J. Atmos. Sci.*, **43**, 505-531.
- Sellers, P. J., D. A. Randall, G. J. Collatz, J. A. Berry, C. B. Field, D. A. Dazlich, C. Zhang, G. D. Collelo, and L. Bounoua, 1996: A revised land surface parameterization (SiB2) for atmospheric GCMs. Part I: Model formulation. *J. Climate*, **9**, 676-705.
- Sen, O. L., W. J. Shuttleworth, and Z.-L. Yang, 2000: Comparative evaluation of BATS2, BATS and SiB2 with Amazon data. *J. Hydrometeorol.*, **1**, 135-153.
- Slingo, J. M., 1980: A cloud parameterization scheme derived from GATE data for use with a numerical model. *Quart. J. Roy. Meteorol. Soc.*, **106**, 747-770.
- Slingo, J. M., 1987: The development and verification of a cloud prediction scheme for the ECMWF model. *Quart. J. Roy. Meteorol. Soc.*, **113**, 899-927.
- Stephens, G. L., 1978: Radiation profiles in extended water clouds. II: Parameterization schemes. *J. Atmos. Sci.*, **35**, 2123-2132.
- Stewart, J. B., 1988: Modeling Surface Conductance of Pine Forest. *Agric. For. Meteorol.*, **43**, 19-35.
- Steyn, D. G., 1990: An advective mixed-layer model for heat and moisture incorporating an analytic expression for moisture entrainment. *Bound.-Layer Meteorol.*, **53**, 21-31.
- Stull, R. B., 1988: *An Introduction to Boundary Layer Meteorology*. Atmospheric

Sciences Library, Kluwer Academic Publishers, Dordrecht, The Netherlands, 666 pp.

Stull, R. B., and A. G. M. Driedonks, 1987: Application of the transilient turbulence parameterization to atmospheric boundary-layer simulations. *Bound.-Layer Meteorol.*, **40**, 209-239.

Tennekes, H., 1973: A model for the dynamics of the inversion above a convective boundary layer. *J. Atmos. Sci.*, **30**, 558-567.

Tennekes, H., and A. G. M. Driedonks, 1981: Basic entrainment equations for the atmospheric boundary layer. *Bound.-Layer Meteorol.*, **20**, 515-531.

Trenberth, K. E., G. W. Branstator, and P. A. Arkin, 1988: Origins of the 1988 North American drought. *Science*, **242**, 1640-1645.

Troen, I., and L. Mahrt, 1986: A simple model of the atmospheric boundary layer: Sensitivity to surface evaporation. *Bound.-Layer Meteorol.*, **37**, 129-148.

van den Hurk, B. J. J. M., and A. C. M. Beljaars, 1996: Impact of some simplifying assumptions in the new ECMWF surface scheme. *J. Appl. Meteorol.*, **35**, 1333-1343.

van den Hurk, B. J. J. M., and A. A. M. Holtslag, 1997. On the bulk parameterization of surface fluxes for various conditions and parameter ranges. *Bound.-Layer Meteorol.*, **82**, 119-134.

van den Hurk, B. J. J. M., C. Peters-Lidard, P. Houser, B. Holtslag, and P. Dirmeyer, 2004: Towards implementation of the "Local-Coupled" (LoCo) GLASS theme. Unpublished document.

van den Hurk, B. J. J. M., A. Verhoef, A. R. van den Berg, and H. A. R. de Bruin, 1995: An intercomparison of three vegetation/soil models for a sparse vineyard canopy. *Quart. J. Roy. Meteorol. Soc.*, **121**, 1867-1889.

van den Hurk, B. J. J. M., P. Viterbo, A. C. M. Beljaars, and A. K. Betts, 2000: Offline validation of the ERA40 surface scheme. European Centre for Medium-Range

Weather Forecasts, Technical Memorandum No. 295, January.

van Genuchten, M. Th., 1980: A closed-form equation for predicting the hydraulic conductivity of unsaturated soils. *Soil Sci. Soc. Amer. J.*, **44**, 892-898.

van Ulden, A. P., and A. A. M. Holtslag, 1985: Estimation of atmospheric boundary layer parameters for diffusion applications. *J. Clim. Appl. Meteorol.*, **24**, 1198-1207.

van Ulden, A. P., and J. Wieringa, 1996: Atmospheric boundary layer research at Cabauw. *Bound.-Layer Meteorol.*, **78**, 39-69.

Vandenberg, J. A., and T. Louters, 1988: The variability of soil-moisture diffusivity of loamy to silty soils on Marl, determined by the hot air method. *J. Hydrology*, **97**, 235-250.

Viterbo, P., and A. C. M. Beljaars, 1995: An improved land surface parameterization scheme in the ECMWF model and its validation. *J. Climate*, **8**, 2716-2748.

Vogelezang, D. H. P., and A. A. M. Holtslag, 1996: Evaluation and model impacts of alternative boundary-layer height formulations. *Bound.-Layer Meteorol.*, **81**, 245-269.

Webb, E. K., 1970: Profile relationships: the log-linear range, and extension to strong stability. *Quart. J. Roy. Meteorol. Soc.*, **96**, 67-90.

Wessels, H. R. A., 1983: Soil moisture measurements 1977-1981 at the Cabauw micrometeorology field. KNMI Technical Report FM-83-19, Royal Netherlands Meteorological Institute (KNMI), De Bilt, Netherlands.

Wessels, H. R. A., 1984: Cabauw meteorological data tapes 1973-1984; description of instrumentation and data processing for the continuous measurements. KNMI Technical Report WR-84-6, Royal Netherlands Meteorological Institute (KNMI), De Bilt, Netherlands.

Wetzel, P. J., and J.-T. Chang, 1987: Concerning the relationship between evaporation and soil moisture. *J. Clim. Appl. Meteorol.*, **26**, 18-27.

Wetzel, P. J., S. Argentini, and A. Boone, 1996: Role of land surface in controlling daytime cloud amount: Two case studies in the GCIP-SW area. *J. Geophys. Res.*, **101**, 7359-7370.

Wilde, N. P., R. B. Stull, and E. W. Eloranta, 1985: The LCL zone and cumulus onset. *J. Clim. Appl. Meteorol.*, **24**, 640-657.

Wilson, M. F., A. Henderson-Sellers, R. E. Dickinson, and P. J. Kennedy, 1987: Sensitivity of the biosphere-atmosphere transfer scheme (BATS) to the inclusion of variable soil characteristics. *J. Clim. Appl. Meteorol.*, **26**, 341-362.

Wood, E. F., D. P. Lettenmaier, X. Liang, D. Lohmann, A. Boone, S. Chang, F. Chen, Y. Dai, C. Desborough, R. E. Dickinson, Q. Duan, M. Ek, Y. M. Gusev, F. Habets, P. Irannejad, R. Koster, K. E. Mitchell, O. N. Nasonova, J. Noilhan, J. Schaake, A. Schlosser, Y. Shao, A. B. Shmakina, D. Verseghy, K. Warrach, P. Wetzel, Y. Xue, Z.-L. Yang, and Q.-c. Zeng, 1998: The project for intercomparison of land-surface parameterization schemes (PILPS) phase 2(c) Red-Arkansas river basin experiment: 1. Experiment description and summary intercomparisons. *Global Planet. Change*, **19**, 115-135.

Zepp, H., and A. Belz, 1992: Sensitivity and problems in modeling soil-moisture conditions. *J. Hydrology*, **131**, 227-238.

Zeng, X., Y. J. Dai, R. E. Dickinson, and M. Shaikh, 1998: The role of root distribution for land climate simulation over land. *Geophys. Res. Letters*, **25**, 4533-4536.

Samenvatting

In dit proefschrift wordt de interactie van het landoppervlak met de atmosfeer onder convectieve omstandigheden onderzocht. Dit wordt gedaan met behulp van een een-dimensionaal (koloms) model en met datasets verkregen op Cabauw (1978, midden Nederland) en gedurende the Hydrological and Atmospheric Pilot Experiment - Modélisation du Bilan Hydrique (HAPEX-MOBILHY, 1986, zuidwest Frankrijk). Het kolomsmodel omvat een gedetailleerde beschrijving van de processen bij het landoppervlak en in de atmosferische grenslaag. De gevoeligheid van de land - atmosfeer wisselwerking voor de beschrijving van hydrologische processen in de bodem laat zien dat de effecten op oppervlaktefluxen en grenslaagontwikkeling het sterkst zijn bij gematigde tot lage waarden van bodemwatergehalte. Dit geldt in het bijzonder voor kale grond. Grenslaagbewolking wordt gereguleerd door de evolutie van relatieve vochtigheid (RH) aan de top van de grenslaag. Hierbij spelen de interactie van bodemwater, de verwarming vanaf het oppervlak, de initiële ABL conditie en de vochtinhoud en temperatuurstratificatie boven de ABL een belangrijke rol, tezamen met een aantal concurrerende terugkoppelingsmechanismen. Een formulering voor de fractionele bedekkingsgraad is ontwikkeld, gebaseerd op een Gaussische distributie van totaal-water RH aan de top van de ABL. De distributie omvat turbulente variaties als functie van droge lucht entrainment aan de ABL-top en mesoschaal variaties als functie van horizontale domein grootte. De gemodelleerde wolkenfractie blijkt gevoeliger te zijn voor de voorgeschreven gemiddelde verticale beweging dan voor aanpassingen in de coëfficiënten van de wolkenfractie formulering. Diverse verbeteringen in het landoppervlakmodel zijn geïmplementeerd en getest door observaties te vergelijken met off-line modelberekeningen zonder dat parameters in het model werden aangepast. Bij het gebruik van dit verbeterde landoppervlakmodel in het gekoppelde land-atmosfeermodel werden realistische oppervlaktefluxen en atmosferische profielen gesimuleerd voor convectieve omstandigheden. Tenslotte werd

doormiddel van modelsimulaties, analytische methoden en observaties aangetoond dat, als de stabiliteit boven de ABL niet te zwak is, het effect van meer bodemwater is dat de RH aan de ABL top toeneemt en daarmee ook de bedekkingsgraad. Hiervoor moet wel in aanvang voldoende vocht in de ABL aanwezig zijn en tevens mag de lucht boven de ABL niet te droog zijn. Bij zwakke stabiliteit boven de ABL, treedt juist bij droge bodems een toename van ABL-top RH op en daarmee een grotere bedekkingsgraad. Ook hier geldt dat er in aanvang dan wel voldoende vocht in de ABL aanwezig moet zijn en tevens mag de lucht boven de ABL niet te droog zijn.

Curriculum vitae

Michael Bryan Ek was born on 19 October 1956 in Portland, Oregon, USA. During 1975-1983 he attended Portland State University and Oregon State University (OSU), receiving a B.S. in 1980 and an M.S. with a minor in math and statistics in 1983, both in Atmospheric Sciences from OSU. The M.S. thesis was on the effects of atmospheric stability on potential evaporation under the direction of Prof.dr. Larry Mahrt. Working with the U.S. National Weather Service and as a private consulting meteorologist in Alaska and then Seattle from 1983-1986 gave Michael important insights into the issues of operational meteorology, particularly as related to fire weather, and snow avalanches and mountain weather. In 1986-1987 he returned to OSU where he received a B.S. in Math and Science Education, and subsequently took a position at OSU in 1988 as a research assistant and instructor in the Department of Atmospheric Sciences (later the College of Oceanic and Atmospheric Sciences), again working with Larry Mahrt on issues in land-surface and atmospheric boundary layer (ABL) research. In 1989 he began a collaboration with Bert Holtslag who was visiting Larry at OSU for the summer; Michael continued to work on similar land-surface and ABL research with Bert who was at the Royal Netherlands Meteorological Institute (KNMI). Michael came to KNMI as a visiting scientist during 1995-1996, where he began working on his PhD with Bert, who at that time was a professor at Utrecht University/IMAU. In 1999, Michael took a position as a University Corporation for Atmospheric Research (UCAR) visiting scientist at the National Centers for Environmental Prediction (NCEP)/Environmental Modeling Center in Suitland, Maryland, USA. At NCEP, Michael maintained his land-surface and ABL research in an operational setting, and continued his collaboration and PhD work with Bert Holtslag, now professor and head of the Meteorology and Air Quality Section at Wageningen University.

Michael has worked on a number of research projects by various funding agencies on atmospheric boundary layers, and land-atmosphere and ocean-atmosphere interaction. He has been a reviewer for several scientific journals, as well as a proposal reviewer and panel member in evaluating different research programs. He has also participated in a number of international groups, e.g. the Project for the Intercomparison of Land-Surface Parameterization Schemes (PILPS) and the Global Land/Atmosphere System Study (GLASS), the GEWEX (Global Energy and Water Cycle Experiment) Cloud System Studies (GCSS)/Boundary Layer Cloud working group, and the Tropical Oceans Global Atmosphere – Coupled Ocean Atmosphere Response Experiment (TOGA-COARE) field program as part of the Climate Variability and Predictability (CLIVAR) program. He is currently a member of the Weather Research and Forecast (WRF) mesoscale model land-surface working group, and a participant in and science panel member for the GEWEX Atmospheric Boundary Layer Study (GABLS).

List of peer-reviewed publications by the author

First-author publications

Ek, M., and A. A. M. Holtslag, 2005: Evaluation of a land-surface scheme at Cabauw. *Theoretical Appl. Climatology*, **80**, 213-227, doi:10.1007/s00704-004-0101-4.

Ek, M., and A. A. M. Holtslag, 2004: Influence of soil moisture on boundary-layer cloud development. *J. Hydrometeorol.*, **5**, 86-99.

Ek, M., K. E. Mitchell, Y. Lin, E. Rogers, P. Grunmann, V. Koren, G. Gayno, and J. D. Tarpley, 2003: Implementation of Noah land-surface model advances in the NCEP operational mesoscale Eta model. *J. Geophys. Res.*, **108**(D22), 8851, doi:10.1029/2002JD003296.

Ek, M., and R. H. Cuenca, 1994: Variation in soil parameters: Implications for modeling surface fluxes and atmospheric boundary-layer development. *Bound.-Layer Meteorol.*, **70**, 369-383.

Ek, M., and L. Mahrt, 1994: Daytime evolution of relative humidity at the boundary-layer top. *Mon. Wea. Rev.*, **122**, 2709-2721.

Ek, M., and L. Mahrt, 1991: A model for boundary-layer cloud cover. *Annales Geophysicae*, **9**, 716-724.

Co-author publications

Levy, G., and **M. Ek**, 2005: Towards a parameterization of surface roughness based on wind tendency. *Bound.-Layer Meteorol.* (submitted)

Cuxart, J., A. A. M. Holtslag, **M. Ek**, and 21 co-authors, 2005: Single-column model intercomparison for a stably stratified atmospheric boundary layer. *Bound.-Layer Meteorol.* (accepted) (See Bibliography for complete list of co-authors.)

Holtslag, A. A. M., and **M. Ek**, 2005: Atmospheric boundary layer climates and land surface interactions (HSA032), in *Encyclopedia of Hydrological Sciences*, Part 3 Meteorology & Climatology, M. G. Anderson and J. J. McDonnell (Eds.), Wiley and Sons, Ltd., Bristol, England. (in press)

Murthy, B. S., S. S. Parasnis, and **M. Ek**, 2004: Interactions of the land-surface with the atmospheric boundary layer: Case studies from LASPEX. *Current Science*, **86**(8), 1128-1134.

Lackmann, G. M., K. Keeter, L. G. Lee, and **M. Ek**, 2002: Model representation of freezing and melting precipitation: Implications for winter weather forecasting. *Wea. Forecasting*, **17**, 1016-1033.

Levy, G., and **M. Ek**, 2001: The simulated response of the marine atmospheric boundary layer in the western Pacific warm pool region to surface flux forcing. *J. Geophys. Res.*, **106**, 7229-7242.

Chang, S., D. Hahn, C.-H. Yang, D. Norquist, and **M. Ek**, 1999: Validation study of the CAPS model land surface scheme using the 1987 Cabauw/PILPS dataset. *J. Appl. Meteorol.*, **38**, 405-422.

Wood, E. F., D. P. Lettenmaier, X. Liang, D. Lohmann, **M. Ek**, and 24 co-authors, 1998: The project for intercomparison of land-surface parameterization schemes (PILPS) phase 2(c) Red–Arkansas river basin experiment: 1. Experiment description and summary intercomparisons. *Global Planet. Change*, **19**, 115-135. (See Bibliography for complete list of co-authors.)

Liang, X., E. F. Wood, D. P. Lettenmaier, D. Lohmann, **M. Ek**, and 24 co-authors, 1998: The project for intercomparison of land-surface parameterization schemes (PILPS) phase 2(c) Red–Arkansas river basin experiment: 2. Spatial and temporal analysis of energy fluxes. *Global Planet. Change*, **19**, 137-159. (See Bibliography for complete list of co-authors.)

Lohmann, D., D. P. Lettenmaier, X. Liang, E. F. Wood, **M. Ek**, and 24 co-authors, 1998: The project for intercomparison of land-surface parameterization schemes (PILPS) phase 2(c) Red–Arkansas River basin experiment: 3. Spatial and temporal analysis of water fluxes. *Global Planet. Change*, **19**, 161-179. (See Bibliography for complete list of co-authors.)

Qu, W., A. Henderson-Sellers, A. Pitman, T. C. F. Abramopoulos, **M. Ek**, and 28 co-authors, 1998: Sensitivity of latent heat flux from PILPS land-surface schemes to perturbations of surface air temperature. *J. Atmos. Sci.*, **55**, 1909-1927. (See Bibliography for complete list of co-authors.)

Chen, T. H., A. Henderson-Sellers, P. Milly, A. Pitman, **M. Ek**, and 43 co-authors, 1997: Cabauw experimental results from the Project for Intercomparison of Land-surface Parameterization Schemes (PILPS). *J. Climate*, **10**, 1194-1215. (See Bibliography for complete list of co-authors.)

Chang, S., and **M. Ek**, 1996: Sensitivity study of the CAPS model land-surface scheme using the 1987 Cabauw/PILPS data set. *Phys. Chem. Earth*, **21**, 205-210.

Chang, S., and **M. Ek**, 1996: Note on "Daytime evolution of relative humidity at the boundary-layer top". *Mon. Wea. Rev.*, **124**, 1323-1326.

Ortega-Farias, S., R. H. Cuenca, and **M. Ek**, 1996: Daytime variation of sensible heat flux estimated by the bulk aerodynamic method for a grass canopy. *Agric. Forest Meteorol.*, **81**, 131-143.

Chen, F., K. Mitchell, J. Schaake, Y. Xue, H.-L. Pan, V. Koren, Q. Y. Duan, **M. Ek**, and A. Betts, 1996: Modeling of land-surface evaporation by four schemes and comparison with FIFE observations. *J. Geophys. Res.*, **101**, 7251-7268.

Cuenca, R. H., **M. Ek**, and L. Mahrt, 1996: Impact of soil water property parameterization on atmospheric boundary-layer simulation. *J. Geophys. Res.*, **101**, 7269-7277.

Holtslag, A. A. M., and **M. Ek**, 1996: Simulation of surface fluxes and boundary layer development over the pine forest in HAPEX-MOBILHY. *J. Appl. Meteorol.*, **35**, 202-213.

Kim, J., and **M. Ek**, 1995: A simulation of the surface energy budget and soil water content over the HAPEX-MOBILHY forest site. *J. Geophys. Res.*, **100**, 20,845-20,854.

Mahrt, L., and **M. Ek**, 1993: Spatial variability of turbulent fluxes and roughness lengths in HAPEX-MOBILHY. *Bound.-Layer Meteorol.*, **65**, 381-400.

Mahrt, L., and **M. Ek**, 1984: The influence of atmospheric stability on potential evaporation. *J. Clim. Appl. Meteorol.*, **23**, 222-234.